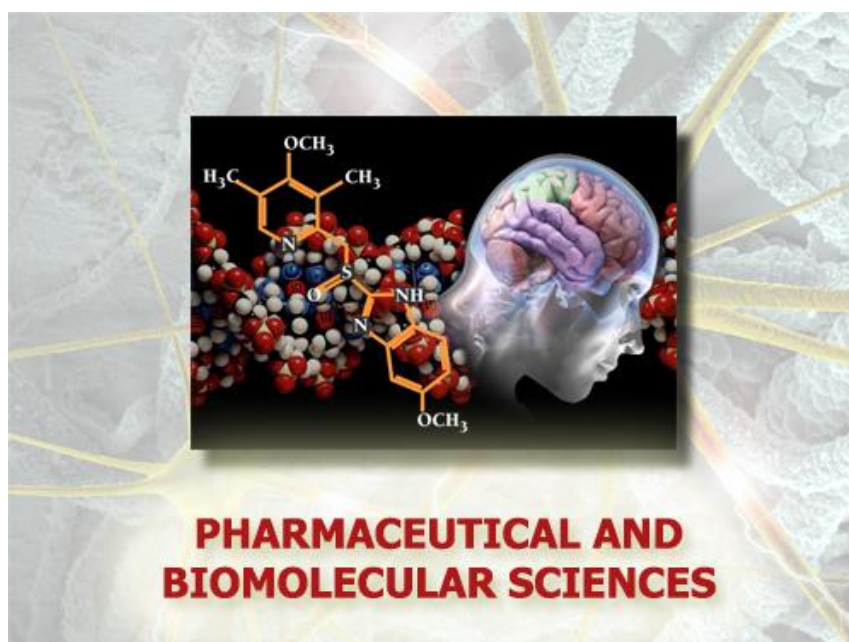


Università degli Studi di Torino



PhD School of Natural Sciences and Innovative Technologies

**Ph.D. Program in  
Pharmaceutical and Biomolecular Sciences  
(XXXIII cycle)**



**TITLE**

**Synthesis of new AAZTA bifunctional  
chelators for the development of innovative  
PET imaging agents**

Candidate: Ivan Hawala

Tutors: Prof. Silvio Aime  
Prof. Enzo Terreno



**Università degli Studi di Torino**



**Ph.D. program in Pharmaceutical and Biomolecular Sciences**

**Department of Molecular Biotechnology and Health Sciences**

**CYCLE: XXXIII**

**THESIS TITLE: SYNTHESIS OF NEW AAZTA BIFUNCTIONAL CHELATORS FOR THE DEVELOPMENT OF INNOVATIVE PET IMAGING AGENTS**

**CANDIDATE: IVAN HAWALA**

**TUTORS: PROF. SILVIO AIME  
PROF. ENZO TERRENO**

**PHD PROGRAM COORDINATOR: PROF GIANMARIO MARTRA**

**ACADEMIC YEARS: 2017-2020**

**SETTORE SCIENTIFICO-DISCIPLINARE DI AFFERENZA: Health-Diagnostic**



## **Abstract**

Molecular imaging applications increase every day the number of available technologies able to fight against cancer diseases. Each imaging technique has been developed during last decades with the purpose of monitoring, diagnosing and threat different kind of tumor related occurrences. Positron emission tomography (PET) plays an essential role in medical imaging, with a wide range of applications covering, among the others, oncology, neurology and cardiology. With the invention of clinical PET scanners and dedicated small animal PET scanners, there have been numerous studies about the development of PET tracers. Most current PET scanners are only available in hybrid PET/computed tomography (CT) configuration. The poor spatial resolution of a PET system (4-5mm) makes difficult the interpretation of PET images due to the lack of identifiable anatomical structures. The need for an accurate anatomical localization of the PET signal was the motivation for the PET/CT systems.

A polyaminopolycarboxylate heptadentate ligand based on a 1,4-diazepine scaffold (AAZTA) has been thoroughly studied as chelator for  $Gd^{3+}$  ions for MRI applications. This ligand has already been proven to form thermodynamically stable and kinetically inert Gallium complexes and an AAZTA-RGD peptide conjugate was recently shown to complex  $^{68}Ga$  at room temperature in acetate buffer at pH 3.8.

The project aims to design and synthesize novel AAZTA derivatives suitable for the conjugation with peptides (targeting probes), fluorophores (OI probes) or other relevant molecular vectors, to be included in a 'cold kit', which allows the labelling with PET's radionuclides, obtained from a cyclotron or eluted from a commercial generator.

# INDEX

<b>ABSTRACT</b> .....	<b>5</b>
<b>I.BACKGROUND</b> .....	<b>8</b>
1.1 MOLECULAR IMAGING (MI) .....	8
1.1.1 Positron emission tomography .....	10
1.1.2 Single-photon emission computed tomography .....	12
1.1.3 Optical Imaging.....	13
1.2 BIFUNCTIONAL CHELATING AGENTS .....	15
1.2.1 Acyclic chelators.....	17
1.2.2 Macrocyclic chelators.....	18
1.2.3 AAZTA.....	19
1.3 BIOCONJUGATION .....	23
1.3.1 Antibodies .....	23
1.3.2 Non-Ig therapeutic proteins.....	24
1.3.3 Peptides.....	27
1.4 PEPTIDE CHEMISTRY .....	28
1.4.1 Solid Phase Peptide Synthesis .....	30
1.4.2 Native Chemical Ligation .....	33
1.5 BIOLOGICAL TARGETS .....	34
1.5.1 Prostate-specific membrane antigen (PSMA) .....	34
1.5.2 Urokinase-type plasminogen activator receptor (uPAR).....	36
REFERENCES: .....	38
<b>II. DESIGN AND SYNTHESIS OF NOVEL AAZTA DERIVATIVES</b> .....	<b>45</b>
2.1 PURPOSE.....	45
2.2 MATERIALS AND METHODS.....	45
2.3 EXPERIMENTAL SYNTHESIS PROCEDURES .....	47
2.4 RESULTS AND DISCUSSIONS .....	53
2.5 CONCLUSIONS .....	53
2.5 SUPPORTING INFORMATION .....	55
<b>III. DESIGN AND SYNTHESIS OF NOVEL PSMA DERIVATIVES</b> .....	<b>60</b>
3.1 PURPOSE.....	60
3.2 MATERIALS AND METHODS.....	60
3.3 EXPERIMENTAL SYNTHESIS PROCEDURES .....	61
3.4 RESULTS AND DISCUSSIONS .....	64
3.5 CONCLUSIONS .....	65
3.5 SUPPORTING INFORMATION .....	66
<b>IV. DESIGN, SYNTHESIS AND <i>IN VITRO</i>/<i>IN VIVO</i> EVALUATIONS OF NEW DUAL PET/OI PROBES</b> .....	<b>69</b>
4.1 PURPOSE.....	69
4.2 MATERIALS AND METHODS.....	69
4.3 EXPERIMENTAL PROCEDURES (CHEMICAL SYNTHESIS).....	71
4.4 EXPERIMENTAL PROCEDURES (LABELING WITH NATURAL GALLIUM ISOTOPE) .....	79
4.5 EXPERIMENTAL PROCEDURES ( <i>IN VITRO</i> EXPERIMENTS) .....	81
4.6 EXPERIMENTAL PROCEDURES ( <i>IN VIVO</i> EXPERIMENTS) .....	81
4.7 RESULTS AND DISCUSSIONS .....	82
4.8 CONCLUSIONS .....	88
4.9 SUPPORTING INFORMATION .....	89
<b>V. DESIGN AND SYNTHESIS OF <math>\Gamma</math>-(R,S)-MERCAPTOORNITHINE</b> .....	<b>92</b>
5.1 PURPOSE.....	92
5.2 MATERIALS AND METHODS.....	94
5.3 EXPERIMENTAL CHEMICAL SYNTHESIS PROCEDURES .....	95
5.4 RESULTS AND DISCUSSIONS .....	98
5.5 CONCLUSIONS .....	98

5.6 SUPPORTING INFORMATION .....	99
<b>VI. GENERAL CONCLUSIONS .....</b>	<b>105</b>
<b>MANUSCRIPT 1 .....</b>	<b>107</b>
SYNTHESIS, RADIOLABELING AND PRE-CLINICAL EVALUATION OF [ <sup>44</sup> Sc]Sc-AAZTA CONJUGATE PSMA INHIBITOR, A NEW TRACER FOR HIGH-EFFICIENCY IMAGING OF PROSTATE CANCER (UNDER REVISION, EJNMMI).....	107
<b>MANUSCRIPTS 2 .....</b>	<b>131</b>
AN INNOVATIVE APPROACH FOR THE SYNTHESIS OF DUAL MODALITY PEPTIDE IMAGING PROBES BASED ON THE NATIVE CHEMICAL LIGATION(PUBLISHED ON CHEMCOMMUN).....	131

# I.BACKGROUND

## 1.1 MOLECULAR IMAGING (MI)

Molecular imaging (MI) serves as clinical and pre-clinical tool, widely used in diagnosis and/or therapy of pathologies. Historically, MI can be defined as the ability to visualize and quantitatively measure *in vivo* biological and cellular processes.<sup>1, 2</sup> Between all possible advantages related to the use of MI, the ability to characterize pathological diseases in tissues/organs without invasive examinations or surgical procedures with the consequence to develop more personalized treatment planning has a relevant importance. Personalized medicine approach is particularly important to define the best care for patients with advanced stage cancers and poor prognosis - in this case, exposure's risk to undesired side-effects of therapy may affect the quality of remaining life.<sup>3</sup>

Nowadays, different modalities are used in medical imaging. Among these, MRI (Magnetic Resonance Imaging), PET (Positron Emission Tomography), SPECT (Single-photon Emission Computed Tomography), OI (Optical Imaging), US (Ultrasound) and CT (Computed Tomography). Each imaging modality has its own advantages, disadvantages and different clinical applications, as shown in Table 1. The greater number of molecular imaging examinations is performed with MRI, PET and SPECT.

Modality	Advantages	Disadvantages	Common contrast agents	Clinical application examples
<b>CT</b>	<ul style="list-style-type: none"> <li>- Unlimited depth penetration;</li> <li>- high spatial resolution;</li> <li>- whole-body imaging;</li> <li>- short acquisition time;</li> <li>- moderately expensive;</li> <li>- anatomical imaging.</li> </ul>	<ul style="list-style-type: none"> <li>- Irradiation exposure;</li> <li>- limited soft tissue contrast;</li> <li>- only for anatomical and functional imaging.</li> </ul>	<ul style="list-style-type: none"> <li>- Barium;</li> <li>- iodine;</li> <li>- krypton;</li> <li>- Xenon.</li> </ul>	<ul style="list-style-type: none"> <li>- Tumor perfusion<sup>4</sup>.</li> </ul>
<b>PET</b>	<ul style="list-style-type: none"> <li>- Unlimited depth penetration;</li> <li>- whole-body imaging;</li> <li>- quantitative MI;</li> <li>- possible to combine with CT or MRI for anatomical information.</li> </ul>	<ul style="list-style-type: none"> <li>- Irradiation exposure;</li> <li>- expensive;</li> <li>- low spatial resolution;</li> <li>- long acquisition time.</li> </ul>	<ul style="list-style-type: none"> <li>- <sup>11</sup>C;</li> <li>- <sup>18</sup>F;</li> <li>- <sup>64</sup>Cu;</li> <li>- <sup>68</sup>Ga.</li> </ul>	<ul style="list-style-type: none"> <li>- <sup>18</sup>F-FDG for cancer staging;<sup>5</sup></li> <li>- diagnosis of various diseases.</li> </ul>
<b>SPECT</b>	<ul style="list-style-type: none"> <li>- Unlimited depth penetration;</li> <li>- whole-body imaging;</li> <li>- quantitative;</li> <li>- possible to combine with CT for</li> </ul>	<ul style="list-style-type: none"> <li>- Irradiation exposure;</li> <li>- expensive;</li> <li>- low spatial resolution;</li> <li>- long acquisition time.</li> </ul>	<ul style="list-style-type: none"> <li>- <sup>99m</sup>Tc;</li> <li>- <sup>123</sup>I;</li> <li>- <sup>111</sup>In.</li> </ul>	<ul style="list-style-type: none"> <li>- Diagnosis of various diseases;</li> <li>- radiotherapy of thyroid carcinoma with <sup>131</sup>I-iodine<sup>6</sup>.</li> </ul>



	anatomical information.			
<b>MRI</b>	<ul style="list-style-type: none"> <li>- Unlimited depth penetration</li> <li>- whole-body imaging;</li> <li>- no ionizing irradiation;</li> <li>- soft tissue contrast;</li> <li>- high spatial resolution.</li> </ul>	<ul style="list-style-type: none"> <li>- Expensive;</li> <li>- limited detection sensitivity of molecular contrast agents;</li> <li>- long acquisition time.</li> </ul>	<ul style="list-style-type: none"> <li>- Gadolinium (Gd<sup>3+</sup>);</li> <li>- iron oxide particles (SPIO, USPIO);</li> <li>- manganese oxide;</li> <li>- <sup>19</sup>F.</li> </ul>	<ul style="list-style-type: none"> <li>- SPIOs for lymph node metastases detection in prostate cancer;<sup>7</sup></li> <li>- characterization of focal hepatic lesions;<sup>8</sup></li> <li>- Perfusion imaging of the heart.<sup>9</sup></li> </ul>
<b>OI</b>	<ul style="list-style-type: none"> <li>- No ionizing irradiation;</li> <li>- relatively high spatial resolution;</li> <li>- real-time imaging/short acquisition time;</li> <li>- external or internal (endoscopy) applications;</li> <li>- inexpensive;</li> <li>- highly quantitative and sensitive.</li> </ul>	<ul style="list-style-type: none"> <li>- Limited depth penetration;</li> <li>- whole-body imaging not possible.</li> </ul>	<ul style="list-style-type: none"> <li>- Fluorescent molecules and dyes;</li> <li>- Light absorbing nanoparticles.</li> </ul>	<ul style="list-style-type: none"> <li>- OCT imaging of atherosclerosis;<sup>10</sup></li> <li>- OCT imaging for colonoscopy screening;<sup>11</sup></li> <li>- Raman imaging of skin cancer.<sup>12</sup></li> </ul>
<b>US</b>	<ul style="list-style-type: none"> <li>- No ionizing irradiation;</li> <li>- high spatial resolution;</li> <li>- real-time imaging/short acquisition time;</li> <li>- external or internal (endoscopy) applications;</li> <li>- inexpensive;</li> <li>- highly sensitive.</li> </ul>	<ul style="list-style-type: none"> <li>- Whole-body imaging not possible;</li> <li>- operator dependency.</li> </ul>	<ul style="list-style-type: none"> <li>- Contrast microbubbles.</li> </ul>	<ul style="list-style-type: none"> <li>- Characterization of focal liver lesions;<sup>13</sup></li> <li>- echocardiography;<sup>14</sup></li> <li>- tumor perfusion of cancer.<sup>15</sup></li> </ul>

**Table 1:** Advantages and disadvantages of some imaging modalities used with targeted or non-targeted contrast agents in clinic. Adapted from Pysz et al.<sup>3</sup>

Clinical molecular imaging is currently carried out often with PET and SPECT, and novel libraries of targeted radiopharmaceuticals for both imaging and dual-imaging/therapy are available. Optical, ultrasound, and other hybrid acoustic imaging strategies (e.g., photoacoustic imaging) propose real-time and inexpensive approaches, which may be well suited for routine clinical applications such as early disease detection and screening protocols involving frequent imaging examinations. The following sections highlight the main clinical and preclinical utilities related to the imaging probes synthesized during this PhD project: PET, SPECT and OI.

### 1.1.1 Positron emission tomography

Positron emission tomography is a unique technique widely used in molecular imaging because of its clear-cut recognition and its proven clinical value in the management of tumor affected patients.<sup>16</sup> Based on the annihilation process<sup>16</sup>, PET gained more attention for detection and visualization of a number of disease states in metabolism, oncology, inflammation, neurology and musculoskeletal systems.<sup>17</sup> PET has certain limitations (i.e. spatial resolution): integration of PET and computed tomography (PET/CT) provides precise localization of the lesions, thereby increasing specificity of the examination.<sup>18</sup> CT data are used to correct PET emission images for photonic self-attenuation by human body. When attenuation correction is carried out, a quantitative measurements of standardized uptake value (SUV) can be obtained.<sup>19</sup>

PET imaging modality needs radiopharmaceuticals labeled with positron emitting radionuclides such as <sup>11</sup>C, <sup>15</sup>O, <sup>13</sup>N and <sup>18</sup>F which are produced by cyclotrons. On the other hand, some radioisotopes can be easily afforded from commercial generators (e.g. <sup>68</sup>Ga, <sup>44</sup>Sc, <sup>82</sup>Rb).

Radionuclide	Half-life	$\beta^+$ branching ratio (%)	Positron energy (MeV)	Production method
<sup>11</sup> C	20.4 min	99	0.97	<sup>14</sup> N(p, $\alpha$ ) <sup>11</sup> C
<sup>15</sup> O	2 min	100	1.70	<sup>15</sup> N(p, $\alpha$ ) <sup>15</sup> O
<sup>13</sup> N	10 min	100	1.19	<sup>16</sup> O(p,n) <sup>13</sup> N
<sup>18</sup> F	110 min	97	0.65	<sup>18</sup> O(p,n) <sup>18</sup> F
<sup>44</sup> Sc	3.97 h	94	1.47	<sup>44</sup> Ca(p,n) <sup>44</sup> Sc or <sup>44</sup> Ti/ <sup>44</sup> Sc generator
<sup>64</sup> Cu	12.7 h	18	0.65	<sup>64</sup> Ni(p,n) <sup>64</sup> Cu
<sup>68</sup> Ga	68 min	89	1.88	<sup>68</sup> Ge/ <sup>68</sup> Ga generator
<sup>82</sup> Rb	1.27 min	65	3.4	<sup>82</sup> Sr/ <sup>82</sup> Rb generator
<sup>89</sup> Zr	78.4 h	23	0.91	<sup>89</sup> Y(p,n) <sup>89</sup> Zr
<sup>124</sup> I	100.2 h	23	1.54	<sup>124</sup> Te(p,n) <sup>124</sup> I

**Table 2:** Some examples of PET radionuclides.<sup>20, 21</sup>

[<sup>18</sup>F]-FDG (Fluorodeoxyglucose), covering over 90% of PET clinical practices, has become the most used radiotracer worldwide.<sup>22</sup> FDG, radiopharmaceutical glucose analog, has an half-life of 110 minute and it is routinely used during screenings of brain metabolism.<sup>23</sup> Malignant tumors have an increased uptake of glucose due to the high number of specific membrane transporter proteins than normal tissues.<sup>24</sup> However, Fluorodeoxyglucose is not tumor specific so it is necessary to be aware of all false negative and false positive in tumor diagnoses.<sup>25</sup> This consideration requires the development of more specific targeting agents to identify more accurately the presence of cancers in human body.





#### Gallium-68

Gallium 68 is one of the earliest used PET radionuclide in clinical medicine (1963)<sup>26</sup>, about 15 years before FDG<sup>27</sup>.

The incoming of PETs radionuclide generators gave to hospital structures and research centers which do not have the availability of an in-house cyclotron production, the possibility to get

with a reasonable cost in a short time lapse, a fresh eluted radioisotope ready-to-use for radiolabeling reactions.<sup>28</sup> Specifically, <sup>68</sup>Ge/<sup>68</sup>Ga generators increase the interest in scientific communities due to particular advantages from the use of gallium:

- high positive branching (89%) and positron energy (1.88 MeV);
- <sup>68</sup>Ge/<sup>68</sup>Ga generators are manufactured under GMP (Good Manufacturing Practice) conditions;
- 270-day half-life of the parent <sup>68</sup>Ge allows the use of this generator efficiently up to 1 year or even more;
- <sup>68</sup>Ga half-life of 68 minutes, matches the pharmacokinetics of many peptides and other small targeting molecules with fast clearance and localization of the target.

	Eckert & Ziegler Cyclotron Co. Ltd.	Eckert & Ziegler IGG100 and IGG101 GMP; Pharm. Grade	I.D.B. Holland B.V.	Isotope Technologies Garching
				
Column matrix	TiO <sub>2</sub>	TiO <sub>2</sub>	SnO <sub>2</sub>	SiO <sub>2</sub> /organic
Eluent	0.1 M HCl	0.1 M HCl	0.6 M HCl	0.05 M HCl
<sup>68</sup> Ge breakthrough	<0.005%	<0.001%	~0.001%	<0.005%
Eluate volume	5 mL	5 mL	6 mL	4 mL
Chemical impurity	Ga: <1 µg/mCl Ni < 1µg/mCl	Fe: <10 µg/GBq Zn: <10 µg/GBq	<10 ppm (Ga, Ge, Zn, Ti, Sn, Fe, Al, Cu)	Only Zn from decay
Weight	11.7 kg	10 kg    14 kg	26 kg	16 kg

**Figure 1:** Examples of <sup>68</sup>Ge/<sup>68</sup>Ga generators.<sup>29</sup>

<sup>68</sup>Ge/<sup>68</sup>Ga generators have been improved in the last two decades, and they have been fully described in several reviews.<sup>30, 31</sup> Decristoforo et al. described a fully automatic synthesis for <sup>68</sup>Ga-labeled peptides with high radiochemical yields.<sup>32</sup> A huge number of excellent literature manuscripts have been published, in order to demonstrate the potential of Gallium-labeled biomolecules in nuclear medicine. Different distributors in Russia, USA and Europe increase the availability of these commercial generators using effective and convenient purification steps. Thanks to this enhancement of generators characteristics, <sup>68</sup>Ga has become as useful in PET as <sup>99m</sup>Tc proved for SPECT imaging.<sup>33</sup>

<sup>68</sup>Ga-labeled radiopeptides have been pre-clinically studied for the targeting of somatostatin<sup>34</sup>, bombesin<sup>35</sup> and melanocortin 1 receptors<sup>36</sup>. Pharmacokinetic proprieties of these peptide-based pharmaceuticals well match the short half-life of the radionuclide (68 min); <sup>68</sup>Ga-based peptides are increasing the recognition of new radiopharmaceutical classes, showing very fast blood clearance and fast target accumulation. Short half-life of <sup>68</sup>Ga allowed an improved dosimetry and repeat imaging, making these agents ideal for the use in clinic.

### 1.1.2 Single-photon emission computed tomography

Single-photon emission computed tomography, in combination with CT, is a clinical application particularly relevant in oncological and non-oncological applications. As in PET, the combination of dual-modality imaging techniques leads to improved specificity and sensitivity by matching of co-acquired functional and anatomical images.<sup>6</sup> One of the reasons of the incoming of SPECT/CT, was the need of more rapid acquisitions and accurate attenuation corrections as well as localization capabilities.<sup>37</sup> Despite spatial resolution of PET scan is 5 mm, while that of SPECT is about 10 mm<sup>38</sup>, low cost and fast acquisition time, makes SPECT a valid alternative, for example with labeled WBCs<sup>39</sup> (white blood cells) or when FDG-PET is not available during prediction of Alzheimer dementia.<sup>40</sup>

<sup>99m</sup>Tc, <sup>111</sup>In, <sup>67</sup>Ga and <sup>123</sup>I represent the main used SPECT radionuclides. <sup>99m</sup>Tc depicts the isotope with the largest area of application due to its decay characteristics, availability and ease of production (<sup>99</sup>Mo/<sup>99m</sup>Tc generators).<sup>41</sup>

Radionuclide	Half-life (h)	Principal photon emission energies (MeV)	Type of emission	Production method
<sup>123</sup> I	13.2	0.16	Electron capture	Cyclotron
<sup>99m</sup> Tc	6	0.14	Isomeric transition	Cyclotron or <sup>99</sup> Mo/ <sup>99m</sup> Tc generator
<sup>111</sup> In	67.9	0.17/0.25	Electron capture	Cyclotron
<sup>67</sup> Ga	78.3	0.09/0.19/0.30	Electron capture	Cyclotron
<sup>201</sup> Tl	73.1	0.17	Electron capture	Cyclotron

**Table 3:** Commonly used SPECT isotopes.

#### Technetium-99m

Technetium-99m is commonly used in bone scans (BS) as a valuable and versatile nuclear medicine tool. The examination is usually performed employing the radioisotope in diphosphonate complex form, either methylene diphosphonate forming <sup>99m</sup>Tc-MDP or hydroxydiphosphonate (HDP) forming <sup>99m</sup>Tc-HDP. <sup>99m</sup>Tc is one of the most used radionuclide because it is reasonable inexpensive and it has favorable characteristics for molecular imaging tools as good spatial resolution, an ideal photopeak of 140 KeV for gamma cameras, and it has a relatively short half-life (6 hours) which permits a satisfactory time for acquisition without excessive radiation dose to patients.<sup>42</sup>

Tc-99m is eluted from <sup>99</sup>Mo/<sup>99m</sup>Tc generator in its highest oxidation form (+7). It can be used for diagnostic examinations alone, but it is often used to label different organic and inorganic moieties. It is unreactive in its native oxidation form, and, for this reason, a reduction with a chemical reductant (+1), (+2), (+5), became necessary before use. Today, almost 80% of radiopharmaceuticals are based on <sup>99m</sup>Tc.<sup>43</sup>

### 1.1.3 Optical Imaging

Optical imaging (OI) and spectroscopy use non-ionizing radiations in visible and near-infrared (NIR) region (400-1500 nm). In this topic, natural or room light have been used as excitation source for chromophores (light absorbing molecules).<sup>44</sup> Different mechanisms are available for OI, among these, scattering, light absorption, fluorescence and bioluminescence.<sup>45</sup> Differently from high-energy rays, NIR photons are highly scattered in human tissue and they have approximately 1 mm of propagation.<sup>46</sup> Appropriate filters in front of the detectors can be used to obtain appropriate fluorescence measurements.<sup>45</sup>

Many organisms present different absorption proprieties: oxy- and deoxy-haemoglobin, lipids and waters as well as intrinsic fluorescence of several substances among which are elastin, keratin, phospholipids, tryptophan and metabolites NAD and FAD.<sup>47-49</sup> Furthermore, exogenous contrast could be added to the possibilities exploited by *in vivo* OI since a huge amount of absorbing and fluorescent forms of contrast are now available for *in vivo* use, and many of these can be targeted with biomolecular and biochemical targets<sup>50</sup>: organic and inorganic dyes<sup>51</sup>, quantum dots<sup>52</sup>, nanoparticles<sup>53</sup> and fluorescent proteins<sup>54</sup>.

The most significant factor that interfere with the improving of *in vivo* optical imaging is light scattering which involve a strong attenuation in all tissues with the consequence of limited ability to form high-resolution images.<sup>50</sup>

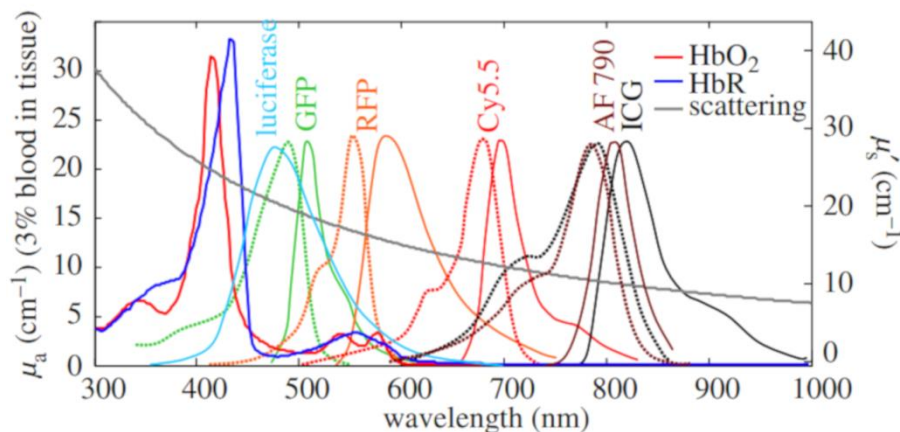


**Figure 2:** Autofluorescence, haemoglobin absorption spectra and scattering compared with common fluorescent dye spectra. Absorption spectra of oxy- and deoxy-haemoglobin (HbO<sub>2</sub> and HbR), luciferase emission, and excitation (dots) and emission (solid) spectra of common fluorophores (GFP/RFP = green/red fluorescent protein, AF790 = Alexa-Fluor 790, ICG = indocyanine green (Invitrogen)). Reduced scattering spectrum is approximated using:  $m_s = A/(b - \lambda)$ , where  $A = 1.14 \times 10^{-7} m(b-1)$  and  $b = 1.3$ <sup>50</sup>

## Image-guided surgery (Fluorescence)

Surgical precision is particularly important in neurosurgery where damage can result in permanent disabilities or death. Consequently, surgeons have fitted modern imaging techniques for the use during surgical operations.<sup>55</sup> Modern day image-guided surgery has been developed thanks to the integration of coordinate based systems with advanced imaging and personal computers.

Image-guided surgery can be defined as any invasive therapy carried out with image assistance on the treated organs. This term, includes generally endoscopy, fluoroscopy, intraoperative CT or MRI, ultrasound and stereotaxis.<sup>56</sup>

Several imaging systems are currently used worldwide. They all consists in a light source, spectrally-resolved, exciting a fluorophore within a turbid medium such as blood, bile or lymph. These fluorophores emits light which is imaged onto a charge-coupled device camera, taking care of filter out the excitation light.<sup>57, 58</sup>

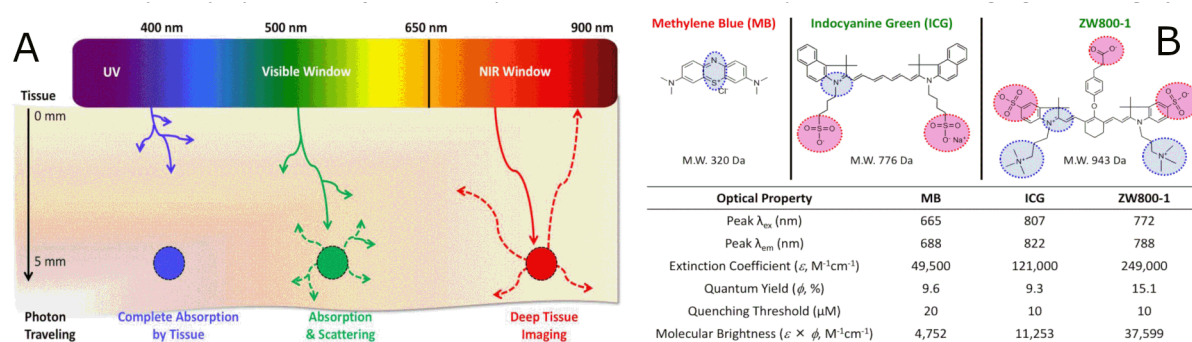


**Figure 3:** The NIR window and NIR fluorophores for image-guided surgery. (A) *In vivo* penetration of fluorescence light and photon travel according to wavelength<sup>59</sup>, and (B) chemical structures and optical proprieties of NIR fluorophores for Methylene Blue (MB), Indocyanine Green, and Zwitterionic Near-Infrared fluorophore-800 (ZW800). From Das et al.<sup>60</sup>

## 1.2 BIFUNCTIONAL CHELATING AGENTS

Bifunctional chelating agents (BFCAs) are chemical structures which contains two separate portions: a strong chelating moiety and a reactive functional group.<sup>61</sup>As shown in Table 1, molecular imaging may exploit different techniques based, for example, on microbubbles, fluorescent dyes, metal ions and radioactive isotopes.

Metals constitute the largest part of the periodic table of elements, most of them existing in several oxidation states and various isotopes of which many are radioactive.<sup>62</sup>Some metals can be employed alone, exploiting the related natural metabolism to diagnose or treat certain pathologies (e.g. Iodine-131). Differently, some radionuclides can be attached directly on natural and non-natural ligands, following, even in this case, an *in vivo* biodistribution by passive accumulation (e.g. <sup>18</sup>FDG). However, a consistent number of metals and radiometals, need to be complexed to chelators to prevent direct toxicity of the free form. Gadolinium is a toxic lanthanide heavy metal, because it has a similar size in comparison with calcium. This similarity may interfere with calcium-dependending biological processes.<sup>63</sup>

Each modality needs certain ions characteristics:

- paramagnetic ions like Gadolinium and Manganese are employed as contrast agents in MRI<sup>64-66</sup> ;
- beta emitting radionuclides like Gallium-68, Scandium-44 or Fluorine-18 are employed in PET<sup>30, 67, 68</sup>;
- gamma emitting radionuclides like Technetium-99m and indium-111 are employed in SPECT<sup>69, 70</sup>;

The most frequent method to label the metal of interest to molecular vectors occurs through BFCAs which contains, as mentioned before, two separate moieties both to functionalize the ligand with targeting molecules and to efficiently perform the metal's labelling. Different kinds of chelators can be used for this purpose. Polyamino polycarboxylic ligands are particularly efficient in this topic because of their high complex stabilities with different metal ions, which avoid *in vivo* release of the metal ion with consequences on biological processes.<sup>71</sup> Basically, BFCAs can be divided in two main groups: acyclic (e.g. EDTA, DTPA) and macrocyclic chelators (e.g. DOTA, NOTA, AAZTA).

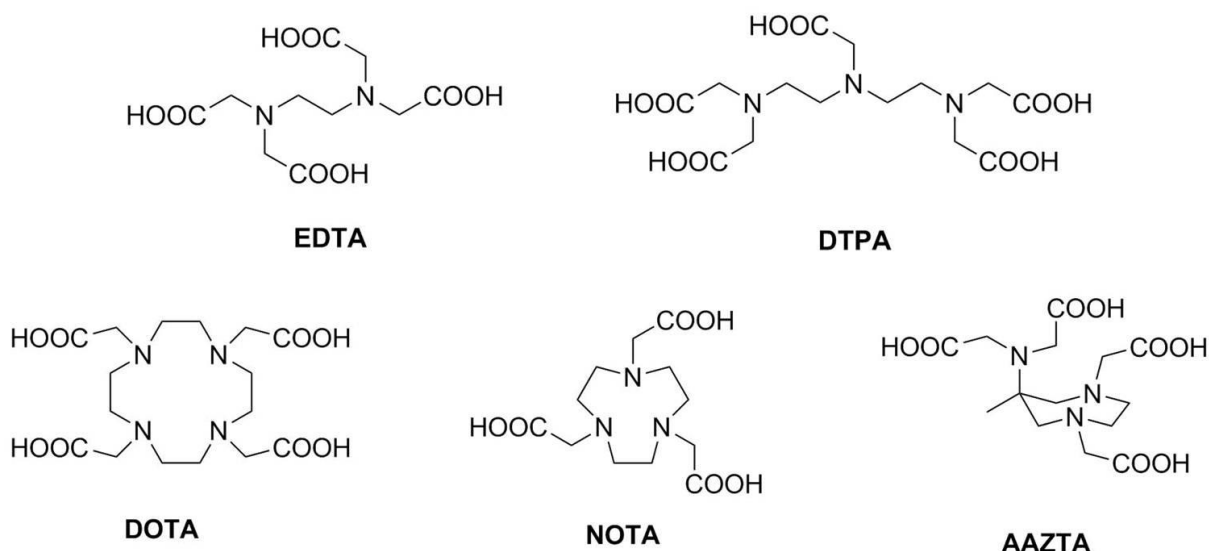


**Figure 4:** Chemical structure of some acyclic and macrocyclic chelators.

Usually, macrocyclic ligands complexes show higher thermodynamic stability but are kinetically more inert when complexed, requiring longer reaction times and/or higher temperatures. Acyclic ligands usually require mild conditions for labelling but they are more conducive to release the metal ion *in vivo* because of transmetallation by endogenous metal ions competition or transchelation by endogenous ligands.<sup>61,72</sup> The choice of the most suitable ligand is a fundamental point in the design of the final bioconjugate and depends both on the metal ion to be labelled and the vector to be attached.

A wide variety of functional chemical groups can be attached on the chelator portion in order to allow the conjugation with targeting molecules, which exhibit a variety of reactive residues. Carboxylic group (-COOH) is one of the most used group due to the huge amount of primary amine residues in potential targeting entities (e.g. lysine, Abs, peptides).<sup>73</sup> Reacting with primary amine residues, -COOH easily forms unreversible and biological accepted amide bonds.<sup>74</sup> Maleimide serves as specific and straightforward tool for selective reaction with thiols, present in cysteine residues, under mild conditions.<sup>75</sup> A particular attention on maleimide's chemistry is due to the fact that thiols, commonly present in peptides and proteins, reacts with maleimides approximately 1000 faster than amines at neutral pH<sup>76</sup>, giving a highly selective conjugation method.

Chelators design for metal coordination is limited only by imagination, providing a rich library of metal-based pharmaceuticals designed for any specific diagnostic and/or treatment disease.<sup>62</sup>



### 1.2.1 Acyclic chelators

DTPA (diethylenetriaminopentaacetic acid) and EDTA (ethylenediaminetetraacetic acid) represent two of the most widely used acyclic chelators, changing in number of donor atoms (see Fig.4). DTPA, probably the most used among these two linear chelators, has been synthesized for the first time by Frost in 1956.<sup>77</sup> The first approved MRI gadolinium based contrast agent (Magnevist®) is a DTPA complex. Later, DTPA-based chelators have been proposed for complexation of different radionuclides employed in nuclear medicine (e.g. <sup>111</sup>In, <sup>67-68</sup>Ga, <sup>99m</sup>Tc, <sup>90</sup>Y, <sup>212</sup>Bi).<sup>78-81</sup> The transformation of at least one carboxylic function of DTPA is a required condition to allow the use of this chelator as BFCA, affecting on the other hand the complex stability. The decreasing stability effect is due to the substitution of an anionic donor atom (carboxylate) with a non-ionic functional group (amide).<sup>82</sup> In the case of Gadolinium, the decreasing stability effect has been studied giving the conclusion that a significant release of the metal under physiological conditions cannot be considered negligible.<sup>83</sup> The simplest DTPA-based BFCA can be obtained by transformation of the chelator into a reactive mixed anhydride which may efficiently reacts with peptides or proteins.<sup>82, 84</sup> Unfortunately, this method gives also a small amount of bisanhydrides which cannot be avoided. To solve this inconvenience, partial and selective protections on carboxylic functions become necessary, building the tri-protected DTPA which allows a selective chemistry during anhydride conversion from carboxylic acids.<sup>85</sup>

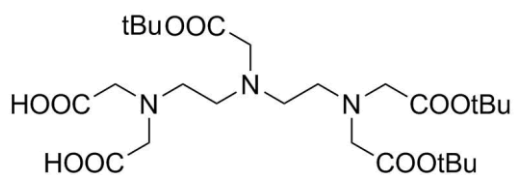


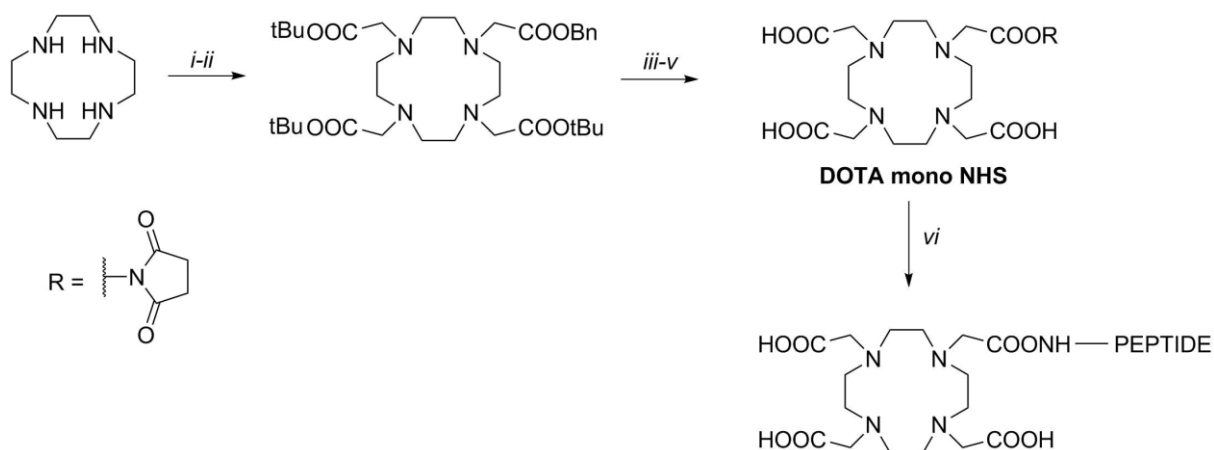
**Figure 5:** Tri-protected DTPA.

Tri-protected DTPA has been employed directly in solid phase synthesis for bioconjugation with somatostatin<sup>86</sup>, bombesin<sup>87</sup> and neurotensin<sup>88</sup> peptide analogues, with the final purpose of radiolabelling with <sup>111</sup>In. Tetra-protected DTPA overcomes the cross-linked or multimeric undesired products which can be obtained in solution chemistry.<sup>89, 90</sup> This would be just an example of the incredible versatility of such kind of chelators.

## 1.2.2 Macrocyclic chelators

DOTA (1,4,7,10-tetraazacyclododecane-1,4,7,10-tetraacetic acid) and NOTA (1,4,7-triazacyclononane-1,4,7-triacetic acid) based structures surely represent two of the most used cyclic chelators, offering a wide range of selective coordination properties in the realm of metal cations complexation. As mentioned in the introduction of this chapter, cyclic chelators overcome the problem of low kinetic stability of acyclic-based complexes.

DOTA, synthesized for the first time by Stetter and Frank in 1976<sup>91</sup>, became one of the best chelating agent for lanthanides, forming complexes with high thermodynamic stability and kinetic inertness.<sup>92, 93</sup> Analogously to DTPA, when a carboxylic donor group of DOTA is converted into a non-donor carboxamide, the stability constant decreases by two/three fold in the majority of metal complexes achieved with different ions. Differently from acyclic chelators, in the case of macrocyclic ones, the kinetic inertness remains almost the same.<sup>94</sup> A very simple strategy to obtain a single carboxylic group derivatization has been developed as in the case of DTPA.<sup>82</sup> Activated esters can be also easily obtained *in situ* in presence of EDC (1-Ethyl-3-(3-dimethylaminopropyl)carbodiimide) and NHS (N-Hydroxysuccinimide), to be subsequently conjugated to different proteins in neutral buffer, adding, when it is required, a co-solvent.<sup>95-97</sup> This is a very straightforward method to conjugate DOTA with good yields under mild conditions. Nevertheless, this approach presents some inconvenience: DOTA-NHS has to be used in excess to statistically reduce cross-linking due to activation of more than one carboxylic arm; doubly substituted DOTA-conjugates cannot be totally avoided even in solid phase synthesis; functionalization results to be unpredictable because of the high hydrolysis susceptibility of the ester groups.<sup>98</sup> To avoid these problems, DOTA mono NHS has been synthesized adopting a protection-deprotection approach, passing through DOTA tris *tert*-butyl ester.<sup>99</sup>

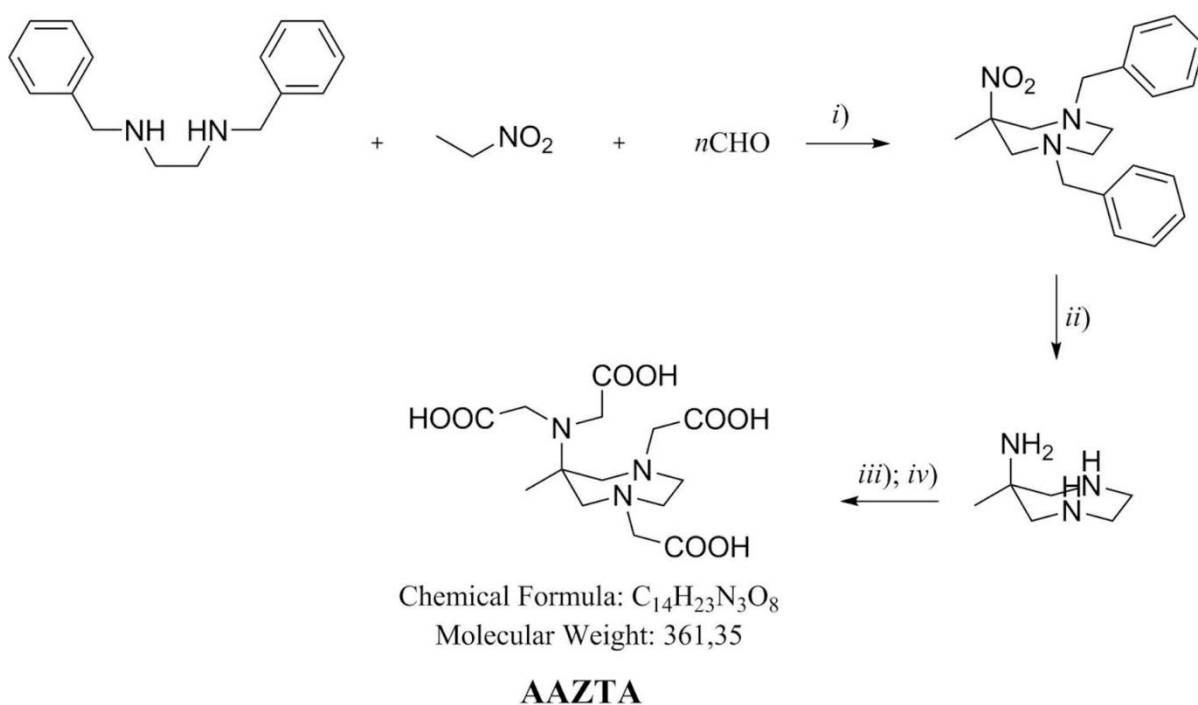


**Scheme 1:** Synthesis of DOTA mono NHS and amide bond formation with peptides: *i*)  $\text{BrCH}_2\text{COOBn}$ , *ii*)  $\text{BrCH}_2\text{COOtBu}$ , *iii*)  $\text{H}_2$ , Pd/C, *iv*) NHS, EDC, *v*) TFA, *vi*) PEPTIDE-NH<sub>2</sub>. Adapted from Lattuada et al.<sup>61</sup>

Apart being one of the first choice chelator for lanthanide's metal complexation, DOTA forms high stable complexes with a significant range of trivalent (e.g. <sup>68</sup>Ga, <sup>90</sup>Y and <sup>111</sup>In) and divalent (e.g. <sup>64</sup>Cu) radioisotopes opening a new scenario over diagnosis and therapy in the field on nuclear medicine.<sup>30, 68, 100</sup>

### 1.2.3 AAZTA

1,4-Bis(hydroxycarbonylmethyl)-6-[bis(hydroxycarbonylmethyl)]amino-6-methylperhydro-1,4-diazepine, namely AAZTA, is an heptadentate pseudo-macrocyclic chelator synthesized for the first time by Aime et al.<sup>101</sup> The simplicity of the synthesis pathway and the corresponding gadolinium (III) chelate potentiometric and relaxometric behaviour, made AAZTA a good candidate to obtain novel MRI CAs (contrast agents).<sup>94</sup> Several studies have been carried out in order to evaluate the influence of each parameter on relaxivity and *in vitro/vivo* stability of such complexes. Later, scientific interest moved to different metals, discovering several AAZTA-metal complexations (e.g. Mn, Eu, Yb)<sup>102, 103</sup>. The increase of nuclear medicine studies towards radiolabelling reactions with different chelators (DOTA, NOTA, NODAGA), moves scientific community attention on this simple and versatile chelator, describing numerous advantages related to beta emitting radionuclides complexation, such as <sup>68</sup>Ga and <sup>44</sup>Sc.<sup>104, 105</sup> AAZTA synthesis consists in 4 step, starting from 2-nitroethane, with a 48% overall yield (Scheme 2).



**Scheme 2:** Synthesis of AAZTA: *i)*  $\Delta$ , EtOH; *ii)* Pd/C,  $H_2$ , MeOH/ $H_2O$ ; *iii)*  $BrCH_2COOtBu$ ,  $K_2CO_3$ ,  $CH_3CN$ ; *iv)* TFA.

The simplest version of this chelator can be realized starting from nitroethane that reacts with *N,N'*-dibenzyl-diethyl-diamine (DBED) in presence of paraformaldehyde (PFA) through a Nitro-Mannich reaction. After the formation of the diazepine ring, nitro and benzyl groups have been removed under hydrogen atmosphere in presence of Pd/C metal catalyst. After that, the *N*-alkylation of all primary and secondary amines, a subsequent cleavage of all *t*Bu protective groups with TFA, give AAZTA. Specifically, this chelator cannot be functionalized with other scaffolds: in these terms, we can say that this native AAZTA chelator is unspecific.

Many manuscripts have been published in the last 15 years (Fig. 6), increasing significantly the number of available AAZTA bifunctional derivatives.<sup>103, 106-109</sup>

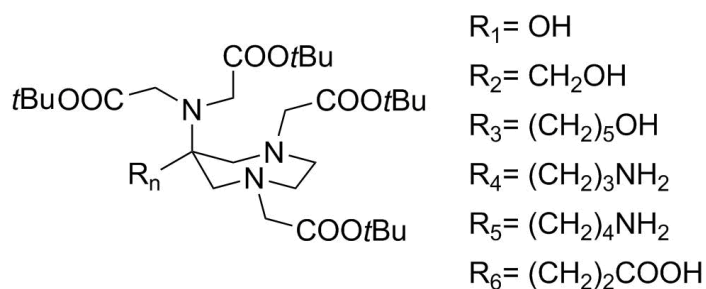
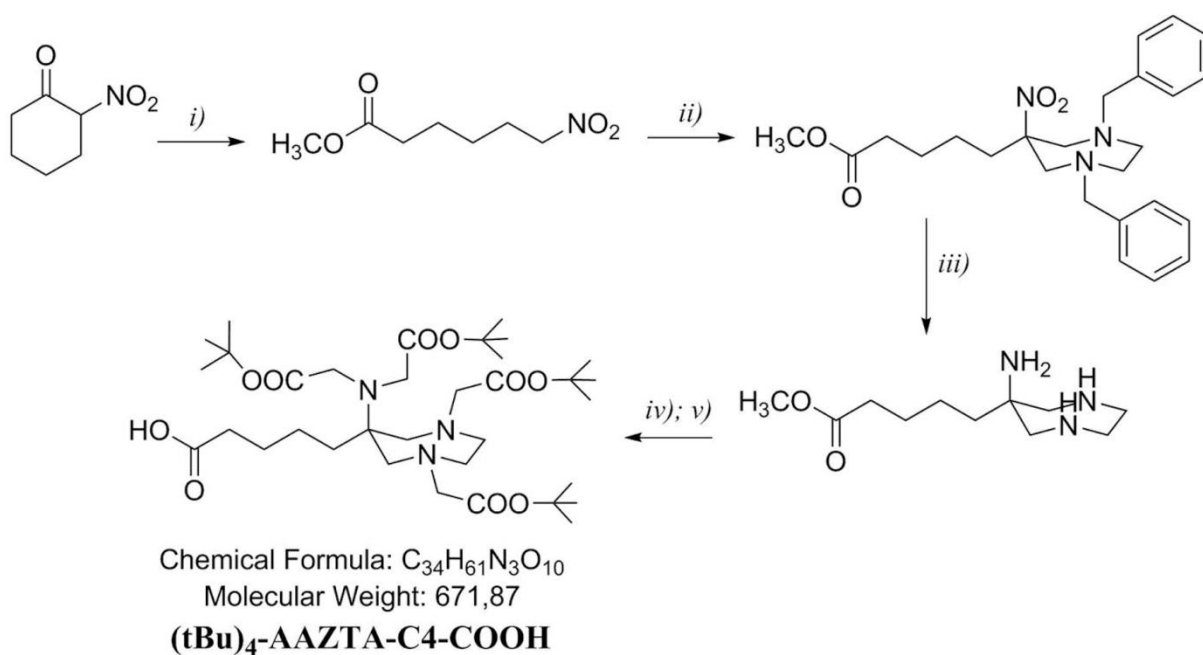


**Figure 6:** Some examples of AAZTA based derivatives

The most used derivative during this thesis project was  $(t\text{Bu})_4\text{-AAZTA-C4-COOH}$  (Scheme 3)<sup>110</sup>. The synthesis scheme 3 shows how procedure has some differences in comparison with AAZTA (Scheme 2)<sup>101</sup>. The main difference is the building block: 2-nitroethane for AAZTA and 6-nitrohexanoic acid methyl ester (synthesized from 2-nitrocyclohexanone following Ballini et al. protocol<sup>111</sup>) for  $(t\text{Bu})_4\text{-AAZTA-C4-COOH}$ .



**Scheme 3:** Synthesis of  $(t\text{Bu})_4\text{-AAZTA-C4-COOH}$ : *i)* Amberlyst A21, MeOH; *ii)* DBED, PFA,  $\Delta$ , EtOH; *iii)* Pd/C,  $\text{H}_2$ , MeOH; *iv); v)* BrCH<sub>2</sub>COOtBu, K<sub>2</sub>CO<sub>3</sub>, Na<sub>2</sub>SO<sub>4</sub>,  $\Delta$ , CH<sub>3</sub>CN; *v)* LiOH, TFA/H<sub>2</sub>O.

In comparison with unfunctionalized AAZTA chelator,  $(t\text{Bu})_4\text{-AAZTA-C4-COOH}$  and other AAZTA derivative examples shown in Fig. 6, can be functionalized with peptides, proteins, antibodies or other biomolecules to give a targeting molecule that, after a complexation with different metal/radiometal gives a targeting contrast agent.

During this three years PhD research project, a novel library of AAZTA derivatives have been synthesized.

## AAZTA complexation properties<sup>112</sup>

In the previous paragraphs, different chelators have been introduced, describing the potential of such chemical structures in the field of complexation with metal ions. The consistent amount of BFCAs, which can be readapted in order to get the best solution in the development of contrast agents, have been described. In this paragraph, a more detailed AAZTA labelling characteristics will be considered, paying a particular attention on gallium, which has been used for the chelation of the final products synthesized during this PhD project.

As incredible as useful contribute in this terms has been given by Baranyai and coworkers, carrying out equilibrium, kinetic and structural studies of AAZTA complexes with  $\text{Ga}^{3+}$ ,  $\text{In}^{3+}$  and  $\text{Cu}^{2+}$ .<sup>112</sup> It is already known how gallium and indium form stable complexes with carboxylates, hydroxamate, phenolate and amine included in numerous ligands which have been thoroughly studied so far.<sup>113-115</sup> Till now, well-known macrocyclic polyamino-polycarboxylic acid based complexes as NOTA<sup>116, 117</sup> and DOTA<sup>118</sup> (Fig. 4) are mostly used in nuclear medicine *in vivo* applications. NOTA forms highly stable complexes with gallium ( $\log K_{\text{Ga}}(\text{NOTA}) = 31.0$ )<sup>119</sup>. However, despite its significantly lower stability constants ( $\log K_{\text{Ga}}(\text{DOTA}) = 26.05$ )<sup>120, 121</sup>, bioconjugation studies are usually achieved on DOTA derivatives due to the fully availability to the corresponding bifunctional compounds. Stability constant related to  $\text{Ga}^{3+}$ -AAZTA complex, results to be 22.18, showing a similar value in comparison with DTPA ( $\log K_{\text{Ga}}(\text{DTPA}) = 24.3$ )<sup>122</sup>. To obtain the stability data, pH-potentiometric titrations and  $^1\text{H}$ - $^{71}\text{Ga}$  NMR studies in the pH range between 1.7 and 12 have been performed by Baranyai et al. I consider more than appropriate to report the graph showing the trend of  $\text{Ga}^{3+}$ -AAZTA complexation in the pH selected range (Fig. 7).

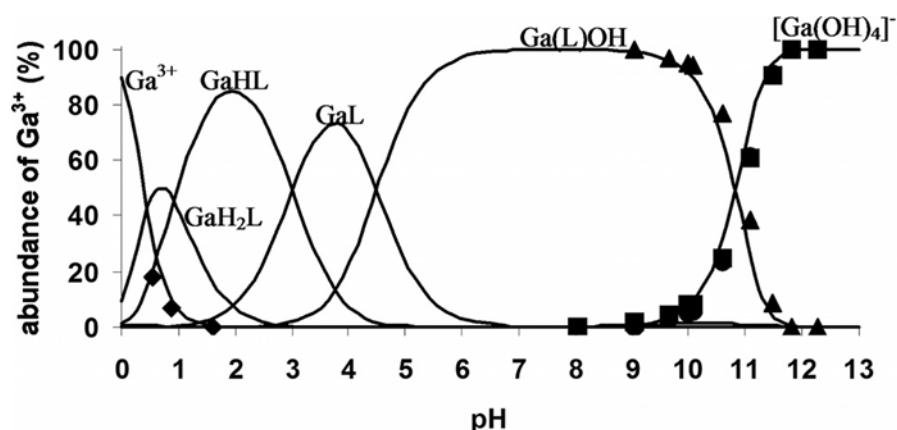


**Figure 7:** Percentage of the  $\text{Ga}^{3+}_{\text{aq}}$  ( $\blacklozenge$ ),  $[\text{Ga}(\text{AAZTA})\text{OH}]$  ( $\blacktriangle$ ), free AAZTA (HL and L) ( $\bullet$ ) and  $[\text{Ga}(\text{OH})_4]^-$  ( $\blacksquare$ ) species calculated from the  $^1\text{H}$  and  $^{71}\text{Ga}$  NMR spectra of the  $\text{Ga}^{3+}$ -AAZTA system. The species distribution was calculated from the equilibrium data obtained by pH-potentiometric titration.  $[\text{Ga}^{3+}] = [\text{AAZTA}] = 0.023 \text{ M}$ ,  $0.1 \text{ M KCl}$ ,  $25 \text{ }^\circ\text{C}$ .

From Baranyai et al.

The complexation process begins at a very low pH value, reaching the complete formation of protonated  $\text{GaH}(\text{AAZTA})$  complex specie at pH around 1.5. Considering the trend of  $\text{Ga}$ -AAZTA species formation, we can define how the graph clearly highlights pH around 4 as the best labeling condition for  $\text{Ga}^{3+}$ -AAZTA reaching almost 80% of  $\text{Ga}(\text{AAZTA})$  specie at this value. To reinforce this conclusion, it is equally appropriate to report  $^1\text{H}$ -NMR data behavior in function of the pH (Fig. 8).

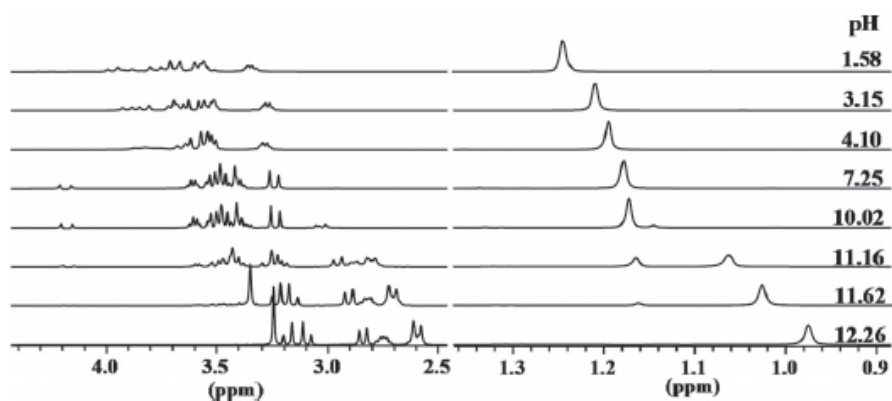


**Figure 8:**  $^1\text{H-NMR}$  spectra of the  $\text{Ga}^{3+}$ -AAZTA system as a function of pH.  $[\text{Ga}^{3+}] = [\text{AAZTA}] = 0.023 \text{ m}$ ,  $0.1 \text{ m KCl}$ ,  $400 \text{ MHz}$ ,  $25 \text{ }^\circ\text{C}$ . From Baranyai et al.

At  $\text{pH} = 4.0$ , the  $^1\text{H-NMR}$  spectrum of  $\text{Ga}(\text{AAZTA})$  contains several broad multiplets which can be justified with the formation of the relatively rigid coordination cage achieved by three nitrogen atoms and three carboxylate groups (one carboxy group is free) of AAZTA.

After appropriate evaluations on complexation stability, it was important to estimate the kinetic inertness of such complex, in order to understand if  $\text{Ga}^{3+}$ -AAZTA remains stable without showing significant decomplexation rate under physiological conditions. The endogenous metal ions that compete with  $\text{Ga}^{3+}$  in the blood plasma are first of all  $\text{Ca}^{2+}$ ,  $\text{Zn}^{2+}$  and  $\text{Cu}^{2+}$ . Considering that at physiological pH the predominant specie is  $\text{Ga}(\text{AAZTA})\text{OH}$ , it was possible to identify by Baranyai the kinetic inertness of the complex at  $\text{pH} 7.5$  and at  $\text{Ca}^{2+}$ ,  $\text{Cu}^{2+}$  and  $\text{Zn}^{2+}$  concentrations similar to those found in plasma.<sup>123</sup> Without going in more specific details, under such conditions, it was possible to calculate the dissociation rate of  $\text{Ga}(\text{AAZTA})\text{OH}$ , which results 20-fold slower than the rate of radioactive decay of  $^{68}\text{Ga}$  ( $t_{1/2}=67.71 \text{ min}$ ).

Despite the values of stability constant and kinetic inertness of  $\text{Ga}(\text{NOTA})$ ,  $\text{Ga}(\text{DOTA})$  and their derivatives result higher than those of  $\text{Ga}(\text{AAZTA})$ , AAZTA could be considered a good alternative for gallium labelling because of its high conditional stability, very fast formation and relatively slow decomplexation rate of  $\text{Ga}(\text{AAZTA})\text{OH}$ .

## 1.3 BIOCONJUGATION

Pharmaceuticals have been largely represented by small molecules; however, biomolecules like proteins and peptides have recently become important competitors. The enormous potential of these scaffolds have been raised up in the last decades because of the opportunity to improve pharmacokinetic proprieties *via* chemical modifications and/or functionalizations.<sup>124</sup>

Various methodologies have been adopted in this application field. Among these, the introduction of unnatural aminoacids, serves as an improvement of biodistribution properties and/or as increase of binding specificity. Chelators can be attached by bioconjugation reactions, in order to functionalize targeting molecules which can be subsequently labeled with metalor radiometal ions, useful in different imaging modalities (e.g. MRI, PET, SPECT).<sup>125</sup> Specifically, natural or unnatural residues can be modified to improve their biological efficacy in treatment and/or diagnosis of different oncological and non-oncological occurrences.

In this chapter, different classes of targeting agents will be considered, in order to give an overview of the bioconjugation scenario in the development of molecular imaging probes, focusing on site-specific chemistry.

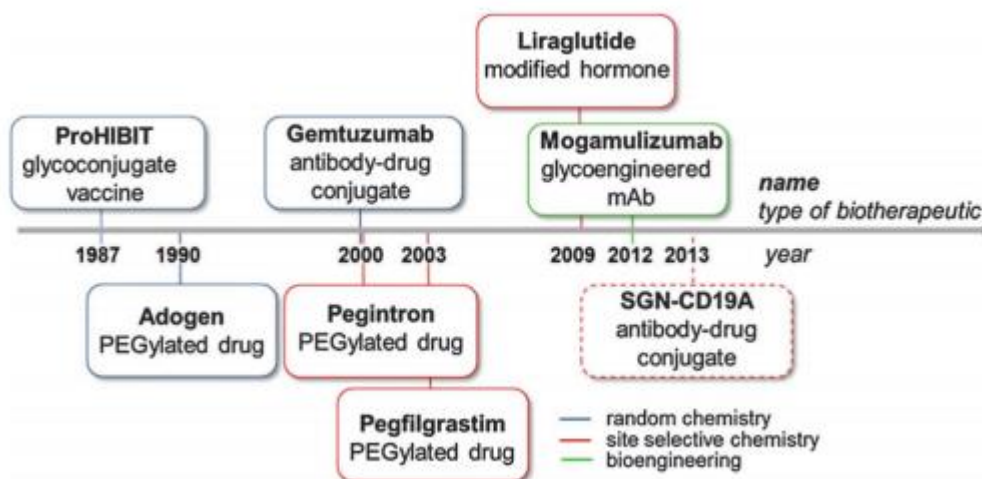


**Figure 9:** Important milestones achieved with bioconjugate medicines show how the scientific discoveries in protein modifications through chemical approaches and bioengineering over the last twenty years are influencing the pharma industry. Licensed biomedicines are indicated with a full frame line, products in clinical trials with a dotted frame line.<sup>126</sup>

### 1.3.1 Antibodies

Recently, a huge number of FDA (Food and Drug Administration) approved therapeutic antibodies (Abs) are prescribed during treatments for rheumatoid and psoriatic arthritis, cancer, psoriasis and Chron's disease.<sup>127</sup>

Antibodies have some advantages over small molecules because of their exceptional target specificity and long circulating half-life mediating by neonatal Fc receptors.<sup>128</sup> On the other hand, antibody drugs can give potential immunogenicity hard to predict, problematic expression and purification procedures, low therapeutic efficacy due to their difficult to penetrate solid tumors.<sup>129</sup>

Considerable interest in the development of chemical approaches for precise site-selective modification of Abs with chemotherapeutic drugs in order to increase treatment efficacy is currently in progress. Cysteine modification has gained popularity in Abs bioconjugation despite primary amine derivatization because of its limited abundance in native and synthesized proteins in comparison with lysine residues.<sup>130</sup>

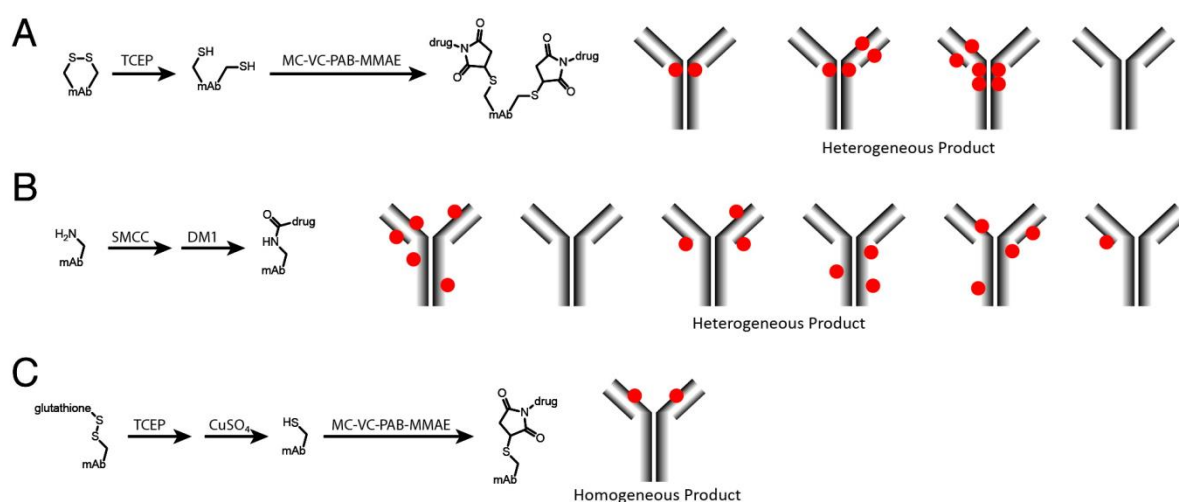


**Figure 10:** Schemes for non-specific (A and B) and site-specific (C) drug conjugation to an Antibody. (A) After reduction of the interchain disulfide bonds with TCEP or DTT, MC-VC-PAB-MMAE (maleimidocaproyl-valinecitrulline-p-amino-benzyloxycarbonyl-monomethylauristatin E) was conjugate to the resulting cysteine side chain thiols through maleimide functional group. The resulting conjugate was a heterogeneous mixture of Abs with different numbers of drugs connected to the eight cysteine residues involved in interchain disulfide bonds. (B) DM1 (mertansine) was attached to the Ab with a maleimidocyclohexanecarboxylate bifunctional linker (SMCC) through the Ab lysine side chain amines. The resulting conjugate was a heterogeneous mixture with zero to eight drugs per Ab attached to as many as 40 different lysine residues.<sup>131</sup> (C) Site directed mutagenesis was utilized to install one additional cysteine residue in each heavy chain. Over Ab expression this cysteine was found in a disulfide bond with glutathione. Reduction of all solvent exposed disulfide bonds followed by re-oxidation of the native disulfide bonds with CuSO<sub>4</sub> resulted in a single thiol on each heavy chain which could be modified with a maleimide-based drug such as MC-VC-PAB-MMAE. This gave a homogeneous product with exactly two drugs attached at the mutant cysteine sites. Adapted from Behrens et al.<sup>132</sup>









### 1.3.2 Non-Ig therapeutic proteins



Despite all disadvantages, antibodies are appealing tumor targeting agents. Non Immunoglobulin (Non-Ig) scaffold are, differently to Abs, single domain proteins which do not require post-translational modification and can directly be multimerize.<sup>133</sup> Proteins non-ig form based can be used to avoid the inconveniences related to Abs. These scaffolds are formed by fragments already present as natural substances in humans (e.g. Adnectins, DARPin)s<sup>134, 135</sup> or bacteria (e.g. Affibodies, Nanobodies)<sup>136, 137</sup> or designed *de novo* (Alphabodies).<sup>138</sup>

The imaging field of ImmunoPET combines the high affinity of Ab fragments with nuclear medicine, to improve diagnosis, staging and monitoring of diseases.<sup>20</sup> These scaffolds can be modified with polyethyleneglycol (PEG), obtaining longer half-life *in vivo*, and labeled for radionuclide therapy and diagnostic purposes.<sup>139</sup>

Affibodies and nanobodies have extremely low molecular weight and after appropriate functionalization with chelators, demonstrate to have higher tumor/organ ratio than antibody equivalent trastuzumab.<sup>139</sup>

Format	Composition	Valency	Approx. MW (kDa)	Typical Serum $t_{1/2}$	Clearance Route	Suggested Reference
 Intact IgG	$(V_H + V_L)_2$	Bivalent	150-160	1-3 weeks	Hepatic	Ogasawara et al., 2013
 F(ab') <sub>2</sub>	$(V_H C_H1 + V_L + C_L)_2$	Bivalent	110	8-10 h	Hepatic	Lütje et al., 2014
 Minibody	$(scFv + C_H3)_2$	Bivalent	75	5-10 h	Hepatic	Tavaré et al., 2014
 Fab	$V_H C_H1 + V_L + C_L$	Monovalent	50-55	12-20 h	Renal	Chakravarty et al., 2014
 Diabody	$(scFv)_2$	Bivalent	50	3-5 h	Renal	Tavaré et al., 2014b
 scFv	$V_H + V_L$	Monovalent	28	2-4 h	Renal	Kim et al., 2014
 Nanobody	$V_H H$ (Camelid)	Monovalent	12-15	30-60 m	Renal	Bannas et al., 2014
 Affibody	Z domain of protein A ( <i>S. aureus</i> )	Monovalent	7	30-60 m	Renal	Strand et al., 2014

**Figure 11:** Antibody fragments: summary of main properties of Abs, recombinant and enzymatic fragments and smaller scaffold. From Freise et al.<sup>140</sup>

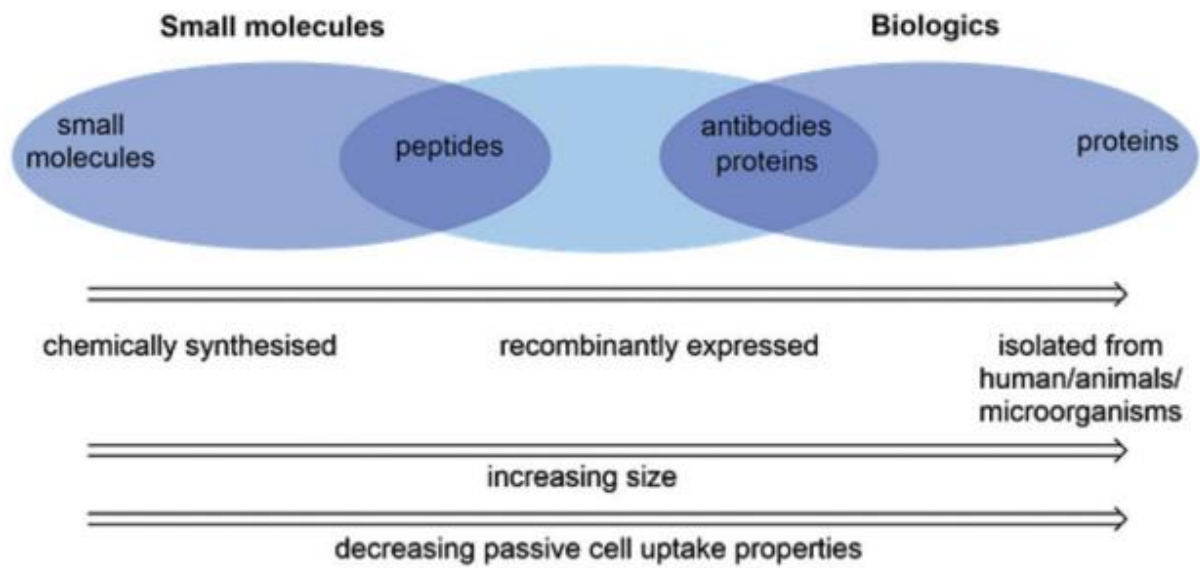


**Figure 12:** Characteristics of small molecules and biologics, with peptides and proteins falling in between. Note: the ability of peptides to enter cells is enabled by basic residues in their sequences.<sup>124</sup>

### 1.3.3 Peptides

Peptides can be situated between small molecules and biologics categories. Since most biological scaffolds are isolated from humans, animals and microorganisms, they are not so compliant to chemical modifications. On the contrary, peptides are chemically synthesized, allowing introduction of unnatural amino acids to improve specificity and biodistribution properties.<sup>126, 141</sup>

Theoretically, peptides are ideal pharmaceutical candidates as their structure and size give them the possibility to avoid protein-protein interactions (PPIs) more specifically than small molecules by mimicking those interactions.<sup>142-144</sup> Unfortunately, it is not always so simple because a peptide sequence is more likely as a random coil when is separated from its usual closing residues in the rest of the protein. Furthermore, the length required to cross a binding site within the cell is probably too long for the peptide to diffuse into the cell and it is not so probable for the peptide sequence to reach its biological target before being degraded by *in vivo* proteases. Small protein structures with the desired  $\alpha$ -helical strand supported by neighboring  $\alpha$ -helical or conformation stabilizations performed by chemical modifications, can be a good solution.<sup>124</sup>

Peptide stapling strategies induce covalent bond formation between two residues within a peptide sequence thought to be able to form  $\alpha$ -helix.<sup>145</sup>

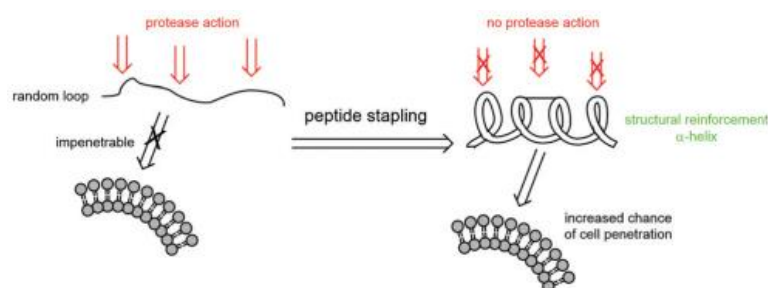


**Figure 13:** Structural reinforcement by stapling.<sup>145</sup>

If correct positions are chosen, chemical stapling will be successful, and the peptide forms a conformationally rigid  $\alpha$ -helix exhibiting improved properties as compared to the unstapled and unstructured form. As reported by Walesky et al., metathesis between olefins and non-natural olefinic-containing side chains efficiently staples *via* Grubb's catalysis.<sup>145</sup>

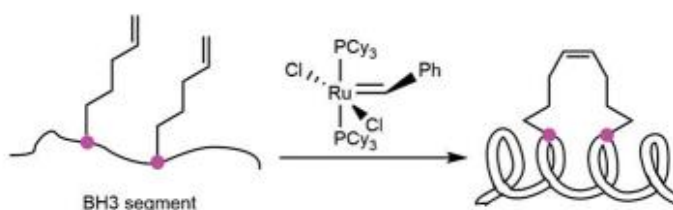


**Figure 14:** Stapling residues via ring-closing metathesis<sup>145</sup>

Several orthogonal reactions have been carried out for peptide stapling, among these CuAAC (copper(I)-catalyzed alkyne-azide cycloaddition)<sup>146</sup>, alkene-tetrazole cycloadditions<sup>147</sup>, disulfide bond formation<sup>148</sup>, oxime formation<sup>149</sup>, perfluoroarylation<sup>150</sup> and thioether formation<sup>151, 152</sup>.

## 1.4 PEPTIDE CHEMISTRY

Peptides have deeply influenced the development of the modern pharmaceutical industry and have contributed significantly to the advancement of biological and chemical science.<sup>153</sup>

Peptides represent a powerful class of medicines often used in multiple occurrences and constitutes indispensable, life-preserving pharmacology.<sup>154-156</sup> Being of limited molecular size and surely much smaller than most protein based, peptides enables the relationship of peptide chemical structure to function to be quickly interrogated by synthesis methods that have developed over the last fifty years.<sup>157, 158</sup> Over sixty peptide-based drugs are commercially available in the global market, with hundreds of these at various stages of commercial development and many more in preclinical phases. Technically all disease areas are included at some level with endocrinology, cancer, infectious and cardiovascular diseases being most prevalent.<sup>159</sup>

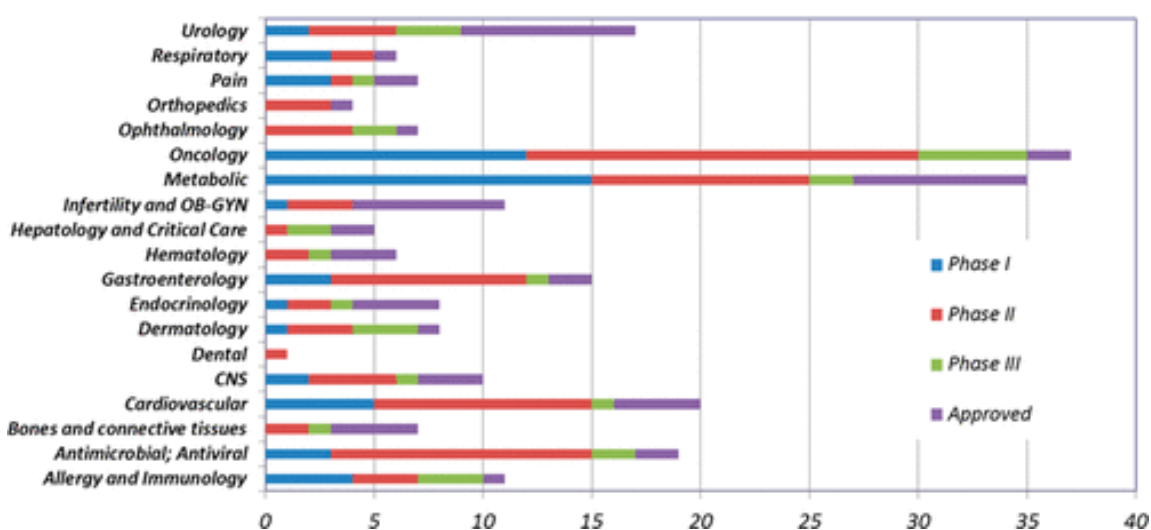


Figure 15: Number of peptide approved or in active development.<sup>153</sup>

As drug discovery is directed at small molecules, peptides research has evolved in the direction of multimode pharmacology, where single molecules are able to interact with multiple receptors in an additive and occasionally in a synergistic way to achieve superior efficacy usually at reduced administered dose.<sup>160-162</sup> Peptide and small molecule bioconjugates reinforce the advantages of peptide-based pharmacology with traditional medicinal chemistry.<sup>159</sup>

The two most used chemical techniques for peptide production are solid phase peptide synthesis (SPPS) and solution phase synthesis (SPS).

Classical SPS puts its bases on the coupling of single amino acids in solution media. The fragment condensation method has been used for the synthesis of long peptides. In this case, short fragments of the required peptide are first synthesized, then coupled together to form a long peptide. The main advantage of SPS for peptide chemical synthesis is that the intermediate products can be purified to afford the final desired peptide in high levels of purity.<sup>163, 164</sup> Oxytocin (neuromodulating nonapeptide and relevant hormone in sexual reproduction), porcine gastrin releasing peptide (hormone stimulating secretion of gastric acid), and human insulin (a 51 amino acid peptide hormone regulating carbohydrate metabolism in the body) are some examples of peptide hormones that were synthesized by

SPS. Although SPS can be scaled up in an easy and inexpensive manner, the long reaction time remains a disadvantage.

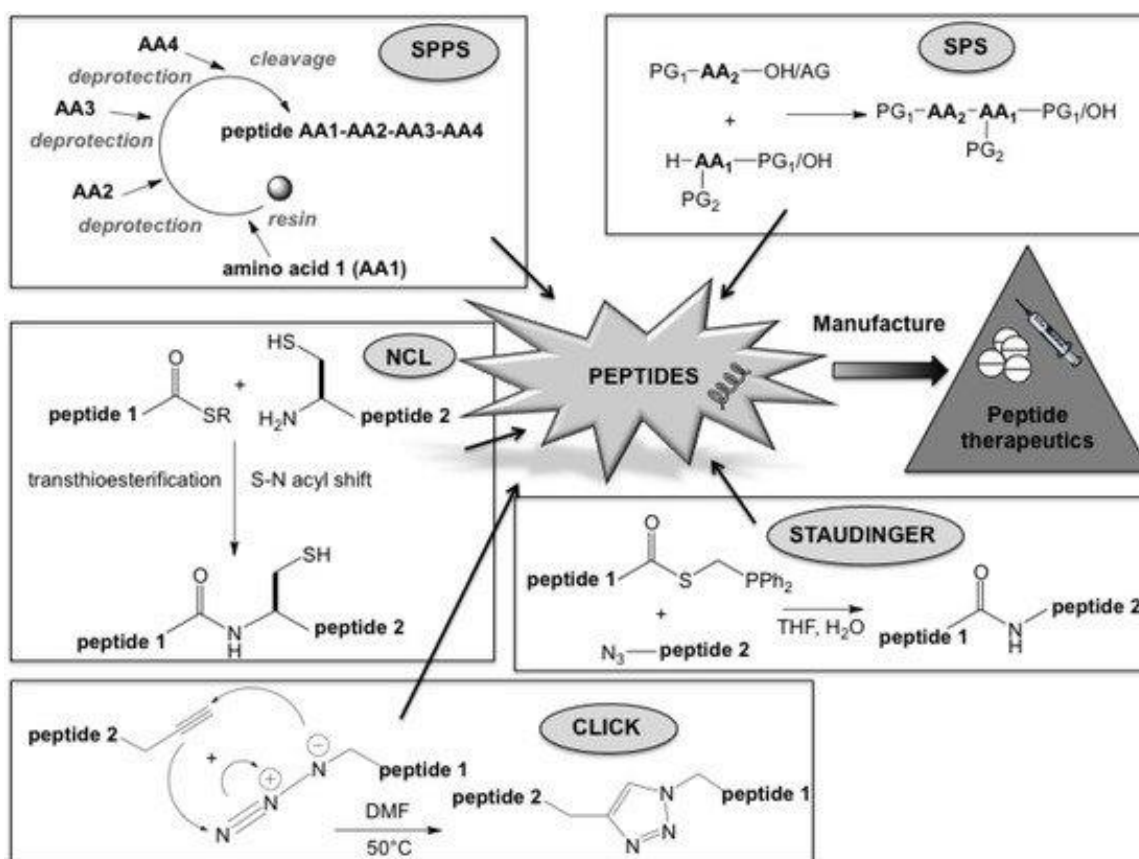


**Figure 16:** Schematic representation of peptide production.<sup>165</sup>

In the next paragraphs, different chemical approaches related to peptide synthesis will be shown to better understand the synthetic pathways adopted during the novel library synthesis of the compounds obtained during this thesis project.

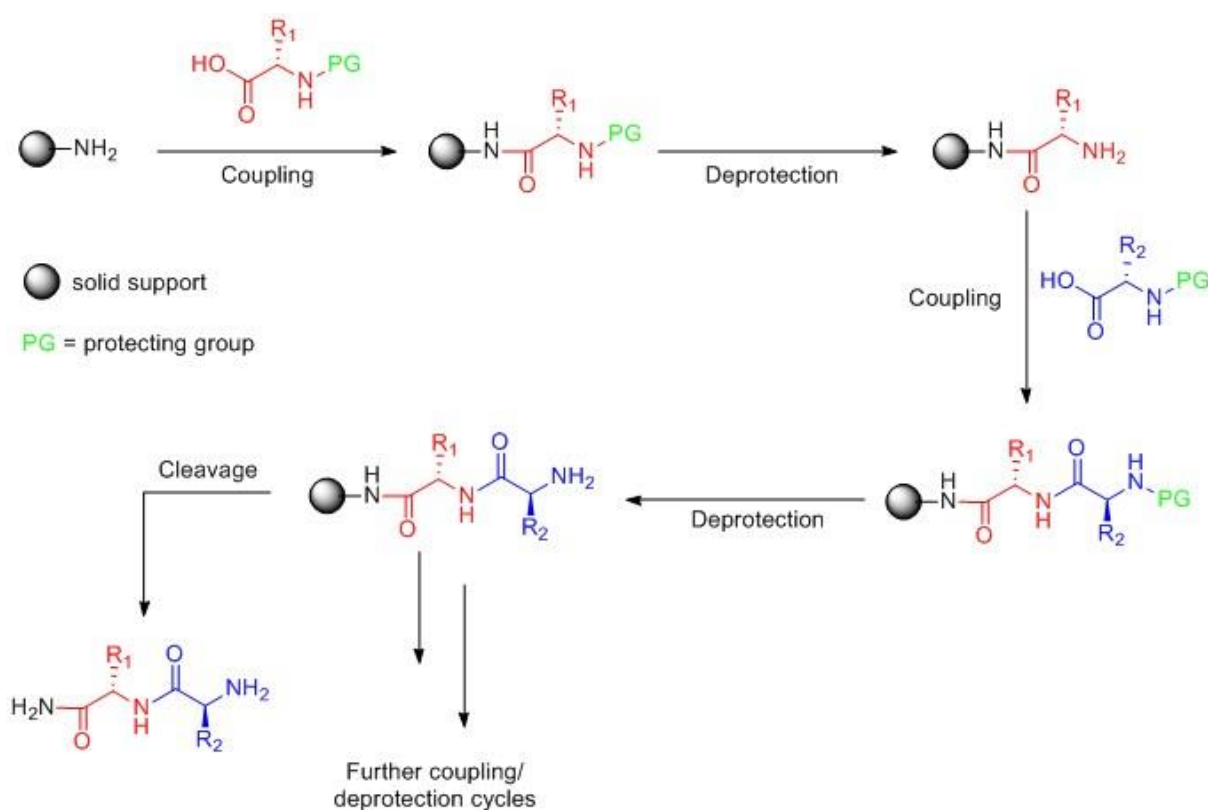
### 1.4.1 Solid Phase Peptide Synthesis

Introduced for the first time by Merrifield in 1963, Solid Phase Peptide Synthesis (SPPS) definitely changed the strategy of peptide synthesis and simplified the repetitive and tedious purification steps associated with solution chemistry.<sup>166</sup>

With the incredible advances reached with this new chemical approach, SPPS also permitted the development of automation phase synthesis. SPPS has become the method of choice for peptide synthesis even if sometimes, solution chemistry can be selected for larger production scales.

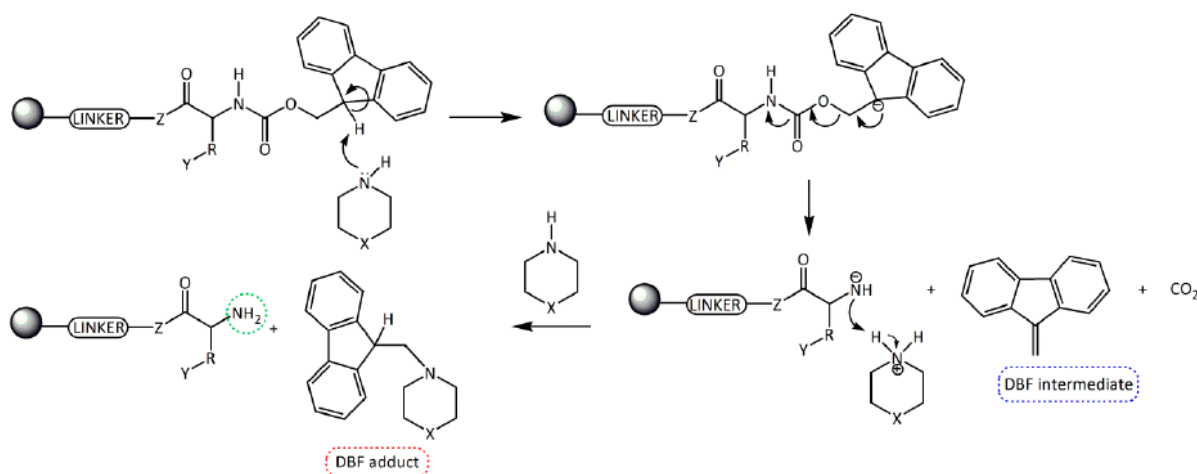
The use of a solid support to build peptide sequences, gave obvious advantages. Despite the high concentration and large excess of starting materials required for this methodology, all side products and excess of reagents can be washed out by simple filtration from the growing peptide anchored to the solid support. This can be considered the milestone of SPPS, because all purification steps that would be required in solution chemistry can be avoided, significantly improving the overall yield and time needed to obtain the product.

Compared to other chemical approaches, SPPS is simple, repetitive and the essential chemical steps, deprotection and coupling, alternated only by a washing step to remove excess reactants and by-products, can be achieved easily.<sup>166</sup>



Scheme 4: SPPS strategy.

SPPS can be historically divided into two subcategories following a Boc (t-butyloxycarbonyl) or Fmoc (fluorenylmethyloxycarbonyl chloride) chemistry. The majority of synthetic peptides are currently prepared by Fmoc solid-phase peptide synthesis.<sup>167</sup> Boc SPPS is now generally only used for particular applications. Nevertheless, the limited use of Boc chemistry is related to the use of anhydrous HF (hydrogen fluoride) or TFMSA (trifluoromethanesulfonic acid) and the use of TFA (trifluoroacetic acid) in each cycle for the removal of the protecting group.<sup>168</sup> At the beginning, the success of the Fmoc based chemistry was due to its availability by non-chemists as biologists realized they could prepare peptides in a short lack of time, suitable for antibody production using inexpensive instruments and avoid the use of strong acidic conditions<sup>169</sup>. Fmoc SPPS is of easy automation not just because there is no need for corrosive TFA in the deprotection cycles, but even because the deprotection of the Fmoc group releases a fluorene group with strong UV absorption properties that gives a useful indicator of synthesis achievement.<sup>170</sup> For peptide chemists, Fmoc approach provided a solution to the previous problems related to Boc method as the deprotection conditions were compatible with modified peptides, such as phosphorylated and glycosylated peptides and for peptide libraries.<sup>158</sup>



**Scheme 5:** Fmoc deprotection mechanism.<sup>171</sup>

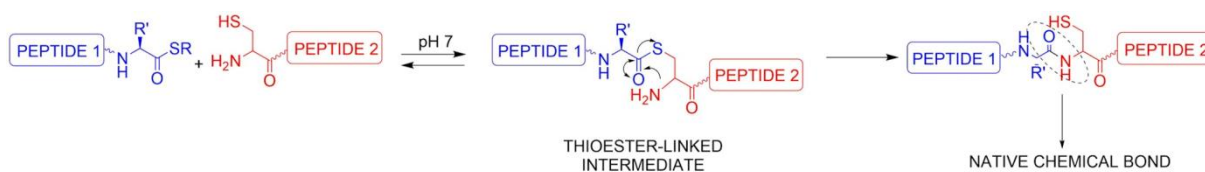
Nevertheless, SPPS has some limitations. The major limitations of SPPS included incomplete coupling and deprotection steps, accumulation of side products, and aggregation of the growing peptides.<sup>172, 173</sup> Microwave (MW)-assisted SPPS approach allows the improvement of the coupling efficiency during peptide synthesis, without any degradation of the solid support.<sup>172</sup> Fmoc deprotection and coupling reactions are not only accelerated with higher temperature, but also alternating electric field of the MW. Furthermore, during peptide elongation, MW can limit chain aggregation, allowing for easier access of the reagents to the solid phase reaction support and reducing the Fmoc deprotection and coupling reaction times.<sup>174</sup> Synthesis of proteins performed by SPPS was also not so feasible because the average length of a protein is about 250 amino acids.<sup>175</sup> To overcome SPPS limitations, innovative techniques for protein synthesis have been developed; chemical ligation has been one of the most successful.<sup>165</sup> The coupling between two peptide fragments, prior thiol capture strategy, was introduced by Kemp *et al.*<sup>176</sup> Other ligation methods have been developed, among these, native chemical ligation (NCL), expressed protein ligation (EPL), and

Staudinger ligation. In addition, the *O*-acyl isopeptide, also known as 'click' or 'switch' peptide, method is particularly useful for the chemical assembly of highly aggregation-prone polypeptides.<sup>177</sup>



### 1.4.2 Native Chemical Ligation

Native chemical ligation (NCL) has played a fundamental role in the revolution of peptide chemistry. NCL allows the coupling between two peptide fragments through a covalent peptide bond at the site of ligation.<sup>178</sup> As mentioned in the previous paragraph, NCL overcomes the limitations of SPPS by allowing chemists to synthesize peptides that are longer than 50 amino acids.<sup>179, 180</sup> Another relevant feature of NCL is the absence of racemization at the ligation's site. Studies carried out by Lu et al. demonstrated that the chemical ligation product had no racemization within a limit of less than 1% D-amino acids.<sup>181</sup> Regio- and chemoselectivity of this chemical approach made it very appealing for chemists' community. Ligation selectivity allows the reaction only in presence of two specific groups: a thioester and a N-Terminal cysteine. The high reaction selectivity improves tremendously the specificity of the reaction with very low possibility to obtain by-products.



**Scheme 6:** Native chemical ligation mechanism.

The selectivity of the reaction between a C-Terminal thioester and a N-Terminal cysteine enables to use totally unprotected peptide fragments. The reaction is carried out under mild aqueous conditions at neutral pH, with a denaturing agent, such as guanidine, to avoid the formation of secondary structural elements that would otherwise interfere with the transformation. The ligation proceeds through a trans-thioesterification step in which the nucleophilic thiol portion of the Cys residue attacks the carbonyl carbon of the thioester, extruding a thiol and forming a new intermolecular thioester intermediate. This intermediate then quickly rearranges *via* an S-N acyl shift, in which the terminal amine from the thiol fragment attacks the newly formed thioester to form a native amide bond, thus restoring the thiol side chain of Cys.<sup>182</sup> The presence of internal cysteine does not affect the reaction selectivity as no possible transposition could form the native peptide bond.<sup>183</sup>

## 1.5 BIOLOGICAL TARGETS

### 1.5.1 Prostate-specific membrane antigen (PSMA)

Prostate Cancer (PCa) is the leading cause of cancer death in men and it is the third most common cause of death in the world.<sup>184</sup> The standard diagnostic strategy of prostate cancer relies on the determination of the Prostate-Specific Antigen (PSA) in the blood, rectal exploration screening and biopsies. The clinical benefit of these diagnoses, however, is rather uncertain and the need for more specific imaging tools to view and identify early prostate cancer, appears necessary. New imaging agents, allowing more accurately and earlier detection of the disease, will allow better patient outcome and quality of life.

Prostate-specific membrane antigen (PSMA) is an extracellular hydrolase highly upregulated in metastatic and hormone-refractory prostate carcinomas.<sup>185</sup> PSMA is a type II membrane glycoprotein with an extensive extracellular domain (44–750 amino acids) and plays a significant role in prostate carcinogenesis and progression.<sup>186</sup>

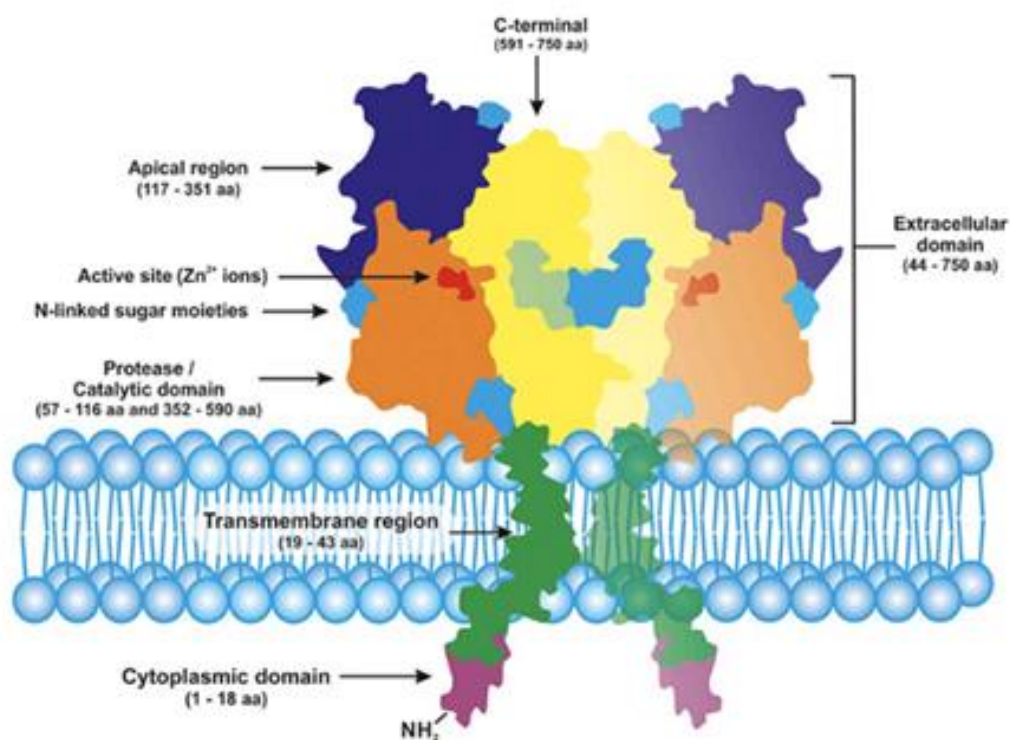


**Figure 17:** Schematic representation of PSMA/GCPII transmembrane protein (homodimer).<sup>187, 188</sup>

PSMA inhibitors fall into three families: phosphorous-based, thiol-based and urea-based. Urea-based inhibitors have a high affinity and specificity for PSMA and fast and efficient internalization in LNCaP cells.<sup>189</sup> Several small compounds for labelling PSMA have been developed and are currently being investigated as imaging probes for PET. The <sup>68</sup>Ga-labelled PSMA inhibitor Glu-NH-CO-NH-Lys(Ahx)-HBED\_CC (Urea-based) is the most widely studied agent.<sup>190</sup>

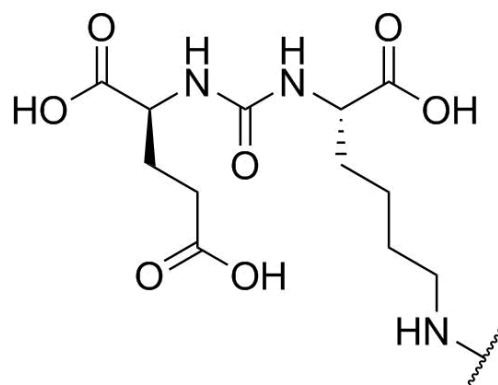


**Figure 18:** Chemical structure of the PSMA binding motif.

A series of novel Glu-urea-X heterodimers for targeting PSMA were successfully synthesized using the Glu-urea-Lys building block (PSMA binding motif).<sup>191</sup> Different PSMA-ligand derivatives were synthesized: the modification of the linker was designed to improve the binding potential and pharmacokinetics for theranostic applications. The results of Benesova et al. group of Uppsala held to further elucidate the structure-activity relationships (SAR) of the resulting PSMA inhibitors. Both *in vitro* and *in vivo* experiments of 18 synthesized PSMA inhibitor variants showed that systematic chemical modification of the linker has a significant impact on the tumor-targeting and pharmacokinetic properties.<sup>192</sup> The most promising spacer selected from Benesova et al. SAR study has been chosen by our research group to develop a new PSMA binding motif derivative imaging probe conjugated with AAZTA ligand to allow the subsequent complexation with PETs radionuclides.

## 1.5.2 Urokinase-type plasminogen activator receptor (uPAR)

The urokinase-type plasminogen activator receptor (uPAR) is a GPI (Glycosylphosphatidylinositol)-anchored cell membrane receptor, formed by three homologous domains (DI, DII, DIII).

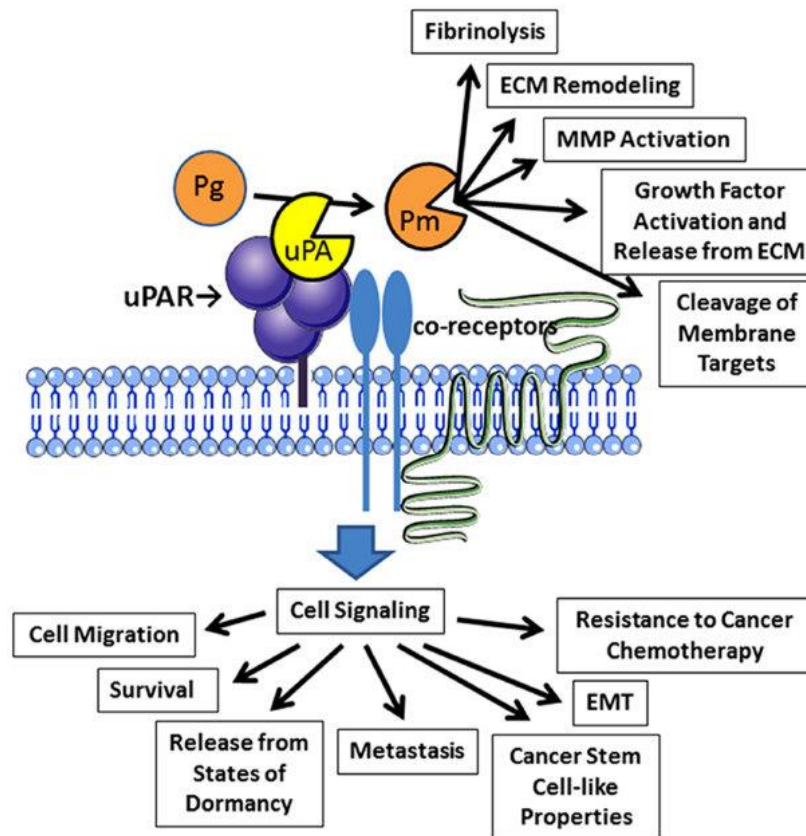


**Figure 19:** Activities of uPAR in cancer cells. Binding of uPA to uPAR promotes activation of plasminogen (Pg) to form plasmin (Pm). Plasmin then expresses diverse activities near the cell surface. uPAR also collaborates with a system of co-receptors to activate cell-signaling. Reported outcomes of uPAR-initiated cell-signaling in cancer cells are shown.<sup>193</sup>

It is mainly involved in urokinase (uPA) proteolytic activity, being responsible for degradation of extracellular matrix components, on the cell surface.<sup>194</sup> uPAR is reported to be over expressed in a wide number of human cancers, strictly correlated with a poor prognosis, early stage invasion and metastasis.<sup>195</sup> High levels of uPAR have been also found in primary tumors and serum of non-small cell lung (NSCLC)<sup>196, 197</sup> and colorectal cancer (CRC).<sup>198, 199</sup> uPAR is an adhesion receptor as it binds vitronectin (VN), an abundant component of temporary extracellular matrix.<sup>200</sup> Direct interaction between uPAR and VN is critical for causing changes morphology, migration and signaling of the cell<sup>201</sup> and seems to be a fundamental requirement for the induction of epithelial mesenchymal transition (EMT)<sup>202</sup>. Furthermore, uPAR regulates cellular adhesion, migration, proliferation and survival<sup>203</sup> through interactions with other transmembrane receptors (e.g. integrins, G-protein-coupled chemotaxis receptors and tyrosine kinase receptors).<sup>204</sup>

There are two main approaches in the search for peptide-based uPAR ligands. The first one exploits a random selection in a display library, whereas the other relies on synthesizing peptide derivatives based on uPA, the natural uPAR-binding ligand.<sup>205</sup> A family of 15-mer

linear peptide was synthesized as antagonists of uPA-uPAR interaction through the selection in a random phage-display library (laboratory technique for the study of protein–protein, protein–peptide, and protein–DNA interactions that uses bacteriophages).<sup>206</sup> The selected lead phage peptide was subjected to the maturation and stabilization affinity performed by combinatorial chemistry obtaining the resulting 9-mer core peptide AE105 (D-Cha-F-s-r-Y-L-W-S)<sup>207</sup> which resulted to be specific and with high-affinity binding to human uPAR ( $K_d \approx 0.4$  nM).

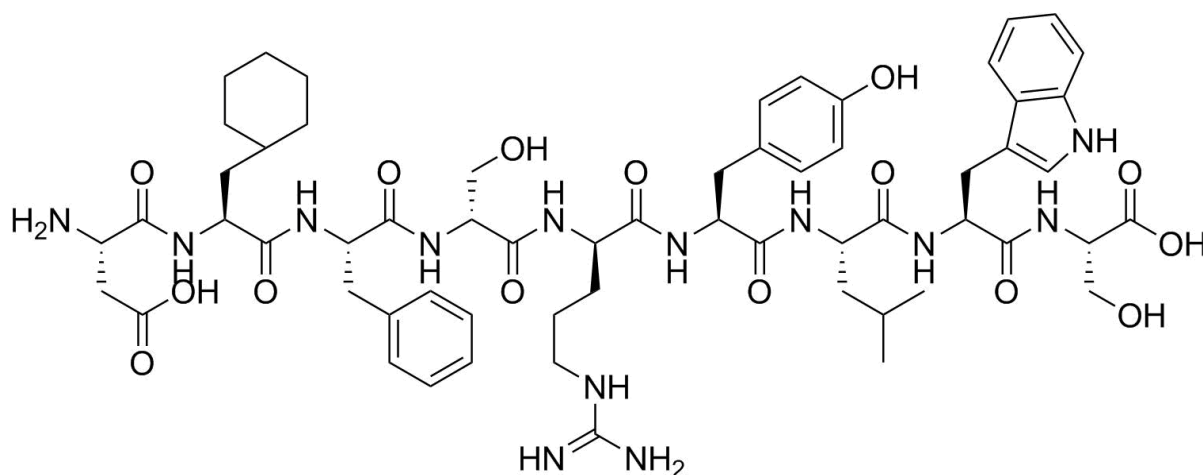


**Figure 20:** Chemical structure of AE105 peptide.

Later on, AE105 and its derivatives, AE120 [(D-Cha-F-s-r-Y-L-W-S)<sub>2</sub>-βA-K<sup>c</sup>] and AE170 (K-S-D-Cha-F-s-k-CHg-L-W-S-S-K) have been applied in a variety of experimental settings.<sup>208</sup> To date, most uPAR-targeted imaging and therapy studies are based on AE105 and its corresponding derivatives.

## References:

1. D. A. Mankoff, *J Nucl Med*, 2007, **48**, 18N, 21N.
2. T. E. Peterson and H. C. Manning, *J Nucl Med Technol*, 2009, **37**, 151-161.
3. M. A. Pysz, S. S. Gambhir and J. K. Willmann, *Clin Radiol*, 2010, **65**, 500-516.
4. C. S. Ng, X. Wang, S. C. Faria, E. Lin, C. Charnsangavej and N. M. Tannir, *AJR Am J Roentgenol*, 2010, **194**, 166-171.
5. D. J. Margolis, J. M. Hoffman, R. J. Herfkens, R. B. Jeffrey, A. Quon and S. S. Gambhir, *Radiology*, 2007, **245**, 333-356.
6. G. Mariani, L. Bruselli, T. Kuwert, E. E. Kim, A. Flotats, O. Israel, M. Dondi and N. Watanabe, *Eur J Nucl Med Mol Imaging*, 2010, **37**, 1959-1985.
7. M. G. Harisinghani, J. Barentsz, P. F. Hahn, W. M. Deserno, S. Tabatabaei, C. H. van de Kaa, J. de la Rosette and R. Weissleder, *N Engl J Med*, 2003, **348**, 2491-2499.
8. M. G. Harisinghani, K. S. Jhaveri, R. Weissleder, W. Schima, S. Saini, P. F. Hahn and P. R. Mueller, *Clin Radiol*, 2001, **56**, 714-725.
9. M. Al-Mallah and R. Y. Kwong, *Rev Cardiovasc Med*, 2009, **10**, 134-141.
10. I. K. Jang, G. J. Tearney, B. MacNeill, M. Takano, F. Moselewski, N. Iftima, M. Shishkov, S. Houser, H. T. Aretz, E. F. Halpern and B. E. Bouma, *Circulation*, 2005, **111**, 1551-1555.
11. T. D. Wang, S. Friedland, P. Sahbaie, R. Soetikno, P. L. Hsiung, J. T. Liu, J. M. Crawford and C. H. Contag, *Clin Gastroenterol Hepatol*, 2007, **5**, 1300-1305.
12. C. A. Lieber, S. K. Majumder, D. L. Ellis, D. D. Billheimer and A. Mahadevan-Jansen, *Lasers Surg Med*, 2008, **40**, 461-467.
13. S. R. Wilson, H. J. Jang, T. K. Kim, H. Iijima, N. Kamiyama and P. N. Burns, *AJR Am J Roentgenol*, 2008, **190**, 691-695.
14. G. B. Schnell, A. J. Kryski, L. Mann, T. J. Anderson and I. Belenkie, *Can J Cardiol*, 2007, **23**, 1043-1048.
15. N. Celli, S. Gaiani, F. Piscaglia, G. Zironi, V. Camaggi, S. Leoni, R. Righini and L. Bolondi, *Eur J Gastroenterol Hepatol*, 2007, **19**, 3-14.
16. A. K. Shukla and U. Kumar, *J Med Phys*, 2006, **31**, 13-21.
17. M. D. Farwell, D. A. Pryma and D. A. Mankoff, *Cancer*, 2014, **120**, 3433-3445.
18. G. K. von Schulthess, H. C. Steinert and T. F. Hany, *Radiology*, 2006, **238**, 405-422.
19. T. F. Hany, H. C. Steinert, G. W. Goerres, A. Buck and G. K. von Schulthess, *Radiology*, 2002, **225**, 575-581.
20. R. Fu, L. Carroll, G. Yahioğlu, E. O. Aboagye and P. W. Miller, *ChemMedChem*, 2018, **13**, 2466-2478.
21. S. K. Imam, *Cancer Biother Radiopharm*, 2005, **20**, 163-172.
22. S. Vallabhajosula, L. Solnes and B. Vallabhajosula, *Semin Nucl Med*, 2011, **41**, 246-264.
23. E. Lotan, K. P. Friedman, T. Davidson and T. M. Shepherd, *Isr Med Assoc J*, 2020, **22**, 178-184.
24. R. L. Wahl, *J Nucl Med*, 1996, **37**, 1038-1041.
25. N. M. Long and C. S. Smith, *Insights Imaging*, 2011, **2**, 679-698.
26. H. O. Anger and A. Gottschalk, *J Nucl Med*, 1963, **4**, 326-330.
27. T. Ido, C. Wan, V. Casella, J. Fowler, A. Wolf, M. Reivich and D. Kuhl, *J Labeled Compounds Radiopharm*, 1978, 174-183.
28. W. A. Breeman and A. M. Verbruggen, *Eur J Nucl Med Mol Imaging*, 2007, **34**, 978-981.
29. I. Velikyan, *Molecules*, 2015, **20**, 12913-12943.
30. M. Fani, J. P. André and H. R. Maecke, *Contrast Media Mol Imaging*, 2008, **3**, 67-77.
31. M. Asti, G. De Pietri, A. Fraternali, E. Grassi, R. Sghedoni, F. Fioroni, F. Roesch, A. Versari and D. Salvo, *Nucl Med Biol*, 2008, **35**, 721-724.
32. C. Decristoforo, R. Knopp, E. von Guggenberg, M. Rupprich, T. Dreger, A. Hess, I. Virgolini and R. Haubner, *Nucl Med Commun*, 2007, **28**, 870-875.
33. S. R. Banerjee and M. G. Pomper, *Appl Radiat Isot*, 2013, **76**, 2-13.

34. S. Froidevaux, E. Hintermann, M. Török, H. R. Mäcke, C. Beglinger and A. N. Eberle, *Cancer Res*, 1999, **59**, 3652-3657.
35. J. Schuhmacher, H. Zhang, J. Doll, H. R. Mäcke, R. Matys, H. Hauser, M. Henze, U. Haberkorn and M. Eisenhut, *J Nucl Med*, 2005, **46**, 691-699.
36. S. Froidevaux, M. Calame-Christe, J. Schuhmacher, H. Tanner, R. Saffrich, M. Henze and A. N. Eberle, *J Nucl Med*, 2004, **45**, 116-123.
37. M. Ljungberg and P. H. Pretorius, *Br J Radiol*, 2018, **91**, 20160402.
38. B. Palumbo, *Nucl Med Commun*, 2008, **29**, 730-735.
39. L. Burrioni, C. D'Alessandria and A. Signore, *J Nucl Med*, 2007, **48**, 1227-1229.
40. C. A. Sanchez-Catasus, G. N. Stormezand, P. J. van Laar, P. P. De Deyn, M. A. Sanchez and R. A. Dierckx, *Curr Alzheimer Res*, 2017, **14**, 127-142.
41. S. L. Pimlott and A. Sutherland, *Chem Soc Rev*, 2011, **40**, 149-162.
42. C. Adams and K. Banks, *Bone Scan*, StatPearls, 2019.
43. D. D. Dokić, *Med Pregl*, 2005, **58**, 180-184.
44. J. Culver, W. Akers and S. Achilefu, *J Nucl Med*, 2008, **49**, 169-172.
45. V. Ntziachristos, J. Ripoll, L. V. Wang and R. Weissleder, *Nat Biotechnol*, 2005, **23**, 313-320.
46. M. S. Patterson, B. Chance and B. C. Wilson, *Appl Opt*, 1989, **28**, 2331-2336.
47. A. E. Cerussi, A. J. Berger, F. Bevilacqua, N. Shah, D. Jakubowski, J. Butler, R. F. Holcombe and B. J. Tromberg, *Acad Radiol*, 2001, **8**, 211-218.
48. W. R. Zipfel, R. M. Williams, R. Christie, A. Y. Nikitin, B. T. Hyman and W. W. Webb, *Proc Natl Acad Sci U S A*, 2003, **100**, 7075-7080.
49. E. M. Hillman, *J Biomed Opt*, 2007, **12**, 051402.
50. E. M. Hillman, C. B. Amoozegar, T. Wang, A. F. McCaslin, M. B. Bouchard, J. Mansfield and R. M. Levenson, *Philos Trans A Math Phys Eng Sci*, 2011, **369**, 4620-4643.
51. S. Bloch, F. Lesage, L. McIntosh, A. Gandjbakhche, K. Liang and S. Achilefu, *J Biomed Opt*, 2005, **10**, 054003.
52. X. Michalet, F. F. Pinaud, L. A. Bentolila, J. M. Tsay, S. Doose, J. J. Li, G. Sundaresan, A. M. Wu, S. S. Gambhir and S. Weiss, *Science*, 2005, **307**, 538-544.
53. E. I. Altinoğlu, T. J. Russin, J. M. Kaiser, B. M. Barth, P. C. Eklund, M. Kester and J. H. Adair, *ACS Nano*, 2008, **2**, 2075-2084.
54. M. Chalfie, Y. Tu, G. Euskirchen, W. W. Ward and D. C. Prasher, *Science*, 1994, **263**, 802-805.
55. D. E. Azagury, M. M. Dua, J. C. Barrese, J. M. Henderson, N. C. Buchs, F. Ris, J. M. Cloyd, J. B. Martinie, S. Razzaque, S. Nicolau, L. Soler, J. Marescaux and B. C. Visser, *Curr Probl Surg*, 2015, **52**, 476-520.
56. R. D. Bucholz, *J Image Guid Surg*, 1995, **1**, 1-3.
57. G. Spinoglio, F. Priora, P. P. Bianchi, F. S. Lucido, A. Licciardello, V. Maglione, F. Grosso, R. Quarati, F. Ravazzoni and L. M. Lenti, *Surg Endosc*, 2013, **27**, 2156-2162.
58. S. Gioux, H. S. Choi and J. V. Frangioni, *Mol Imaging*, 2010, **9**, 237-255.
59. E. A. Owens, S. Lee, J. Choi, M. Henary and H. S. Choi, *Wiley Interdiscip Rev Nanomed Nanobiotechnol*, 2015, **7**, 828-838.
60. P. Das, S. Santos, G. K. Park, I. Hoseok and H. S. Choi, *Korean J Thorac Cardiovasc Surg*, 2019, **52**, 205-220.
61. L. Lattuada, A. Barge, G. Cravotto, G. B. Giovenzana and L. Tei, *Chem Soc Rev*, 2011, **40**, 3019-3049.
62. J. Greiser, W. Weigand and M. Freesmeyer, *Pharmaceuticals (Basel)*, 2019, **12**.
63. A. D. Sherry, P. Caravan and R. E. Lenkinski, *J Magn Reson Imaging*, 2009, **30**, 1240-1248.
64. C. F. Geraldès and S. Laurent, *Contrast Media Mol Imaging*, 2009, **4**, 1-23.
65. M. Bottrill, L. Kwok and N. J. Long, *Chem Soc Rev*, 2006, **35**, 557-571.
66. Z. Zhang, S. A. Nair and T. J. McMurry, *Curr Med Chem*, 2005, **12**, 751-778.
67. M. Shokeen and C. J. Anderson, *Acc Chem Res*, 2009, **42**, 832-841.
68. K. Tanaka and K. Fukase, *Org Biomol Chem*, 2008, **6**, 815-828.
69. W. W. Lee and K.-S. Group, *Nucl Med Mol Imaging*, 2019, **53**, 172-181.

70. O. Israel, O. Pellet, L. Biassoni, D. De Palma, E. Estrada-Lobato, G. Gnanasegaran, T. Kuwert, C. la Fougère, G. Mariani, S. Massalha, D. Paez and F. Giammarile, *Eur J Nucl Med Mol Imaging*, 2019, **46**, 1990-2012.
71. G. Anderegg, F. Arnaud-Neu, R. Delgado, J. Felcman and K. Popov, *Pure Appl. Chem.* , 2005 **77**, 1445
72. N. R. Puttagunta, W. A. Gibby and V. L. Puttagunta, *Invest Radiol*, 1996, **31**, 619-624.
73. M. Brinkley, *Bioconjug Chem*, 1992, **3**, 2-13.
74. E. Valeur and M. Bradley, *Chem Soc Rev*, 2009, **38**, 606-631.
75. B. H. Northrop, S. H. Frayne and U. Choudhary, *Polym. Chem.*, 2015, **6**, 3415-3430.
76. S. Ravi, V. R. Krishnamurthy, J. M. Caves, C. A. Haller and E. L. Chaikof, *Acta Biomater*, 2012, **8**, 627-635.
77. A. E. Frost, *Nature*, 1956, **178**, 322.
78. O. A. Gansow, M. W. Brechbiel, S. Mirzadeh, D. Colcher and M. Roselli, *Cancer Treat Res*, 1990, **51**, 153-171.
79. C. H. Cummins, E. W. Rutter and W. A. Fordyce, *Bioconjug Chem*, 1991, **2**, 180-186.
80. P. Chaumet-Riffaud, I. Martinez-Duncker, A. L. Marty, C. Richard, A. Prigent, F. Moati, L. Sarda-Mantel, D. Scherman, M. Bessodes and N. Mignet, *Bioconjug Chem*, 2010, **21**, 589-596.
81. H. Essien, J. Y. Lai and K. J. Hwang, *J Med Chem*, 1988, **31**, 898-901.
82. P. F. Sieving, A. D. Watson and S. M. Rocklage, *Bioconjug Chem*, 1990, **1**, 65-71.
83. C. Cabella, S. G. Crich, D. Corpillo, A. Barge, C. Ghirelli, E. Bruno, V. Lorusso, F. Uggeri and S. Aime, *Contrast Media Mol Imaging*, 2006, **1**, 23-29.
84. G. E. Krejcarek and K. L. Tucker, *Biochem Biophys Res Commun*, 1977, **77**, 581-585.
85. S. Achilefu, R. R. Wilhelm, H. N. Jimenez, M. A. Schmidt and A. Srinivasan, *J Org Chem*, 2000, **65**, 1562-1565.
86. S. Achilefu, H. N. Jimenez, R. B. Dorshow, J. E. Bugaj, E. G. Webb, R. R. Wilhelm, R. Rajagopalan, J. Jöhler and J. L. Erion, *J Med Chem*, 2002, **45**, 2003-2015.
87. M. de Visser, H. F. Bernard, J. L. Erion, M. A. Schmidt, A. Srinivasan, B. Waser, J. C. Reubi, E. P. Krenning and M. de Jong, *Eur J Nucl Med Mol Imaging*, 2007, **34**, 1228-1238.
88. F. Alshoukr, C. Rosant, V. Maes, J. Abdelhak, O. Raguin, S. Burg, L. Sarda, J. Barbet, D. Tourwé, D. Pelaprat and A. Gruaz-Guyon, *Bioconjug Chem*, 2009, **20**, 1602-1610.
89. Y. Arano, T. Uezono, H. Akizawa, M. Ono, K. Wakisaka, M. Nakayama, H. Sakahara, J. Konishi and A. Yokoyama, *J Med Chem*, 1996, **39**, 3451-3460.
90. F. Leclercq, M. Cohen-Ohana, N. Mignet, A. Sbarbati, J. Herscovici, D. Scherman and G. Byk, *Bioconjug Chem*, 2003, **14**, 112-119.
91. H. Stetter and W. A. Frank, *Angew. Chem., Int. Ed. Engl.*, 1976, **15** 686
92. M. K. Moi, S. J. DeNardo and C. F. Meares, *Cancer Res*, 1990, **50**, 789s-793s.
93. J. F. Desreux, *Inorg. Chem.*, 1980, **19**, 1319.
94. P. Caravan, J. J. Ellison, T. J. McMurphy and R. B. Lauffer, *Chem Rev*, 1999, **99**, 2293-2352.
95. M. R. Lewis, J. Y. Kao, A. L. Anderson, J. E. Shively and A. Raubitschek, *Bioconjug Chem*, 2001, **12**, 320-324.
96. M. R. Lewis, A. Raubitschek and J. E. Shively, *Bioconjug Chem*, 1994, **5**, 565-576.
97. R. Albert, P. Smith-Jones, B. Stolz, C. Simeon, H. Knecht, C. Bruns and J. Pless, *Bioorg Med Chem Lett*, 1998, **8**, 1207-1210.
98. S. X. Lu, E. J. Takach, M. Solomon, Q. Zhu, S. J. Law and F. Y. Hsieh, *J Pharm Sci*, 2005, **94**, 788-797.
99. C. Li, P. T. Winnard, T. Takagi, D. Artemov and Z. M. Bhujwala, *J Am Chem Soc*, 2006, **128**, 15072-15073.
100. W. A. Volkert and T. J. Hoffman, *Chem Rev*, 1999, **99**, 2269-2292.
101. S. Aime, L. Calabi, C. Cavallotti, E. Gianolio, G. B. Giovenzana, P. Losi, A. Maiocchi, G. Palmisano and M. Sisti, *Inorg Chem*, 2004, **43**, 7588-7590.
102. L. Tei, G. Gugliotta, M. Fekete, F. K. Kálmán and M. Botta, *Dalton Trans*, 2011, **40**, 2025-2032.
103. E. M. Elemento, D. Parker, S. Aime, E. Gianolio and L. Lattuada, *Org Biomol Chem*, 2009, **7**, 1120-1131.



104. G. Nagy, D. Szikra, G. Trencsényi, A. Fekete, I. Garai, A. M. Giani, R. Negri, N. Masciocchi, A. Maiocchi, F. Uggeri, I. Tóth, S. Aime, G. B. Giovenzana and Z. Baranyai, *Angew Chem Int Ed Engl*, 2017, **56**, 2118-2122.
105. B. P. Waldron, D. Parker, C. Burchardt, D. S. Yufit, M. Zimny and F. Roesch, *Journal*, 2013, **49**, 579-581.
106. G. Gugliotta, M. Botta, G. B. Giovenzana and L. Tei, *Bioorg Med Chem Lett*, 2009, **19**, 3442-3444.
107. R. S. Sengar, S. J. Geib, A. Nigam and E. C. Wiener, *Acta Crystallogr C*, 2010, **66**, o174-175.
108. E. Gianolio, G. B. Giovenzana, A. Ciampa, S. Lanzardo, D. Imperio and S. Aime, *ChemMedChem*, 2008, **3**, 60-62.
109. 2006.
110. L. Manzoni, L. Belvisi, D. Arosio, M. P. Bartolomeo, A. Bianchi, C. Brioschi, F. Buonsanti, C. Cabella, C. Casagrande, M. Civera, M. De Matteo, L. Fugazza, L. Lattuada, F. Maisano, L. Miragoli, C. Neira, M. Pilkington-Miksa and C. Scolastico, *ChemMedChem*, 2012, **7**, 1084-1093.
111. R. Ballini, M. Petrini and V. Polzonetti, *Synthesis*, 1992, 355-357.
112. B. Zsolt, U. Fulvio, M. Alessandro, G. Giovanni B., C. Camilla, T. Anett, T. Imre, B. István, B. Attila, B. Erno and A. Silvio, *Journal*, 2013, 147-162.
113. W. R. Harris and A. E. Martell, *Inorg. Chem.*, 1976, **15**, 713-720.
114. E. Boros, C. L. Ferreira, J. F. Cawthray, E. W. Price, B. O. Patrick, D. W. Wester, M. J. Adam and C. Orvig, *J Am Chem Soc*, 2010, **132**, 15726-15733.
115. D. J. Clevette and C. Orvig, *Polyhedron*, 1990, **9**, 151-161
116. A. S. Craig, D. Parker, H. Adams and N. A. Bailey, *Chem. Commun.*, 1989, 1793-1794.
117. J. Notni, P. Hermann, J. Havlíčková, J. Kotek, V. Kubíček, J. Plutnar, N. Loktionova, P. J. Riss, F. Rösch and I. Lukes, *Chemistry*, 2010, **16**, 7174-7185.
118. N. A. Viola, R. S. Rarig Jr., W. Ouellette and R. P. Doyle, *Polyhedron*, 2006 **25**, 3457-3462
119. E. T. Clarke and A. E. Martell, *Inorg. Chim. Acta*, 1991 **181** 273-280
120. E. T. Clarke and A. E. Martell, *Inorg. Chim. Acta*, 1991, **190**, 37-46
121. V. Kubíček, J. Havlíčková, J. Kotek, G. Tircsó, P. Hermann, E. Tóth and I. Lukes, *Inorg Chem*, 2010, **49**, 10960-10969.
122. R. Delgado, M. do Carmo Figueira and S. Quintino, *Talanta*, 1997, **45**, 451-462.
123. P. M. May, D. R. Williams and P. W. Linder, *J. Chem. Soc., Dalton Trans.*, 1977, 588-595.
124. S. B. Gunnoo and A. Maddar, *Org Biomol Chem*, 2016, **14**, 8002-8013.
125. M. Morais and M. T. Ma, *Drug Discov Today Technol*, 2018, **30**, 91-104.
126. Q. Y. Hu, F. Berti and R. Adamo, *Chem Soc Rev*, 2016, **45**, 1691-1719.
127. A. L. Nelson, E. Dhimolea and J. M. Reichert, *Nat Rev Drug Discov*, 2010, **9**, 767-774.
128. D. C. Roopenian and S. Akilesh, *Nat Rev Immunol*, 2007, **7**, 715-725.
129. C. Hamers-Casterman, T. Atarhouch, S. Muyldermans, G. Robinson, C. Hamers, E. B. Songa, N. Bendahman and R. Hamers, *Nature*, 1993, **363**, 446-448.
130. P. A. Szijj, C. Bahou and V. Chudasama, *Drug Discov Today Technol*, 2018, **30**, 27-34.
131. J. R. Junutula, H. Raab, S. Clark, S. Bhakta, D. D. Leipold, S. Weir, Y. Chen, M. Simpson, S. P. Tsai, M. S. Dennis, Y. Lu, Y. G. Meng, C. Ng, J. Yang, C. C. Lee, E. Duenas, J. Gorrell, V. Katta, A. Kim, K. McDorman, K. Flagella, R. Venook, S. Ross, S. D. Spencer, W. Lee Wong, H. B. Lowman, R. Vandlen, M. X. Sliwkowski, R. H. Scheller, P. Polakis and W. Mallet, *Nat Biotechnol*, 2008, **26**, 925-932.
132. C. R. Behrens and B. Liu, *MAbs*, 2014, **6**, 46-53.
133. K. Škrlec, B. Štrukelj and A. Berlec, *Trends Biotechnol*, 2015, **33**, 408-418.
134. D. Lipovsek, *Protein Eng Des Sel*, 2011, **24**, 3-9.
135. A. Plückthun, *Annu Rev Pharmacol Toxicol*, 2015, **55**, 489-511.
136. J. Löfblom, J. Feldwisch, V. Tolmachev, J. Carlsson, S. Ståhl and F. Y. Frejd, *FEBS Lett*, 2010, **584**, 2670-2680.
137. S. Oloketuyi, C. Dilkaute, E. Mazzega, J. Jose and A. de Marco, *Appl Microbiol Biotechnol*, 2019, **103**, 4443-4453.

138. J. Desmet, K. Verstraete, Y. Bloch, E. Lorent, Y. Wen, B. Devreese, K. Vandenbroucke, S. Loverix, T. Hettmann, S. Deroo, K. Somers, P. Henderikx, I. Lasters and S. N. Savvides, *Nat Commun*, 2014, **5**, 5237.
139. A. Orlova, A. Jonsson, D. Rosik, H. Lundqvist, M. Lindborg, L. Abrahmsen, C. Ekblad, F. Y. Frejd and V. Tolmachev, *J Nucl Med*, 2013, **54**, 961-968.
140. A. C. Freise and A. M. Wu, *Mol Immunol*, 2015, **67**, 142-152.
141. N. Krall, F. P. da Cruz, O. Boutureira and G. J. Bernardes, *Nat Chem*, 2016, **8**, 103-113.
142. C. H. Douse, S. J. Maas, J. C. Thomas, J. A. Garnett, Y. Sun, E. Cota and E. W. Tate, *ACS Chem Biol*, 2014, **9**, 2204-2209.
143. L. Nevola and E. Giralt, *Chem Commun (Camb)*, 2015, **51**, 3302-3315.
144. M. M. Harris, Z. Coon, N. Alqaeisoom, B. Swords and J. M. Holub, *Org Biomol Chem*, 2016, **14**, 440-446.
145. L. D. Walensky, A. L. Kung, I. Escher, T. J. Malia, S. Barbuto, R. D. Wright, G. Wagner, G. L. Verdine and S. J. Korsmeyer, *Science*, 2004, **305**, 1466-1470.
146. S. A. Kawamoto, A. Coleska, X. Ran, H. Yi, C. Y. Yang and S. Wang, *J Med Chem*, 2012, **55**, 1137-1146.
147. M. M. Madden, A. Muppidi, Z. Li, X. Li, J. Chen and Q. Lin, *Bioorg Med Chem Lett*, 2011, **21**, 1472-1475.
148. Z. Li, R. Huang, H. Xu, J. Chen, Y. Zhan, X. Zhou, H. Chen and B. Jiang, *Org Lett*, 2017, **19**, 4972-4975.
149. C. M. Haney, M. T. Loch and W. S. Horne, *Chem Commun (Camb)*, 2011, **47**, 10915-10917.
150. A. M. Spokoyny, Y. Zou, J. J. Ling, H. Yu, Y. S. Lin and B. L. Pentelute, *J Am Chem Soc*, 2013, **135**, 5946-5949.
151. F. M. Brunel and P. E. Dawson, *Chem Commun (Camb)*, 2005, 2552-2554.
152. A. Iyer, D. Van Lysebetten, Y. Ruiz García, B. Louage, B. G. De Geest and A. Madder, *Org Biomol Chem*, 2015, **13**, 3856-3862.
153. A. Henninot, J. C. Collins and J. M. Nuss, *J Med Chem*, 2018, **61**, 1382-1414.
154. J. L. Lau and M. K. Dunn, *Bioorg Med Chem*, 2018, **26**, 2700-2707.
155. K. Fosgerau and T. Hoffmann, *Drug Discov Today*, 2015, **20**, 122-128.
156. A. A. Kaspar and J. M. Reichert, *Drug Discov Today*, 2013, **18**, 807-817.
157. A. J. Mijalis, D. A. Thomas, M. D. Simon, A. Adamo, R. Beaumont, K. F. Jensen and B. L. Pentelute, *Nat Chem Biol*, 2017, **13**, 464-466.
158. R. Behrendt, P. White and J. Offer, *J Pept Sci*, 2016, **22**, 4-27.
159. R. He, B. Finan, J. P. Mayer and R. D. DiMarchi, *Molecules*, 2019, **24**.
160. A. Moya-García, T. Adeyelu, F. A. Kruger, N. L. Dawson, J. G. Lees, J. P. Overington, C. Orengo and J. A. G. Ranea, *Sci Rep*, 2017, **7**, 10102.
161. A. Anighoro, J. Bajorath and G. Rastelli, *J Med Chem*, 2014, **57**, 7874-7887.
162. A. S. Reddy and S. Zhang, *Expert Rev Clin Pharmacol*, 2013, **6**, 41-47.
163. L. A. Carpino, S. Ghassem, D. Ionescu, M. Ismail and D. T. Sadat-Aalae, Geouge A. Mansour, E.M.E. Siw ruk, Gary A. Eynon, John S. Morgan, Berry., *Org. Proc. Res. Dev.*, 2003, **7**, 28-37.
164. Y. Nishiuchi, T. Inui, H. Nishio, J. Bódi, T. Kimura, F. I. Tsuji and S. Sakakibara, *Proc Natl Acad Sci U S A*, 1998, **95**, 13549-13554.
165. S. Chandrudu, P. Simerska and I. Toth, *Molecules*, 2013, **18**, 4373-4388.
166. M. Amblard, J. A. Fehrentz, J. Martinez and G. Subra, *Mol Biotechnol*, 2006, **33**, 239-254.
167. R. Sheppard, *J Pept Sci*, 2003, **9**, 545-552.
168. M. Muttenthaler, F. Albericio and P. E. Dawson, *Nat Protoc*, 2015, **10**, 1067-1083.
169. G. Walter, *J Immunol Methods*, 1986, **88**, 149-161.
170. S. Eissler, M. Kley, D. Bächle, G. Loidl, T. Meier and D. Samson, *J Pept Sci*, 2017, **23**, 757-762.
171. O. F. Luna, J. Gomez, C. Cárdenas, F. Albericio, S. H. Marshall and F. Guzmán, *Molecules*, 2016, **21**.
172. S. L. Pedersen, A. P. Tofteng, L. Malik and K. J. Jensen, *Chem Soc Rev*, 2012, **41**, 1826-1844.
173. D. S. King, C. G. Fields and G. B. Fields, *Int J Pept Protein Res*, 1990, **36**, 255-266.

174. I. Friligou, E. Papadimitriou, D. Gatos, J. Matsoukas and T. Tselios, *Amino Acids*, 2011, **40**, 1431-1440.
175. A. L. Berman, E. Kolker and E. N. Trifonov, *Proc Natl Acad Sci U S A*, 1994, **91**, 4044-4047.
176. D. Kemp, S. Leung and D. Kerkman, *Tetrahedron Lett.*, 1981, **22**, 181-184.
177. M. Skwarczynski and Y. Kiso, *Curr Med Chem*, 2007, **14**, 2813-2823.
178. P. E. Dawson, T. W. Muir, I. Clark-Lewis and S. B. Kent, *Science*, 1994, **266**, 776-779.
179. P. E. Dawson and S. B. Kent, *Annu Rev Biochem*, 2000, **69**, 923-960.
180. T. W. Muir, P. E. Dawson and S. B. Kent, *Methods Enzymol*, 1997, **289**, 266-298.
181. W. Lu, M. A. Qasim and S. B. H. Kent, *J. Am. Chem. Soc.*, 1996, **118**, 8518-8523.
182. A. C. Conibear, E. E. Watson, R. J. Payne and C. F. W. Becker, *Chem Soc Rev*, 2018, **47**, 9046-9068.
183. S. B. Kent, *Chem Soc Rev*, 2009, **38**, 338-351.
184. R. Siegel, J. Ma, Z. Zou and A. Jemal, *CA Cancer J Clin*, 2014, **64**, 9-29.
185. M. Weineisen, J. Simecek, M. Schottelius, M. Schwaiger and H. J. Wester, *EJNMMI Res*, 2014, **4**, 63.
186. D. A. Silver, I. Pellicer, W. R. Fair, W. D. Heston and C. Cordon-Cardo, *Clin Cancer Res*, 1997, **3**, 81-85.
187. J. C. Evans, M. Malhotra, J. F. Cryan and C. M. O'Driscoll, *Br J Pharmacol*, 2016, **173**, 3041-3079.
188. C. Bařinka, C. Rojas, B. Slusher and M. Pomper, *Curr Med Chem*, 2012, **19**, 856-870.
189. M. Eder, M. Schäfer, U. Bauder-Wüst, W. E. Hull, C. Wängler, W. Mier, U. Haberkorn and M. Eisenhut, *Bioconjug Chem*, 2012, **23**, 688-697.
190. T. Maurer, M. Eiber, M. Schwaiger and J. E. Gschwend, *Nat Rev Urol*, 2016, **13**, 226-235.
191. K. P. Maresca, S. M. Hillier, F. J. Femia, D. Keith, C. Barone, J. L. Joyal, C. N. Zimmerman, A. P. Kozikowski, J. A. Barrett, W. C. Eckelman and J. W. Babich, *J Med Chem*, 2009, **52**, 347-357.
192. M. Benešová, U. Bauder-Wüst, M. Schäfer, K. D. Klika, W. Mier, U. Haberkorn, K. Kopka and M. Eder, *J Med Chem*, 2016, **59**, 1761-1775.
193. S. L. Gonias and J. Hu, *Front Pharmacol*, 2015, **6**, 154.
194. N. Montuori, V. Cosimato, L. Rinaldi, V. E. Rea, D. Alfano and P. Ragno, *Thromb Haemost*, 2013, **109**, 309-318.
195. A. P. Mazar, *Clin Cancer Res*, 2008, **14**, 5649-5655.
196. N. Montuori, A. Mattiello, A. Mancini, P. Tagliatalata, M. Caputi, G. Rossi and P. Ragno, *Int J Cancer*, 2003, **105**, 353-360.
197. C. E. Almasi, I. J. Christensen, G. Høyer-Hansen, K. Danø, H. Pappot, H. Dienemann and T. Muley, *Lung Cancer*, 2011, **74**, 510-515.
198. A. F. Lomholt, G. Høyer-Hansen, H. J. Nielsen and I. J. Christensen, *Br J Cancer*, 2009, **101**, 992-997.
199. A. F. Lomholt, I. J. Christensen, G. Høyer-Hansen and H. J. Nielsen, *Acta Oncol*, 2010, **49**, 805-811.
200. Y. Wei, D. A. Waltz, N. Rao, R. J. Drummond, S. Rosenberg and H. A. Chapman, *J Biol Chem*, 1994, **269**, 32380-32388.
201. C. D. Madsen, G. M. Ferraris, A. Andolfo, O. Cunningham and N. Sidenius, *J Cell Biol*, 2007, **177**, 927-939.
202. R. D. Lester, M. Jo, V. Montel, S. Takimoto and S. L. Gonias, *J Cell Biol*, 2007, **178**, 425-436.
203. G. van der Pluijm, B. Sijmons, H. Vloedgraven, C. van der Bent, J. W. Drijfhout, J. Verheijen, P. Quax, M. Karperien, S. Papapoulos and C. Löwik, *Am J Pathol*, 2001, **159**, 971-982.
204. C. D. Mauro, A. Pesapane, L. Formisano, R. Rosa, V. D'Amato, P. Ciciola, A. Servetto, R. Marciano, R. C. Orsini, F. Monteleone, N. Zambrano, G. Fontanini, A. Servadio, G. Pignataro, L. Grumetto, A. Lavecchia, D. Bruzzese, A. Iaccarino, G. Troncone, B. M. Veneziani, N. Montuori, S. Placido and R. Bianco, *Sci Rep*, 2017, **7**, 9388.
205. D. Li, S. Liu, H. Shan, P. Conti and Z. Li, *Theranostics*, 2013, **3**, 507-515.
206. R. J. Goodson, M. V. Doyle, S. E. Kaufman and S. Rosenberg, *Proc Natl Acad Sci U S A*, 1994, **91**, 7129-7133.

207. M. Ploug, S. Østergaard, H. Gårdsvoll, K. Kovalski, C. Holst-Hansen, A. Holm, L. Ossowski and K. Danø, *Biochemistry*, 2001, **40**, 12157-12168.
208. M. C. Kriegbaum, M. Persson, L. Haldager, W. Alpízar-Alpízar, B. Jacobsen, H. Gårdsvoll, A. Kjær and M. Ploug, *Curr Drug Targets*, 2011, **12**, 1711-1728.

## II. DESIGN AND SYNTHESIS OF NOVEL AAZTA DERIVATIVES

### 2.1 Purpose

In this chapter, the design and synthesis of all novel AAZTA derivatives will be described. The library has been created in order to obtain a range of possibilities for the conjugation with differently derivatized biomolecules. All AAZTA based bifunctional chelators have been synthesized with different functional groups that allow the subsequent reaction with targeting scaffolds. Basically, the first paragraph is dedicated to the description of the improvement of the synthesis of  $(t\text{Bu})_4\text{-AAZTA-C4-COOH}$ , the mainly used AAZTA derivative for peptide derivatization through bioconjugation reactions. In the following paragraphs, four AAZTA derivatives have been successfully synthesized in order to extend bioconjugation reaction possibilities on the base of the exposed chemical groups by peptides and/or biomolecules.

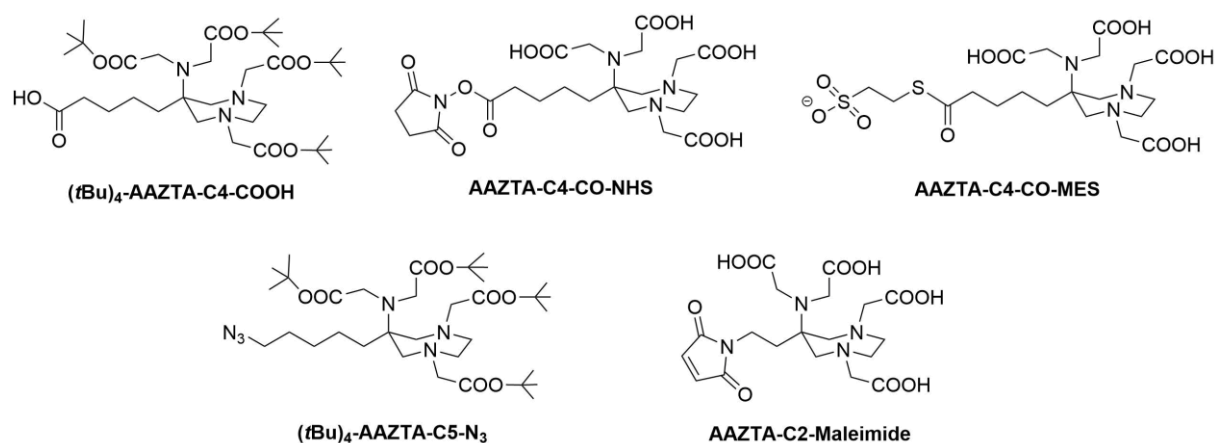


**Figure 2.1:** Chemical structures of AAZTA derivative library.

AAZTA-C4-CO-NHS can be used as a reacting scaffold for the conjugation with primary amines, to obtain a stable and biologically accepted amide bond. The chelator preactivated as a thioester, AAZTA-C4-CO-MES, as will be shown in Chapter IV, will be used for the chemoselective chemical ligation reaction with N-terminal cysteine peptides to form, even in this case, an amide bond. Azide and maleimide AAZTA derivatives may find interesting applications in the field of click chemistry, reacting respectively with terminal alkynes, to give a 1,2,3-triazole (Huisgen cycloaddition<sup>1</sup>) and primary thiols, to give a stable and irreversible thioether linkage<sup>2</sup>.

### 2.2 Materials and Methods

All reagents were purchased from Sigma Aldrich (Darmstadt, Germany). All solvents were purchased by VWR International (Radnor, USA) and were used without further purifications. Mass spectra with electrospray ionization (ESI) were recorded on a SQD 3100 Mass Detector (Waters). The HPLC-MS analytical and preparative analysis were carried out on a Waters AutoPurification system (3100 Mass Detector, 600 Quaternary Pump Gradient Module, 2767 Sample Manager and 2487 UV/Visible Detector). Analytical HPLC analyses were performed using a Waters 2695 Alliance Separation Module equipped with a Waters 2998 Photodiode Array Detector. Desalting processes were performed with an AKTA purifier equipped with UV-

900 lamp, P-900 pumps, FRAC-920 collector, 907 Inj valve, PV-908 Outlet valve. NMR spectra were recorded at 298 K on a Bruker AVANCE 600 spectrometer. CD<sub>3</sub>OD and NMR tube were purchased from Sigma Aldrich. 6-[Bis[2-(1,1-dimethylethoxy)-2-oxoethyl]amino]-6-(5-carboxypentyl)tetrahydro-1H-1,4-diazepine-1,4(5H)-Diacetic acid  $\alpha,\alpha'$ -bis(1,1-dimethylethyl)ester ((*tBu*)<sub>4</sub>-AAZTA-C4-COOH) was synthesized in accordance with Manzoni et al protocol.<sup>3</sup>

## 2.3 Experimental synthesis procedures

### 2.3.1 Improved synthesis of (tBu)<sub>4</sub>-AAZTA-C4-COOH

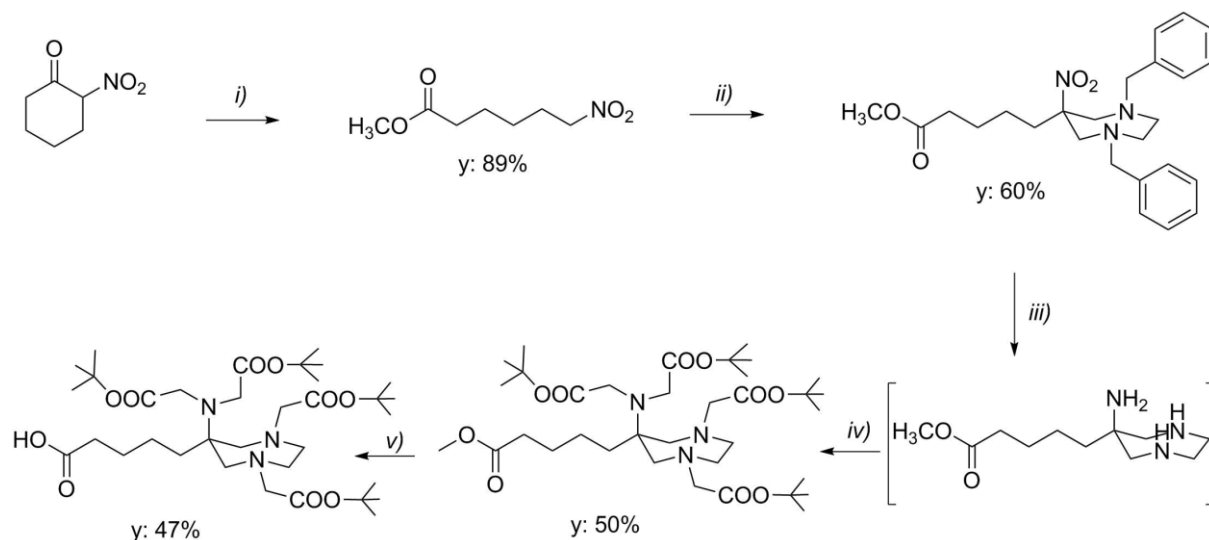


**Figure 2.2:** Synthesis scheme of (tBu)<sub>4</sub>-AAZTA-C4-COOH and step yields from Manzoni et al: *i)* Amberlyst A21, MeOH; *ii)* DBED(N,N'-Dibenzylethylenediamine), PFA(Paraformaldehyde), Δ, EtOH; *iii)* Pd/C, H<sub>2</sub>, MeOH; *iv)* tBBA(tert-Butyl bromoacetate), K<sub>2</sub>CO<sub>3</sub>, Na<sub>2</sub>SO<sub>4</sub>, Δ, CH<sub>3</sub>CN; *v)* LiOH, TFA/H<sub>2</sub>O. Overall yield: 13%.<sup>3</sup>

Steps *i* to *iv* have been carried out following Manzoni et. al procedure. Step *v* has been performed as follows:<sup>4, 5</sup>

6eq of NaOH as powder (369 mg) were added to a solution of (tBu)<sub>4</sub>-AAZTA-C4-COOCH<sub>3</sub> (1.27 g; 1.85 mmol) in H<sub>2</sub>O/*i*Pro 1:1 (70 mL). The solution was stirred at room temperature for 15 h. The *i*Pro was evaporated *in vacuo* and the pH of the solution was brought to 7 by addition of HCl 1M (product precipitation). The aqueous residue was extracted with EtOAc (3x10 mL). The organic phases were collected, dried (Na<sub>2</sub>SO<sub>4</sub>), filtered and evaporated. The final product was obtained without further purification as a pale yellow oil. (1.10 g; 1.64mmol). y: 89%. ESI-MS (*m/z*): calcd: For C<sub>34</sub>H<sub>61</sub>N<sub>4</sub>O<sub>10</sub> (M+H)<sup>+</sup> 672.44 found: 672.48.

### 2.3.2 AAZTA-C4-CO-NHS

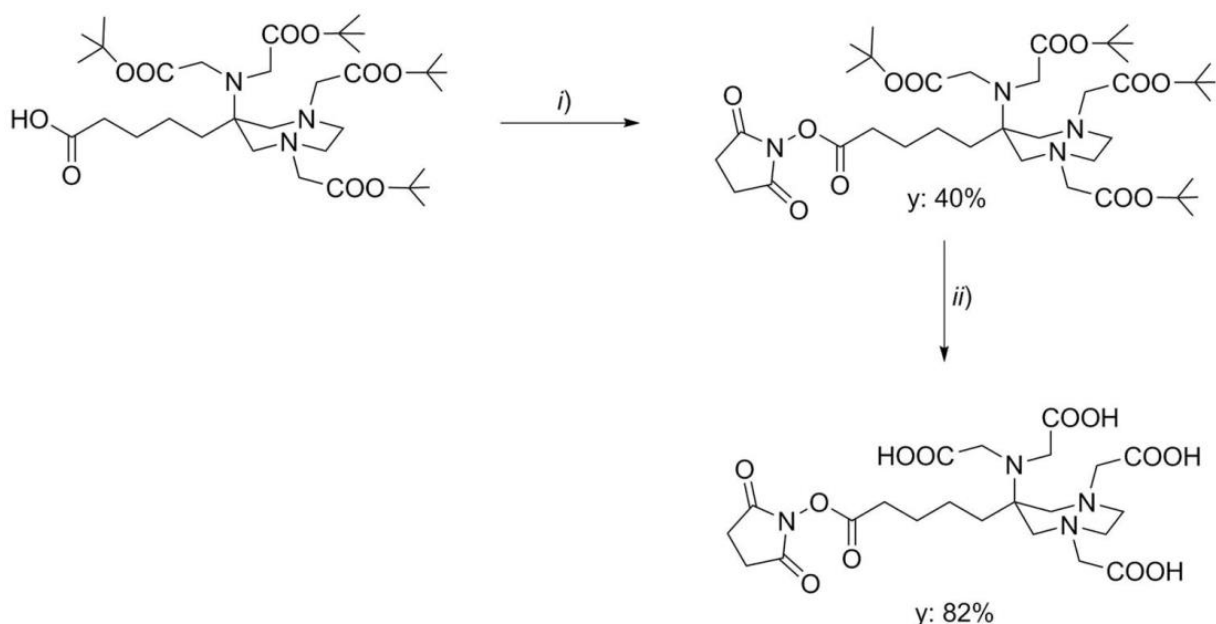


**Figure 2.3: Synthesis scheme of AAZTA-C4-CO-NHS:**

*i)* DCC, NHS, DMAP, CH<sub>2</sub>Cl<sub>2</sub>, RT, 2h; *ii)* TFA:CH<sub>2</sub>Cl<sub>2</sub>; Overall yield: 33%.

*i)* In a round bottom flask, 246mg of (tBu)<sub>4</sub>-AAZTA-C4-COOH were dissolved in CH<sub>2</sub>Cl<sub>2</sub> (10 mL). 1.2eq of NHS (N-Hydroxysuccinimide), 1.1 eq of DCC (N,N'-Dicyclohexylcarbodiimide) and 0.2 of DMAP (4-Dimethylaminopyridine) were added to the solution. The solution was stirred 4h at RT. The precipitate (dicyclohexylurea) was filtered and the solvent was evaporated *in vacuo*. The crude product was purified on a gravimetric silica chromatography with Hex/AcOEt 3:2. The purity of the product was checked by analytical HPLC-MS by employing an Atlantis DC18 5um, 4.6X150mm column. Eluent: (A) 0.1% TFA in H<sub>2</sub>O, (B) 0.1% TFA in CH<sub>3</sub>CN. Gradient profile; linear gradient from 40% to 100% of B in 20 min, isocratic at 100% for 10 min. Flow rate of 1 mL/min and UV detection at 254 nm. RT: 11.30 min. <sup>1</sup>H-NMR (CDCl<sub>3</sub>, 600 MHz): δ 1.45 (s, 36H), 1.75 (tr, 6H), 2.65 (tr, 6H), 2.85 (tr, 6H), 3.40 (tr, 6H), 3.60 (tr, 4H). Purity 89%. p: 112.6mg. Yield: 40%. ESI-MS (*m/z*): calcd: For C<sub>38</sub>H<sub>64</sub>N<sub>4</sub>O<sub>12</sub> (M+H)<sup>+</sup> 769.95 found: 769.44.

*ii)* The product obtained from the previous step was put in ice bath and a solution 2:1 of TFA/CH<sub>2</sub>Cl<sub>2</sub> was added dropwise. After 30 minutes the ice bath was removed and the solution was left to stir overnight at RT. The solution was evaporated with addition of toluene to form the azeotrope. p: 53mg. Yield: 82%. Overall yield: 33%. ESI-MS (*m/z*): calcd: For C<sub>22</sub>H<sub>32</sub>N<sub>4</sub>O<sub>12</sub> (M+H)<sup>+</sup> 545.51 found: 545.37



### 2.3.3 AAZTA-C4-CO-MES

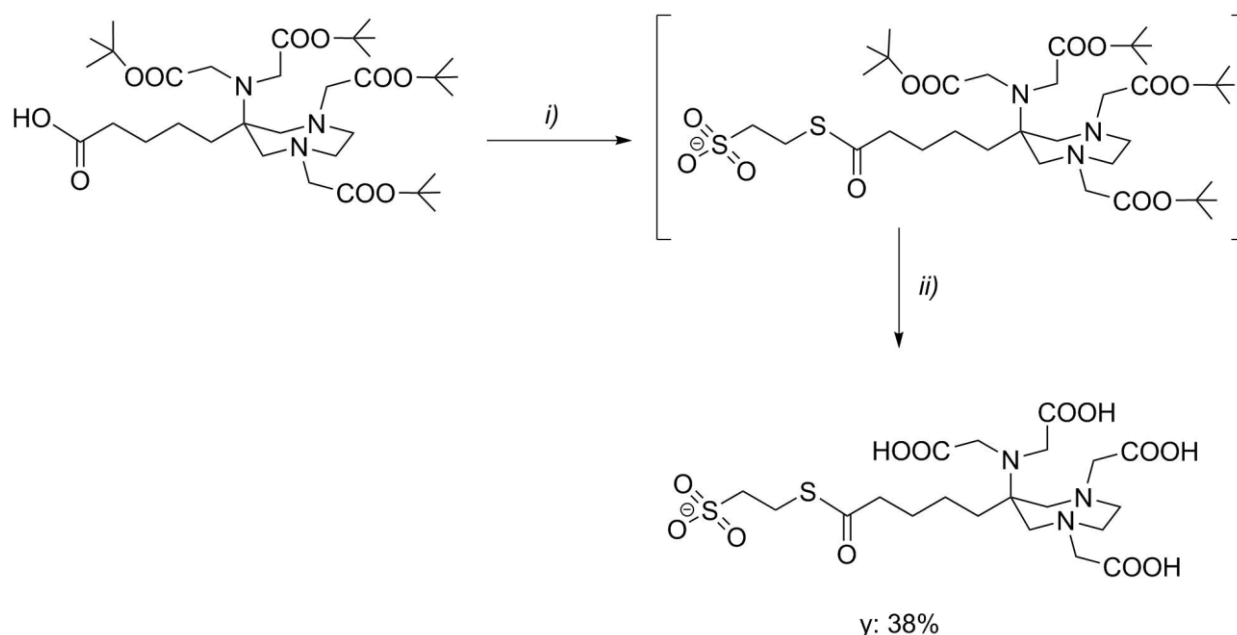


**Figure 2.4: Synthesis scheme of AAZTA-C4-CO-MES:**

*i)* EDC, MESNA, DMAP, CH<sub>2</sub>Cl<sub>2</sub>, RT; *ii)* TFA/TIS/H<sub>2</sub>O; Overall yield: 38%.

In a round bottom flask, 108.1 mg of (tBu)<sub>4</sub>-AAZTA-C4-COOH (1 eq, 0.161 mmol) were dissolved in 5 mL of CH<sub>2</sub>Cl<sub>2</sub>. The solution was cooled at 273 K and DMAP (0.09 eq, 1.8 mg) and EDC (1 eq, 30.8 mg) were added. After 10 minutes the ice bath was removed and MESNA (sodium 2-mercaptoethane sulfonate) (0.9 eq, 23.8 mg) were added to the solution and the reaction was stirred overnight at room temperature. The solvent was evaporated and the obtained product re-dissolved in 5 mL of TFA/TIS/H<sub>2</sub>O (95:2.5:2.5) and the reaction was stirred overnight at room temperature. The solvent was evaporated and the final purification was achieved by preparative RP-HPLC on Waters AutoPurification system by employing an Atlantis prepD<sup>®</sup> C18OBD 5 $\mu$ m (19X100 mm) column. Eluent: (A) 0.1% TFA in H<sub>2</sub>O, (B) 0.1% TFA in CH<sub>3</sub>CN. Gradient profile: isocratic at 10% of B for 2.8 min, linear gradient from 10% to 35% of B in 5.7 min, linear gradient from 35% to 100% in 2.8 min, isocratic at 100% for 1 min. Flow rate; 15 mL/min. AAZTA-C4-CO-MES was isolated as a homogenous peak with a retention time of ca 5 minutes. The solvent was removed *in vacuo* and the product lyophilized from water to give AAZTA-C4-CO-MES as a white solid (35 mg, 38%). The purity of the product was checked by analytical UPLC-MS by employing an ACQUITY UPLC<sup>®</sup> Peptide BEH C18 column (300 $\text{\AA}$ , 1.7 $\mu$ m, 2.1X100mm). Eluent: (A) 0.05% TFA in H<sub>2</sub>O, (B) 0.05% TFA in CH<sub>3</sub>CN. Gradient profile; linear gradient from 5% to 50% of B in 7 min, linear gradient from 50% to 100% in 3 min, isocratic at 100% for 3 minutes. Flow rate of 0.4 mL/min and UV detection at 210 nm. Purity 95%. ESI-MS (*m/z*): calcd: For C<sub>20</sub>H<sub>33</sub>N<sub>3</sub>O<sub>12</sub>S<sub>2</sub> (M+H)<sup>+</sup> 572.16 found: 572.31. <sup>1</sup>H-NMR (CD<sub>3</sub>OD, 600 MHz):  $\delta$  1.63 (tr, 6H), 2.37 (t, J=7.45 Hz, 2H), 2.62 (t, J=7.45, 4H), 3.02 (tr, 4H), 3.26 (tr, 2H), 3.58 (tr, 2H), 3.74 (s, 8H).

All characterization data are reported in Manuscript 2, pag. 152-153.

### 2.3.4 (tBu)<sub>4</sub>-AAZTA-C5-N<sub>3</sub>

(tBu)<sub>4</sub>-AAZTA-C5-OH was used as starting material and it was synthesized in according with Gianolio *et al.* protocol.<sup>6</sup>

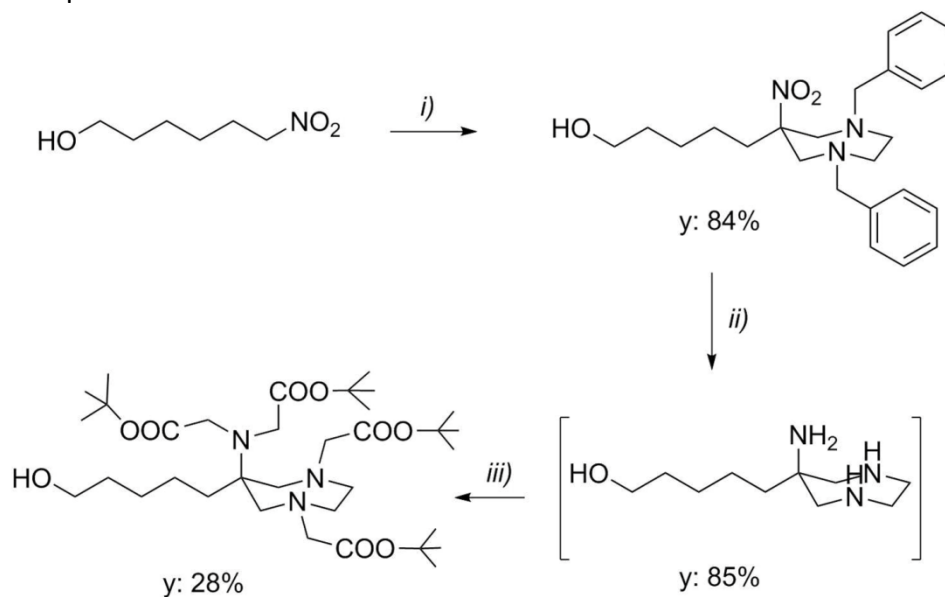


**Figure 2.5: Synthesis scheme of (tBu)<sub>4</sub>-AAZTA-C5-OH and step yields from Gianolio *et al.*:**  
*i)* DBED, PFA, Δ, EtOH/Toluene; *ii)* Pd/C, NH<sub>4</sub>HCO<sub>2</sub>, MeOH; *iii)* tBBA, K<sub>2</sub>CO<sub>3</sub>, Δ, NMP; Overall yield: 20%.

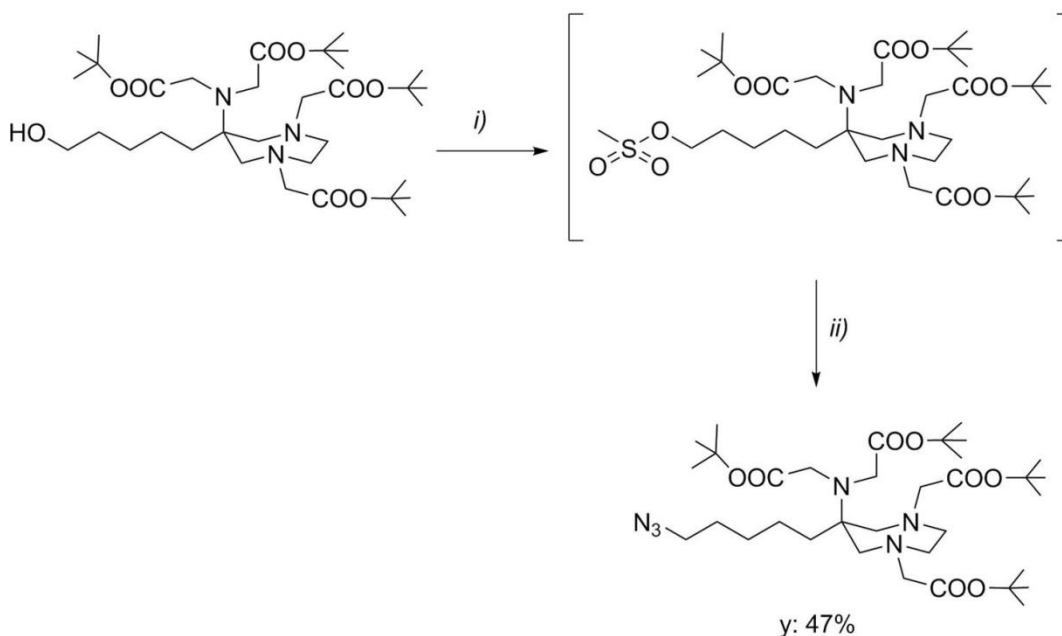


**Figure 2.6: Synthesis scheme of (tBu)<sub>4</sub>-AAZTA-C5-N<sub>3</sub>:**  
*i)* MsCl, pyridine, 0°C, 1h; *ii)* NaN<sub>3</sub>, DMF, 50°C, ON; Overall yield: 47%.

In a three neck 25mL round bottom flask 0.5g of (tBu)<sub>4</sub>-AAZTA-C5-OH (1 eq, 0.760 mmol) were dissolved in 10mL of dry pyridine and the obtained solution was brought to 0°C with an ice bath. 2.2eq of methansulfonic chloride (MsCl, 129uL). After the MsCl adding, the solution became yellow. After 30 minutes the ice bath was removed and the solution was stirred at RT

for additional 30min. The solution was diluted with 10mL of ethyl acetate and the solution was brought again to 0°C with an ice bath. 5-10mL of water were added drop wise to neutralize the MsCl not reacted. The solution was extracted with ethyl acetate (4X10mL). The organic phase was anhydrified with Na<sub>2</sub>SO<sub>4</sub>, filtered and evaporated *in vacuo*.

The yellow pale oil obtained from the previous step was re-dissolved in 10mL of dimethylformamide and 3eq of NaN<sub>3</sub> were added (148mg, 2.28mmol). The solution was stirred overnight at 50°C. 1 additional equivalent of NaN<sub>3</sub> was added to the solution and it was left to stir overnight at 50°C. The solution was diluted with 15mL of water and extracted with ethyl acetate (4X10mL). The organic phase was anhydrified with Na<sub>2</sub>SO<sub>4</sub>, filtered and evaporated *in vacuo*. The crude product was purified over flash chromatography with Hexane/AcOEt (10:1→4:1). p: 243mg. Overall Yield: 47%. ESI-MS (*m/z*): calcd: For C<sub>34</sub>H<sub>62</sub>N<sub>6</sub>O<sub>8</sub> (M+H)<sup>+</sup> 683.90.16 found: 683.53. <sup>1</sup>H-NMR (CD<sub>3</sub>OD, 600 MHz): δ 1.42 (tr, 5H), 1.52 (s, 36H), 1.65 (tr, 5H), 2.68 (tr, 4H), 2.80 (tr, 2H), 3.04 (d, J=7.45, 2H), 3.27 (s, 4H), 3.65 (s, 4H).

### 2.3.5AAZTA-C2-maleimide<sup>7</sup>

(*t*Bu)<sub>4</sub>-AAZTA-C<sub>2</sub>-NH<sub>2</sub> was used as starting material and it was synthesized in according with the related BRACCO protocol (confidential).

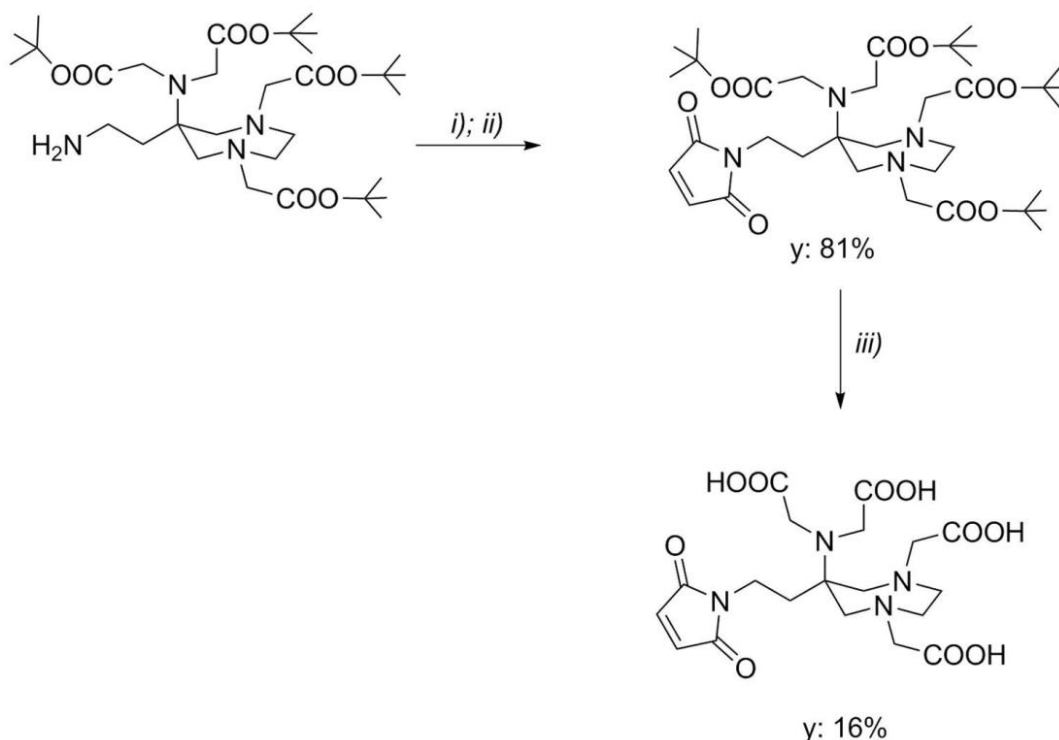


**Figure 2.7: Synthesis scheme of (*t*Bu)<sub>4</sub>-AAZTA-C<sub>2</sub>-maleimide:**

i) Maleic anhydride, CHCl<sub>3</sub>, RT;

ii) Acetic anhydride, 95°C, 2h; iii) TFA:TIS (triisopropylsilane); Overall yield: 13%.

*i-ii*) To a solution of (*t*Bu)<sub>4</sub>-AAZTA-C<sub>2</sub>-NH<sub>2</sub> (80.1 mg, 0.13 mmol) in CHCl<sub>3</sub>, was added 1 equivalent of maleic anhydride. The obtained solution was stirred overnight at RT under inert atmosphere of argon. The solvent was evaporated and the crude product was dissolved in 2 mL of acetic anhydride and 1 equivalent of CH<sub>3</sub>COONa was added. The solution was heated to 95-100°C (the solution became dark) and stirred for 2 hours. The crude product was purified on gravimetric silica chromatography with CH<sub>2</sub>Cl<sub>2</sub>/MeOH 98:2 to afford the pure product, ready for the final cleavage. p: 73 mg; y: 81%.

*iii*) The product obtained from the previous step (73 mg) was dissolved in 2 mL of a solution 95:5 of TFA/TIS and stirred overnight at room temperature. The solvent was evaporated *in vacuo* and the product was precipitated in cold Et<sub>2</sub>O. Final purification was achieved by preparative HPLC by employing an *Atlantis prepD*<sup>®</sup> C18OBD 5 $\mu$ m (19X100 mm) column. Eluent: (A) 0.1% TFA in H<sub>2</sub>O, (B) 0.1% TFA in CH<sub>3</sub>CN. Gradient profile; linear gradient from 5% to 10% of B in 2.84 min, linear gradient from 10% to 25% of B in 2.84 min, isocratic at 25% for 1.16 min, linear gradient from 25% to 50% in 1.66 min, isocratic at 50% for 1.5 min. Flow rate; 20 mL/min. AAZTA-C<sub>2</sub>-maleimide was isolated as a homogenous peak with retention time of 5 min. The solvent was removed *in vacuo* and the product lyophilized from water to give a white solid (8 mg; overall yield: 13%). The purity of the product was checked by analytical HPLC-MS by employing an *Atlantis DC18* 5 $\mu$ m, 4.6X150mm column. Eluent: (A) 0.1% TFA in H<sub>2</sub>O, (B) 0.1% TFA in CH<sub>3</sub>CN. Gradient profile; linear gradient from 5% to 10% of B in 10 min, linear gradient from 10% to 30% of B in 2 min, linear gradient from 30% to 50% of

B in 3 min, linear gradient from 50% to 100% of B in 3 min, isocratic at 100% for 2 min. Flow rate of 1 mL/min and UV detection at 215 nm. RT: 7.52 min. Purity 95%. ESI-MS ( $m/z$ ): calcd: For  $C_{19}H_{26}N_4O_{10}$  ( $M+H$ )<sup>+</sup> 471.44 found: 471.23.

## 2.4 Results and discussions

A novel library of AAZTA derivatives has been synthesized opening more possibilities for proteins and/or peptides functionalization.

The first paragraph (2.3.1) describes how the overall yield of the synthesis of  $(tBu)_4$ -AAZTA-C4-COOH (reported by Manzoni *et al.*) has been raised up modifying the conditions of the last synthesis step (Fig. 2.1, step  $v$ ). The first protocol improvement consists in the substitution of the reaction solvent, and the solution used to adjust the pH before the final liquid/liquid separation: *i*PrOH/H<sub>2</sub>O instead THF as solvent, 1M HCl instead 5M AcOH as pH adjusting solution. No further silica purification has been carried out after the hydrolysis of the methyl group. Final step yield has been increased from 47% to 89%, improving the overall yield from 13% to 24%.

$(tBu)_4$ -AAZTA-C4-CO-NHS (2.3.2) has been obtained with an overall yield of 33%. Synthesis pathway and characterization of AAZTA-C4-CO-MES (2.3.3) has been fully described in Manuscript 2, pag. 131.

Azide AAZTA derivative has been synthesized from  $(tBu)_4$ -AAZTA-C5-OH (Gianolio *et al.*, see 2.3.4). Final product has been obtained with an overall yield of 47%. Final characterizations with HPLC-MS and <sup>1</sup>H-NMR have been carried out to evaluate the purity of the compound.

$(tBu)_4$ -AAZTA-C2-maleimide (2.3.5) has been obtained from  $(tBu)_4$ -AAZTA-C2-NH<sub>2</sub>, another important AAZTA key intermediate, which has been previously synthesized following a confidential BRACCO protocol. Final product has been obtained with 13% overall yield.

## 2.5 Conclusions

In conclusion, five different AAZTA derivatives have been successfully synthesized to be used for biomolecules functionalization. The diversity of the AAZTA side chain functional groups allows the specific reaction with a large range of targeting molecules.

Overall yield and reaction conditions of synthesis step  $v$  of  $(tBu)_4$ -AAZTA-C4-COOH, have been significantly improved for two main reasons: solvent changing and avoiding the final silica purification step. Despite THF is a good solvent, it may cause cancer in animals.<sup>8</sup> We can certainly say that the substitution of this solvent with *i*PrOH/H<sub>2</sub>O could be considered an improvement for human health. Nevertheless, the main difference between the two procedures consists in the *non*-purification after the final hydrolysis. In Manzoni *et al.* protocol, 5M AcOH has been used to adjust the pH. The inconvenient with the use of this acid is its boiling point (118 °C) and the high solubility in organic solvents (i.e. AcOEt, used in the separation process). Some traces of AcOH still remained in the organic phase after separation, so it was very hard to eliminate without a silica purification. The use of an aqueous solution to adjust the pH (1M HCl) allows the avoiding of the final purification step. Furthermore, since

silica has a slightly acidic composition, a big loss of the last carboxylic acid derivative during the purification was the main cause of the very low yield of the last step (47%).

(*tBu*)<sub>4</sub>-AAZTA-C4-COOH has been used as key intermediate for the synthesis of the NHS (2.3.2) and the thioester (2.3.3) derivatives. The NHS derivative can be used for attaching AAZTA to primary amine, largely present as at N-terminal sites of proteins and/or peptides as on lysine residues. Thioester has been used to perform the chemo- and stereo-selective reaction with N-terminal cysteines (see Manuscript 2, pag. 131) based on the Native Chemical Ligation (NCL) approach (see 1.4.2, pag. 33).

Not less important is the azide derivative (2.3.4) very appealing compound for coupling reactions performed in the field of "Click" chemistry (e.g. azide-alkyne).

Maleimide AAZTA (2.3.5) can be considered a very important intermediate because of the selective reaction between maleimide and thiol. Maleimide reacts with sulfidriols forming a strong, irreversible thioether linkage.<sup>9</sup> It can be used to conjugate scaffolds such as peptides/proteins/Abs which expose a cysteine residue.

1. M. Danese, M. Bon, G. Piccini and D. Passerone, *Phys Chem Chem Phys*, 2019, **21**, 19281-19287.
2. K. Renault, J. W. Fredey, P. Y. Renard and C. Sabot, *Bioconjug Chem*, 2018, **29**, 2497-2513.
3. L. Manzoni, L. Belvisi, D. Arosio, M. P. Bartolomeo, A. Bianchi, C. Brioschi, F. Buonsanti, C. Cabella, C. Casagrande, M. Civera, M. De Matteo, L. Fugazza, L. Lattuada, F. Maisano, L. Miragoli, C. Neira, M. Pilkington-Miksa and C. Scolastico, *ChemMedChem*, 2012, **7**, 1084-1093.
4. P. Minazzi, L. Lattuada, I. G. Menegotto and G. B. Giovenzana, *Org Biomol Chem*, 2014, **12**, 6915-6921.
5. Z. Wu, Z. Zha, S. R. Choi, K. Plössl, L. Zhu and H. F. Kung, *Nucl Med Biol*, 2016, **43**, 360-371.
6. E. Gianolio, G. B. Giovenzana, A. Ciampa, S. Lanzardo, D. Imperio and S. Aime, *ChemMedChem*, 2008, **3**, 60-62.
7. D. Fles, R. Vukovic, A. E. Kuzmic, G. Bogdanic, V. Pilizota, D. Karlovic, K. Markus, K. Wolsperger and V.-T. Drazen, *Croat Chem Acta*, 2003, **76**, 69-74.
8. R. S. Chhabra, R. A. Herbert, J. H. Roycroft, B. Chou, R. A. Miller and R. A. Renne, *Toxicol Sci*, 1998, **41**, 183-188.
9. B. H. Northrop, S. H. Frayne and U. Choudhary, *Polym. Chem.*, 2015, **6**, 3415-3430.

## 2.5 Supporting information

XTerraC8 anal H2O-CH3CN TFA

ihg15pureaaztacoh 62 (10.352) Cm (61.66)

1: Scan ES+  
3.19e7

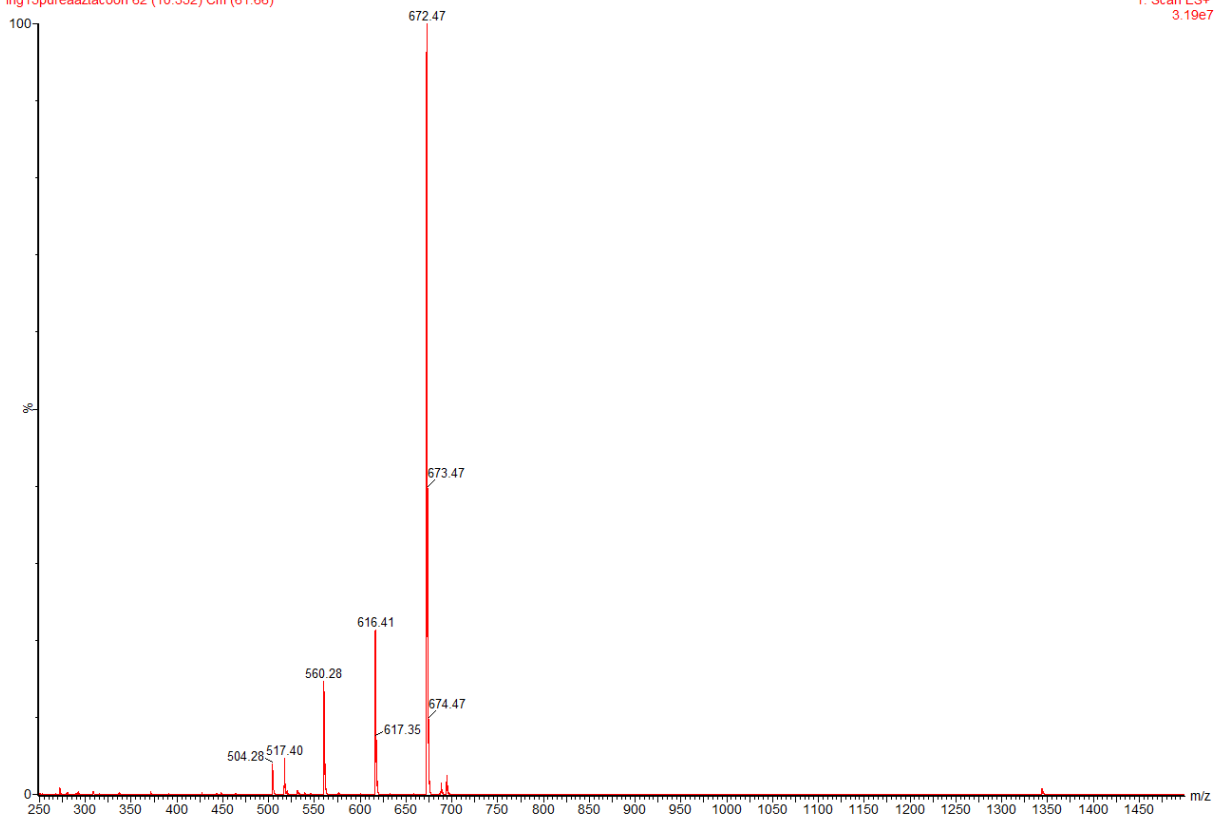


Figure S2.1: Mass spectrum of  $(tBu)_4$ -AAZTA-C4-COOH (2.3.1).

XTerraC8 anal H2O-CH3CN TFA

ihg23pureaaztanhs

2: Diode Array  
254  
Range: 1.638e-2  
Area, Height

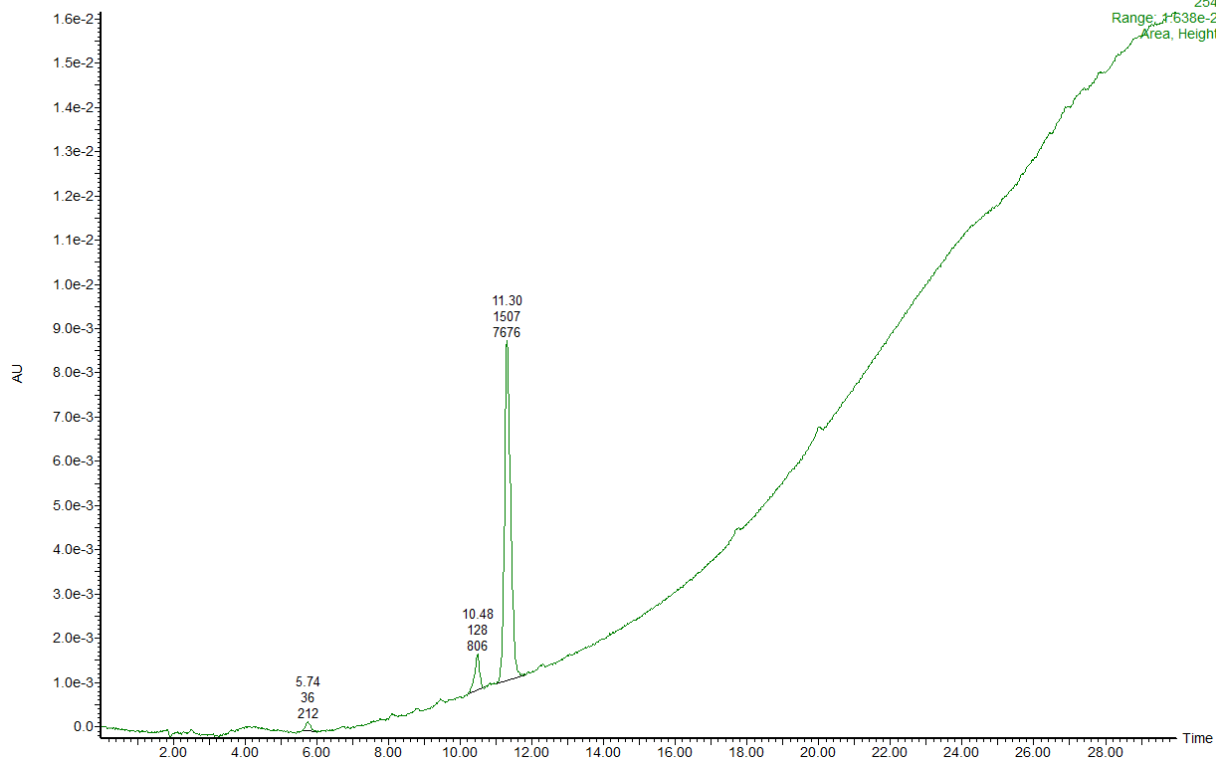


Figure S2.2: HPLC chromatogram revealed at 254 nm of pure  $(tBu)_4$ -AAZTA-C4-CO-NHS (2.3.2).

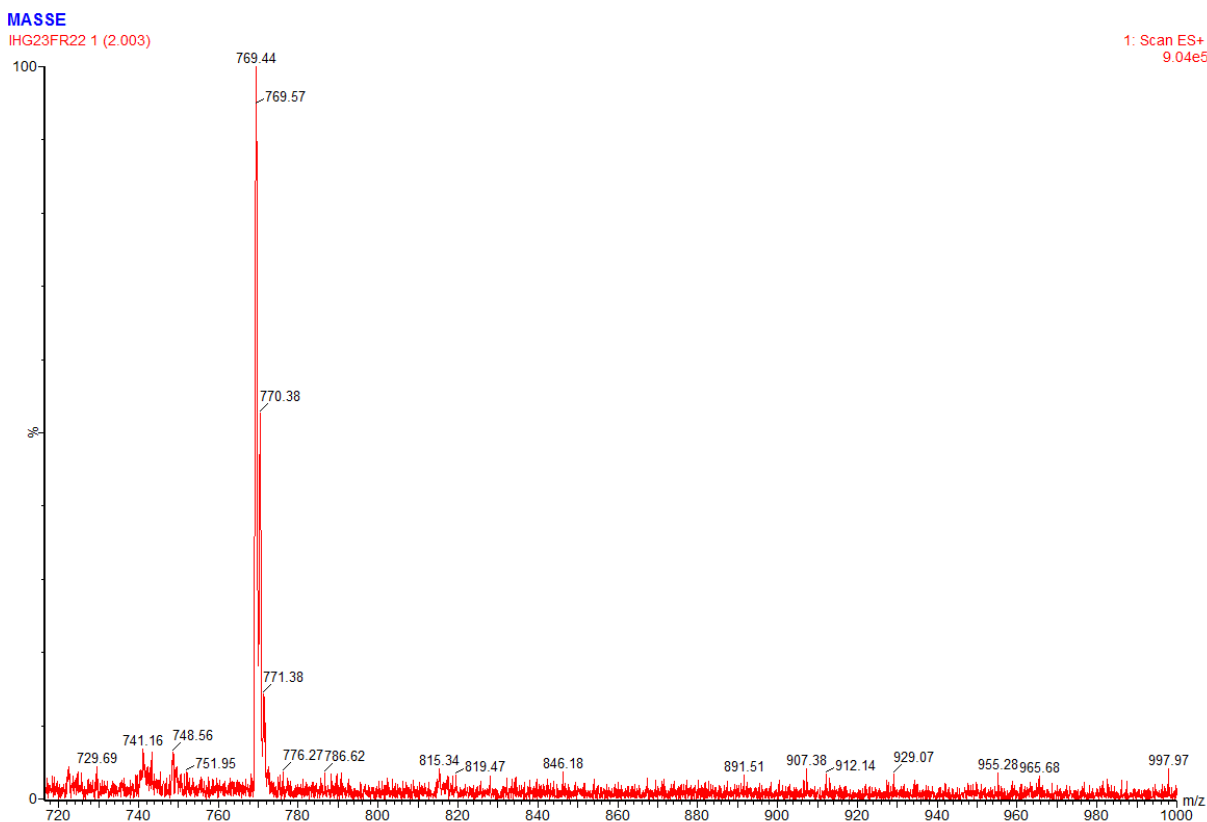


Figure S2.3: Mass spectrum of pure (tBu)<sub>4</sub>-AAZTA-C4-CO-NHS (2.3.2).

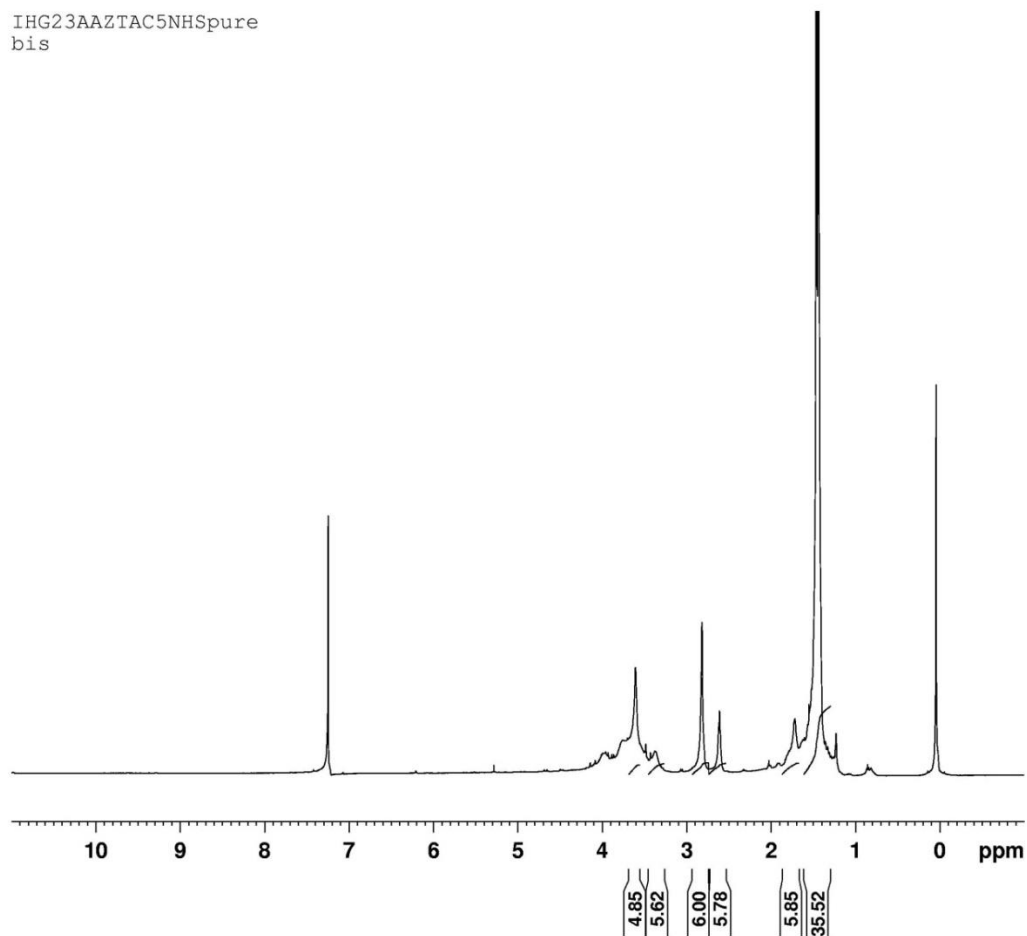


Figure S2.4: <sup>1</sup>H-NMR spectrum of (tBu)<sub>4</sub>-AAZTA-C4-CO-NHS (2.3.2).



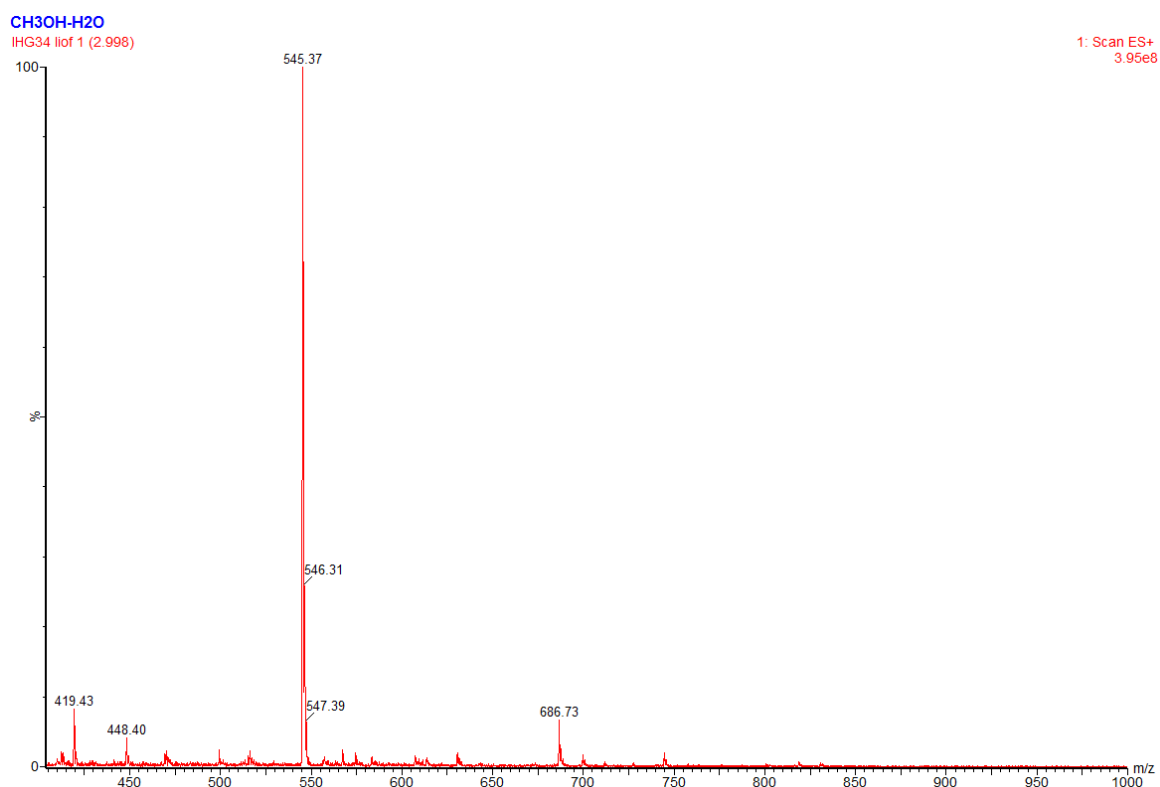


Figure S2.5:  $^1\text{H}$ -NMR spectrum of AAZTA-C4-CO-NHS (2.3.2).



Figure S2.6: Mass spectrum of pure  $(t\text{Bu})_4\text{-AAZTA-C5-N}_3$  (2.3.3).

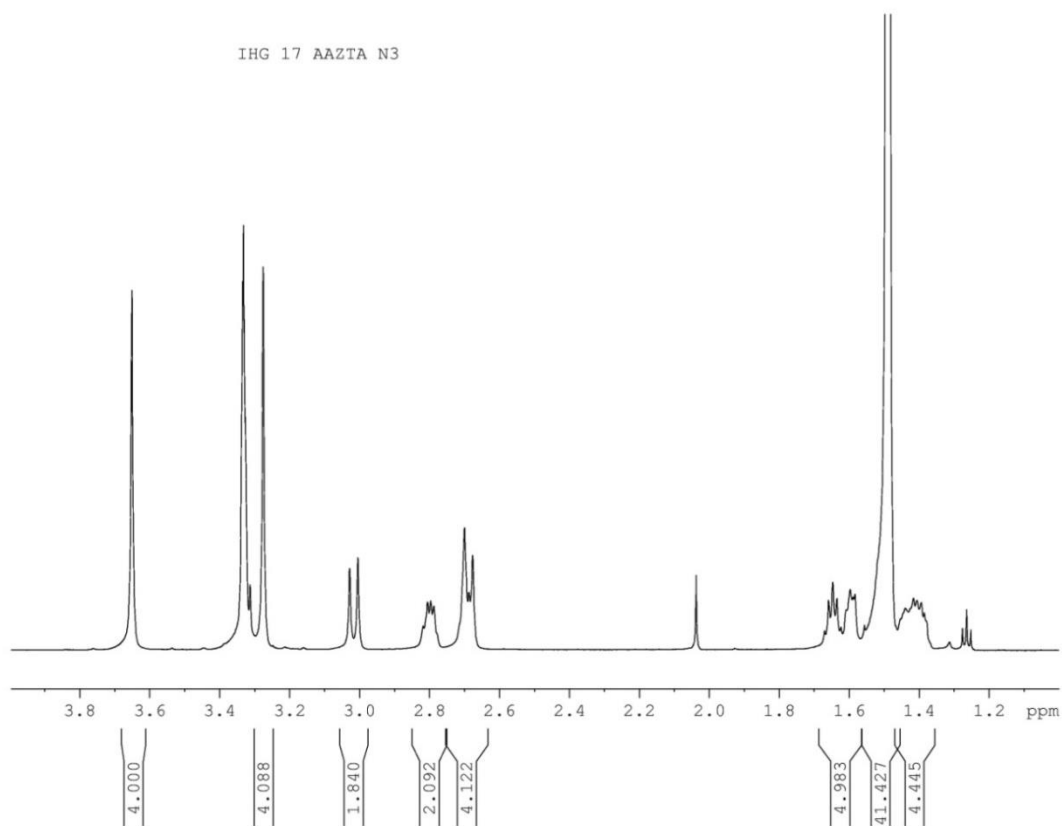


Figure S2.7:  $^1\text{H}$ -NMR spectrum of  $(t\text{Bu})_4\text{-AAZTA-C5-N}_3$  (2.3.4).

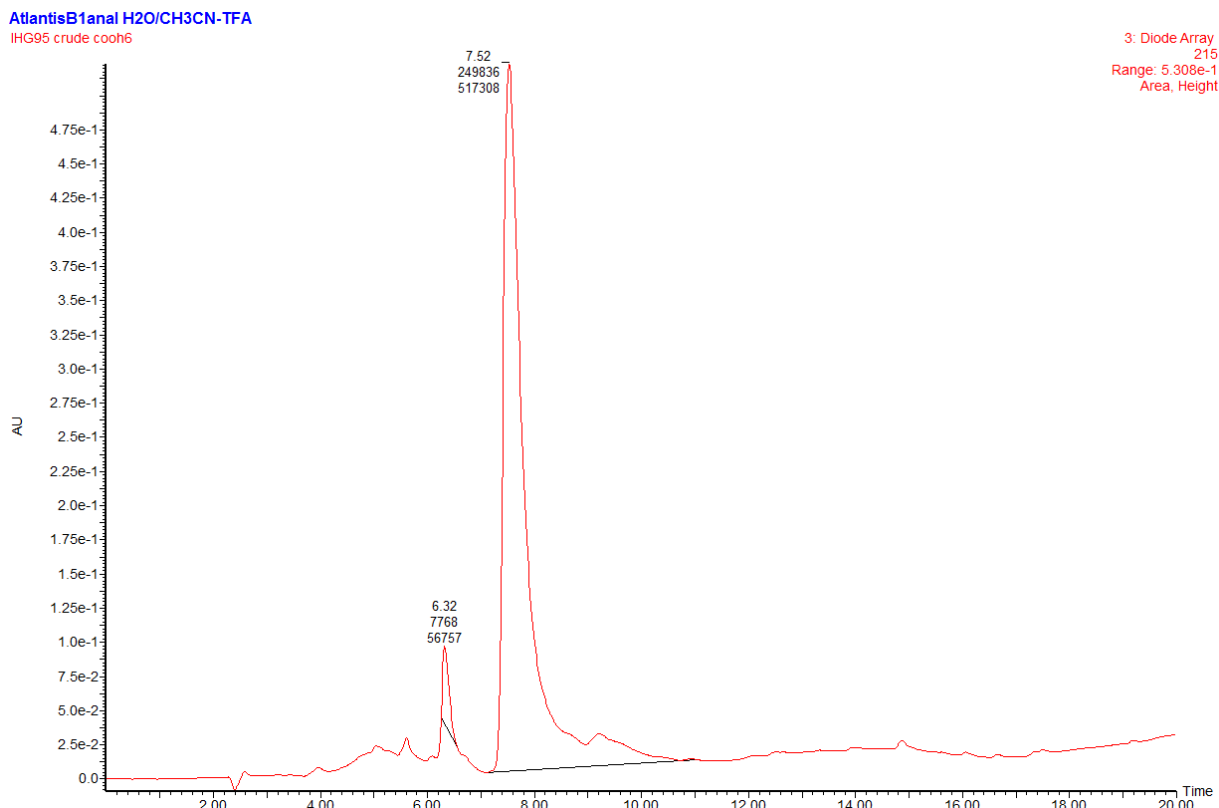


Figure S2.8: HPLC chromatogram revealed at 215 nm of pure AAZTA-C2-Maleimide (2.3.5).

AtlantisC18prep H2O-TFA

IHG95 PREP5 246 (5.168) Cm (245.254)

1: Scan ES+  
2.09e7

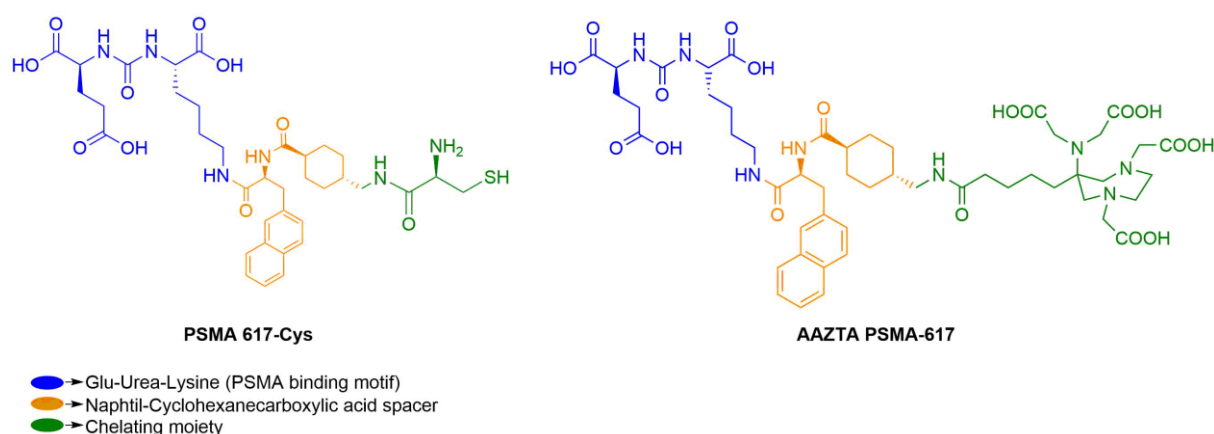


Figure S2.9: Mass spectrum of pure AAZTA-C2-Maleimide (2.3.5).

### III. DESIGN AND SYNTHESIS OF NOVEL PSMA DERIVATIVES

#### 3.1 Purpose

In this chapter, the design and synthesis of novel PSMA derivatives will be described. Two different PSMA derivatives have been successfully synthesized, obtaining two new imaging probes which can be used in diagnosis of prostate cancer by PET and SPECT imaging techniques. As anticipated in Chapter I, paragraph 1.5.1, a thiol-urea based scaffold has been selected for this purpose (Glu-Urea-Lysine) because of his extended literature reported activity in the detention of PSMA. Based on Benesova et al SAR (Structure-Activity relationship) studies, a naphthyl-cyclohexanecarboxylic acid spacer has been chosen to improve the inhibitory activity to the PSMA receptor. The following paragraphs will show synthesis methodologies and characterizations.



**Figure 3.1:** Chemical structures of PSMA derivatives.

#### 3.2 Materials and Methods

9-Fluorenylmethoxycarbonyl (Fmoc), tert-butyloxycarbonyl (Boc) protected amino acids and 2-Chlorotrytil Chloride Resin, 2-(1H-benzotriazol-1-yl)-1,1,3,3-tetramethyluronium hexafluorophosphate (HBTU), N,N-Diisopropylethylamine (DIPEA) and Hexafluoroisopropanol (HFIP) were purchased from IRIS Biotech (Marktredwitz, Germany) and Sigma Aldrich (Darmstadt, Germany). All solvents were purchased by VWR International (Radnor, USA) and were used without further purifications. NMR spectra were recorded at 303 K on a Bruker AVANCE 600 spectrometer. Mass spectra with electrospray ionization (ESI) were recorded on a SQD 3100 Mass Detector (Waters). The HPLC-MS preparative analysis were carried out on a Waters AutoPurification system (3100 Mass Detector, 600 Quaternary Pump Gradient Module, 2767 Sample Manager and 2487 UV/Visible Detector). Analytical HPLC analyses were performed using a Waters 2695 Alliance Separation Module equipped with a Waters 2998 Photodiode Array Detector.

(*tBu*)<sub>4</sub>-AAZTA-C4-COOH was synthesized in accordance with Manzoni *et al.* protocol.<sup>1</sup> PSMA binding motif was synthesized following Maresca *et al.* protocol.<sup>2</sup>

### 3.3 Experimental synthesis procedures

#### 3.3.1 PSMA 617-Cys

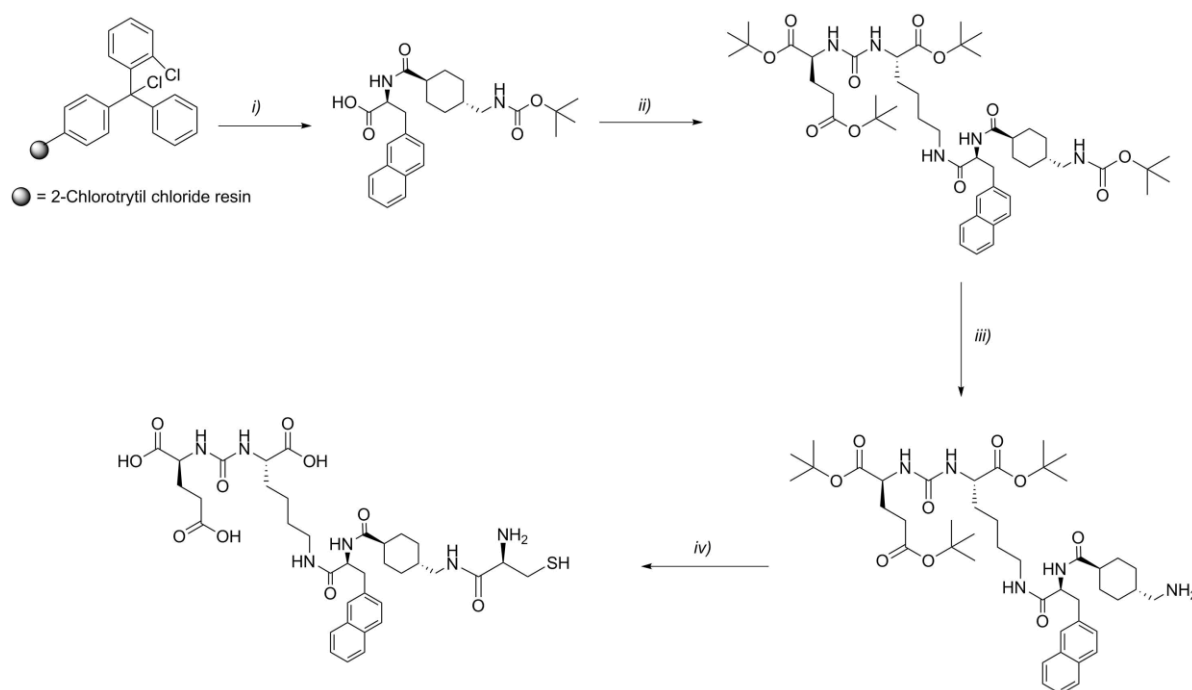


**Figure 3.2: Synthesis scheme of PSMA 617-Cys:**

*i)* Fmoc-L-2NaI-OH, DIPEA, CH<sub>2</sub>Cl<sub>2</sub>/DMF/Piperidine 4:1; Boc-4-Amc-OH, DIPEA, HBTU, DMF; HFIP/DCM 1:4; *ii)* PSMA binding motif, HBTU, DIPEA; *iii)* TFA/CH<sub>2</sub>Cl<sub>2</sub>, 1h, 0°C. *iv)* Boc-Cys(trt)-OH, HATU, DIPEA; TFA/TIS.

*i)* 200 mg of a 2-Chlorotrytyl chloride resin (loading 1.22 mmol/g) were pre-swelled into a SPPS manual reactor vessel with 10 mL of methylene chloride (CH<sub>2</sub>Cl<sub>2</sub>) during 30 min. The first Fmoc protected amino acid (AA) (Fmoc-L-2NaI-OH) was loaded on the resin during 2.5 h (2 eq, 0.488 mmol, 213.5 mg) with 3 eq. of DIPEA (128 μL). After the anchoring of the first AA, the resin was end-capped with a solution of Methanol/DIPEA 6:1 during 30 min (3 mL). The resin was washed with dimethylformamide (DMF), and the cleavage solution was added to the reactor vessel (piperidine:DMF 1:4) and stirred for 30 minutes. The resin was washed with DMF and the second AA was added to the reactor vessel (Boc-4-Amc-OH, 2 eq, 125.6 mg, 0.488 mmol) with 4 eq. of DIPEA (170 μL) and 1.8 eq of HBTU (166.6 mg, 0.439 mmol). After two hours, the resin was washed with DMF and the fully protected peptide was cleaved from the resin with a solution of HFIP(hexafluoro-2-propanol)/CH<sub>2</sub>Cl<sub>2</sub> 1:4 for 5 minutes. The solvent was evaporated *in vacuo* and the product was used for the next step without further purification (white solid).

*ii)* The compound obtained from the previous step was dissolved in CH<sub>2</sub>Cl<sub>2</sub> and DIPEA (3 eq, 128 μL) and HBTU (0.9 eq., 83 mg) were added to the solution. Then a solution of PSMA binding motif<sup>2</sup> (1 eq, 119 mg) was added to the solution and the reaction was stirred overnight at room temperature. The solvent was evaporated and the crude product was purified by silica gravimetric chromatography with CH<sub>2</sub>Cl<sub>2</sub>→CH<sub>2</sub>Cl<sub>2</sub>/Methanol 95:5 to afford the pure intermediate as a pale yellow oil (82.7 mg).

*iii*) The compound obtained from the previous step was dissolved in 3 mL of CH<sub>2</sub>Cl<sub>2</sub> at 0°C. 300 µL of trifluoroacetic acid (TFA) were added dropwise and the reaction was stirred for 1 h at 0°C. 10 mL of sat. NaHCO<sub>3</sub> were added to the solution and the product was extracted with CHCl<sub>3</sub>. The solvent was evaporated to obtain the fully protected product with a free primary amine on the *N*-terminal position of the 4-Acm-OH AA.

*iv*) In a round bottom flask 41.5 mg of Boc-Cys(trt)-OH were dissolved in CH<sub>2</sub>Cl<sub>2</sub> and 3 eq of DIPEA and 1 eq of HBTU were added to the solution. Then a solution of the compound obtained from the previous step in CH<sub>2</sub>Cl<sub>2</sub> was added to the Boc-Cys(trt)-OH solution and the reaction was stirred overnight at room temperature. The solution was washed three times with water, then the solvent was evaporated and the product re-dissolved in a solution of TFA/triisopropylsilane 95:5 (4 mL). The reaction was stirred overnight at room temperature. The solvent was evaporated and the crude product precipitated with cold Et<sub>2</sub>O.

The final product was purified by preparative HPLC by employing an Atlantis prepD<sup>®</sup> C18 OBD 5 µm (19X100 mm) column. Eluent: (A) 0.1% TFA in H<sub>2</sub>O, (B) 0.1% TFA in CH<sub>3</sub>CN. Gradient profile: isocratic at 25% of B for 5.69 min, linear gradient from 25% to 37.5% of B in 2.85 min, linear gradient from 37.5% to 100% in 1.70 min, isocratic at 100% of B for 1.8 min. Flow rate: 20 mL/min. PSMA 617-Cys was isolated as a homogenous peak with retention time of about 9 min. All fractions containing the final product are collected, evaporated and lyophilized to give PSMA 617-Cys as a white solid. The purity of the product was monitored by analytical HPLC using an Atlantis DC18 5 µm (4.6X150 mm) column. Gradient profile: isocratic at 25% of B for 1 minute, linear gradient from 25% to 32% of B in 16 minutes, isocratic at 32% of B for 6 minutes, linear gradient from 32% to 90% of B in 1 minute, isocratic at 90% of B for 4 minutes, linear gradient from 90% to 100% of B in 1 minute, isocratic at 100% of B for 1 minute. Flow rate; 1 mL/min; λ: 254 nm. RT: 9.32 min. HPLC Purity: 99%. p: 12.3 mg, overall yield: 7%. ESI-MS (*m/z*): calcd: For C<sub>36</sub>H<sub>51</sub>N<sub>6</sub>O<sub>10</sub>S (*M/Z*)<sup>+</sup> 759.89 found: 759.28. <sup>1</sup>H-NMR (DMSO-*d*<sub>6</sub>, 600 MHz): δ 0.85 (m, 3H), 0.88 (t, 1H), 1.06 (m, 1H), 1.18 (m, 2H), 1.34 (m, 2H), 1.41 (d, 2H, J= 5.7 Hz), 1.50 (m, 2H), 1.66 (m, 4H), 1.93 (m, 1H), 2.10 (m, 2H), 2.28 (m, 2H), 3.02 (m, 5H), 4.03 (m, 1H), 4.10 (m, 1H), 4.55 (m, 1H), 6.30 (m, 2H), 7.40 (d, 1H, J= 8.5 Hz), 7.46 (m, 2H), 7.69 (s, 1H), 7.79 (t, 2H, J= 8.4 Hz), 7.86 (d, 1H, J= 7.8 Hz).

### 3.3.2 AAZTA PSMA 617

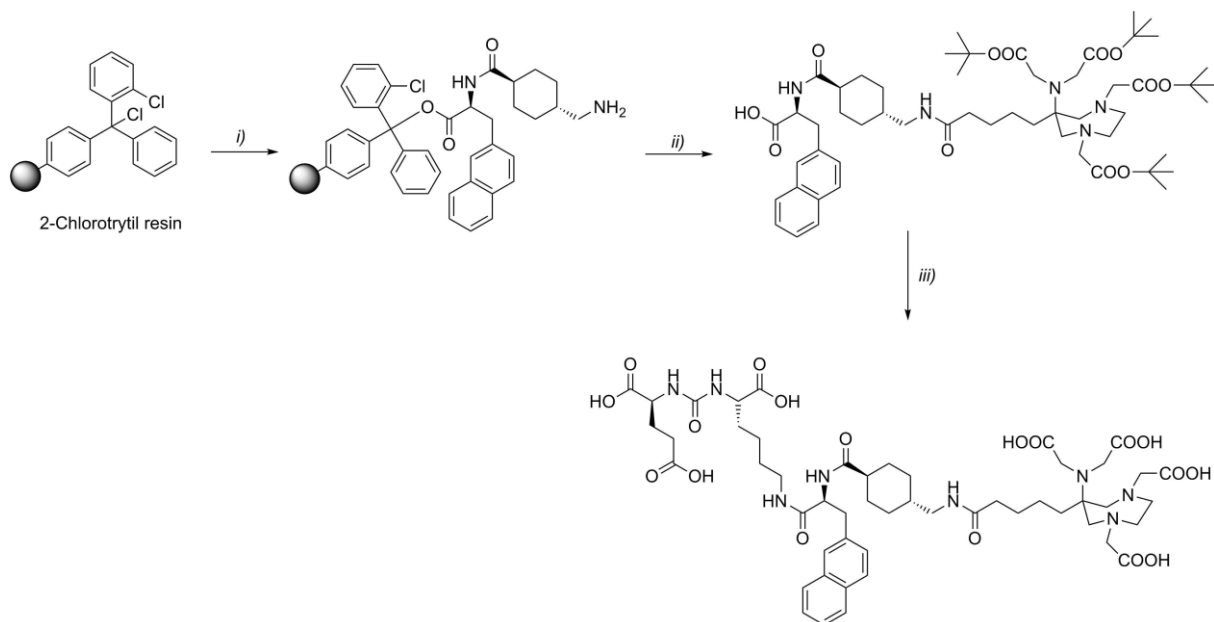


**Figure 3.3: Synthesis scheme of AAZTA-PSMA 617:**

*i)* Fmoc-L-2-Nal-OH, DIPEA, CH<sub>2</sub>Cl<sub>2</sub>; MeOH/DIPEA 3:0.5; DMF/Piperidine 4:1; *ii)* Fmoc-4-Amc-OH, DIPEA, HBTU, DMF; DMF/Piperidine 4:1; *iii)* (tBu)<sub>4</sub>-AAZTA-C4-COOH, HBTU, DIPEA, DMF; HFIP, CH<sub>2</sub>Cl<sub>2</sub>; PSMA-binding motif, DIPEA, CH<sub>2</sub>Cl<sub>2</sub>; TFA/TIS 95/5.

*i)* 400 mg of a 2-Chlorotrytil chloride resin (loading 1.63mmol/g) were pre-swelled with 10 mL of CH<sub>2</sub>Cl<sub>2</sub> for 10 minutes. The first Fmoc protected AA (Fmoc-L-2-Nal-OH) was loaded on the resin during 2.5 h (2 eq, 1.304mmol, 570.6 mg) with 3 eq. of DIPEA (341 uL). After the anchoring of the first AA, the resin was end-capped with a solution of MeOH/DIPEA 3:0.5 for 30 minutes (10 mL). The resin was washed with DMF, and the cleavage solution was added to the reactor (piperidine:DMF 1:4) and stirred for 30 minutes. The resin was washed with DMF and the second AA was added to the reactor (Fmoc-4-Amc-OH, 2 eq, 494.8 mg, 1.304mmol) with 3 eq. of DIPEA (341uL) and 1.6eq of HBTU (395.6 mg, 1.043mmol). After two hours, the resin was washed with DMF.

*ii)* (tBu)<sub>4</sub>-AAZTA-C4-COOH (1.5 eq, 657 mg, 0.978 mmol) was added to the reactor with 3 eq. of DIPEA (341 uL) and 1.2 eq. of HBTU (296.9 mg, 0.78 mmol). After 2 h the resin was washed with DMF, CH<sub>2</sub>Cl<sub>2</sub>, Et<sub>2</sub>O and the fully protected peptide was cleaved from the resin with a solution of HFIP/CH<sub>2</sub>Cl<sub>2</sub> 1:4 for 5 minutes. The solvent was evaporated *in vacuo* and the product was used for the next step without further purification (797 mg, white solid).

*iii)* The compound obtained from the previous step was dissolved in CH<sub>2</sub>Cl<sub>2</sub> and DIPEA (8 eq; 0.9 mL) and HBTU (0.9 eq; 222.5 mg) were added to the solution. Then a solution of PSMA binding motif (1 eq; 318 mg; 0.652 mmol) was added to the solution and the reaction was stirred overnight at room temperature. The solvent was evaporated and the crude product was purified by silica gravimetric direct phase chromatography with CH<sub>2</sub>Cl<sub>2</sub>/MeOH 98:2 → CH<sub>2</sub>Cl<sub>2</sub>/MeOH 7:3 to afford the pure product as pale yellow oil (423 mg). The totally protected pure product was dissolved in 10 mL of TFA/TIS 95:5 and stirred overnight at room temperature. The solvent was evaporated and the product precipitated in cold Et<sub>2</sub>O to obtain the crude product.

The product was purified by preparative HPLC by employing an Atlantis prepD<sup>®</sup>C18OBD 5 $\mu$ m (19X100 mm) column. Eluent: (A) 0.1% TFA in H<sub>2</sub>O, (B) 0.1% TFA in CH<sub>3</sub>CN. Gradient profile; isocratic at 25% of B for 8.58 min, linear gradient from 25% to 80% of B in 2.84 min, linear gradient from 80% to 100% in 0.58 min, isocratic at 100% of B for 1.8 min; Flow rate; 20 mL/min. AAZTA PSMA was isolated as a homogenous peak with retention time of ca 8 min. The purity of the product was monitored by analytical HPLC using the same gradient profile and solvent mixtures as above but with Atlantis DC18 5 $\mu$ m (4.6X150mm) column. Flow rate of 1 mL/min and UV detection at 230 nm. The TFA was removed by a desalting process on AKTA purifier with a Mono S HR 5/5 packed with XAD1600D resin; Eluent: (A) H<sub>2</sub>O, (B) CH<sub>3</sub>CN. Gradient profile; isocratic at 16% of B for 5 min, linear gradient from 16% to 100% of B in 5 min, isocratic at 100% of B for 5 min. Flow rate: 0.5 mL/min. The fractions containing the pure product were evaporated *in vacuo* and lyophilized from water to give a white solid. HPLC Purity: 97%. ESI-MS (*m/z*): calcd: For C<sub>51</sub>H<sub>72</sub>N<sub>8</sub>O<sub>18</sub> (M/Z)<sup>+</sup>1085.18 found: 1085.46; for C<sub>51</sub>H<sub>72</sub>N<sub>8</sub>O<sub>18</sub> (M+2H)<sup>2+</sup>543.59 found: 543.26. <sup>1</sup>H-NMR (CDCl<sub>3</sub>, 600 MHz):  $\delta$  0.82 (tr, 3H), 1.06 (t, J<sub>1</sub>=12.6 Hz, J<sub>2</sub>=12.8 Hz, 1H), 1.29 (tr, 13H), 1.49 (tr, 2H), 1.68 (tr, 5H), 1.93 (tr, 1H), 2.04 (t, J=7.5 Hz, 1H), 2.25 (tr, 3H), 2.85 (t, J=5.81 Hz, 2H), 2.96 (tr, 2H), 3.05 (tr, 1H), 3.11 (dd, 1H), 3.21 (s, 2H), 3.44 (s, 3H), 3.61 (s, 3H), 3.77 (s, 3H), 4.03 (tr, 1H), 4.12 (q, J<sub>1</sub>=5.34, J<sub>2</sub>= 8.06, 1H), 4.11 (q, J<sub>1</sub>=5.34, J<sub>2</sub>=8.06, 1H), 4.54 (q, J<sub>1</sub>=5.45, J<sub>2</sub>=8.57, 1H), 6.29 (tr, 1H), 7.46 (quint, J<sub>1</sub>= 8.84, J<sub>2</sub>=15.91, 2H), 7.69 (s, 1H), 7.79 (t, J=7.82, 2H), 7.85 (d, J=7.82, 1H). AAZTA-PSMA (3):63.6 mg. Overall yield: 9%.

### 3.4 Results and discussions

PSMA 617-Cys and AAZTA-PSMA 617 have been obtained respectively with 7% and 9% of overall yield and 99% and 97% of HPLC purity. The first step of both syntheses have been performed in a manual reaction vessel for SPPS, following a Fmoc protocol (1.6.1). A 2-chlorotrytil chloride resin has been used for the loading of the first AA (Fmoc-L-2Nal-OH) pre-dissolved in CH<sub>2</sub>Cl<sub>2</sub>. After a deprotection of the Fmoc group, the second AA (Boc-4-Amc-OH for PSMA 617-Cys and Fmoc-4-Amc-OH for AAZTA-PSMA 617) was anchored to the first AA. From this point the syntheses have followed two different ways. Regarding the PSMA 617-Cys, the dimer was cleaved from the resin maintaining the Boc protection on the second AA with a solution 1:4 of HFIP/CH<sub>2</sub>Cl<sub>2</sub>. After the coupling with PSMA binding motif, the totally protected intermediate obtained from the second step, has been successfully purified on a gravimetric silica column eluted with a gradient of CH<sub>2</sub>Cl<sub>2</sub>/MeOH (100:0 to 95:5). In the third step, the Boc protecting group has been selectively removed with a controlled cleavage with TFA/TIS at 0°C. In the fourth and last synthesis step, the trityl-protected cysteine has been attached to the product obtained from the previous step, in presence of HBTU as activator and DIPEA as base. After last total deprotection carried out with TFA/TIS, the product was purified with a preparative HPLC-MS to afford the pure PSMA 617-Cys. Coming back to AAZTA-PSMA 617, the second Fmoc-protected AA have been linked to the first one, attached during the resin loading. The Fmoc group was removed with the de-block solution (DMF/piperidine) and the reaction with (*tBu*)<sub>4</sub>-AAZTA-C4-COOH has been carried out in the manual reaction vessel for SPPS in presence of HBTU and DIPEA. As done with PSMA 617-Cys, a solution of HFIP/CH<sub>2</sub>Cl<sub>2</sub> has been used to mildly remove the compound from the solid support, avoiding the deprotection of the AAZTA *tBu* protecting groups. After the coupling of the PSMA binding motif, a silica gravimetric purification (CH<sub>2</sub>Cl<sub>2</sub>/MeOH from 98:2 to 7:3) and a subsequent deprotection with TFA and purification by preparative HPLC-MS, AAZTA-PSMA 617 has been efficiently obtained.



### 3.5 Conclusions

A synthetic strategy to easily obtain two different PSMA derivatives have been described. The combination of solid phase synthesis and solution chemistry allows the achievement of the purpose, performing just 2 purifications during all synthesis pathway: the first one on gravimetric silica chromatography (direct phase) and the second one on a preparative HPLC chromatographic system (reverse phase). Both product can be directly use as "cold" kit, which allow the subsequent complexation with PET or SPECT radionuclides. Specifically, AAZTA-PSMA 617 have been efficiently labeled with Scandium-44 and tested *in vivo* as reported in Manuscript 1, pag.107. Otherwise, PSMA 617-cys have been efficiently labeled with <sup>99m</sup>Tc as reported in patent N°WO2018109164.

1. L. Manzoni, L. Belvisi, D. Arosio, M. P. Bartolomeo, A. Bianchi, C. Brioschi, F. Buonsanti, C. Cabella, C. Casagrande, M. Civera, M. De Matteo, L. Fugazza, L. Lattuada, F. Maisano, L. Miragoli, C. Neira, M. Pilkington-Miksa and C. Scolastico, *ChemMedChem*, 2012, **7**, 1084-1093.
2. K. P. Maresca, S. M. Hillier, F. J. Femia, D. Keith, C. Barone, J. L. Joyal, C. N. Zimmerman, A. P. Kozikowski, J. A. Barrett, W. C. Eckelman and J. W. Babich, *J Med Chem*, 2009, **52**, 347-357.

### 3.5 Supporting information

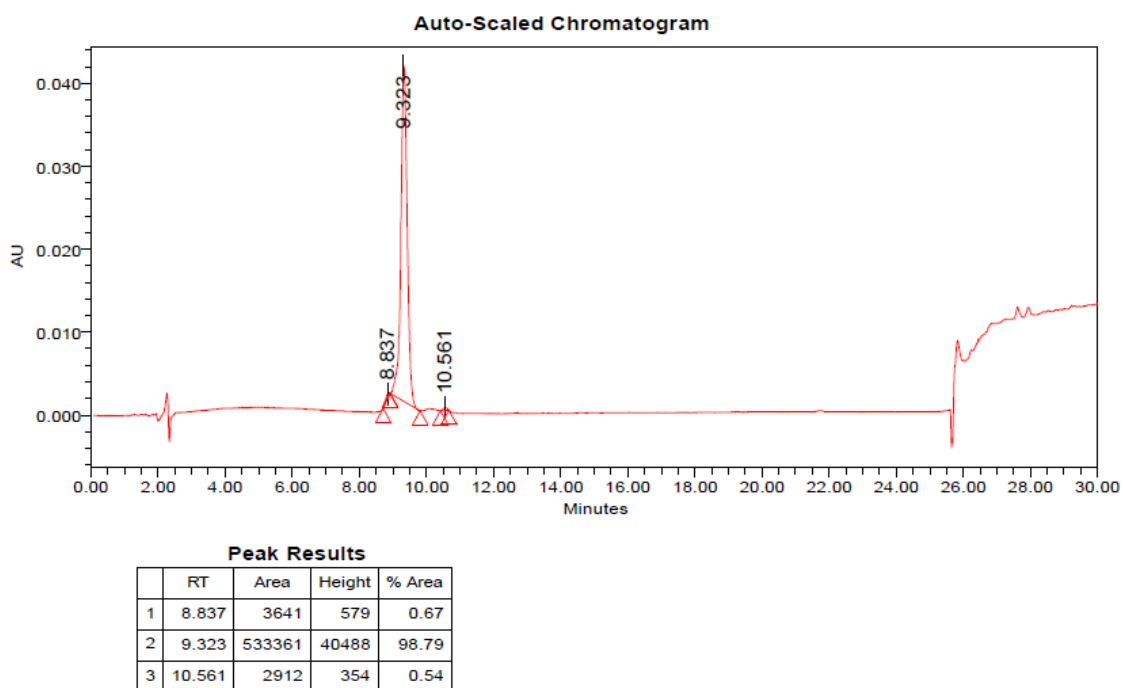


**Figure S3.1:** HPLC chromatogram revealed at 254 nm of pure PSMA 617-Cys.

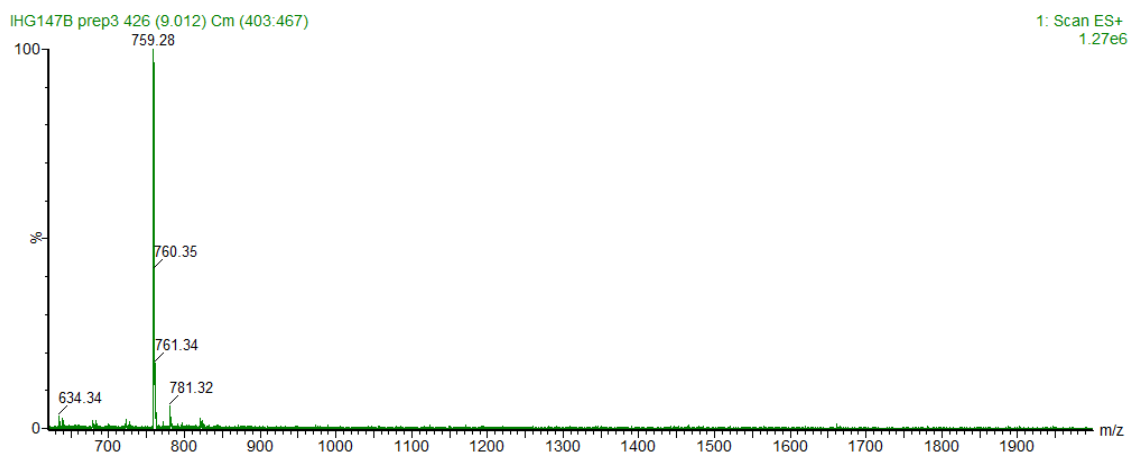


**Figure S3.2:** Mass spectrum of the collected peak during preparative HPLC purification of compound PSMA 617-Cys.

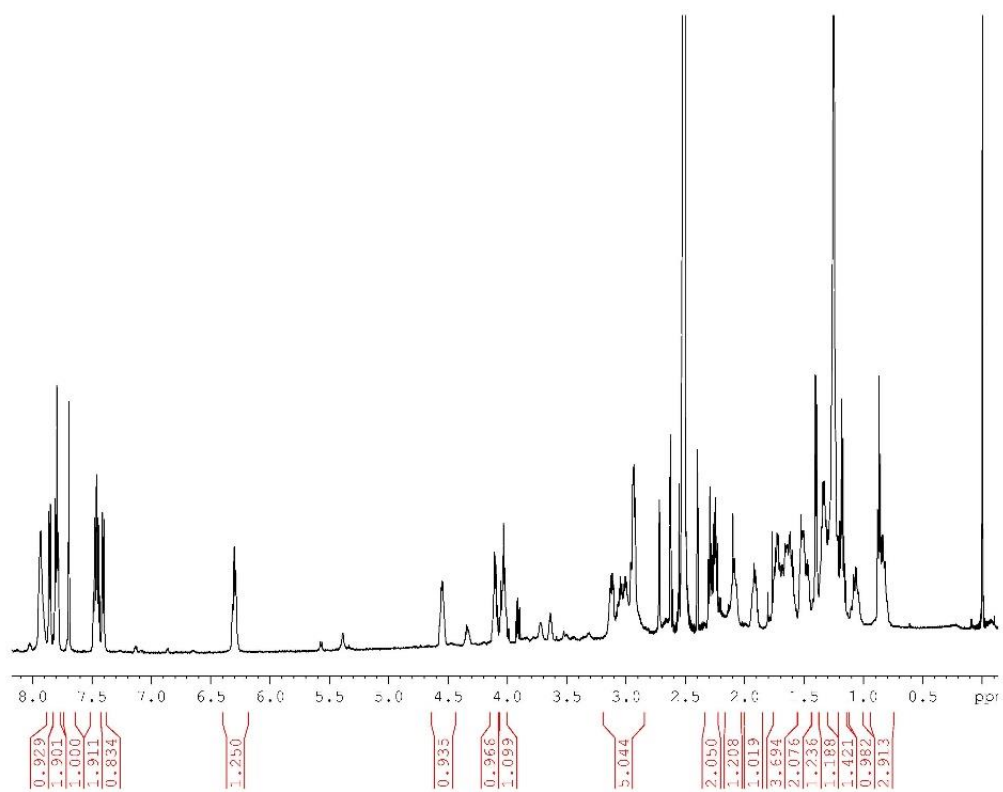


**Figure S3.3:**  $^1\text{H}$ -NMR spectrum in DMSO- $d_6$  at 303K of the pure PSMA 617-Cys.

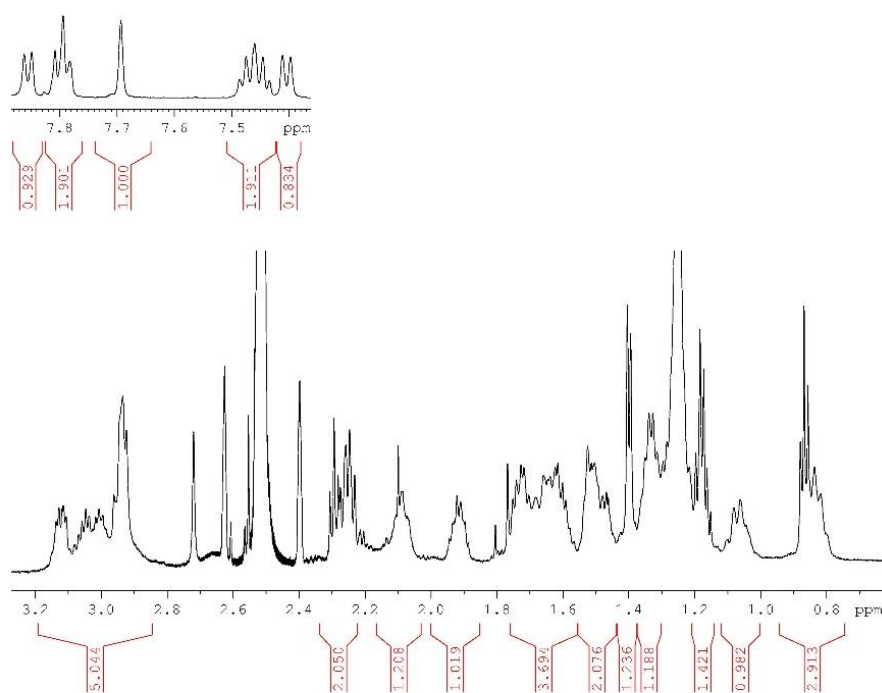
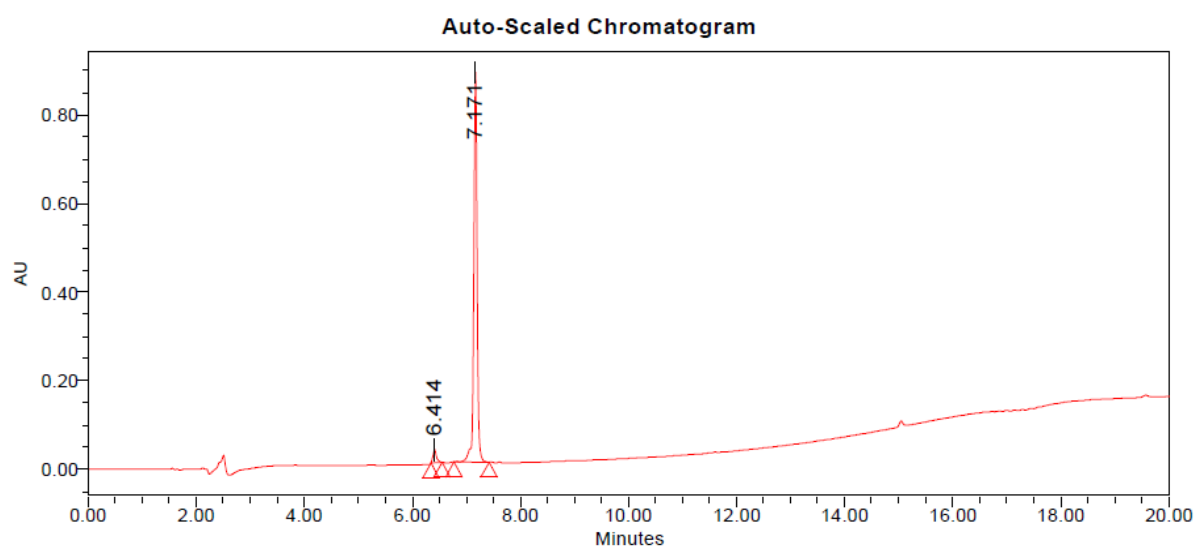


**Figure S3.4:** Expanded  $^1\text{H}$ -NMR spectrum in DMSO- $d_6$  at 303K of the pure PSMA 617-Cys.



**Peak Results**

	RT	Area	Height	% Area
1	6.414	134470	29908	3.39
2	7.171	3836591	880760	96.61

**Figure S3.5:** HPLC chromatogram revealed at 254 nm of pure AAZTA-PSMA 617.

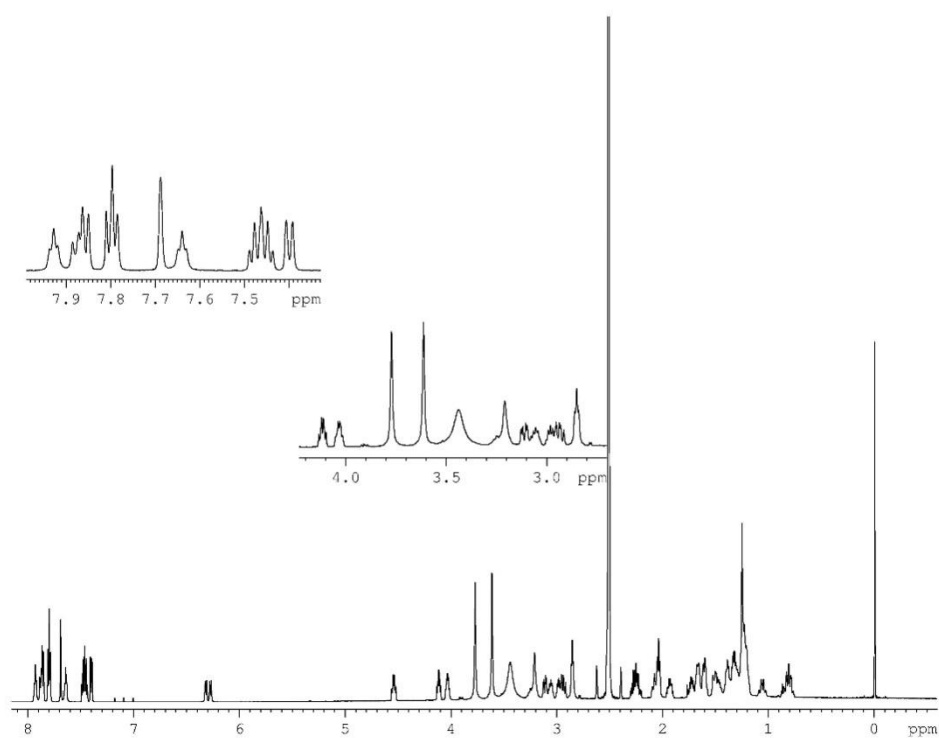
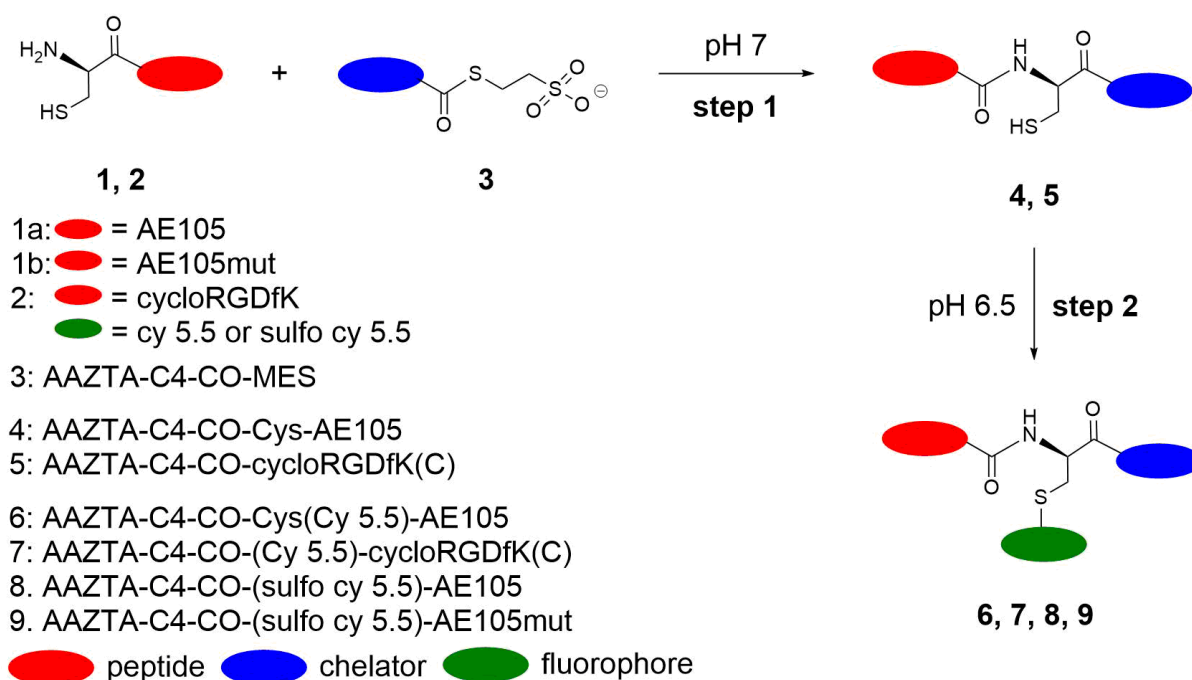


**Figure S3.6:**  $^1\text{H}$ -NMR spectrum in DMSO- $d_6$  at 303K of the pure AAZTA-PSMA 617.

## IV. DESIGN, SYNTHESIS AND *IN VITRO/IN VIVO* EVALUATIONS OF NEW DUAL PET/OI PROBES

### 4.1 Purpose

The aim of this chapter was to synthesize novel targeting AAZTA dual PET/OI probes which include the possibility of labeling with gallium-68 to acquire PET images and a fluorescent dye (i.e. cy 5.5, sulfo cy 5.5) to allow tumor visualization during surgical removal of the mass. To obtain the final products, the synthesis strategy has been developed following an innovative approach based on Native Chemical Ligation (NLC, see paragraph 1.4.2) as shown in scheme 1.



**Scheme 4.1:** General synthesis scheme of the dual labelled peptide based probes: step (1) phosphate buffer pH 7.4, 5 M imidazole, 3 M guanidinium chloride, 50mMTCEP, 1 h, RT; step (2) (sulfo) cy 5.5maleimide, acetate pH 6.5, 3 h, RT.

Synthesis of uPAR antagonist peptide and its corresponding control (AE105 and AE105mut) will be described in the next paragraph. To better understand the purposes of this chapter see Manuscript 2, published on ChemCommun on February 2020.

### 4.2 Materials and Methods

#### *Chemical synthesis*

All Fmoc protected amino acids, preloaded Wang Resin with Fmoc-Ser(*t*Bu)-OH and PyBOP were purchased by Novabiochem (Darmstad, Germany), Sigma Aldrich (Darmstad, Germany) and Iris Biotech (Marktredwitz, Germany). Fmoc-Asp-OAll was purchased by Fluka. Wang ChemMatrix<sup>®</sup> resin was purchased by Biotage (Uppsala, Sweden). Sodium acetate, acetic acid and anhydrous GaCl<sub>3</sub> were purchased by Sigma Aldrich (Darmstad, Germany). Cyanine5.5

maleimide was purchased by Lumiprobe GmbH (Hannover, Germany). All other reagents were purchased by Sigma Aldrich (Darmstadt, Germany). All solvents were purchased by VWR International (Radnor, USA) and were used without further purifications. 6-[Bis[2-(1,1-dimethylethoxy)-2-oxoethyl]amino]-6-(5-carboxypentyl)tetrahydro-1H-1,4-diazepine-1,4(5H)-Diacetic acid  $\alpha,\alpha'$ -bis(1,1-dimethylethyl)ester ((*t*Bu)<sub>4</sub>-AAZTA-C4-COOH) was synthesized in accordance with Manzoni et al protocol.

NMR spectra were recorded at 298 K on a Bruker AVANCE 600 spectrometer. CD<sub>3</sub>OD and NMR tube were purchased from Sigma Aldrich.

Mass spectra with electrospray ionization (ESI) were recorded on a SQD 3100 Mass Detector (Waters) and on an LC-MS system Agilent 1200 Infinity Series (Agilent Technologies). The HPLC-MS analytical and preparative purifications were carried out on a Waters AutoPurification system (3100 Mass Detector 600 Quaternary Pump Gradient Module, 2767 Sample Manager and 2487 UV/Visible Detector) and on a HP 1200 Series (Agilent Technologies). UPLC-MS analyses were performed using a Waters Acquity UPLC H-Class coupled with an ESI source, a quadrupole (QDa) mass analyzer and dual-wavelength UV/Vis TUV Detector. High resolution mass analysis was performed on an Agilent 1200 Infinity Series (Agilent Technologies) equipped with ESI source and a ToF analyzer.

AE105-Cys linear peptide was synthesized automatically with a CEM Microwave Peptide Liberty Synthesizer.

UV-Vis spectra were acquired by a 6715 UV-Vis spectrophotometer (JENWAY) in the spectral range 500-800 nm using rectangular quartz cells having an optical path length of 1 cm (Hellma Analytics).

#### *Cell culture and flow cytometry*

U-87 MG human glioblastoma cell line was purchased from American Type Culture Collection (ATCC, Manassas, VA, USA) and were grown in MEM modified medium (Euroclone, Milan, Italy) supplemented with 1% glutamine, 1% sodium pyruvate, 1% Non-Essential Aminoacids, 100U/mL penicillin, 100 U/mL streptomycin and 10% (v/v) fetal bovine serum (FBS) at 310 K in humidified atmosphere containing 5% of CO<sub>2</sub>.

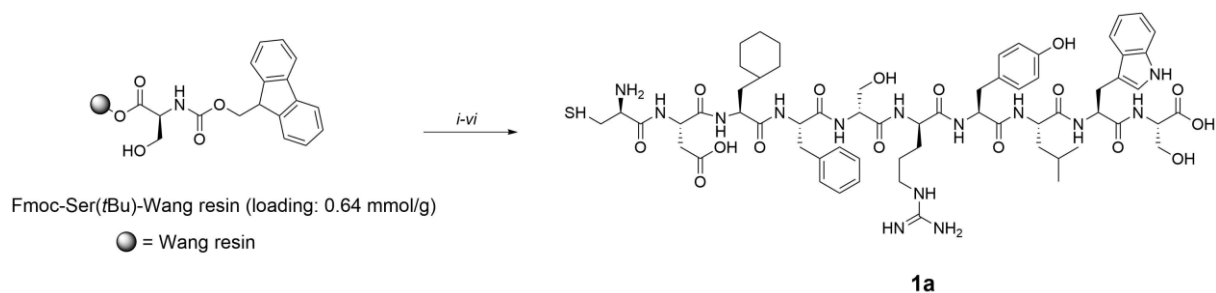
*In vitro* binding evaluations were performed by Guava<sup>®</sup> easyCyte 8 Benchtop Flow Cytometer (Merck Millipore, Burlington, Massachusetts, USA) using RED2 filter (661/19 nm). Fluorescent profiles and binding percentages of the cell populations were obtained and analyzed using InCyte Software (Merck Millipore, Burlington, Massachusetts, USA).

#### *In vivo and ex vivo optical imaging experiments*

The optical imaging experiments were performed on IVIS Instrument SPECTRUM (Perkin Elmer), equipped with a CCD camera and a series of excitation (ex) and emission (em) filters. The OI acquisition parameters to image Cy 5.5 and sulfo Cy 5.5 were: excitation filter, 675nm; emission filter, 720nm; field of view (FOV) for *in vivo* acquisition, 24.8 cm; FOV for *ex vivo* 14 cm; the optimal filter pair were 675 nm (ex) and 720 nm (em). *In vivo* optical imaging (OI) experiments were performed from the 1 to 126 hours after administration of the fluorescent probes. Animals were anesthetized (7-8% sevoflurane for induction, 3-4% for maintenance, in 100% oxygen), and placed into the scanner. Body temperature was maintained at about 37° C using a heated bed. At the end of the imaging sessions, mice were anesthetized and euthanized by cervical dislocation. For each group, *ex vivo* OI experiments were performed on the main organs: brain, lung, liver, kidneys, intestine, heart, testicles and spleen were excised for *ex vivo* analysis.

## 4.3 Experimental procedures (Chemical Synthesis)

### 4.3.1 Cys-AE105 (1a)

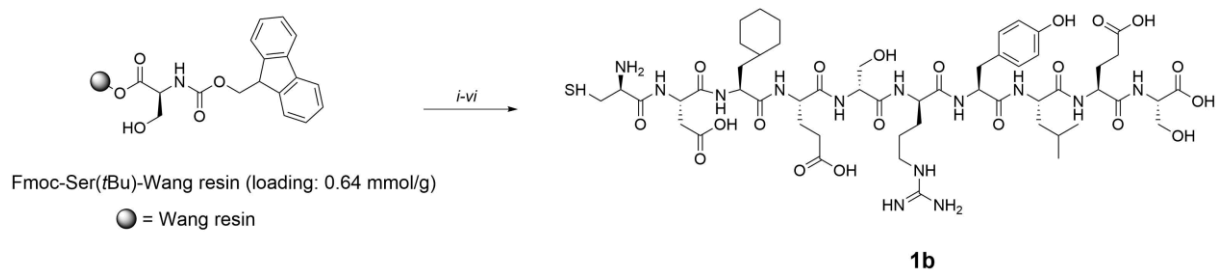


#### Scheme 4.2: Synthesis scheme of Cys-AE105 (1a):

*i*) Fmoc-AA-OH, PyBoP, DIPEA; *ii*) Wash with DMF and CH<sub>2</sub>Cl<sub>2</sub>; *iii*) DMF/Piperidine (4:1); *iv*) Wash with DMF and CH<sub>2</sub>Cl<sub>2</sub>; *v*) repeat step *i-iv*; *vi*) TFA/Phenol/TIS/H<sub>2</sub>O; Overall yield: 29%

The immobilized linear peptide H-Cys(*trt*)-Asp(*t*Bu)-Cha-Phe-D-Ser(*t*Bu)-D-Arg(Pbf)-Tyr(*t*Bu)-Leu-Trp(Boc)-Ser(*t*Bu)-Wang resin was synthesized automatically with the support of microwaves (MW) on a Wang Resin preloaded with H-Ser(*t*Bu)-OH (156 mg, 0.64 mmol/g) by standard Fmoc protocol. Cleavage of Fmoc group was achieved with 20% piperidine in DMF. Each coupling reaction was performed adding to the reaction vessel 5 equivalents of the Fmoc protected amino acid, 10 equivalents of DIPEA and 5 equivalents of the activator agent (PyBOP). The peptide was cleaved from the solid support by addition of TFA/Phenol/H<sub>2</sub>O/TIS (88:5:2:5) overnight at room temperature. Final purification was achieved by preparative RP-HPLC by employing an Atlantis prepD<sup>®</sup> C18OBD 5 $\mu$ m (19X100 mm) column. Eluent: (A) 0.1% TFA in H<sub>2</sub>O, (B) 0.1% TFA in CH<sub>3</sub>CN. Gradient profile; isocratic at 20% of B for 8.52 min, linear gradient from 20% to 40% of B in 8.48 min, linear gradient from 40% to 100% in 2.9 min, isocratic at 100% for 1.1 minutes. Flow rate; 15 mL/min. Cys-AE105 was isolated as a homogenous peak with a retention time of ab. 18 minutes. The solvent was removed *in vacuo* and the product lyophilized from water to give **1a** as a white solid (39 mg, 29%). The purity of the product was checked by analytical UPLC-MS by employing an ACQUITY UPLC<sup>®</sup> Peptide BEH C18 column (300 $\text{\AA}$ , 1.7 $\mu$ m, 2.1X100mm). Eluent: (A) 0.05% TFA in H<sub>2</sub>O, (B) 0.05% TFA in CH<sub>3</sub>CN. Gradient profile; linear gradient from 5% to 50% of B in 7 min, linear gradient from 50% to 100% in 3 min, isocratic at 100% for 3 minutes. Flow rate of 0.4 mL/min and UV detection at 210 nm. Purity 98%. ESI-MS (*m/z*): calcd: For C<sub>67</sub>H<sub>91</sub>N<sub>13</sub>O<sub>21</sub>S<sub>2</sub> (M+2H)<sup>2+</sup> 665.37 found: 665.73. HPLC and MS characterizations are reported in Manuscript 2, pag 152.

### 4.3.2 Cys-AE105mut (1b)<sup>1</sup>



#### Scheme 4.3: Synthesis scheme of Cys-AE105mut (1b):

*i*) Fmoc-AA-OH, PyBoP, DIPEA; *ii*) Wash with DMF and CH<sub>2</sub>Cl<sub>2</sub>; *iii*) DMF/Piperidine (4:1); *iv*) Wash with DMF and CH<sub>2</sub>Cl<sub>2</sub>; *v*) repeat step *i-iv*; *vi*) TFA/Phenol/TIS/H<sub>2</sub>O; Overall yield: 20%.

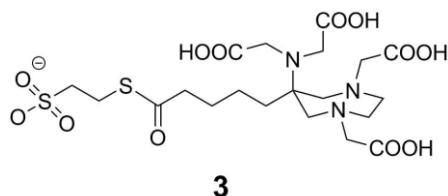
The immobilized linear peptide H-Cys(*trt*)-Asp(*t*Bu)-Cha-Glu(*Ot*Bu)-D-Ser(*t*Bu)-D-Arg(*Pbf*)-Tyr(*t*Bu)-Leu-Glu(*Ot*Bu)-Ser(*t*Bu)-Wang resin was synthesized automatically with the support of microwaves (MW) on a Wang Resin preloaded with H-Ser(*t*Bu)-OH (150 mg, 0.64 mmol/g) by standard Fmoc protocol. Cleavage of Fmoc group was achieved with 20% piperidine in DMF. Each coupling reaction was performed adding to the reaction vessel 5 equivalents of the Fmoc protected amino acid, 10 equivalents of DIPEA and 5 equivalents of the activator agent (PyBOP). The peptide was cleaved from the solid support by addition of TFA/Phenol/H<sub>2</sub>O/TIS (88:5:2:5) overnight at room temperature. Final purification was achieved by preparative RP-HPLC by employing an Atlantis prepD<sup>®</sup> C18OBD 5 $\mu$ m (19X100 mm) column. Eluent: (A) 0.1% TFA in H<sub>2</sub>O, (B) 0.1% TFA in CH<sub>3</sub>CN. Gradient profile; isocratic at 20% of B for 8.52 min, linear gradient from 20% to 40% of B in 8.48 min, linear gradient from 40% to 100% in 2.9 min, isocratic at 100% for 1.1 minutes. Flow rate; 15 mL/min. Cys-AE105 was isolated as a homogenous peak with a retention time of ab. 18 minutes. The solvent was removed *in vacuo* and the product lyophilized from water to give **1b** as a white solid (25 mg, 20%). The purity of the product was checked by analytical HPLC-MS by employing an Atlantis DC18 5 $\mu$ m, 4.6X150mm column. Eluent: (A) 0.1% TFA in H<sub>2</sub>O, (B) 0.1% TFA in CH<sub>3</sub>CN. Gradient profile; linear gradient from 20% to 35% of B in 10 min, isocratic at 35% for 5 min, linear gradient from 35% to 98% in 5 min, isocratic at 98% for 5 min. Flow rate of 1 mL/min and UV detection at 210 nm. RT: 6.97 min. Purity 99%. ESI-MS (*m/z*): calcd: For C<sub>53</sub>H<sub>83</sub>N<sub>13</sub>O<sub>20</sub>S (M+H)<sup>+</sup> 1255.38 found: 1255.69; (M+2H)<sup>2+</sup> 627.59 found: 627.93.

### 4.3.3 CycloRGDFK (C) (2)

The product has been synthesized by L.D.Rosa from Istituto di Biostrutture e Bioimmagini, CNR, Napoli (TO). See preparation of product 2, Manuscript 2, Chapter 5.

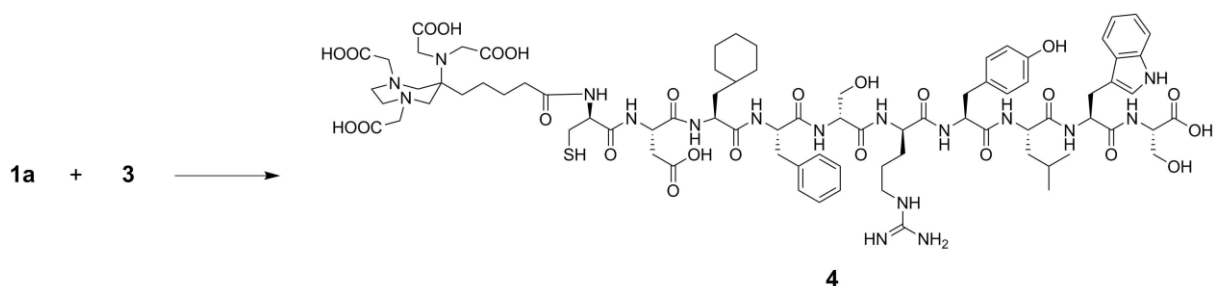


#### 4.3.4 AAZTA-CO-MES (3)



See preparation 2.3.3, Chapter II. HPLC and MS characterizations are reported in Manuscript 2, pag 152-153.

#### 4.3.5 AAZTA-C4-CO-Cys-AE105(4)



#### Scheme 4.4: Synthesis scheme of AAZTA-C4-CO-Cys-AE105 (4):

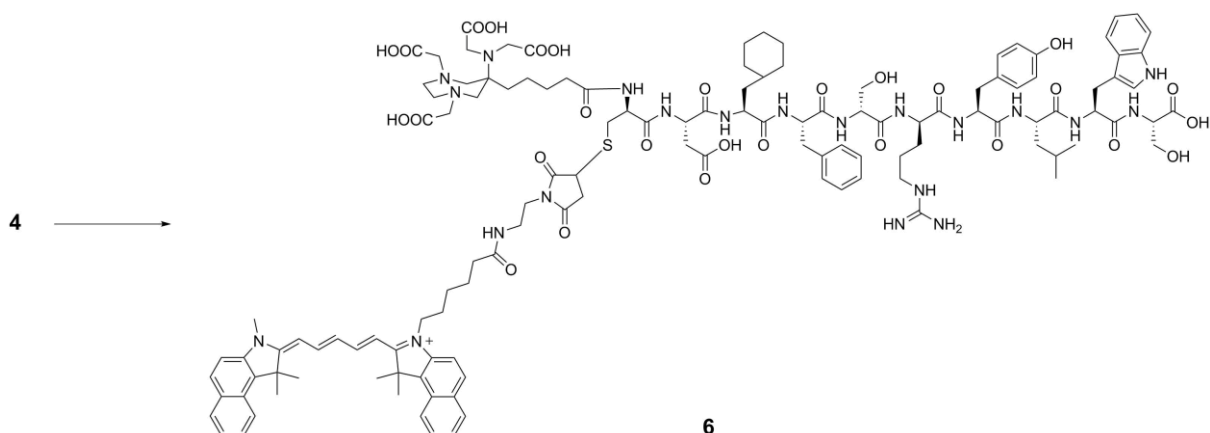
phosphate buffer pH 7.4, 5M imidazole, 3M guanidinium chloride, 50mM TCEP, 1h, RT. Yield: 62%.

2 mg of **1a** (1.50  $\mu\text{mol}$ , 1 eq) were dissolved in 100  $\mu\text{L}$  of ligation buffer (0.2M phosphate buffer pH 7.4, 5M Imidazole, 3M Guanidinium chloride, 50mM TCEP. Final pH: 7.4) and the pH is adjusted to 7.4. A solution of **3** (3.00  $\mu\text{mol}$ , 2 eq) in 100  $\mu\text{L}$  of ligation buffer was added to the previous solution and the pH was adjusted to 7.4. The reaction was stirred for 1 h at room temperature. The reaction was monitored by HPLC-MS. Final purification was achieved by preparative RP-HPLC on Waters AutoPurification system by employing an XBridge™ BEH300 Prep C18 10  $\mu\text{m}$  (10X100 mm) column. Eluent: (A) 0.1% TFA in  $\text{H}_2\text{O}$ , (B) 0.1% TFA in  $\text{CH}_3\text{CN}$ . Gradient profile; isocratic at 20% of B for 10 min, linear gradient from 20% to 35% of B in 10 min, linear gradient from 35% to 100% in 3.33 min, isocratic at 100% for 4 min. Flow rate; 5 mL/min. **4** was isolated as a homogenous peak with a retention time of 22.5 minutes. The solvent was removed *in vacuo* and the product lyophilized from water to give **4** as white solid (1.64 mg, 62%). The purity of the product was checked by analytical UPLC-MS by employing an ACQUITY UPLC® Peptide BEH C18 column (300 $\text{\AA}$ , 1.7 $\mu\text{m}$ , 2.1X100mm). Eluent: (A) 0.05% TFA in  $\text{H}_2\text{O}$ , (B) 0.05% TFA in  $\text{CH}_3\text{CN}$ . Gradient profile; linear gradient from 5% to 50% of B in 7 min, linear gradient from 50% to 100% in 3 min, isocratic at 100% for 3 minutes. Flow rate of 0.4 mL/min and UV detection at 210 nm. Purity 98%. ESI-MS ( $m/z$ ): calcd: For  $\text{C}_{81}\text{H}_{115}\text{N}_{17}\text{O}_{25}\text{S}$  ( $M+2\text{H}$ )<sup>2+</sup> 880.36 found: 880.16. HPLC and MS characterizations are reported in Manuscript 2, pag 154.

#### 4.3.6 AAZTA-C4-CO-cycloRGDFk(C)(5)

The product has been synthesized by L.D.Rosa from Istituto di Biostrutture e Bioimmagini, CNR, Napoli (TO). See preparation of product 5, Manuscript 2, Chapter 5.

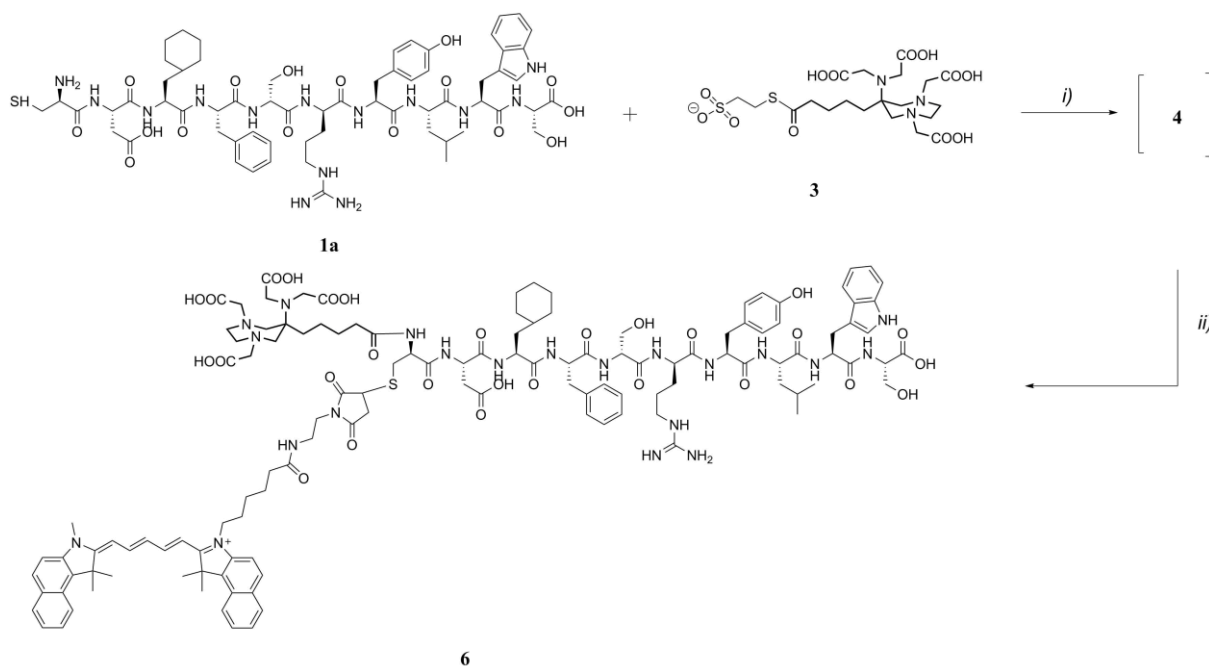
#### 4.3.7 AAZTA-C4-CO-Cys(Cy 5.5)-AE105 (6): procedure 1



**Scheme 4.5: Synthesis scheme of AAZTA-C4-CO-Cys(Cy 5.5)-AE105 (6):**  
cy 5.5 maleimide, acetate pH 6.5, 3h, RT. Yield: 62%.

3.09 mg of **4** (1.76  $\mu\text{mol}$ ) were dissolved in 600  $\mu\text{L}$  of 50 mM acetate at pH 6.5. 1.14 mg of Cyanine 5.5 Maleimide (0.875 eq, 1.53  $\mu\text{mol}$ ) were added to the previous solution and the reaction was stirred at room temperature for 3h. The reaction was monitored by UPLC-MS. Final purification was achieved by preparative RP-HPLC on Waters AutoPurification system by employing an XBridge™ BEH300 Prep C18 10  $\mu\text{m}$  (10 $\times$ 100 mm) column. Eluent: (A) 0.1% TFA in H<sub>2</sub>O, (B) 0.1% TFA in CH<sub>3</sub>CN. Gradient profile; isocratic at 25% of B for 5.25 min, linear gradient from 25% to 50% of B in 15.77 min, isocratic at 50% of B in 5.25 min, linear gradient from 50% to 100% in 5 min, isocratic at 100% for 5 min. Flow rate; 4.5 mL/min. AAZTA-C4-CO-Cys(Cy 5.5)-AE105 (**6**) was isolated as a homogenous peak with a retention time of ab. 24 min (1.68 mg, 39%). The purity of the product was checked by analytical UPLC-MS by employing an ACQUITY UPLC® Peptide BEH C18 column (300 $\text{\AA}$ , 1.7  $\mu\text{m}$ , 2.1 $\times$ 100mm). Eluent: (A) 0.05% TFA in H<sub>2</sub>O, (B) 0.05% TFA in CH<sub>3</sub>CN. Gradient profile; linear gradient from 5% to 50% of B in 7 min, linear gradient from 50% to 100% in 3 min, isocratic at 100% for 3 minutes. Flow rate of 0.4 mL/min and UV detection at 210 nm and 672 nm. Purity<sub>210 nm</sub>: 95%. ESI-MS ( $m/z$ ): calcd: For C<sub>127</sub>H<sub>164</sub>N<sub>21</sub>O<sub>28</sub>S<sup>+</sup> (M+2H)<sup>3+</sup> 822.11found: 822.35.HPLC and MS characterizations are reported in Manuscript 2, pag 155.

#### 4.3.8 AAZTA-C4-CO-Cys(Cy 5.5)-AE105 (6): procedure 2



#### Scheme 4.6: Synthesis scheme of AAZTA-C4-CO-Cys(Cy 5.5)-AE105 (6):

- i) phosphate buffer pH 7.4, 5M imidazole, 3M guanidinium chloride, 50mM TCEP, 1h, RT; ii) cy 5.5 maleimide, 3h, RT. Overall Yield: 22%.

2.5 mg of **1a** (1.88  $\mu\text{mol}$ , 1 eq.) were dissolved in 300  $\mu\text{L}$  of the reaction buffer (0.2M phosphate buffer pH 7.4, 5M imidazole, 3M guanidinium chloride. Final pH: 7.0) and 2.14 mg of **3** (3.75  $\mu\text{mol}$ , 2 eq.) were added to the solution. The obtained solution was stirred at room temperature for 30 min. After the reaction time an UPLC-MS chromatogram shows the total conversion to the desired product.

Subsequently, without performing any further purification, 1.39 mg of Cy 5.5 maleimide (1.87  $\mu\text{mol}$ , 1 eq.) were added to the solution. After 3 h the solution was directly purified on preparative RP-HPLC (same condition of synthesis of **6**). The final product was lyophilized from water to give **6** as dark blue solid (1.0 mg, 22%). The purity of the product was checked by analytical UPLC-MS by employing an ACQUITY UPLC<sup>®</sup> Peptide BEH C18 column (300  $\text{\AA}$ , 1.7  $\mu\text{m}$ , 2.1  $\times$  100mm). Eluent: (A) 0.05% TFA in  $\text{H}_2\text{O}$ , (B) 0.05% TFA in  $\text{CH}_3\text{CN}$ . Gradient profile; linear gradient from 5% to 50% of B in 7 min, linear gradient from 50% to 100% in 3 min, isocratic at 100% for 3 minutes. Flow rate of 0.4 mL/min and UV detection at 210 nm and 672 nm. Purity<sub>210 nm</sub>: 95%. ESI-MS ( $m/z$ ): calcd: For  $\text{C}_{127}\text{H}_{164}\text{N}_{21}\text{O}_{28}\text{S}^+$  ( $M+2\text{H}$ )<sup>3+</sup> 822.11 found: 822.15.

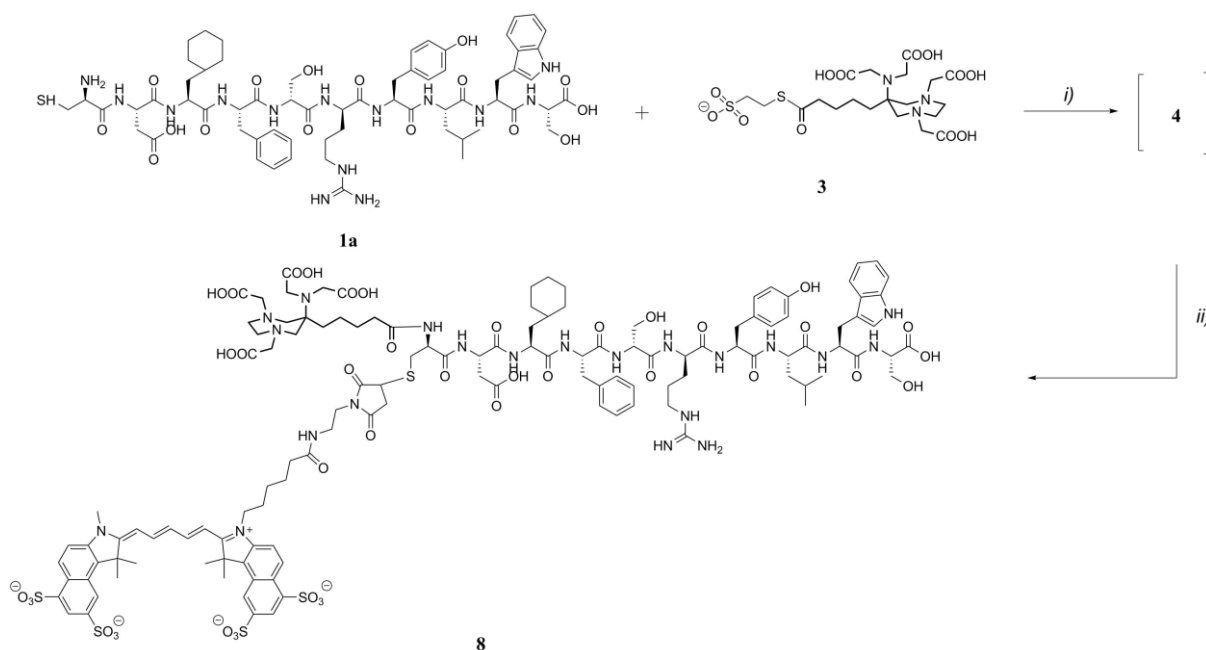
#### 4.3.9 AAZTA-C4-CO-(Cy 5.5)-cycloRGDFk(C) (7): procedure 1

The product has been synthesized by L. D. Rosa from Istituto di Biostrutture e Bioimmagini, CNR, Napoli (TO). See preparation of product 7 (procedure 1), Manuscript 2, Chapter 5.

#### 4.3.10 AAZTA-C4-CO-(Cy 5.5)-cycloRGDFk(C) (7): procedure 2

The product has been synthesized by L. D. Rosa from Istituto di Biostrutture e Bioimmagini, CNR, Napoli (TO). See preparation of product 7 (procedure 2), Manuscript 2, Chapter 5.

### 4.3.11 Synthesis of AAZTA-C4-CO-Cys(sulfoCy 5.5)-AE105 (8): procedure 2



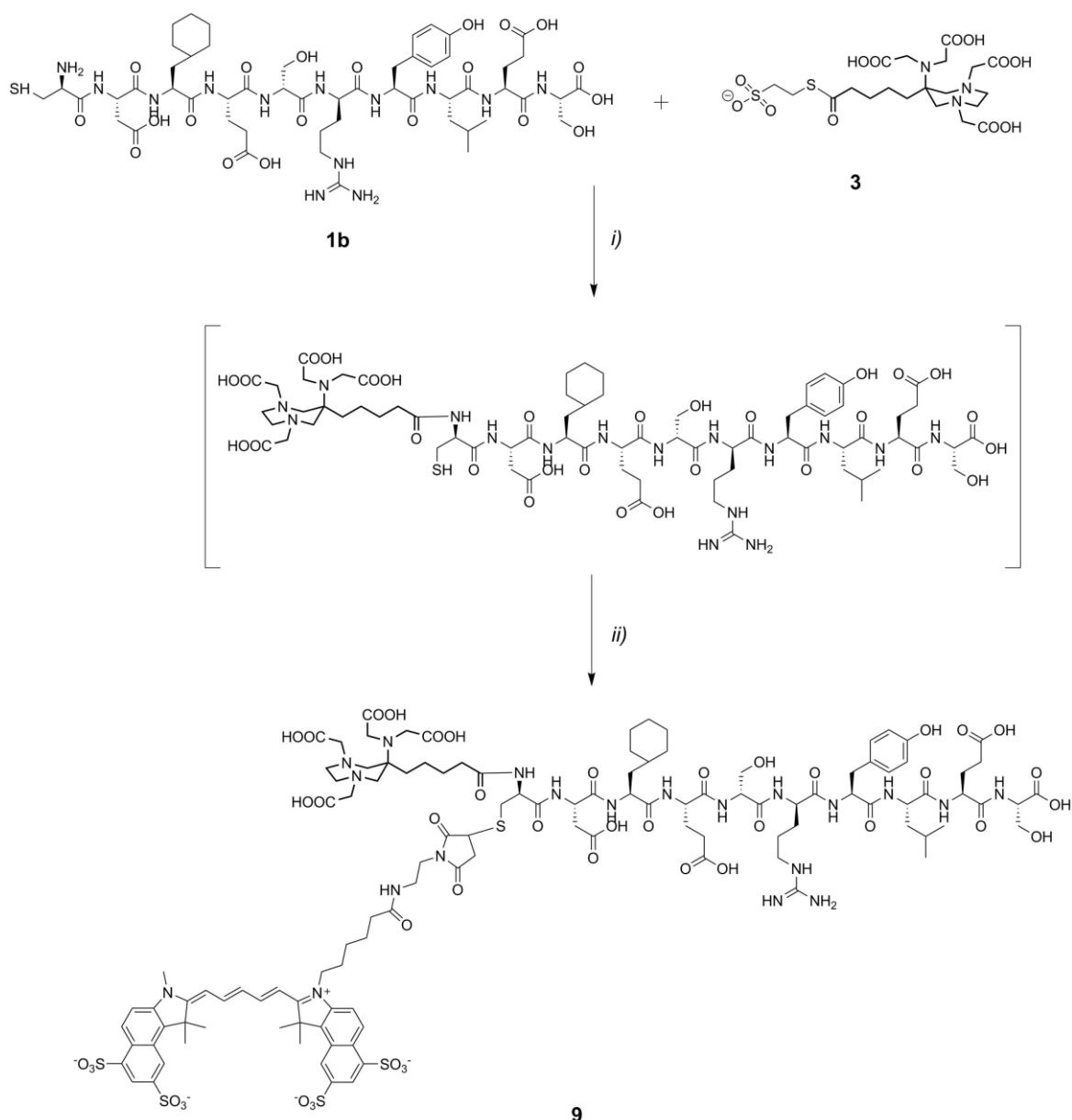
#### Scheme 4.7: Synthesis scheme of AAZTA-C4-CO-Cys(sulfo Cy 5.5)-AE105 (8):

- i) phosphate buffer pH 7.4, 5M imidazole, 3M guanidinium chloride, 50mM TCEP, 1h, RT; ii) sulfo cy 5.5 maleimide, 3h, RT. Overall Yield: 26%.

5 mg of **1a** (3.76  $\mu\text{mol}$ , 1 eq.) were dissolved in 500  $\mu\text{L}$  of the reaction buffer (0.2M phosphate buffer pH 7.4, 5M imidazole, 3M guanidinium chloride. Final pH: 7.0) and 2.85 mg of **3** (4.99  $\mu\text{mol}$ , 1.33 eq.) were added to the solution. The obtained solution was stirred at room temperature for 30 min. After the reaction time an UPLC-MS chromatogram shows the total conversion to the desired product.

Subsequently, without performing any further purification, 4.28 mg of SulfoCy5.5 maleimide (3.76  $\mu\text{mol}$ , 1 eq.) were added to the solution. After 3 h the solution was directly loaded on preparative RP-HPLC. Final purification was achieved on Waters AutoPurification system by employing an XBridge™ BEH300 Prep C18 10  $\mu\text{m}$  (10 $\times$ 100 mm) column. Eluent: (A) H<sub>2</sub>O, (B) CH<sub>3</sub>CN. Gradient profile; isocratic at 25% of B for 5.25 min, linear gradient from 25% to 50% of B in 15.77 min, isocratic at 50% of B in 5.25 min, linear gradient from 50% to 100% in 5 min, isocratic at 100% for 5 min. Flow rate; 4.5 mL/min. The final product was lyophilized from water to give **8** as dark blue solid (2.84 mg, 26%). The purity of the product was checked by analytical HPLC using an XBridge™ DC18 5 $\mu\text{m}$ , 4.6 $\times$ 150mm column. Eluent: (A) TEA buffer pH 7, (B) CH<sub>3</sub>CN. linear gradient from 2% to 20% of B in 20 min, linear gradient from 20% to 50% in 10 min, linear gradient from 50 to 95% of B in 5 min, isocratic at 95% for 5 min. Flow rate of 1 mL/min and UV detection at 210 nm and 672 nm. RT: 22.5 min. Purity<sub>210nm</sub>: 99%. ESI-MS ( $m/z$ ): calcd: For C<sub>127</sub>H<sub>160</sub>N<sub>21</sub>O<sub>40</sub>S<sub>5</sub><sup>+</sup> (M-2H)<sup>2</sup>-1390.05 found: 1390.99

### 4.3.12 Synthesis of AAZTA-C4-CO-Cys(sulfo Cy 5.5)-AE105mut (9): procedure 2



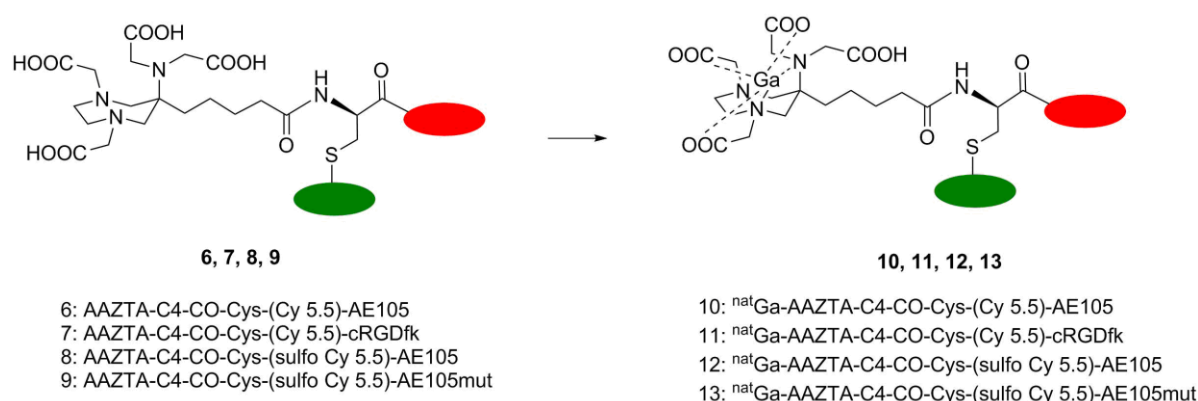
**Scheme 4.8:** Synthesis scheme of AAZTA-C4-CO-Cys(sulfo Cy 5.5)-AE105mut (9): i) phosphate buffer pH 7.4, 5M imidazole, 3M guanidinium chloride, 50mM TCEP, 1h, RT; ii) sulfo cy 5.5 maleimide, 3h, RT. Overall Yield: 85%.

5 mg of **1b** (3.99 $\mu$ mol, 1 eq.) were dissolved in 500 $\mu$ L of the reaction buffer (0.2M phosphate buffer pH 7.4, 5M imidazole, 3M guanidinium chloride. Final pH: 7.4) and 3.41 mg of **3** (5.99  $\mu$ mol, 1.50 eq.) were added to the solution. The obtained solution was stirred at room temperature for 30 min. After the reaction time an UPLC-MS chromatogram shows the total conversion to the desired product.

Subsequently, without performing any further purification, 4.5 mg of SulfoCy5.5 maleimide (3.99  $\mu$ mol, 1 eq.) were added to the solution. After 3 h the solution was directly purified on preparative RP-HPLC. The reaction was monitored by UPLC-MS. Final purification was achieved by preparative RP-HPLC on Waters AutoPurification system by employing an XBridge™ BEH300

Prep C18 10  $\mu\text{m}$  (10 $\times$ 100 mm) column. Eluent: (A) 0.1% TFA in  $\text{H}_2\text{O}$ , (B) 0.1% TFA in  $\text{CH}_3\text{CN}$ . Gradient profile; isocratic at 25% of B for 5.25 min, linear gradient from 25% to 50% of B in 15.77 min, isocratic at 50% of B in 5.25 min, linear gradient from 50% to 100% in 5 min, isocratic at 100% for 5 min. Flow rate; 4.5 mL/min. The final product was lyophilized from water to give **9** as dark blue solid (9.18 mg, 85%). The purity of the product was checked by analytical HPLC using an XBridge™ DC18 5 $\mu\text{m}$ , 4.6 $\times$ 150mm column. Eluent: (A) TEA buffer pH 7, (B)  $\text{CH}_3\text{CN}$ . linear gradient from 2% to 20% of B in 15 min, linear gradient from 20% to 50% in 5 min, linear gradient from 50 to 95% of B in 5 min, isocratic at 95% for 5 min. Flow rate of 1 mL/min and UV detection at 210 nm and 672 nm. RT: 17.4 min. Gradient profile; linear gradient from 5% to 50% of B in 7 min, linear gradient from 50% to 100% in 3 min, isocratic at 100% for 3 minutes. Flow rate of 0.4 mL/min and UV detection at 210 nm and 672 nm. Purity<sub>210nm</sub>: 99%. ESI-MS ( $m/z$ ): calcd: For  $\text{C}_{117}\text{H}_{155}\text{N}_{20}\text{O}_{44}\text{S}_5^+(\text{M}+2\text{H})^{2+}$  1353.96 found: 1355.49;  $(\text{M}+3\text{H})^{3+}$  902.97 found: 903.55.

## 4.4 Experimental procedures (Labeling with natural gallium isotope)



**Scheme 4.9:** General labeling scheme of the dual labelled peptide based probes: **10-11**) 0.1M acetate buffer pH 3.8/CH<sub>3</sub>CN 1:1, 1h, RT; **12-13**) 0.1M acetate buffer pH 3.8.

### 4.4.1 Ga-AAZTA-C4-CO-Cys(Cy 5.5)-AE105 (10)

0.38 mg of **6** (0.154  $\mu\text{mol}$ ) were dissolved in 300  $\mu\text{L}$  of a solution 50:50 of 0.1M acetate buffer at pH 3.8/CH<sub>3</sub>CN. 10  $\mu\text{L}$  of a 1000ppm standard water solution of GaCl<sub>3</sub> were added and the solution was stirred at room temperature for 1h. Product **10** was quantified by UV absorption spectroscopy in ethanol, using the Cy5.5 molar extinction coefficient at 684 nm of  $1.98 \cdot 10^5 \text{ M}^{-1} \text{ cm}^{-1}$ . The purity of the product was checked by analytical UPLC employing an ACQUITY UPLC® Peptide BEH C18 column (300Å, 1.7 $\mu\text{m}$ , 2.1X100mm). Eluent: (A) 0.05% TFA in H<sub>2</sub>O, (B) 0.05% TFA in CH<sub>3</sub>CN. Gradient profile; linear gradient from 5% to 50% of B in 7 min, linear gradient from 50% to 100% in 3 min, isocratic at 100% for 3 minutes. Flow rate of 0.4 mL/min and UV detection at 210nm and 672 nm. Purity<sub>210nm</sub>: 96%. ESI-MS ( $m/z$ ): calcd: For C<sub>127</sub>H<sub>161</sub>GaN<sub>21</sub>O<sub>28</sub>S<sup>+</sup> (M+2H)<sup>3+</sup> 844.42 found: 844.25. High resolution mass spectrometry monoisotopic peak (M+2H)<sup>3+</sup>: calcd: 843.6932; found: 843.6893. HPLC and MS characterizations are reported in Manuscript 2, pag 156.

### 4.4.2 Ga-AAZTA-C4-CO-(Cy 5.5)-cycloRGDfK(C) (11)

0.54 mg of **7** (0.293  $\mu\text{mol}$ ) were dissolved in 450  $\mu\text{L}$  of a solution 50:50 of 0.1M acetate buffer/CH<sub>3</sub>CN at pH 3.8. 20  $\mu\text{L}$  of a 1000ppm standard water solution of GaCl<sub>3</sub> were added and the solution was stirred at room temperature for 1h. The pure **11** was quantified by UV absorption spectroscopy in ethanol, using the Cy5.5 molar extinction coefficient at 684 nm of  $1.98 \cdot 10^5 \text{ M}^{-1} \text{ cm}^{-1}$ . The purity of the product was checked by analytical UPLC by employing an ACQUITY UPLC® Peptide BEH C18 column (300Å, 1.7 $\mu\text{m}$ , 2.1X100mm). Eluent: (A) 0.05% TFA in H<sub>2</sub>O, (B) 0.05% TFA in CH<sub>3</sub>CN. Gradient profile; linear gradient from 5% to 50% of B in 7 min, linear gradient from 50% to 100% in 3 min, isocratic at 100% for 3 minutes. Flow rate of 0.4 mL/min and UV detection at 210 nm and 672 nm. Purity<sub>210nm</sub>:95%. ESI-MS ( $m/z$ ): calcd for C<sub>94</sub>H<sub>119</sub>GaN<sub>17</sub>O<sub>20</sub>S<sup>+</sup>(M+H)<sup>2+</sup>954.94 found: 954.97. High resolution mass spectrometry monoisotopic peak (M+H)<sup>2+</sup>: calcd: 953.8897; found: 953.8832. HPLC and MS characterizations are reported in Manuscript 2, pag 156.

#### **4.4.3 Ga-AAZTA-C4-CO-Cys(sulfo Cy 5.5)-AE105 (12)**

0.30 mg of **8** (0.108  $\mu\text{mol}$ ) were dissolved in 300  $\mu\text{L}$  of acetate buffer at pH 3.8. 7.5  $\mu\text{L}$  of a 1000ppm standard water solution of  $\text{GaCl}_3$  were added and the solution was stirred at room temperature for 1h. The pure **12** was quantified by UV absorption spectroscopy in ethanol, using the sulfoCy5.5 molar extinction coefficient at 673 nm of  $2.35 \cdot 10^5 \text{ M}^{-1} \text{ cm}^{-1}$ .

#### **4.4.4 Ga-AAZTA-C4-CO-Cys(sulfo Cy 5.5)-AE105mut (13)**

1.02 mg of **9** (0.377  $\mu\text{mol}$ ) were dissolved in 500  $\mu\text{L}$  of acetate buffer at pH 3.8. 26  $\mu\text{L}$  of a 1000ppm standard water solution of  $\text{GaCl}_3$  were added and the solution was stirred at room temperature for 1h. The pure **13** was quantified by UV absorption spectroscopy in ethanol, using the sulfo Cy5.5 molar extinction coefficient at 673 nm of  $2.35 \cdot 10^5 \text{ M}^{-1} \text{ cm}^{-1}$ .



## 4.5 Experimental procedures (*In vitro* experiments)

Human U-87 MG glioblastoma cells were used to determine cell binding of Ga-AAZTA-C4-CO-Cys(Cy 5.5)-AE105 (compound **10**) and Ga-AAZTA-C4-CO-(Cy 5.5)-*cyclo*RGDfk(C) (compound **11**). To minimize the non-specific uptake, incubations were performed on ice and followed immediately by flow cytometry. All cells groups( $10^5$ ) were incubated with Ga-AAZTA-C4-CO-Cys-(Cy 5.5)-AE105 or Ga-AAZTA-C4-CO-(Cy 5.5)-*cyclo*RGDfk(C) (0, 0.033, 0.133 and 0.400  $\mu$ g) for 30 min at 273 K. After centrifugation of the tubes and the elimination of the supernatant, cells were washed twice with PBS 1X. 100uL of PBS 1X supplemented with 0.1% BSA were added to each tube.

## 4.6 Experimental procedures (*In vivo* experiments)

### 4.6.1 *In vivo* preliminary dynamic imaging experiments with product **10**

Three million of Human U-87MG glioblastoma cells were subcutaneously injected, under anesthesia, in the flank of 8 immunocompromised athymic mice. Tumor development was assessed by palpation and caliper measurement every 2-3 days. OI experiments were performed when tumor reached the appropriate size, approximately 10-14 days after tumors implantation. U87MG tumor bearing mice (n=2/group) were catheterized by the lateral tail vein and placed into the scanner. The U87MG bearing-mice were injected with 10nmol of probe **10**. *In vivo* dynamic OI acquisitions were performed at 1, 2, 4, 6, 8, 10, 24, 30, 34h on 2 groups (2 mice/group). *Ex vivo* acquisitions have been carried out at 24h on 2 groups (2 mice/group).

### 4.6.2 *In vivo* preliminary dynamic imaging experiments with products **12** and **13**

1.5 million of Human U-87MG glioblastoma cells were subcutaneously injected, under anesthesia, in the flank of 8 immunocompromised athymic mice. Tumor development was assessed by palpation and caliper measurement every 2-3 days. OI experiments were performed when tumor reached the appropriate size, approximately 10-14 days after tumors implantation. U87MG tumor bearing mice (n=2/group) were catheterized by the lateral tail vein and placed into the scanner. The U87MG bearing-mice were injected with 5nmol of probes **12** (group 1) or **13** (group 2). *In vivo* dynamic OI acquisitions were performed at 1, 2, 4, 6, 8, 10, 24h (2 groups, 2 mice/group). *Ex vivo* acquisitions were carried out at 24h on 2 groups (2 mice/group).

## 4.7 Results and discussions

The reported synthesis procedure has allowed for the preparation of a dual labeled peptide based probe. Using two chemoselective reactions, the fluorescent and the chelating moieties have inserted at site-specific positions without the use of protecting groups. The targeting peptide has been modified with the introduction of a cysteine residue, which could be easily inserted during peptide synthesis, minimizing the impact on the overall molecular structure even in the case of short peptide sequences. Even the chelator has to be modified with the introduction of a thioester group (see paragraph 2.3 and Manuscript 2), which reacts selectively with the N-terminal cysteine attached on the peptide sequence. After the ligation reaction between peptide (**1a** or **1b**) and chelator (**3**), a free thiol has become newly accessible for the selective reaction with the maleimide preactivated fluorophore (i.e. cy 5.5 or sulfo cy 5.5). All the bioconjugation reactions have been performed in aqueous solution, under mild conditions and using unprotected reagents, suggesting that an analogous procedure could be easily translated to the preparation of protein-based probes, not presenting exposed Cys residue, through the introduction of an N-terminal cysteine. The syntheses of sulfo cy 5.5 derivatives (products **8** and **9**) have given higher overall yield, after one purification step, instead two purification steps, as done in the case of the non sulfo-derivatives syntheses (products **6** and **7**). All gallium complexation reactions have been performed under very mild conditions, during 10 minutes at room temperature. In the case of probe **6** and **7**, the complexation reactions have been carried out in a solution 50:50 of 0.1M phosphate buffer at pH 7 and acetonitrile, in order to allow the complete dissolving of the non-sulfonated probes. On the other hand, for the complexation of probes **8** and **9**, the reactions have been done in buffer solution only.

Human glioblastoma U-87 MG cells overexpressing either uPAR and  $\alpha v\beta 3$  integrin receptors have been used to assess the binding properties of the synthesized dual probes (compound **10** and **11**) by flow cytometry. Tumour cells ( $10^5$ /well) were incubated in a medium containing different concentrations of **10** or **11** (from 0 to 0.4  $\mu\text{g}$ ) for 30 minutes at 273 K. Representative results from flow cytometry experiments with Ga-AAZTA-C4-CO-Cys(Cy5.5)-AE105 (**10**) and Ga-AAZTA-C4-CO-(Cy5.5)-cycloRGDfK(C) (**11**) are reported in Figures S9 and S10, Manuscript 2, pag.158-159. Both dual probes were able to bind to U-87 MG cells. Furthermore, both probes showed a dose-dependent behaviour (Fig.4.1).

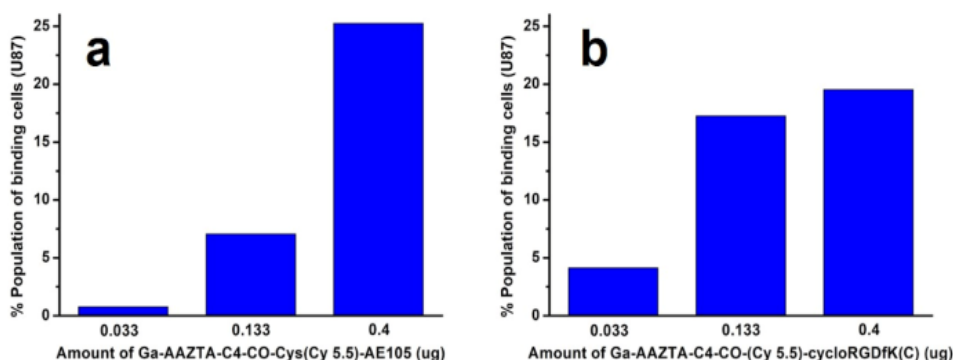


**Figure 4.1** a) Histogram plot of U-87 MG cells ( $10^5$ ) analyzed at FACS after incubation for 1h at 273 K with 0.033, 0.133 and 0.400  $\mu\text{g}$  of Ga-AAZTA-C4-CO-Cys(Cy5.5)-AE105 (**10**); b) Histogram plot of U-87 MG cells ( $10^5$ ) analyzed after incubation for 1h at 273 K with 0.033, 0.133 and 0.400  $\mu\text{g}$  of Ga-AAZTA-C4-CO-(Cy5.5)-cycloRGDfK(C) (**11**).

*In vivo* optical dynamic experiments have been carried out with compounds 10, 12 and 13 to verify *in vivo* binding of the synthesized dual PET/OI probes. The non-sulfonated probe **10**, showed a slow biodistribution profile, reaching tumor site after 14-18h post injection.

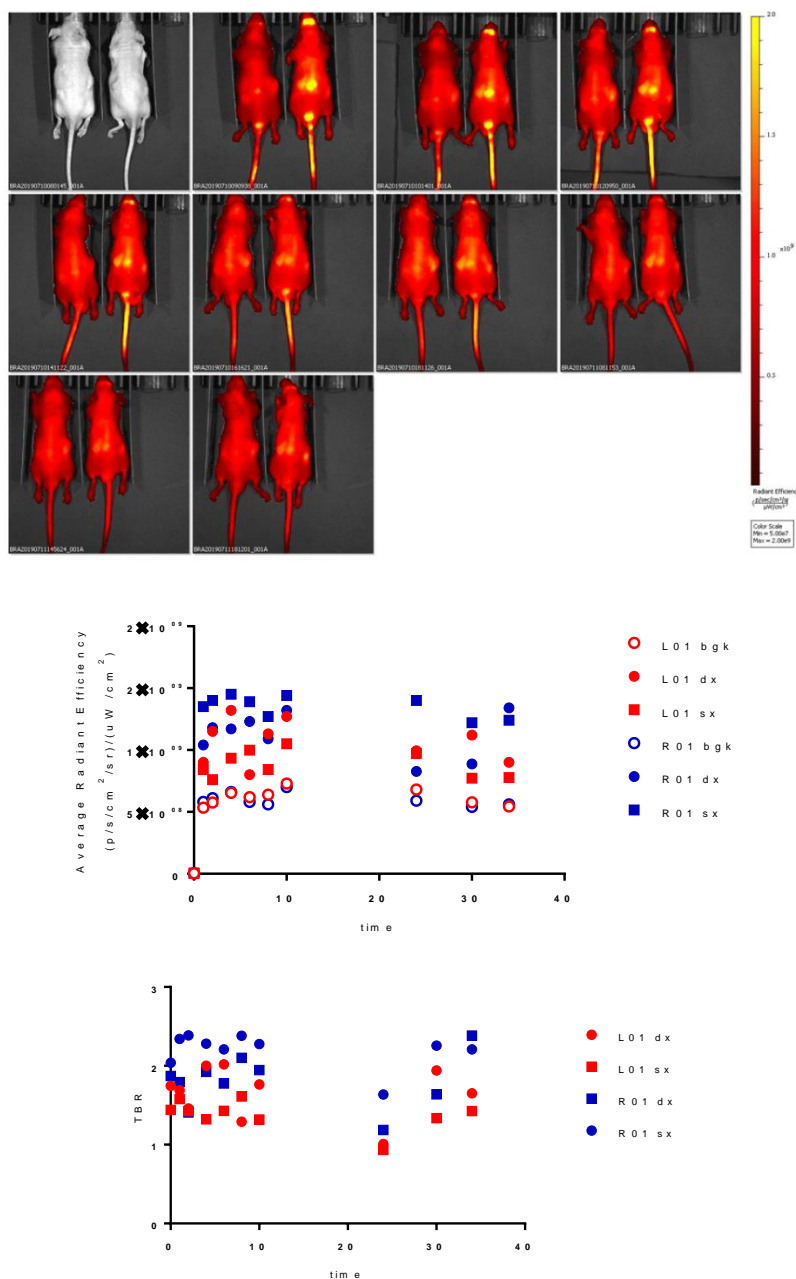


**Figure 4.2:** *In vivo* dynamic images and profiles acquired after inj. of probe **10** (group 1). Time points: pre inj., 1h, 2h, 4h, 6h, 8h, 10h, 24h, 30h. L01: left animal; R01: right animal; TBR: Tumor/Background Ratio.

The images of both groups (1 and 2) show a high background fluorescence after several hours post inj., confirmed also by *ex vivo* ROI evaluations.

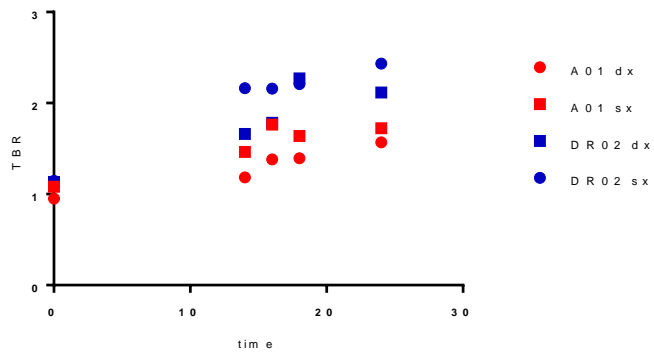
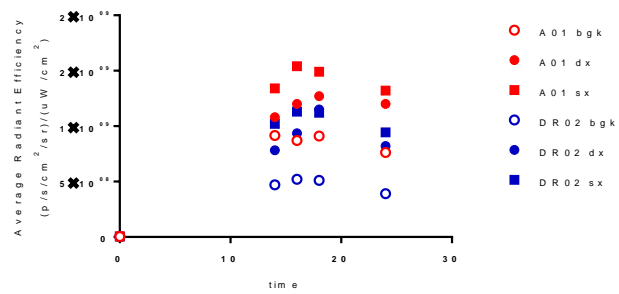
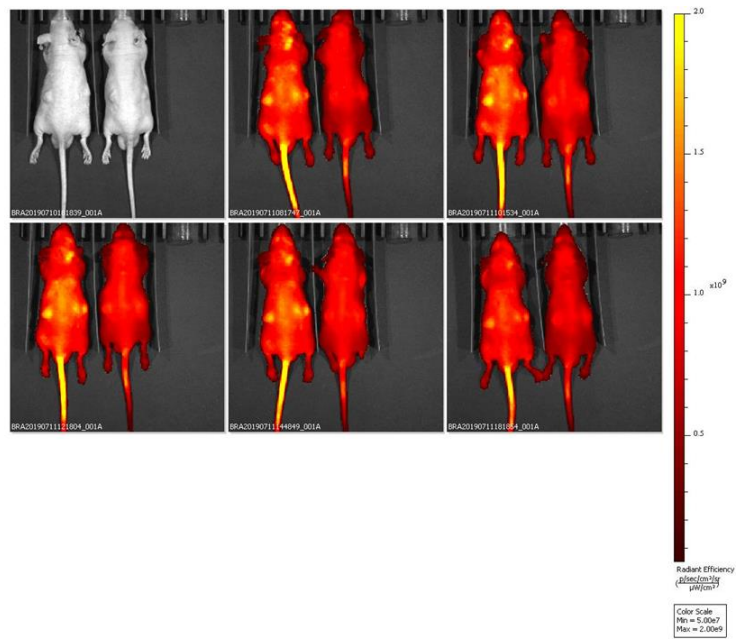


**Figure 4.3:** *In vivo* dynamic images and profiles acquired after inj. of probe **10** (group 2). Time points: pre inj., 14h, 16h, 18h, 20h, 24h. A01: left animal; DR02: right animal.

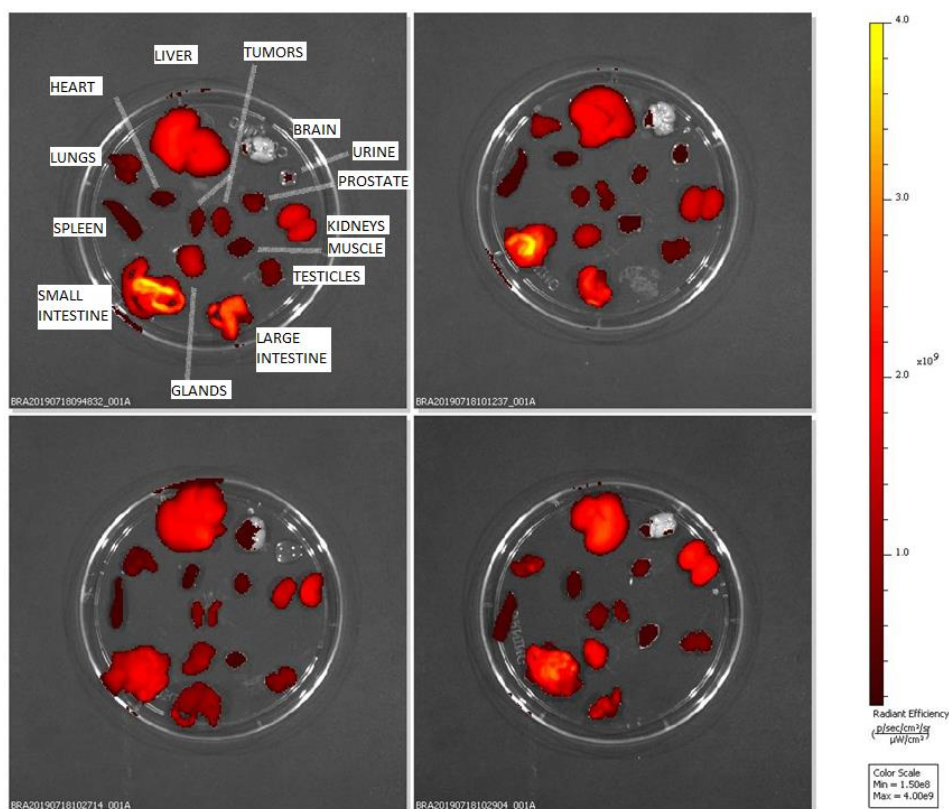


**Figure 4.4:** *Ex vivo* ROI evaluations 24h post inj. of product **10** (group 3 and 4). These preliminary *in vivo* results evidenced the need to improve the chemical structure of the synthesized probes, improving their hydrosolubility. Two sulfo cyanine derivative dual probes (**8** and **9**) have been successfully synthesized following the same innovative approach based on the NCL, as done for probes **6** and **7**. After gallium complexation of the sulfonated uPAR targeting and non targeting peptide probes (**12** and **13**), the products have been injected in U87 MG glioblastoma tumor-bearing mice. With respect the previous optical imaging acquisition, the injected dose was reduced from 10 to 5nmol, in order to decrease the fluorescence background. The *in vivo* dynamic optical imaging acquisition demonstrated how the specific probe reaches the tumor target at 1h post injection, as shown in Figures 4.5.

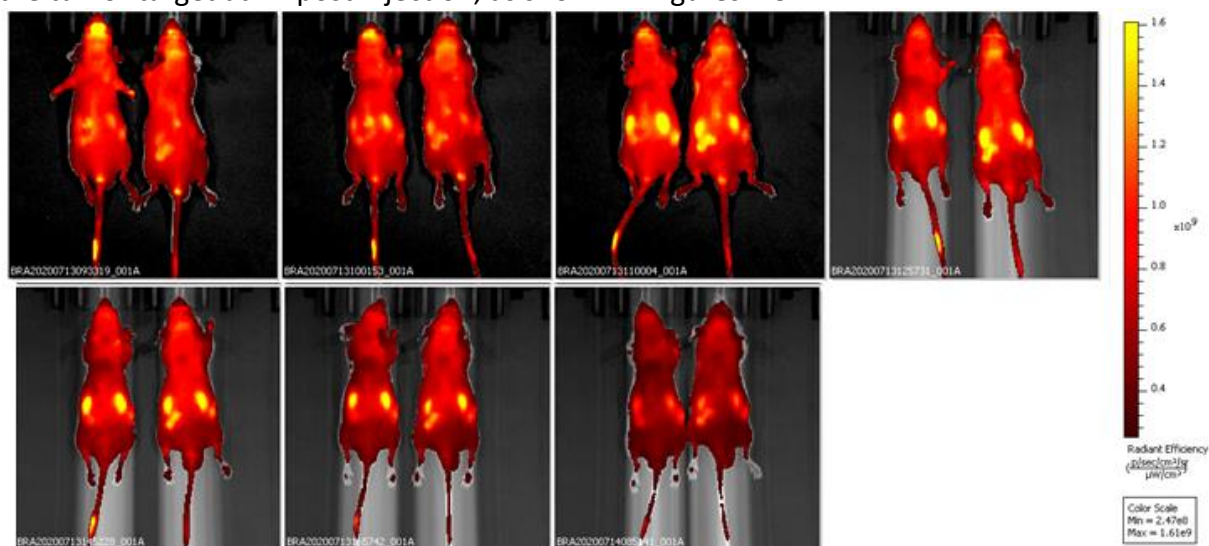


**Figure 4.5:** *In vivo* dynamic images acquired after inj. of probe **12** (group 1). Time points: 30 min, 1h, 2h, 4h, 6h, 8h, 24h.

Despite the good results obtained with the sulfonated probe **12** in comparison with non sulfonated **10**, the uPAR aspecific probe **13** showed a certain affinity for tumor target, as shown in Figure 4.6.

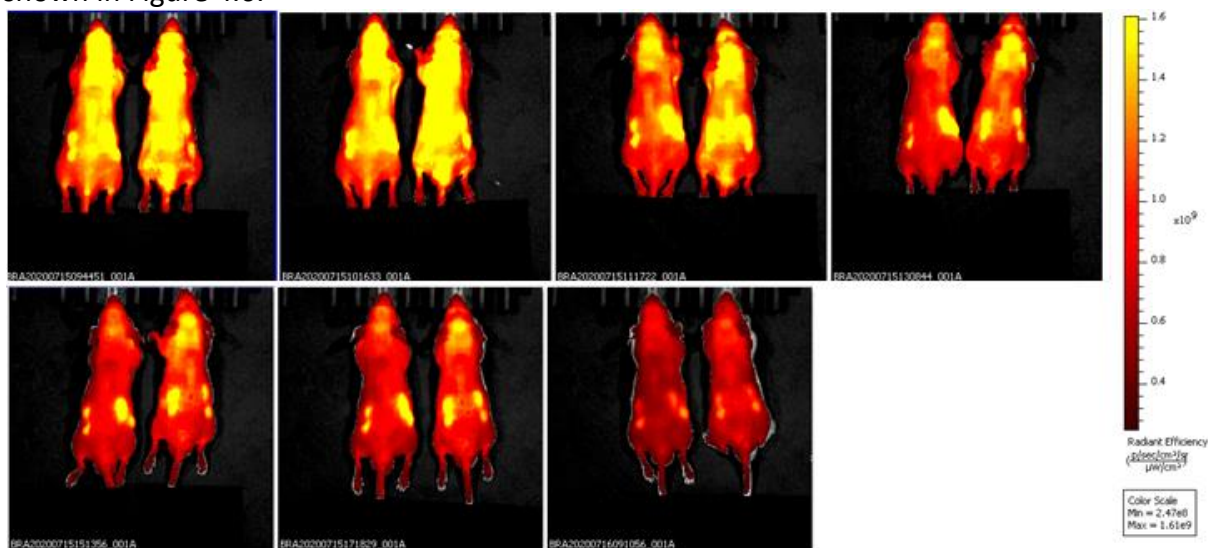


**Figure 4.6:** *In vivo* dynamic images acquired after inj. of probe **13** (group 2).  
Time points: 30 min, 1h, 2h, 4h, 6h, 8h, 24h.

A small but no significant difference between specific probe **12** and aspecific probe **13** can be appreciate observing graphs in Figure 4.7.

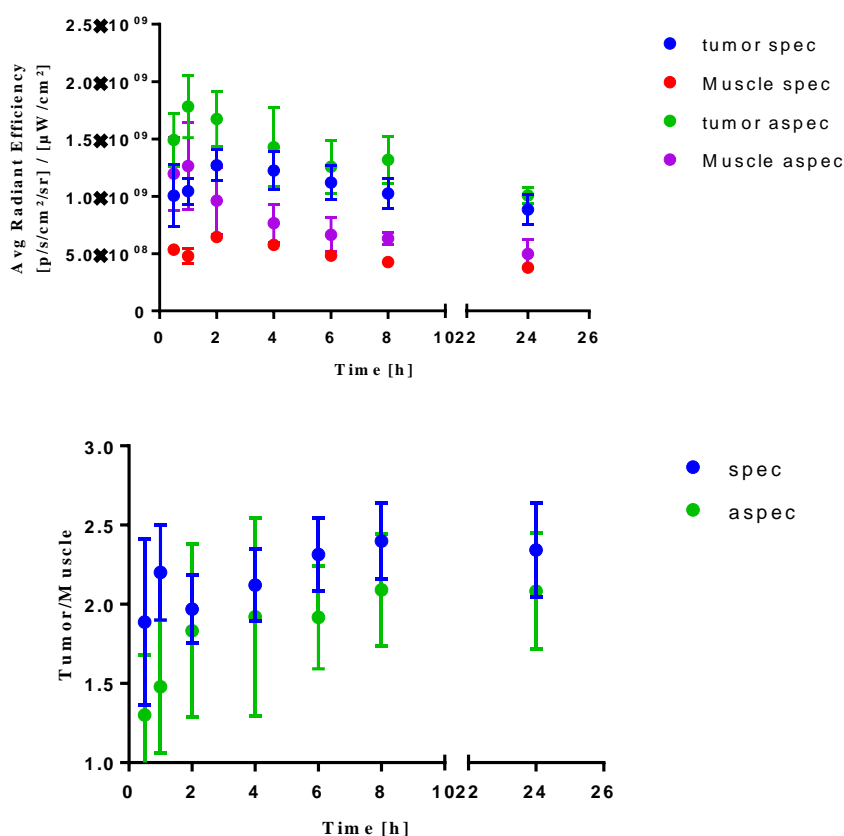


**Figure 4.7:** *In vivo* dynamic profiles after inj. of probe **12** and **13** (group 1 and 2).  
The observed results during *in vivo* dynamic optical imaging acquisitions have been confirmed by the *ex vivo* acquisitions at 24h. Differently from *ex vivo* ROI evaluation of the groups injected with probe **10**, it can be observed in Figure 4.8 and 4.9, how in this case, the tumors exhibit the higher fluorescence in comparison with the other organs.

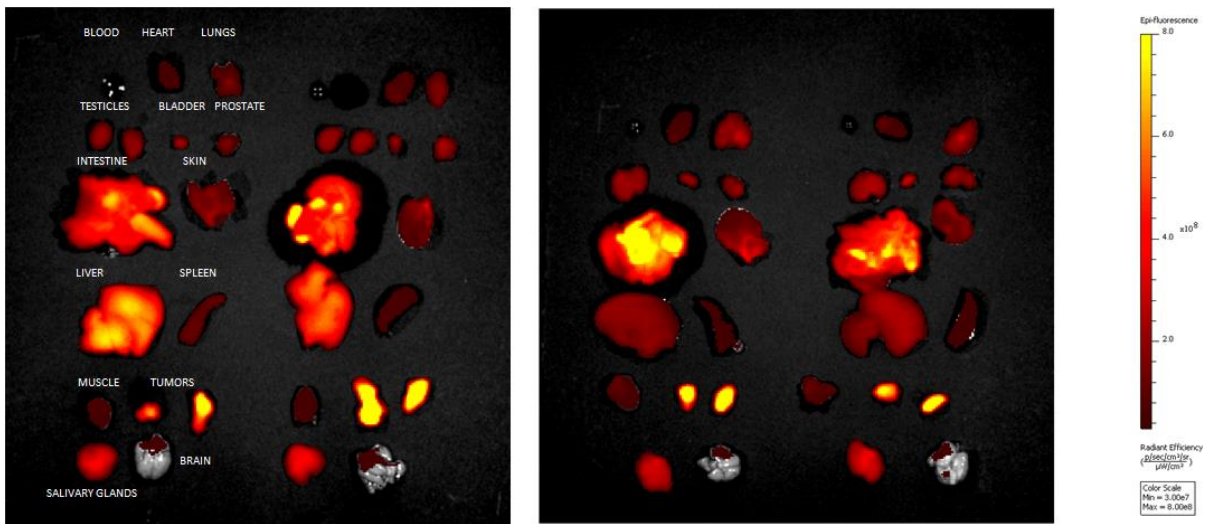


**Figure 4.8:** *Ex vivo* ROI evaluations 24h post inj. of product **12** and **13** (groups 3 and 4).

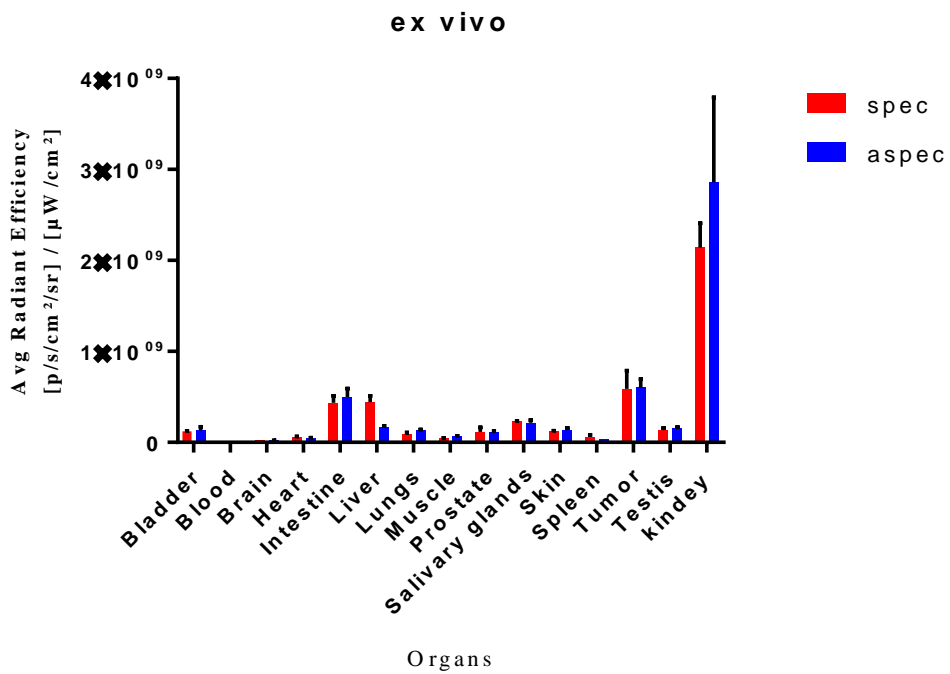


**Figure 4.9:** *Ex vivo* ROI evaluations 24h post inj. in the main organs of product **12** (spec) and **13** (aspec) (groups 3 and 4).

## 4.8 Conclusions

In conclusion, the herein reported results show that a synthesis strategy can be set-up to obtain peptide-containing molecules (e.g. AE105, cycloRGDfK and AE105mut) functionalized with a fluorophore (e.g. cy 5.5 or sulfo cy 5.5) and a chelator (e.g. AAZTA). The reported synthesis procedure can be generally applied to obtain dual imaging probes. Compounds **6**, **7**, **8** and **9** if labelled with Ga-68 could be considered as candidates for dual detection with PET and optical imaging. Such probes might be particularly useful in image-guided surgery via the detection of the fluorescence reporters once the occurrence of successful targeting has been verified pre-surgery by the acquisition of PET images. The use of sulfo cy 5.5 instead cy 5.5 demonstrated a faster biodistribution profile related to the increase of the overall solubility of the probes. The decrease of the dose, from 10 to 5 nmol showed how the background fluorescence of the animals decreased, obtaining better quality imaging acquisitions. Both in vivo and ex vivo acquisitions, showed how Ga-AAZTA-C4-CO-Cys(sulfo Cy 5.5)-AE105 (**12**) improved the biodistribution and elimination profile with respect the probe **10**, matching the half-life of Gallium-68 (68 min). This preliminary in vivo study demonstrate that AE105mut is not feasible as control peptide, showing a no significant difference in terms of binding specificity as reported in literature.



## 4.9 Supporting information

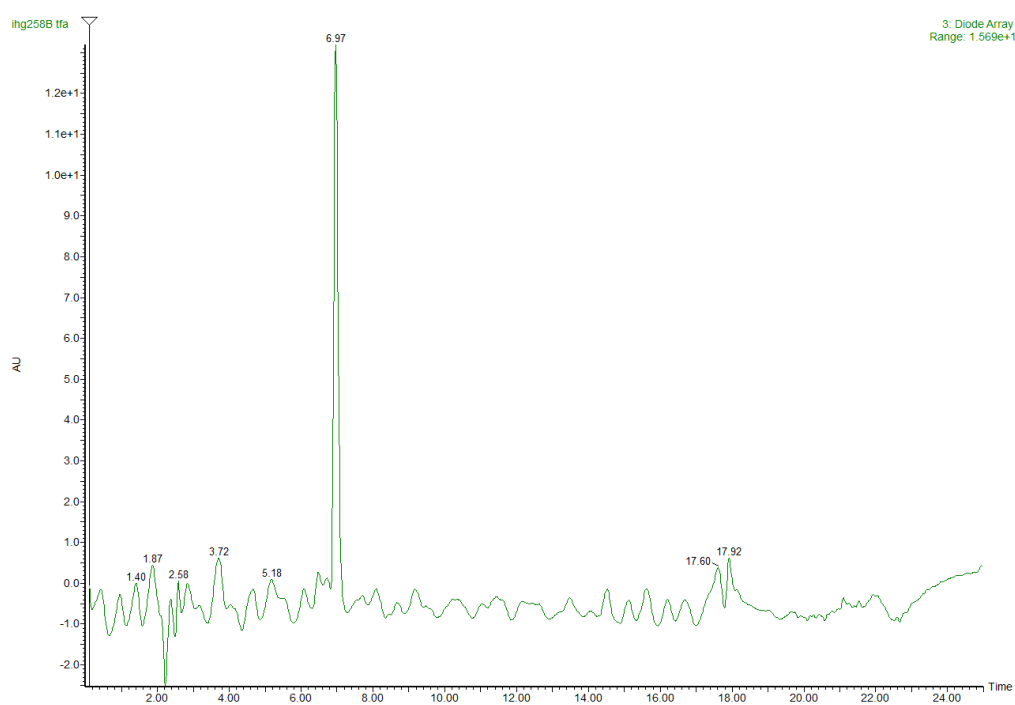
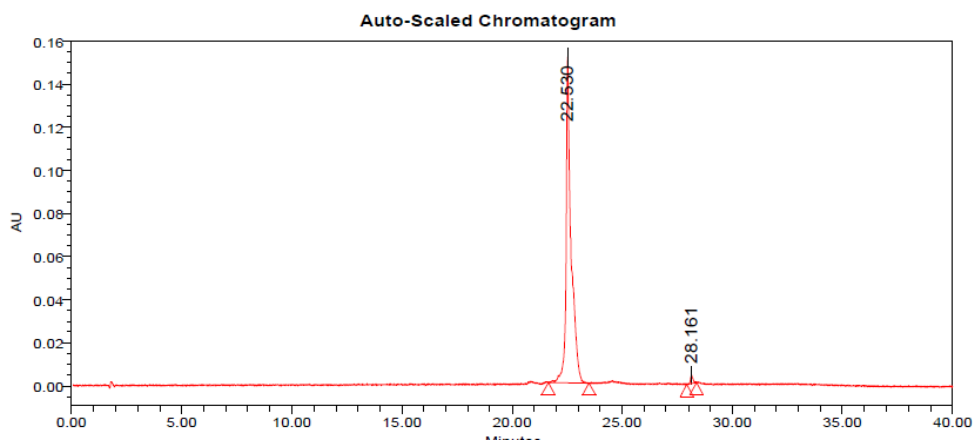


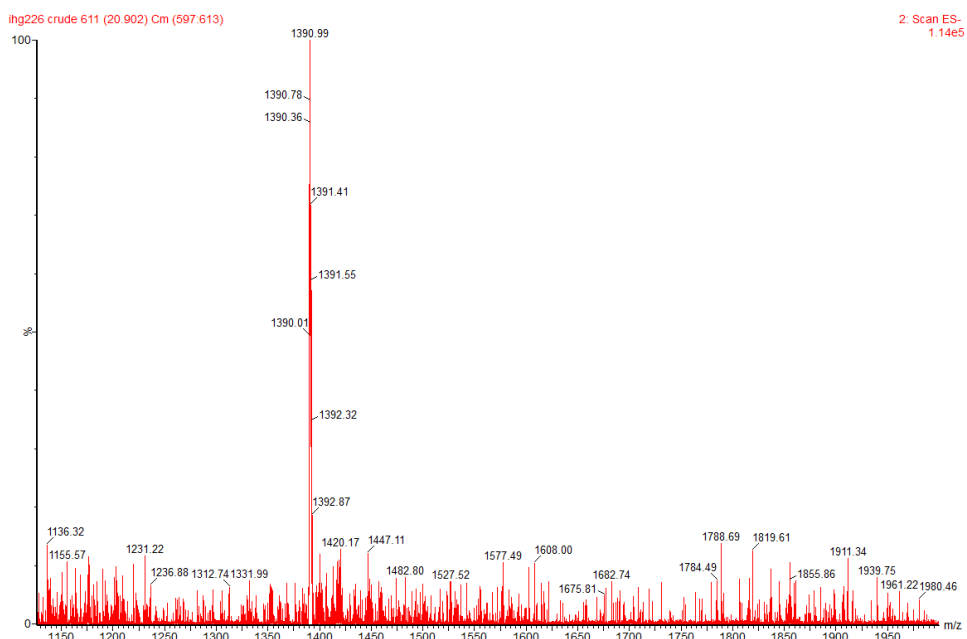
Figure S4.1: HPLC chromatogram revealed at 210 nm of pure **1b**.



Figure S4.2: Mass spectrum of **1b**.



**Figure S4.3:** HPLC chromatogram revealed at 210 nm of pure **8**.



**Figure S4.4:** Mass spectrum of **8**.

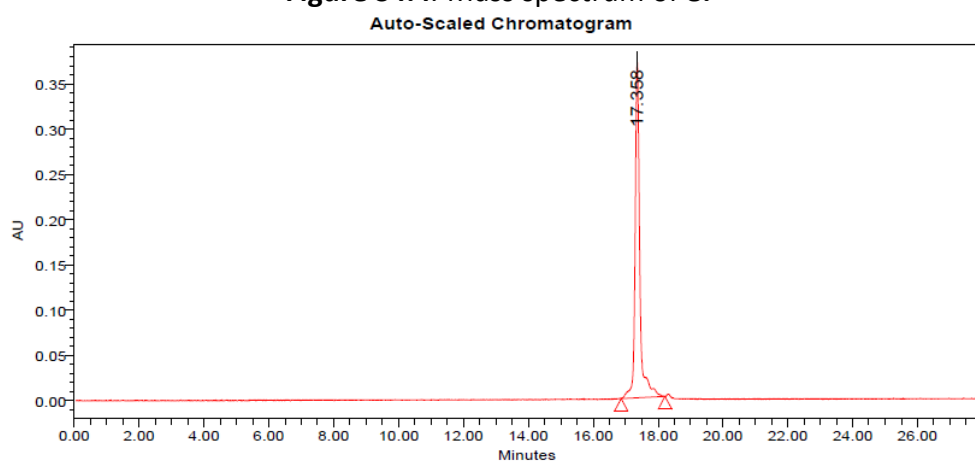


**Figure S4.5:** HPLC chromatogram revealed at 210 nm of pure **9**.

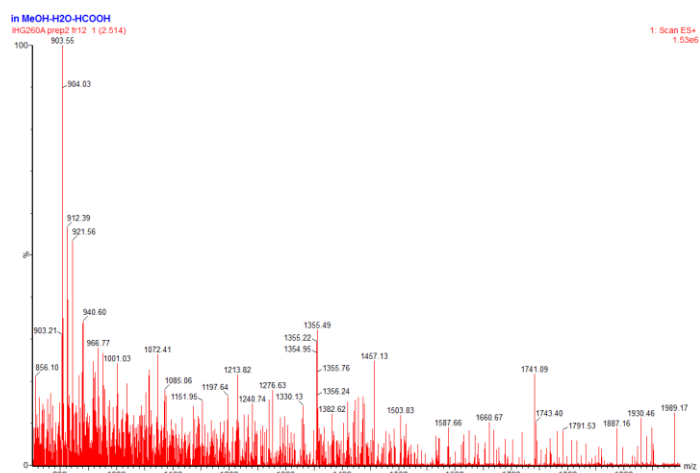


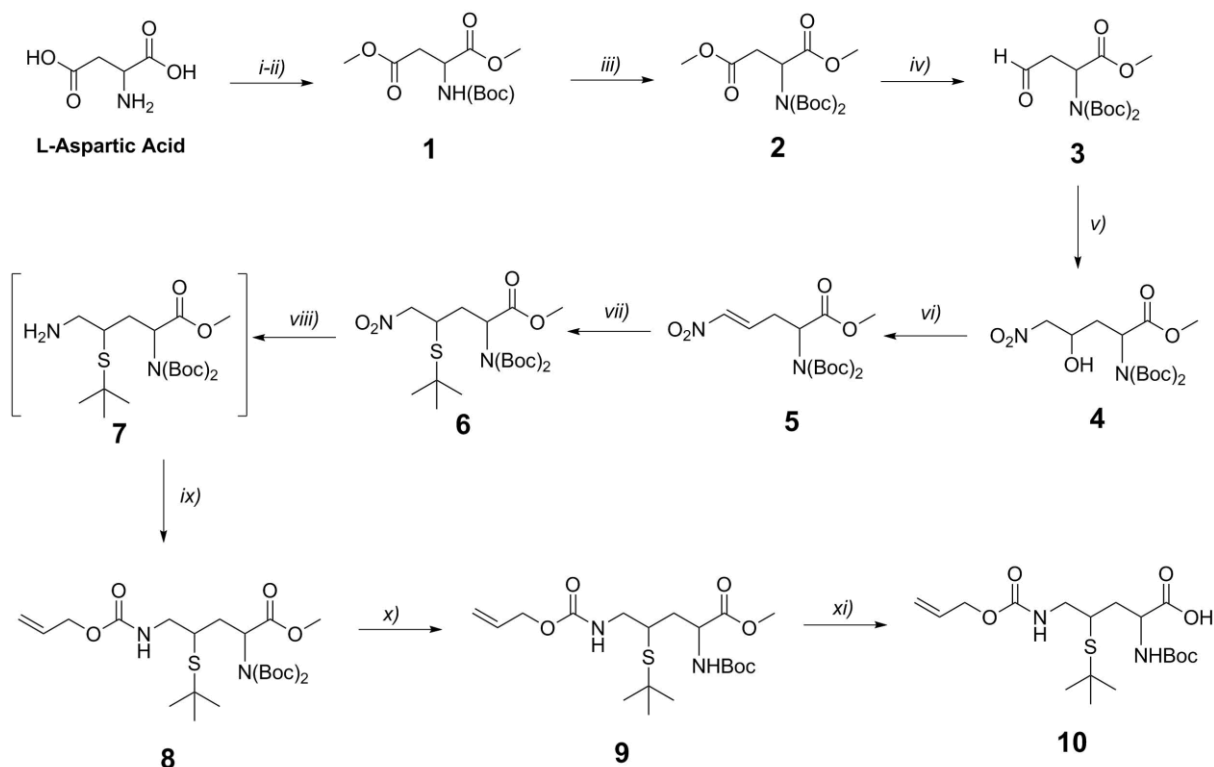
**Figure S4.6: Mass spectrum of 9.**

1. M. Persson, M. Hosseini, J. Madsen, T. J. Jørgensen, K. J. Jensen, A. Kjaer and M. Ploug, *Theranostics*, 2013, **3**, 618-632.

## V. DESIGN AND SYNTHESIS OF $\gamma$ -(R,S)-MERCAPTOORNITHINE

### 5.1 Purpose

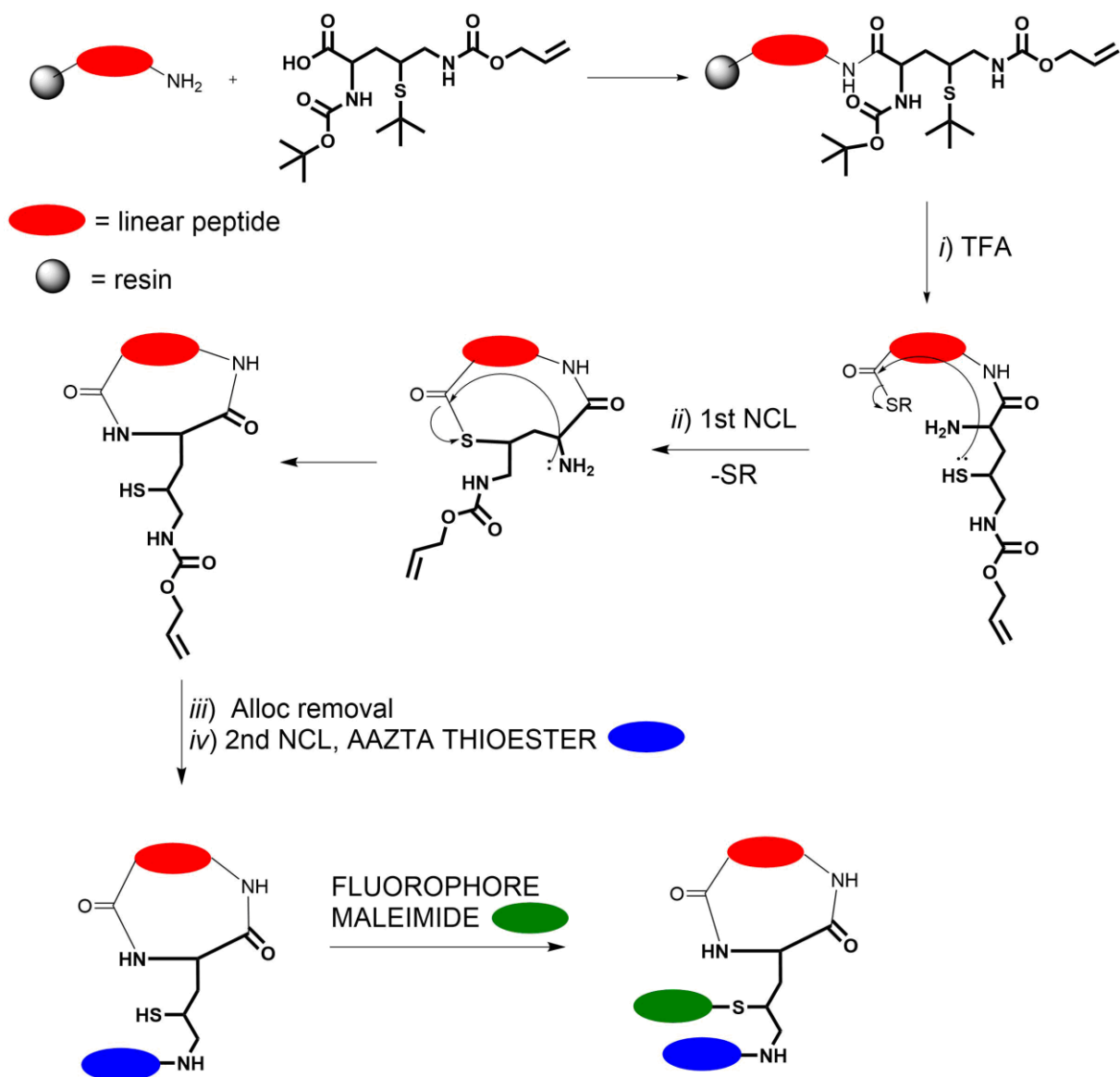
The aim of this chapter was to synthesize a  $\gamma$ -(R,S)-mercaptoornithine in order to obtain a new particular amino acid which can be used, after the anchoring to a linear on-resin peptide, to perform a peptide cyclization, followed by the attachment of a chelator (i.e. AAZTA) and a fluorophore, to easily obtain a dual PET/OI probe. The synthesis pathway consists in 11 steps, as shown in Scheme 1.



**Scheme 1: Synthesis scheme of 10:**

*i)*  $\text{Me}_3\text{SiCl}$ ,  $\text{MeOH}$ ; *ii)*  $(\text{Boc})_2\text{O}$ ,  $\text{Et}_3\text{N}$ ; *iii)*  $\text{Boc}_2\text{O}$ , DMAP (4-dimethylaminopyridine),  $\text{CH}_3\text{CN}$ ; *iv)* DIBAL (diisobutylaluminum hydrate),  $\text{Et}_2\text{O}$ ; *v)*  $\text{CH}_3\text{NO}_2$ , TBAF (*tetra* N-butylammonium fluoride); *vi)*  $\text{Ac}_2\text{O}$ , DMAP,  $\text{Et}_2\text{O}$ ; *vii)* *t*Bu-SH, *n*BuLi, THF; *viii)*  $\text{NaBH}_4$ ,  $\text{NiCl}_2$ ,  $\text{MeOH}/\text{THF}$ ; *ix)* Allyl Chloroformate, TEA (triethylamine), THF; *x)* TFA/ $\text{CH}_2\text{Cl}_2$ ,  $0^\circ\text{C}$ , 1h,  $\text{Boc}_2\text{O}$ ; *xi)* NaOH, *i*Pro/ $\text{H}_2\text{O}$ .<sup>1</sup>

To be used for the previously described purpose, product **10** has to be attached to the N-Terminal position of an on-resin linear peptide (i.e. RGDfk). As fully described by Terrier et al.<sup>2</sup>, a specific resin has to be used for the synthesis of the linear peptide, following the Fmoc Solid phase synthesis protocol, to allow the thioester formation on the C-Terminus. After the anchoring of the linear peptide derivatized with the 'special' aminoacid **10**, the cleavage from the resin could be carried out by TFA addition to the reaction vessel. At the same time, *t*-Bu and Boc protecting groups of the product **10**, could be cleaved to allow the chemoselective reaction between the C-Terminus thioester and the free thiol. After an internal S to N shift, a new native peptide bond (amide) can be formed, giving the peptide cyclization (See Scheme 2).



**Scheme 2:** Schematic simplified chemical representation of the peptide cyclization, chelator attachment, fluorophore derivatization.

After the peptide cyclization, the synthetic strategy relies on the chemical approach described in the previous chapter (see also Manuscript 2).

## 5.2 Materials and Methods

All reagents were purchased by Sigma Aldrich (Darmstad, Germany) and IRIS Biotech (Marktredwiz, Germany). All solvents were purchased by VWR International (Radnor, USA) and were used without further purifications.

NMR spectra were recorded at 298 K on a Bruker AVANCE 600 spectrometer. CDCl<sub>3</sub> and NMR tube were purchased from Sigma Aldrich.

Mass spectra with electrospray ionization (ESI) were recorded on a SQD 3100 Mass Detector (Waters). The HPLC-MS analytical runs were carried out on a Waters AutoPurification system (3100 Mass Detector 600 Quaternary Pump Gradient Module, 2767 Sample Manager and 2487 UV/Visible Detector). UPLC-MS analyses were performed using a Waters Acquity UPLC *H*-Class coupled with and ESI source, a quadrupole (QDa) mass analyzer and dual-wavelength UV/Vis TUV Detector.

## 5.3 Experimental chemical synthesis procedures

### 5.3.1 Dimethyl (S)-2-tert-butoxycarbonylamino-butanodioate (1)

In a three-neck round bottom flask, 5.32 g of L-Aspartic Acid (39.97 mmol) were dissolved in MeOH (120 mL). The solution was brought to 0°C with an ice bath, then Me<sub>3</sub>SiCl (23.2 mL, 4.4 eq.) were added dropwise. The ice bath was removed and the solution was left to stir overnight at room temperature. 36 mL of TEA were added to the reaction solution. Subsequently 9.6 g of Boc<sub>2</sub>O (1.1 eq) were added. The reaction was left to stir overnight at room temperature. The solvent was evaporated *in vacuo*. The obtained with solid was washed with Et<sub>2</sub>O (3X250 mL) on Celite®. The collected supernatant was evaporated and the crude product was purified on flash silica chromatography with CH<sub>2</sub>Cl<sub>2</sub>/MeOH 99:1→97:3 to afford pure **1** as white solid (7.23 g, 69%). <sup>1</sup>H-NMR (CDCl<sub>3</sub>, 600 MHz): δ 1.47 (s, 9H), 2.85 (dd, 1H, J=4.6 Hz), 3.04 (dd, 1H, J=4.39Hz), 3.72 (s, 3H), 3.79 (s, 3H), 4.60 (quint, 1H, J<sub>1</sub>=J<sub>2</sub>=4.33Hz) 5.52 (d, 1H, J=3.82Hz).

### 5.3.2 Dimethyl (2S)-2-{{tert-butoxy}-N-{{tert-butyl}oxycarbonyl}carbonylamino}butane-1,4-dioate(2)

In a three-neck round bottom flask, 7.23 g of **1** were dissolved in CH<sub>3</sub>CN (90 mL). 676 mg of DMAP (0.2 eq.) and 6.64 g of Boc<sub>2</sub>O (1.1 eq.) were added to the obtained solution. The reaction was left to stir at room temperature for 2 h. A second portion of Boc<sub>2</sub>O was added to the solution (3.02 g, 0.5 eq.) and it was left to stir overnight at room temperature. The solvent was evaporated *in vacuo* and the crude product was purified on flash silica chromatography with Petrol Ether/Ethyl Acetate 8:2 to afford pure **2** as white solid (8.91 g, 89%). <sup>1</sup>H-NMR (CDCl<sub>3</sub>, 600 MHz): δ 1.53 (s, 18H), 2.55 (dd, 1H, J=4.7 Hz), 3.27 (dd, 1H, J=7.18Hz), 3.73 (s, 3H), 3.75 (s, 3H), 5.48 (t, 1H, J=6.80Hz).

### 5.3.3 Methyl (2S)-2-{{tert-butoxy}-N-{{tert-butyl}oxycarbonyl}carbonylamino}-4-oxobutanoate (3)

In a two-neck round bottom flash equipped with rubber septum, 4.45 g of **2** were dissolved in dry Et<sub>2</sub>O (125 mL). The solution was brought to -78°C with acetone/N<sub>2</sub> bath. 13.56 mL of a 1M solution of DIBAL in hexane (12.3 mmol, 1.1 eq.) was added dropwise. After the end of the addition, the solution was left to stir at -78°C for 5 minutes and then quenched with H<sub>2</sub>O (1.54 mL, ab. 7 eq.). The solution was stirred for additional 30 minutes, then the solvent was evaporated *in vacuo* and the crude product was purified on flash silica chromatography with Petrol Ether/Ethyl Acetate 95:5→85:15 to afford pure **3** (2.58 g, 63%). <sup>1</sup>H-NMR (CDCl<sub>3</sub>, 600 MHz): δ 1.52 (s, 18H), 2.85 (dd, 1H, J=5.89 Hz), 3.44 (dd, 1H, J=6.91Hz), 3.75 (s, 3H), 5.55 (t, 1H, J=6.40Hz), 9.81 (s, 1H).

### 5.3.4 Methyl (5R,S)-hydroxy-5-nitro-(2S)-2-{{tert-butoxy}-N-{{tert-butyl}oxy carbonyl}-carbonylamino}-pentanoate(4)

In a round bottom flask 2.58 g of **3** were dissolved in 6.9 mL of nitromethane and the obtained solution was brought to -5°C with a CaCl<sub>2</sub>/ice bath. Under inert atmosphere of argon, 1.23 g of TBAF (0.5 eq.) were added. The solution was left to stir at 0°C for 15 minutes. The solvent

was evaporated *in vacuo* and the crude product was purified on flash silica chromatography with Petrol Ether/Ethyl Acetate 8:2→7:3 to afford the pure **4** (3.05 g, 73%). <sup>1</sup>H-NMR (CDCl<sub>3</sub>, 600 MHz): δ 1.55 (tr, 18H), 1.91 (tr, 1H), 2.28 (tr, 1H), 2.56 (tr, 1H), 3.00(tr, 1H), 3.69 (tr, 1H), 3.77 (tr, 3H). ESI-MS (*m/z*): calcd: For C<sub>16</sub>H<sub>28</sub>N<sub>2</sub>O<sub>9</sub> (M+H, Boc loss)<sup>+</sup> 193.17 found: 193.15.

### 5.3.5 Methyl 5-nitro-2-(bis(tert-butoxycarbonyl)amino)-pent-4-enoate(**5**)

In a round bottom flask, 1.24 g of **4** were dissolved in Et<sub>2</sub>O (15.5 mL) and the solution was brought at 0°C with an ice bath. 349 uL of acetic anhydride (1.2 eq.) and 148 mg of DMAP (0.4 eq.) were added to the reaction solution. The solution was stirred until the consumption of the starting material, monitored by TLC (ab. 2h). The solvent was evaporated *in vacuo* and the crude product was purified on flash silica chromatography with Petrol Ether/Ethyl Acetate 85:15 to afford the pure **5** (0.852 g, 72%). The purity of the product was checked by analytical UPLC-MS by employing an ACQUITY UPLC® Peptide BEH C18 column (300Å, 1.7µm, 2.1X100mm). Eluent: (A) 0.05% TFA in H<sub>2</sub>O, (B) 0.05% TFA in CH<sub>3</sub>CN. Gradient profile; linear gradient from 5% to 50% of B in 7 min, linear gradient from 50% to 100% in 3 min, isocratic at 100% for 3 minutes. Flow rate of 0.4 mL/min and UV detection at 254 nm. Purity 99%. ESI-MS (*m/z*): calcd: For C<sub>16</sub>H<sub>26</sub>N<sub>2</sub>O<sub>8</sub> (M+Na)<sup>+</sup>397.38 found: 397.28.

### 5.3.6 Methyl 5-nitro-2-(bis(tert-butoxycarbonyl)amino)-4-(tert-butylthio)pentanoate (**6**)

To a three-neck round bottom flask under inert atmosphere of argon equipped with a rubber septum, 6.5 mL of dry THF were added. 180 uL of *t*-BuSH (1.602, 1.2 eq.) were added to the solution which was brought at -10°C with a NaCl/ice bath. Subsequently 1 mL of a 1.6 M solution of *n*BuLi in hexane (1.602 mmol, 1.2 eq.) were added to the obtained solution which was left to stir at -10°C for 10 minutes. The NaCl/ice bath was removed and the solution was brought at -78°C with an acetone/N<sub>2</sub> bath. 500 mg of **5** (1.335 mmol, 1 eq.), previously dissolved in dry THF, were slowly added to the reaction solution for 10 minutes. The reaction was left to stir at -78°C for 1h and then was quenched with NH<sub>4</sub>Cl (5 mL) and 20 mL of H<sub>2</sub>O were added. The product was extracted with ethyl acetate (3 X 15 mL) and the organic phase was anhydriified with Na<sub>2</sub>SO<sub>4</sub>. The solution was filtered and the solvent was evaporated *in vacuo*. The product has been used for the subsequent step without further purification. (545 mg, 88%). The purity of the product was checked by analytical UPLC-MS by employing an ACQUITY UPLC® Peptide BEH C18 column (300Å, 1.7µm, 2.1X100mm). Eluent: (A) 0.05% TFA in H<sub>2</sub>O, (B) 0.05% TFA in CH<sub>3</sub>CN. Gradient profile; linear gradient from 5% to 50% of B in 7 min, linear gradient from 50% to 100% in 3 min, isocratic at 100% for 3 minutes. Flow rate of 0.4 mL/min and UV detection at 254 nm. Purity 95%. ESI-MS (*m/z*): calcd: For C<sub>20</sub>H<sub>36</sub>N<sub>2</sub>O<sub>8</sub> (M+Na)<sup>+</sup>487.56 found: 487.20.

### 5.3.7 Methyl 5-(((allyloxy)carbonyl)amino)-2-(bis(tert-butoxycarbonyl)amino)-4-(tert-butylthio)pentanoate (**8**)

In a round bottom flask, 106.1 mg of **6** (0.228 mmol) were dissolved in 4 mL of MeOH/THF 1:1. 108.6 mg of NiCl<sub>2</sub>\*6H<sub>2</sub>O (1.2 eq.) were added and the solution was left to stir at room temperature for 10 minutes. 51.75 mg of NaBH<sub>4</sub> (6 eq.) were slowly added portion wise to the solution. The reaction was monitored by TLC until a red spot appears at the base with addition of ninhidryn. The solvent was evaporated *in vacuo* and the product **7** was used for the subsequent step without further purification.



The unstable obtained primary amine (**7**) was re-dissolved in THF (4 mL). 95.3  $\mu$ L of TEA (3 eq.) and 29.1  $\mu$ L of allyl chloroformate (0.274 mmol, 1.2 eq.) were added to the solution which was left to stir for ab. 1h. The solvent was evaporated and the crude product was purified on gravimetric silica chromatography with Petrol Ether/Ethyl Acetate 8:2 to afford the pure **8** (35 mg, 30%). The purity of the product was checked by analytical HPLC-MS by employing an Atlantis DC18 5 $\mu$ m, 4.6X150mm column. Eluent: (A) 0.1% TFA in H<sub>2</sub>O, (B) 0.1% TFA in CH<sub>3</sub>CN. Gradient profile; linear gradient from 40% to 100% of B in 20 min, isocratic at 100% for 10 min. Flow rate of 1 mL/min and UV detection at 210 nm. RT: 25.6 min. Purity 95%. ESI-MS (*m/z*): calcd: For C<sub>24</sub>H<sub>42</sub>N<sub>2</sub>O<sub>8</sub>S (M+H)<sup>+</sup> 519.67 found: 519.39.

### 5.3.8 Methyl 5-(((allyloxy)carbonyl)amino)-2-((tert-butoxycarbonyl)amino)-4-(tert-butylthio)pentanoate(**9**)

In a round bottom flask, 277.7 mg of **8** (0.535 mmol) were dissolved in 10 mL of CH<sub>2</sub>Cl<sub>2</sub>. The solution was brought to 0°C with an ice bath, then 5mL of TFA were added dropwise. After 1h of stirring at RT 150mL of satNaHCO<sub>3</sub> were added and the obtained solution was extracted with ethyl acetate (3X20mL). The organic phase was collected, dried with Na<sub>2</sub>SO<sub>4</sub>, filtered and evaporated *in vacuo*. The obtained oil was re-dissolved in MeOH (5mL) and 1.44 mL of DIPEA were added. The solution was brought at 0°C with an ice bath and 1.1 eq of Boc<sub>2</sub>O (348.1 mg, 0.589 mmol). The solution was stirred at 0°C for 2h. The solvent was evaporated and the crude product was purified on flash silica chromatography with Hexane/Ethyl Acetate (85:15 to 8:2) to afford the pure **9** (180 mg, 80%). The purity of the product was checked by analytical HPLC-MS by employing an Atlantis DC18 5 $\mu$ m, 4.6X150mm column. Eluent: (A) 0.1% TFA in H<sub>2</sub>O, (B) 0.1% TFA in CH<sub>3</sub>CN. Gradient profile; linear gradient from 40% to 100% of B in 20 min, isocratic at 100% for 10 min. Flow rate of 1 mL/min and UV detection at 210 nm. RT: 25 min. Purity 99%. ESI-MS (*m/z*): calcd: For C<sub>19</sub>H<sub>34</sub>N<sub>2</sub>O<sub>6</sub>S (M+H)<sup>+</sup> 419.55 found: 419.27.

### 5.3.9 5-(((allyloxy)carbonyl)amino)-2-((tert-butoxycarbonyl)amino)-4-(tert-butylthio)pentanoic acid (**10**)

3eq of NaOH as powder (51.6 mg) were added to a solution of **9** (180 mg; 0.430mmol) in H<sub>2</sub>O/*i*Pro 1:1 (10 mL). The solution was stirred at room temperature for 6 h. The *i*Pro was evaporated *in vacuo* and the pH of the solution was brought to 7 by addition of HCl 1M. The aqueous residue was extracted with ethyl acetate (3x5 mL). The organic phases were collected, dried (Na<sub>2</sub>SO<sub>4</sub>), filtered and evaporated. The final product was obtained without further purification as a white solid. (138.8mg; 80%).The purity of the product was checked by analytical HPLC-MS by employing an Atlantis DC18 5 $\mu$ m, 4.6X150mm column. Eluent: (A) 0.1% TFA in H<sub>2</sub>O, (B) 0.1% TFA in CH<sub>3</sub>CN. Gradient profile; linear gradient from 40% to 100% of B in 20 min, isocratic at 100% for 10 min. Flow rate of 1 mL/min and UV detection at 210 nm. RT: 24.7 min. Purity 97%. ESI-MS (*m/z*): calcd: For C<sub>18</sub>H<sub>32</sub>N<sub>2</sub>O<sub>6</sub>S (M+H)<sup>+</sup> 405.52 found: 405.27.

## 5.4 Results and discussions

The reported synthesis procedure allows for the preparation of  $\gamma$ -(R,S)-mercaptoornithine, to be used for the previously described purposes (See Purpose).

Synthesis pathway consisted in 11 reaction steps, including 9 purifications performed by direct phase silica chromatography. Each intermediate product has been fully characterized by HPLC, MS and/or  $^1\text{H-NMR}$ . All intermediate has been obtained with high purity percentage, including product **10** (97%). The overall yield results to be 4%.

## 5.5 Conclusions

In conclusion, the herein reported results showed how, starting from L-Aspartic acid, can be obtained  $\gamma$ -(R,S)-mercaptoornithine. This 'special' aminoacid can be easily attached to a linear on-resin peptide, in order to perform a peptide cyclization, a chelator attachment and a fluorophore derivatization, under mild conditions, exploiting an innovative synthetic approach based on the Native Chemical Ligation. The second part of this aim will be carry out more further, as fully describes in scheme 2 of the paragraph 5.1.

## 5.6 Supporting information

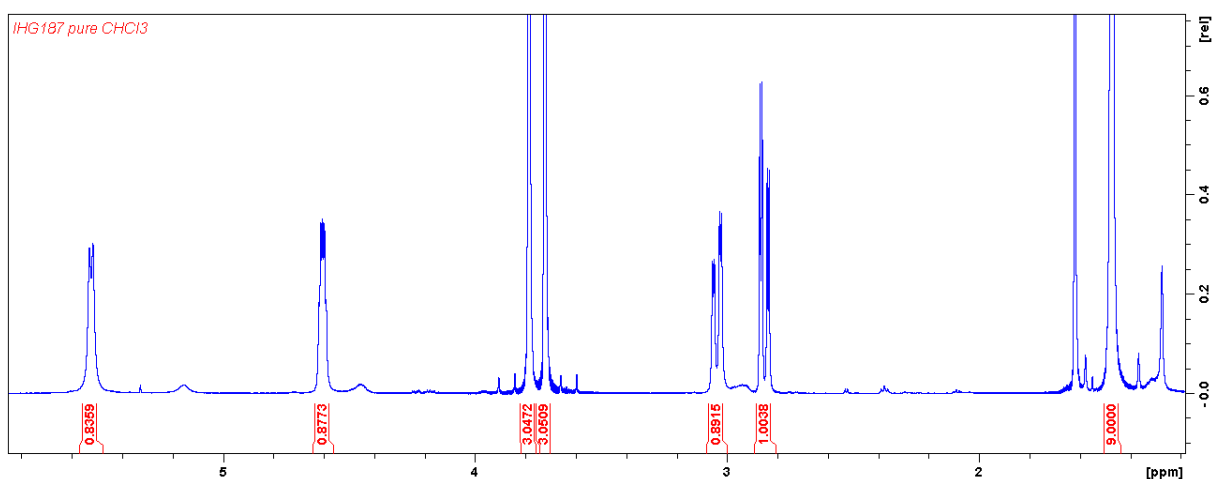


Figure S5.1: <sup>1</sup>H-NMR spectrum in CDCl<sub>3</sub> at 283K of the pure 1.

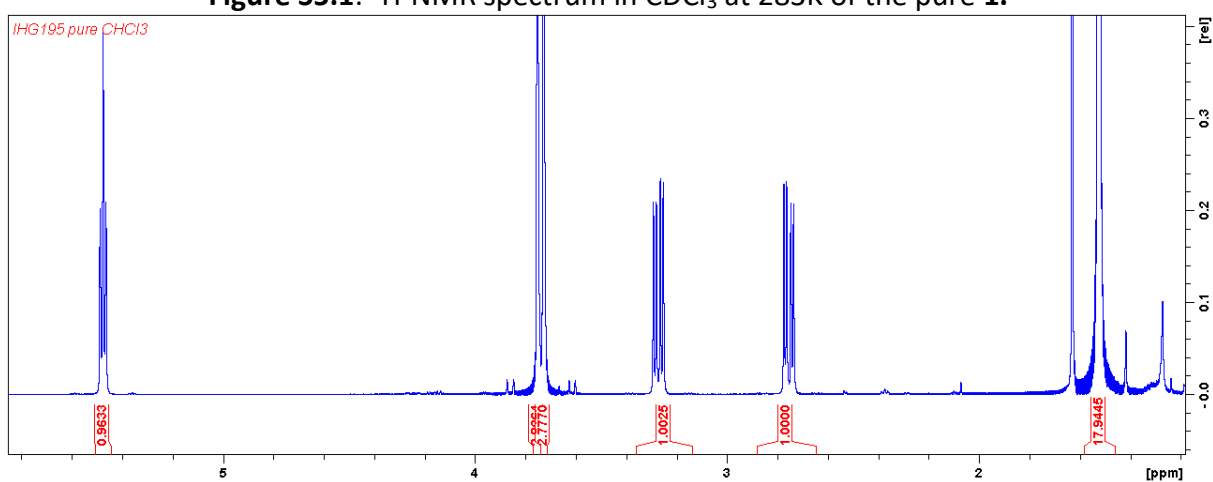


Figure S5.2: <sup>1</sup>H-NMR spectrum in CDCl<sub>3</sub> at 283K of the pure 2.

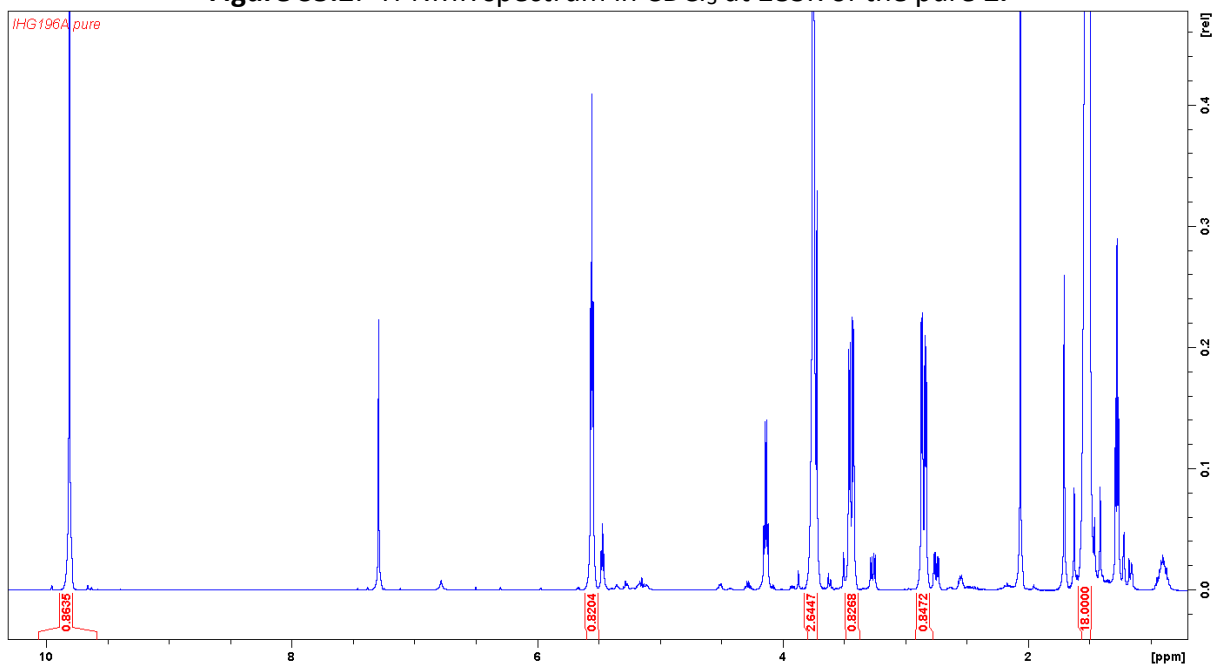
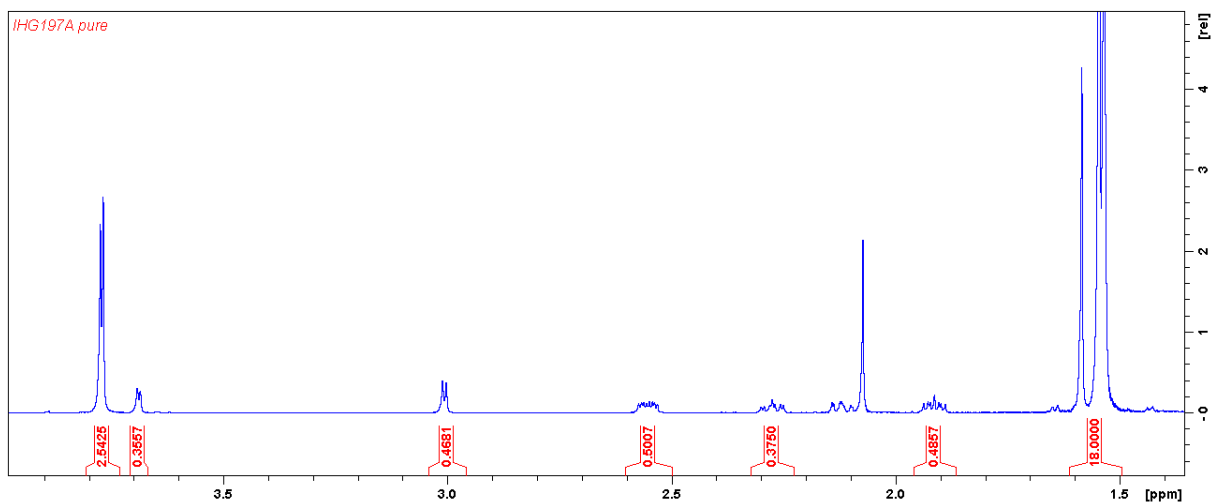


Figure S5.3: <sup>1</sup>H-NMR spectrum in CDCl<sub>3</sub> at 283K of the pure 3.



**Figure S5.4:**  $^1\text{H}$ -NMR spectrum in  $\text{CDCl}_3$  at 283K of the pure **4**.



**Figure S5.5:** HPLC chromatogram revealed at 254nm of pure **5**.

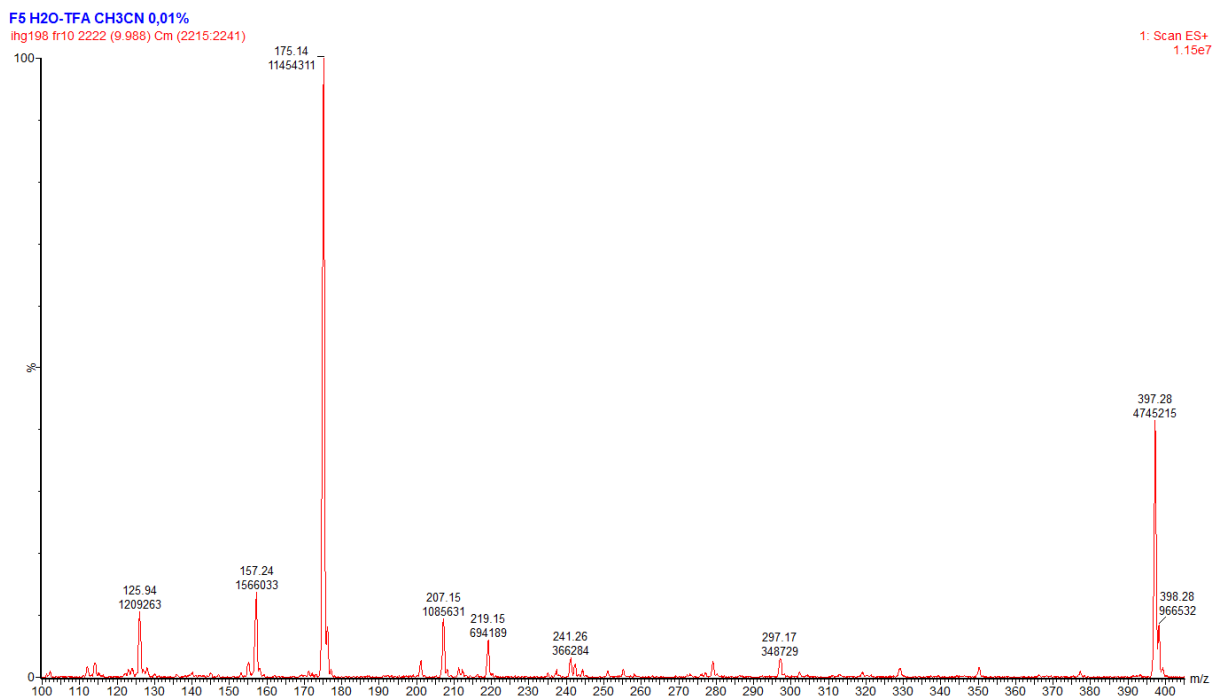


Figure S5.6: Mass spectrum of 5.

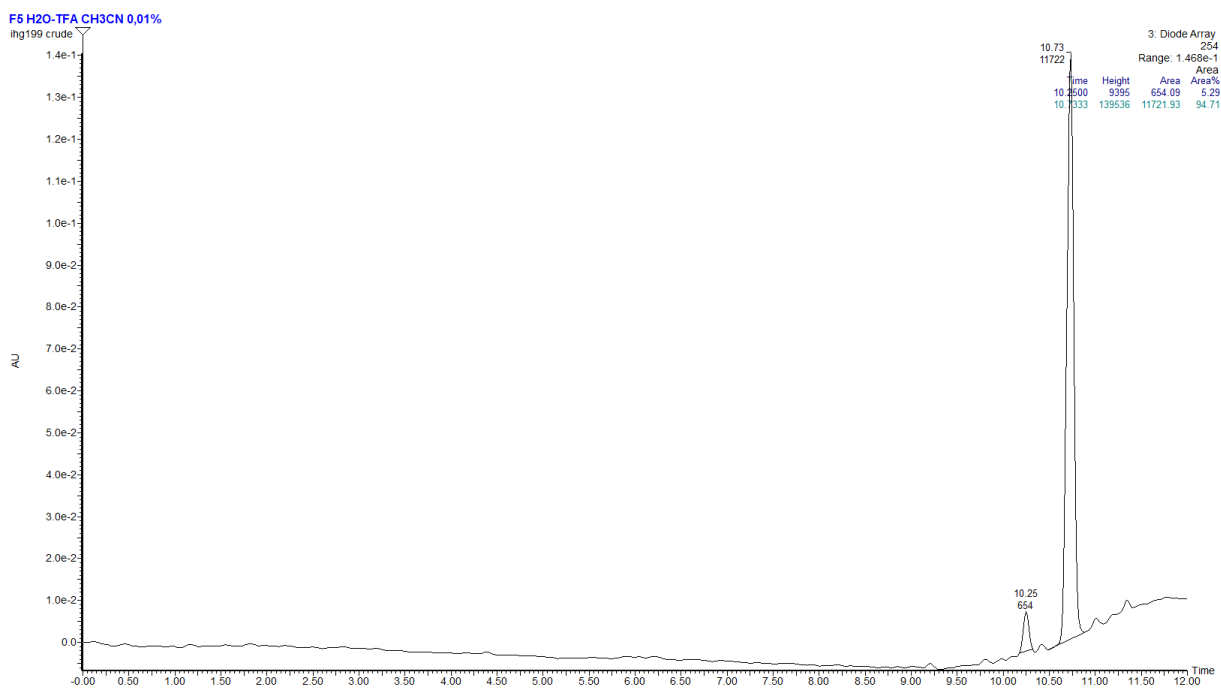
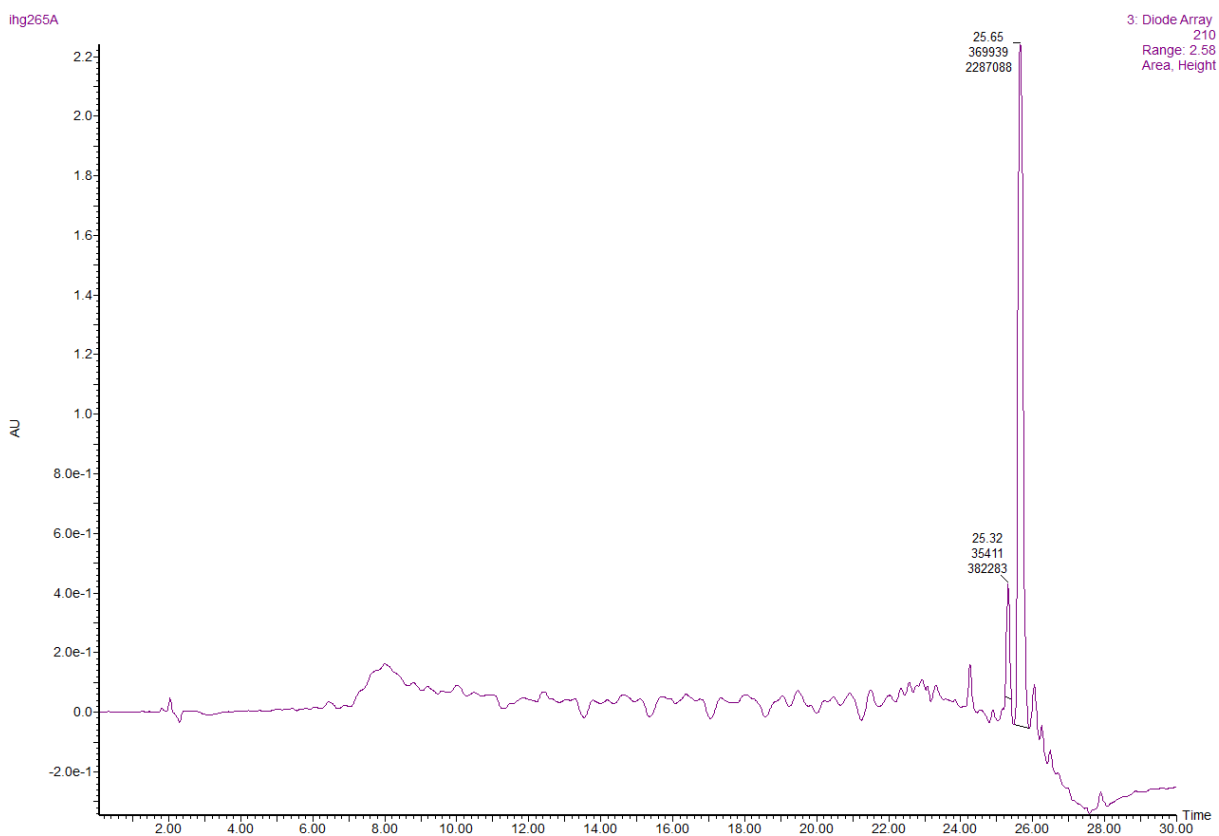
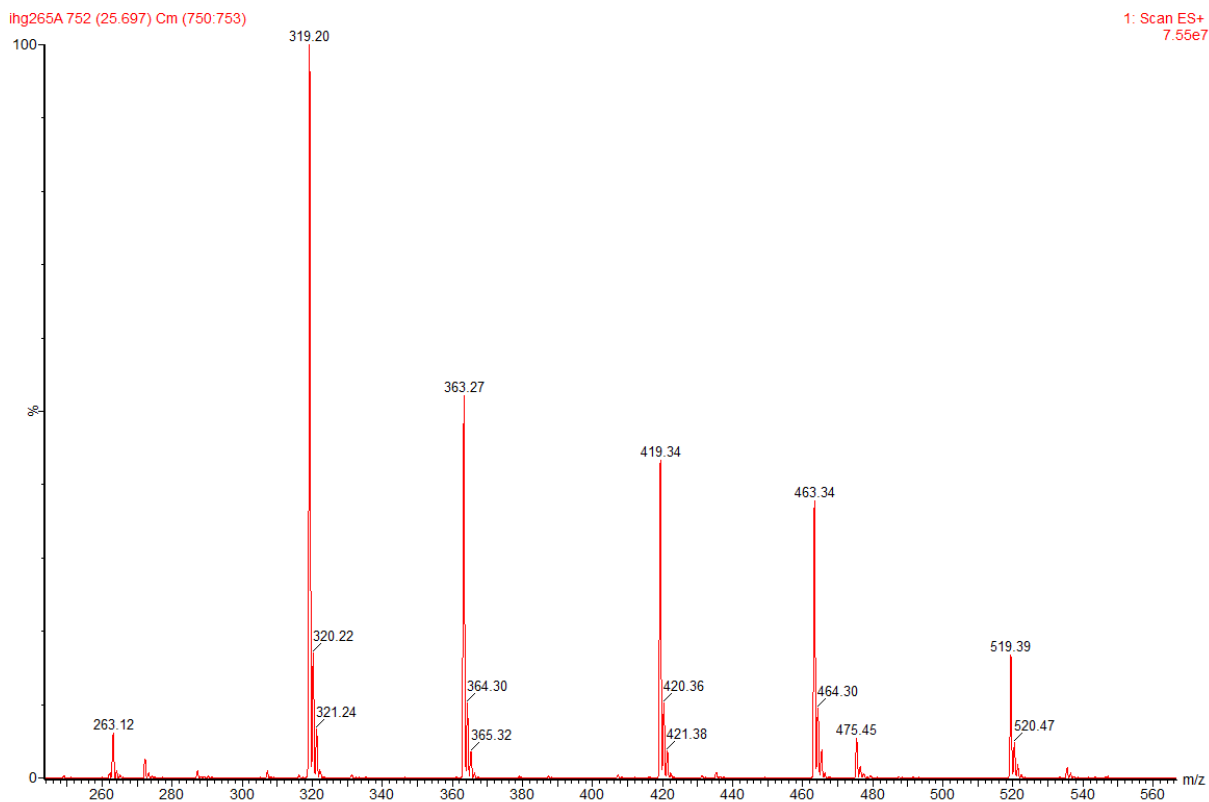


Figure S5.7: HPLC chromatogram revealed at 254nm of pure 6.



**Figure S5.8:** HPLC chromatogram revealed at 210nm of pure **8**.



**Figure S5.9:** Mass spectrum of **8**.

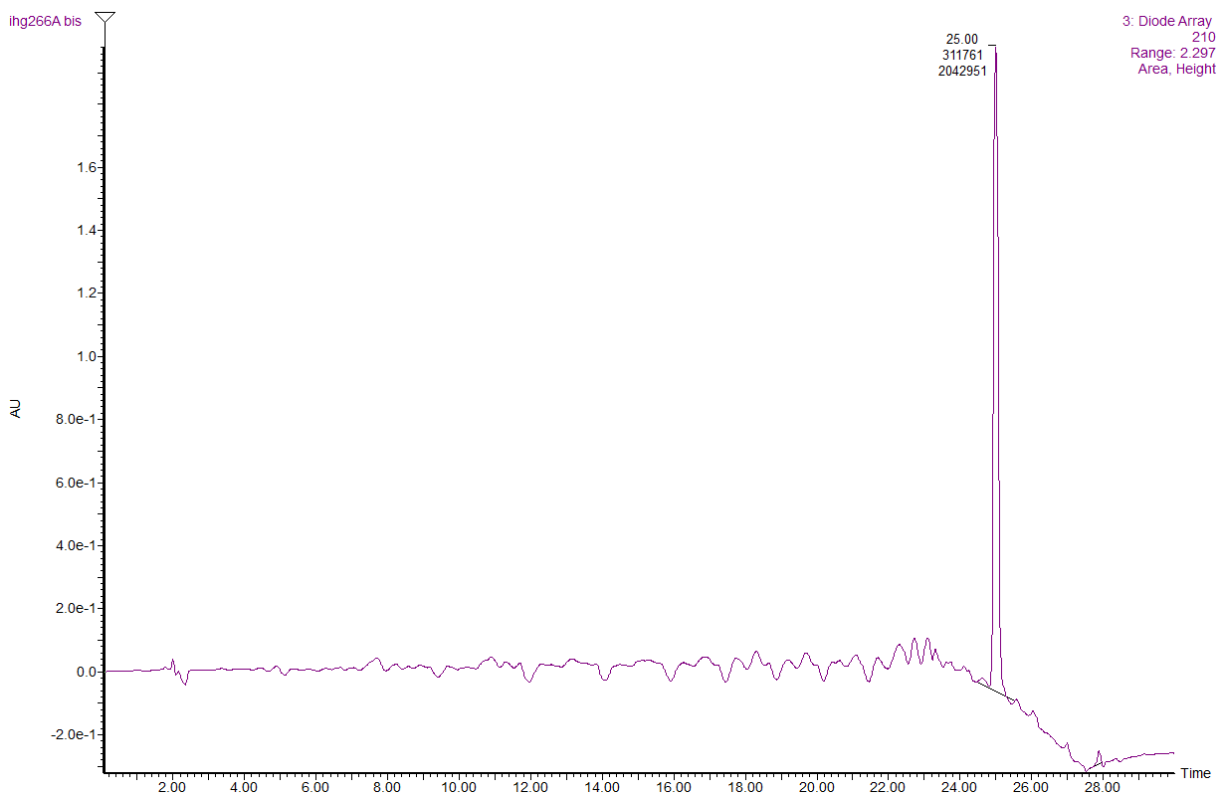


Figure S5.10: HPLC chromatogram revealed at 210nm of pure **9**.

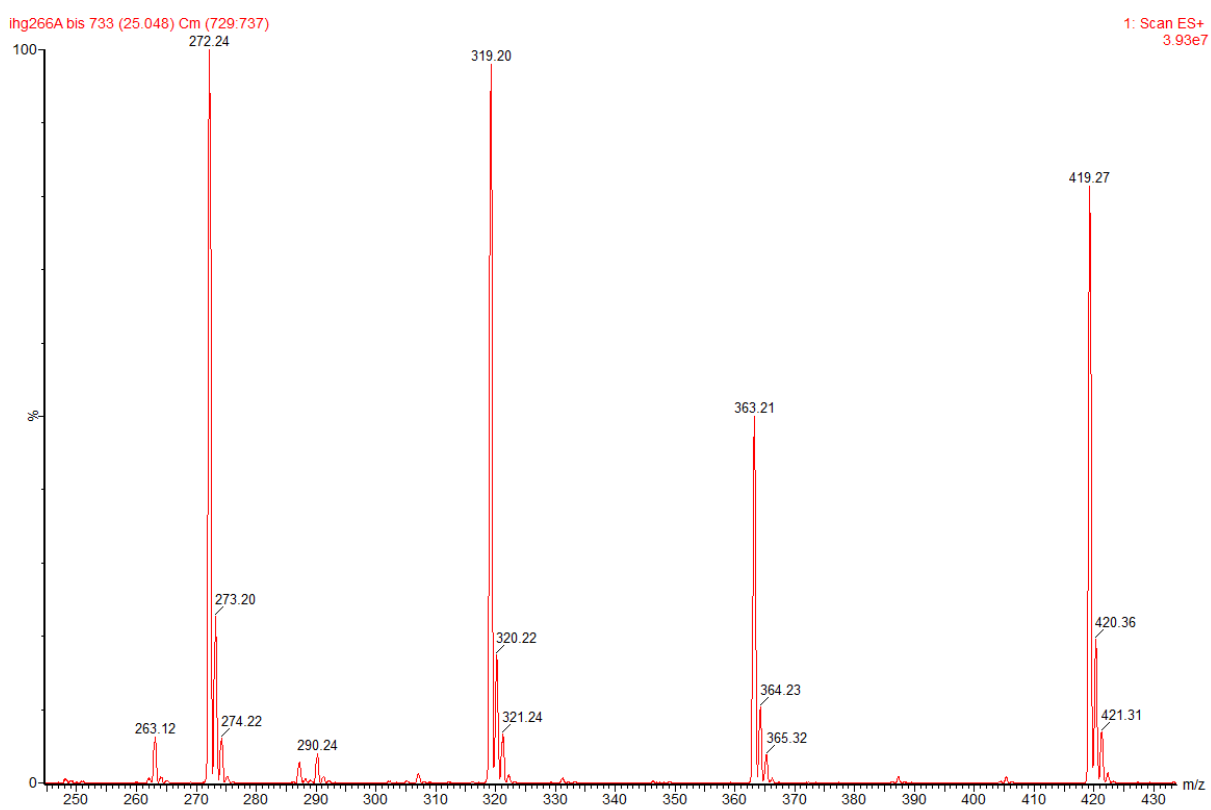
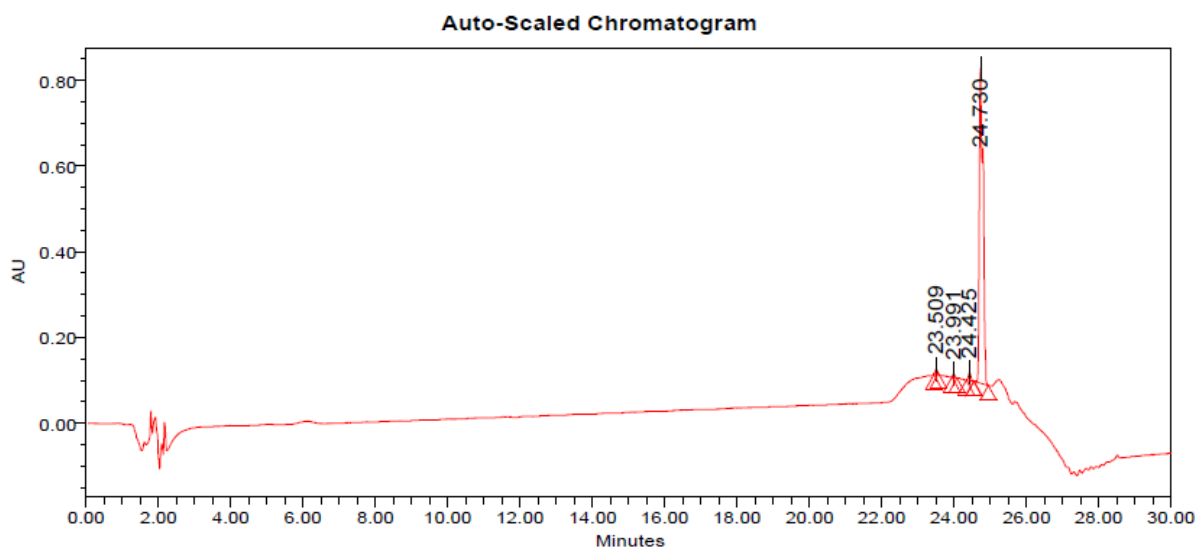


Figure S5.11: Mass spectrum of **9**.



**Peak Results**

	RT	Area	Height	% Area
1	23.509	41926	9843	0.76
2	23.991	30779	8027	0.56
3	24.425	87074	18802	1.58
4	24.730	5344864	734721	97.10

**Figure S5.12:** HPLC chromatogram revealed at 210nm of pure **10**.

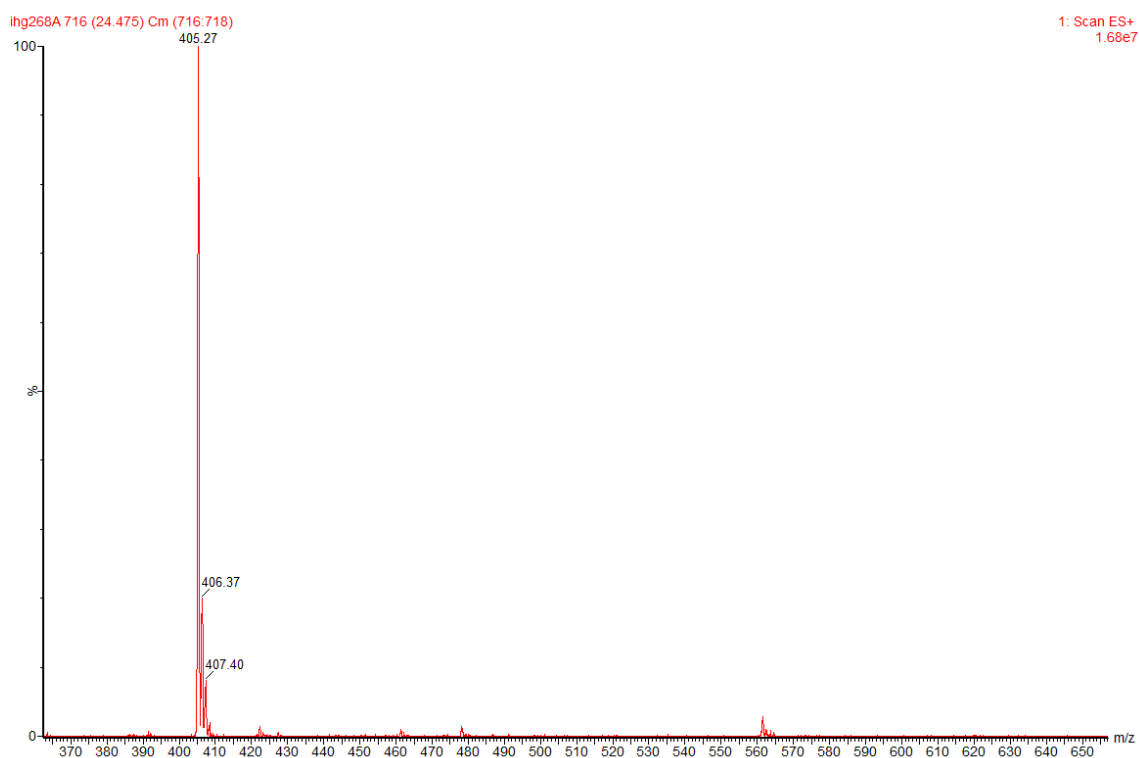


**Figure S5.13:** Mass spectrum of **10**.

1. K. S. Ajish Kumar, M. Haj-Yahya, D. Olschewski, H. A. Lashuel and A. Brik, *Angew Chem Int Ed Engl*, 2009, **48**, 8090-8094.
2. V. P. Terrier, H. Adihou, M. Arnould, A. F. Delmas and V. Aucagne, *Chem Sci*, 2016, **7**, 339-345.



## VI. GENERAL CONCLUSIONS

During this PhD project, several arguments related to molecular imaging's realm have been developed. The main task was the chemical synthesis of new molecular imaging probes, derivatized with AAZTA chelator. Chemical approaches adopted during the three years project, relies on Solid Phase Peptide Synthesis, solution chemistry, Native Chemical Ligation and Click Chemistry. Nevertheless, the activities ranged from chemical synthesis to cell biology, up to *in vivo* experiments.

During the first year, a novel library of AAZTA derivatives have been synthesized, in order to obtain different bioconjugation reaction possibilities in the stage of peptide or other relevant targeting vectors functionalization (CHAPTER 2). New PSMA targeting probes have been successfully obtained, to be used as PET/CT, PET/MRI and SPECT imaging probes (CHAPTER 3 and Manuscript 1).

The second year activities focused on the synthesis of dual PET/OI probes using an innovative chemical synthesis approach based on the Native Chemical Ligation, as fully described in CHAPTER 4 and Manuscript 2. Some of the synthesized probes, have been evaluated from a biological point of view, through *in vitro* evaluations.

During the last year of the PhD project *in vivo* and *ex vivo* experiments have been carried out to evaluate the binding affinity of the uPAR targeting dual imaging probes, synthesized during second and third year.

Last argument of the project relies on the synthesis of a new particular modified amino acid, the  $\gamma$ -(R,S)-mercaptoornithine, which can be exploited, after the anchoring on an on-resin linear peptide, to perform a cyclization, a chelator attachment and a fluorophore derivatization.



## MANUSCRIPT 1

### **Synthesis, radiolabeling and pre-clinical evaluation of [<sup>44</sup>Sc]Sc-AAZTA conjugate PSMA inhibitor, a new tracer for high-efficiency imaging of prostate cancer (Under revision, EJNMMI)**

S. Ghiani<sup>1</sup>, I. Hawala<sup>2</sup>, D.Szikra<sup>3,4</sup>, G.Trencsényi<sup>3,4</sup>, Z. Baranyai<sup>1</sup>, G.Nagy<sup>3</sup>, A.Vágner<sup>3</sup>, R. Stefania<sup>2</sup>, P. Suresh<sup>5</sup>, A.Maiocchi<sup>6</sup>.

<sup>1</sup> Bracco Imaging Spa, Bracco Research Centre, Via Ribes 5, 10010, Colletterto Giacosa (TO), Italy

<sup>2</sup> Dipartimento di Biotecnologie Molecolari e Scienze per la salute, Centro di Imaging Molecolare, Università degli Studi di Torino, Via Nizza 52, 10126, Torino (TO), Italy;

<sup>3</sup>Scanomed Ltd. Nagyerdeikrt. 98, 4032 Debrecen, Hungary

<sup>4</sup>Division of Nuclear Medicine and Translational Imaging, Department of Medical Imaging, Faculty of Medicine, University of Debrecen

<sup>5</sup>Bracco Research USA Inc., 259 Prospect Plains Rd., Bldg. H, Monroe Township, New Jersey 08831, USA

<sup>6</sup>Bracco SpA, Via Caduti di Marcinelle, 13, 20134, Milano, Italy.

**Abstract:**

**Purpose:** The aim of this work was to demonstrate the suitability of AAZTA conjugated to PSMA inhibitor (B28110) labelled with scandium-44 as a new PET tracer for diagnostic imaging of prostate cancer.

**Background:** Nowadays, scandium-44 has received much attention as a potential radionuclide with favourable characteristics for PET applications. A polyaminopolycarboxylate heptadentate ligand based on a 1,4-diazepine scaffold (AAZTA) has been thoroughly studied as chelator for  $Gd^{3+}$  ions for MRI applications. The excellent results of the equilibrium, kinetic, and labeling studies led to a preliminary assessment of the *in vitro* and *in vivo* behaviour of  $[^{44}Sc][Sc-(AAZTA)]^-$  and two derivatives, i.e.  $[^{44}Sc][Sc(CNAAZTA-BSA)]$  and  $[^{44}Sc][Sc(CNAAZTA-cRGDfK)]$ .

**Results:** B28110 was synthesized combining solid phase peptide synthesis (SPPS) and solution chemistry to obtain the desired high purity (97%) product with an overall yield of 9%. Subsequently, the radioactive labeling was performed with scandium-44 produced from natural Calcium target in cyclotron, in good radiochemical yields (RCY) under mild condition (pH 4, 298 K). Stability study in human plasma showed good RCP% of  $[^{44}Sc]Sc-B28110$  up to 24 hours (94.32 %). *In vivo* PET/MRI imaging on LNCaP tumor-bearing mice showed high tracer accumulation in the tumour regions as early as 20 minutes post injection. *Ex vivo* biodistribution studies confirmed that, the accumulation of  $^{44}Sc-PSMA-617$  was two-fold lower, than that of the radiolabeled B28110 probes.

**Conclusions:** This work demonstrated the suitability of B28110 for the complexation with scandium-44 at room temperature and the high performance of resultant new tracer based on AAZTA chelator for the diagnosis of prostate cancer using PET.

**Keywords:** Scandium-44, AAZTA, Prostate-specific membrane antigen (PSMA)-targeted radioligand, PET/MRI.

## Background

Prostate Cancer (PCa) is the leading cause of cancer death in men and it is the third most common cause of death in the world.[1] The standard diagnostic strategy of prostate cancer relies on the determination of the Prostate-Specific Antigen (PSA) in the blood, rectal exploration screening and biopsies. The clinical benefit of these diagnoses, however, is rather uncertain and there is a need for more specific imaging agents, allowing more accurate and early detection of the disease.

Prostate-specific membrane antigen (PSMA) is an extracellular hydrolase highly upregulated in metastatic and hormone-refractory prostate carcinomas.[2] PSMA is a type II membrane glycoprotein with an extensive extracellular domain (44–750 amino acids) and plays a significant role in prostate carcinogenesis and progression.[3]

PSMA inhibitors fall into three families: phosphorous-based, thiol-based and urea-based. Urea-based inhibitors showed a high affinity for PSMA and fast and efficient internalization in LNCaP cells.[4] Several small compounds for labeling PSMA have been developed and are currently investigated as imaging probes for PET with the  $^{68}\text{Ga}$ -labeled urea-based PSMA inhibitor being the most widely studied agent [5, 6]. Different PSMA-ligand derivatives were synthesized: the modification of the linker was designed to improve the binding specificity and pharmacokinetics for theranostic applications. The results of Benesova et al. held to further elucidate the structure-activity relationships (SAR) of the resulting PSMA inhibitors.[7] The most promising spacer selected from the SAR study of Benesova et al. have been adapted (i.e. Glu-NH-CO-NH-Lys-2-naphthyl-L-Ala-cyclohexane) to design a new PSMA inhibitor derivative imaging probe conjugated with AAZTA ligand (B28110), suitable for the complexation of PET radionuclides.

Recently scandium-44 has received much attention as a potential radionuclide with favourable characteristics for PET imaging applications ( $E_{\beta^+}$  mean 0.632 MeV, positron branching 94.27%). The half-life of 3.97 h matches the rate of some slower targeting processes involving peptides and antibody fragments, which renders scandium-44 to be promising for the radioactive labeling of small to medium size biomolecules.[8]

Furthermore, scandium-44 can be considered an appealing candidate to develop new theranostic strategies when combined with radionuclide having radiotherapeutic properties such as the  $\beta^-$ -emitting scandium-47.[9]

Current chelators like 1,4,7,10-tetraazacyclododecane-1,4,7,10-tetraacetic acid (DOTA) have certain limitations[10], in particular providing different coordination for different metals and requiring specific condition (e.g. high temperature, high chelate excess, etc.) for radiolabeling. Other chelators such as 1,4,7-triazacyclononane, 1-glutaric acid-4,7 acetic acid (NODAGA)[11] have shown the potential for convenient preparation of  $^{68}\text{Ga}$ -radiopharmaceuticals at room temperature; however, they cannot be used for larger trivalent metals with a coordination number 8, in particular, those for radionuclide therapy applications (e.g.  $^{90}\text{Y}$ ,  $^{177}\text{Lu}$ ).[12] Even when the labeling was achieved successfully, the stability of  $^{44}\text{Sc}$ -labeled NODAGA-peptides was clearly inferior to that of  $^{44}\text{Sc}$ -labeled DOTA derivatives.[13]

Heptadentate aminopolycarboxylate ligand with a 1,4-diazepine scaffold (AAZTA) has been thoroughly studied as chelator of  $\text{Gd}^{3+}$  ions for MRI applications.[14] This ligand has already been proven to form thermodynamically stable and kinetically inert  $\text{Ga}^{3+}$  complexes[15] and

an AAZTA conjugated with RGD peptide was shown to form complex with  $^{68}\text{Ga}$  at room temperature in acetate buffer at pH 3.8.[16]

Promising results of the equilibrium, kinetic, and labeling studies led to a preliminary assessment of the *in vitro* and *in vivo* behaviour of AAZTA derivatives labeled with scandium-44 radionuclide, [ $^{44}\text{Sc}$ ][Sc(CNAAZTA-BSA)] and [ $^{44}\text{Sc}$ ][Sc(CNAAZTA-cRGDFK)], described by Nagy G et al. recently.[17]

With the aim to obtain  $^{44}\text{Sc}$ -based efficient molecular imaging probe for PCs diagnosis, we designed a new AAZTA chelator conjugate to PSMA inhibitor (B28110) suitable for the complexation of scandium-44 radionuclide at mild condition. B28110 is characterized by the same binding motif of the commercially known DOTA-based PSMA-617.

Herein we report the synthesis of B28110 chelator (Fig. 1) and its labeling with scandium-44 radionuclide. The stability of the resulting [ $^{44}\text{Sc}$ ][Sc-B28110] complex was also carefully evaluated by following the transchelation reaction with DTPA ligand and the de-metallation processes in human plasma. *In vitro* and *in vivo* performance of [ $^{44}\text{Sc}$ ][Sc-B28110] was also investigated and compared with those of the DOTA analogue, PSMA-617.

## Materials and methods

### Materials and Reagents

Materials and reagents used for B28110 synthesis and radiolabeling are reported in ESI.

### Synthesis

6-[Bis[2-(1,1-dimethylethoxy)-2-oxoethyl]amino]-6-(5-carboxypentyl)tetrahydro-1H-1,4-diazepine-1,4(5H)-Diacetic acid  $\alpha,\alpha'$ -bis(1,1-dimethylethyl)ester (AAZTA-C4-COOH *tetra t*-butyl ester) was synthesized as it was described by Manzoni et al. [16]. PSMA binding motif was synthesized as it was published by Maresca et al [6].

*(2-chlorophenyl)(phenyl)(p-tolyl)methyl(2S)-2-((1r,4S)-4-(aminomethyl)cyclohexane-1-carboxamido)-3-(naphthalen-2-yl)propanoate (1)*

400 mg of a 2-Chlorotriyl chloride resin (loading 1.63mmol/g) were pre-swelled with 10 mL of CH<sub>2</sub>Cl<sub>2</sub> for 10 minutes. The first Fmoc protected AA (Fmoc-L-2NaI-OH) was loaded on the resin during 2.5 h (2 eq, 1.304mmol, 570.6 mg) with 3 eq. of DIPEA (341  $\mu$ L). After the anchoring of the first AA, the resin was end-capped with a solution of MeOH/DIPEA 3:0.5 for 30 minutes (10 mL). The resin was washed with DMF, and the cleavage solution was added to the reactor (piperidine:DMF 1:4) and stirred for 30 minutes. The resin was washed with DMF and the second AA was added to the reactor (Fmoc-4-Amc-OH, 2 eq, 494.8 mg, 1.304mmol) with 3 eq. of DIPEA (341 $\mu$ L) and 1.6eq of HBTU (395.6 mg, 1.043mmol). After two hours, the resin was washed with DMF.

*(S)-2-((1r,4S)-4-((5-(6-(bis(2-(tert-butoxy)-2-oxoethyl)amino)-1,4-bis(2-(tert-butoxy)-2-oxoethyl)-1,4-diazepan-6-yl)pentanamido)methyl)cyclohexane-1-carboxamido)-3-(naphthalen-2-yl)propanoic acid (2)*

AAZTA-C4-COOH *tetra t*-butyl ester (1.5 eq, 657 mg, 0.978 mmol) was added to the reactor with 3 eq. of DIPEA (341  $\mu$ L) and 1.2 eq. of HBTU (296.9 mg, 0.78 mmol). After 2 h the resin was washed with DMF, CH<sub>2</sub>Cl<sub>2</sub>, Et<sub>2</sub>O and the fully protected peptide was cleaved from the resin with a solution of HFIP/CH<sub>2</sub>Cl<sub>2</sub> 1:4 for 5 minutes. The solvent was evaporated in vacuo and the product was used for the next step without further purification (2,797 mg, white solid).

B28110,(((S)-5-((S)-2-((1r,4S)-4-((5-(6-(bis(carboxymethyl)amino)-1,4-bis(carboxymethyl)-1,4-diazepan-6-yl)pentanamido)methyl)cyclohexane-1-carboxamido)-3-(naphthalen-2-yl)propanamido)-1-carboxypentyl)carbamoyle)-L-glutamic acid (3)

Compound 2 was dissolved in CH<sub>2</sub>Cl<sub>2</sub> and DIPEA (8 eq; 0.9 mL) and HBTU (0.9 eq; 222.5 mg) were added to the solution. Then a solution of PSMA binding motif (1 eq; 318 mg; 0.652 mmol) was added to the solution and the reaction mixture was stirred overnight at room temperature. The solvent was evaporated and the crude product was purified by silica gravimetric direct phase chromatography with CH<sub>2</sub>Cl<sub>2</sub>/MeOH 98:2  $\rightarrow$  CH<sub>2</sub>Cl<sub>2</sub>/MeOH 7:3 to afford the pure product as pale yellow oil (423 mg). The totally protected pure product was dissolved in 10 mL of TFA/TIS95:5 and stirred overnight at room temperature. The solvent was evaporated and the product precipitated in cold Et<sub>2</sub>O to obtain the crude product. The crude product was purified and characterized as reported in ESI obtaining B28110 (3):63.6 mg, overall yield: 9%.

### Radiolabeling experiments

Scandium-44 was obtained by the irradiation of natural calcium target as detailed in ESI. The highest activity fractions of the obtained eluates were used for labeling experiments at different conditions, stability evaluation and *in vitro* and *in vivo* labeling solution preparation.

Average molar activity for the time of start of incubation (in vitro) were 39.4 GBq/umol for [<sup>44</sup>Sc]Sc-B28110 and 11.3 GBq/umol for [<sup>44</sup>Sc]Sc-PM5A-617. In the case of *in vivo* study, the average molar activity for time of injection were 53.3 GBq/umol for [<sup>44</sup>Sc]Sc-B28110 and 26 GBq/umol for [<sup>44</sup>Sc]Sc-PM5A-617. All details for labeling procedure are reported in ESI.

#### ***DTPA stability***

<sup>44</sup>Sc-labeled B28110 solution was incubated up to 24h in 0.01 M DTPA at pH=7.4 and room temperature and the solution was analyzed at the following time points: 0, 0.17, 2, 19, 24 h. Samples were injected to the HPLC at regular intervals to determine radiochemical purity.

#### ***Plasma stability***

The labeled compound dissolved in PBS was mixed with human plasma purchase from Sigma Aldrich (Darmstadt, Germany) at 37 °C in a 1 mL well closed syringe. At each time point, 50 µl sample was withdrawn and mixed with 50 µl 0.01M pH=4 DTPA solution. Mixture was incubated for 10 minutes at 37 °C. After the incubation the sample was mixed with 25 µl cold 50 % ethanol and 75 µl cold acetonitrile. After the centrifugation of the sample for 5 min at 9000 RPM the supernatant has been analyzed by HPLC measurement.

#### ***Cellular uptake studies***

LNCaP and A2780 cells were trypsinized centrifuged and re-suspended in DMEM and were aliquoted in test tubes at a cell concentration of  $1 \times 10^6 \text{ ml}^{-1}$ . Tubes were incubated for 15, 30, 60 and 90 min in the presence of 0.37 MBq of <sup>68</sup>Ga- or <sup>44</sup>Sc-labeled PSMA-617 or B28110 at 37 °C. After the incubation time samples were washed three times with ice-cold PBS and the radioactivity was measured with a calibrated gamma counter (Perkin Elmer Wizard gammacounter) for 1 min within the <sup>68</sup>Ga-sensitive energy window. Decay-corrected radiotracer uptake was expressed as counts/(min\*( $10^6$  cells)) (cpm). The uptake was expressed as percentage of the total radioactivity of radiotracers added to the cells (%ID /  $10^6$  cells). Each experiment was performed in triplicate and the displayed data represents the means of at least three independent experiments ( $\pm$ SD).

#### ***In vitro binding studies***

For *in vitro* binding studies melanotic LNCaP cells were used. The cells were cultured for 24 h in 24-well plates ( $5 \times 10^4$  per well). Different concentrations of [<sup>44</sup>Sc]Sc-B28110 or [<sup>68</sup>Ga]Ga-B28110 was added in cell culture medium (DMEM) to each well in 200 µl volume. After 30 and 90 min incubation time (in CO<sub>2</sub> incubator at 37 °C) the medium was removed and the cells were washed twice with PBS, then washed twice with glycine (0.2 M) and lysed with NaOH (1 M) for 10 min at 37 °C.

#### ***LNCaP tumor xenograft model***

LNCaP tumor cells ( $5 \times 10^6$  in 150 µl medium-Matrigel (50-50%) mixture/injection site) were injected subcutaneously into CB17 SCID male mice. Each animal received two injections, one in the right shoulder and one in the right thigh to double the imaged tumor numbers per animal. For *ex vivo* and *in vivo* data analysis both tumors were used. Tumor growth was assessed by caliper measurements every two days by the same experienced researcher. The tumor size was calculated using the following formula: (largest diameter × smallest diameter<sup>2</sup>)/2.[18]



### ***In vivo PET/MRI imaging***

*In vivo* experiments were carried out  $26 \pm 3$  days after subcutaneous injection of tumor cells at the tumor volume of  $189 \pm 19$  mm<sup>3</sup>. For *in vivo* imaging studies LNCaP tumor-bearing male CB17SCID mice (n=3) were injected intravenously with approximately 18 MBq [<sup>44</sup>Sc]Sc-B28110 or [<sup>68</sup>Ga]Ga-B28110 or [<sup>44</sup>Sc]Sc-PSMA-617 via the lateral tail vein. *In vivo* dynamic scans (0-90 min), then 20 min static scans were performed at 2.5h. Mice were anaesthetized by 3-1.5% isoflurane (Forane) with a dedicated small animal anesthesia device during the imaging studies. For the determination of the anatomical localization of the organs and tissues whole body T<sub>1</sub>-weighted MRI scans were performed using the preclinical nanoScan PET/MRI system (Mediso Ltd., Hungary). PET/MRI imaging analysis details are reported in ESI.

### ***Ex vivo biodistribution studies***

After *in vivo* PET/MRI imaging animals were euthanized with 5% Forane. Tissue samples were taken from selected organs (brain, fat, gall bladder, heart, small intestines, large intestines kidney, liver, lung, muscle, spleen, stomach, testis, tumor, urine) and the weight and the radioactivity of the samples were measured with calibrated gamma counter (PerkinElmer Wizard2 2480) and the uptake was expressed as %ID/g tissue.

### ***Self-Blocking experiments***

For self-blocking experiments, LNCaP tumor-bearing mice were injected intravenously with B28110 (in 100 µl saline as a blockade, approx. 200-fold of the [<sup>44</sup>Sc]Sc-B28110) and 10 min later [<sup>44</sup>Sc]Sc-B28110 via the lateral tail vein. *In vivo* dynamic scans (0-90 min), then 20 min static scans were performed at 2.5h. *Ex vivo* organ distribution studies were performed 3h after the injection as described above.

### ***Statistical analysis***

Significance was calculated by Mann-Whitney U-test and the significance level was set at  $p \leq 0.05$  unless otherwise indicated. Data are presented as mean  $\pm$ SD of at least three independent experiments.

## Results

### Synthesis

The synthesis of B28110 consists of three main steps: the solid phase synthesis, a solution chemistry step to carry out the PSMA binding motif conjugation and a final purification performed by semi-preparative HPLC. B28110 (compound 3 in Fig.1) was obtained with an overall yield of 9% and a purity of 97% as determined by HPLC.

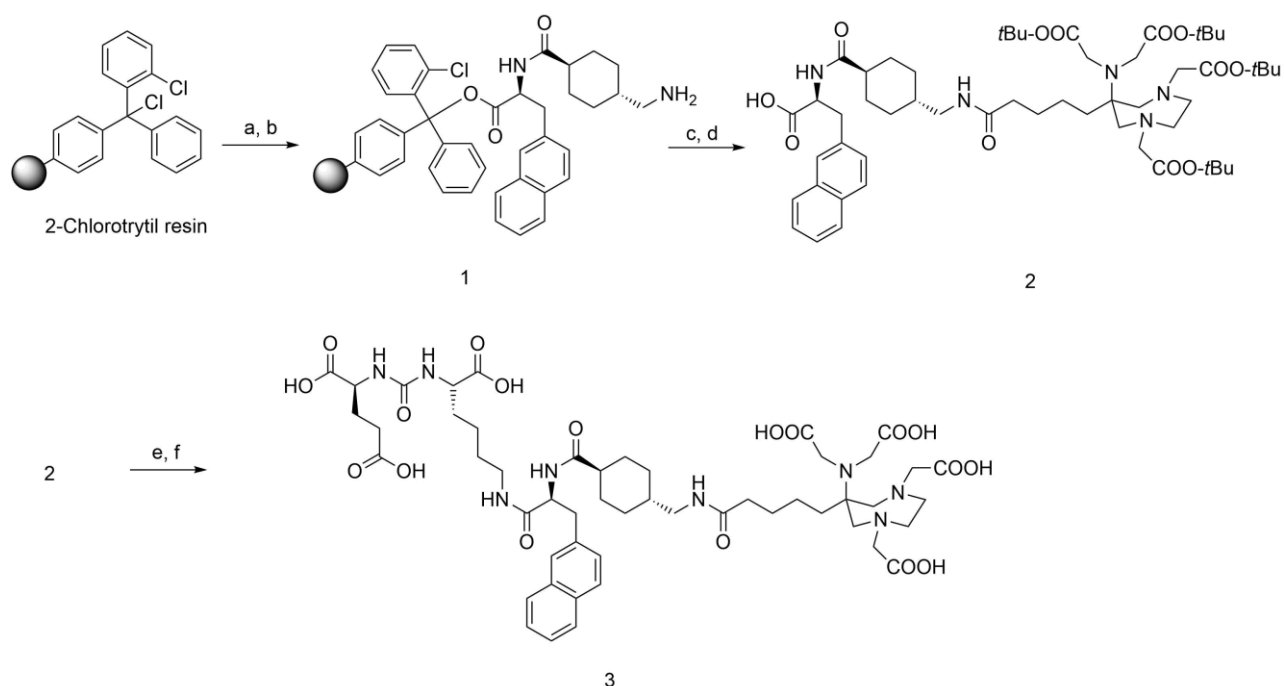


**Fig.1.** Synthesis scheme of B28110 (3): a) *i*- Fmoc-L-2Nal-OH, DIPEA, CH<sub>2</sub>Cl<sub>2</sub>; *ii*-MeOH/DIPEA 3:0.5; *iii*- DMF:Piperidine 4:1; b) *i*- Fmoc-4-Amc-OH, DIPEA, HBTU, DMF; *ii*- DMF:Piperidine 4:1; c) (tBu)<sub>4</sub>-AAZTA-C4-COOH, HBTU, DIPEA, DMF; d) HFIP, CH<sub>2</sub>Cl<sub>2</sub>; e) PSMA-binding motif, DIPEA, CH<sub>2</sub>Cl<sub>2</sub>; f) TFA/TIS 95/5

### Radiolabeling experiments

B28110 was labeled with scandium-44 in the presence of various chelator concentrations to determine the optimal labeling conditions. The effect of buffer, pH, temperature, reaction time and ligand concentration on the labeling of B28110 with scandium-44 have been examined. The effect of buffer was examined in the presence of 0.03, 0.1, 0.3, 1, 3 μM ligand in different buffer: 0.1 M and 1M HEPES, 1 M NH<sub>4</sub>OAc and 1 M NH<sub>4</sub>COOH at pH 4, 95°C in 5 minutes of reaction time (Fig. 2).

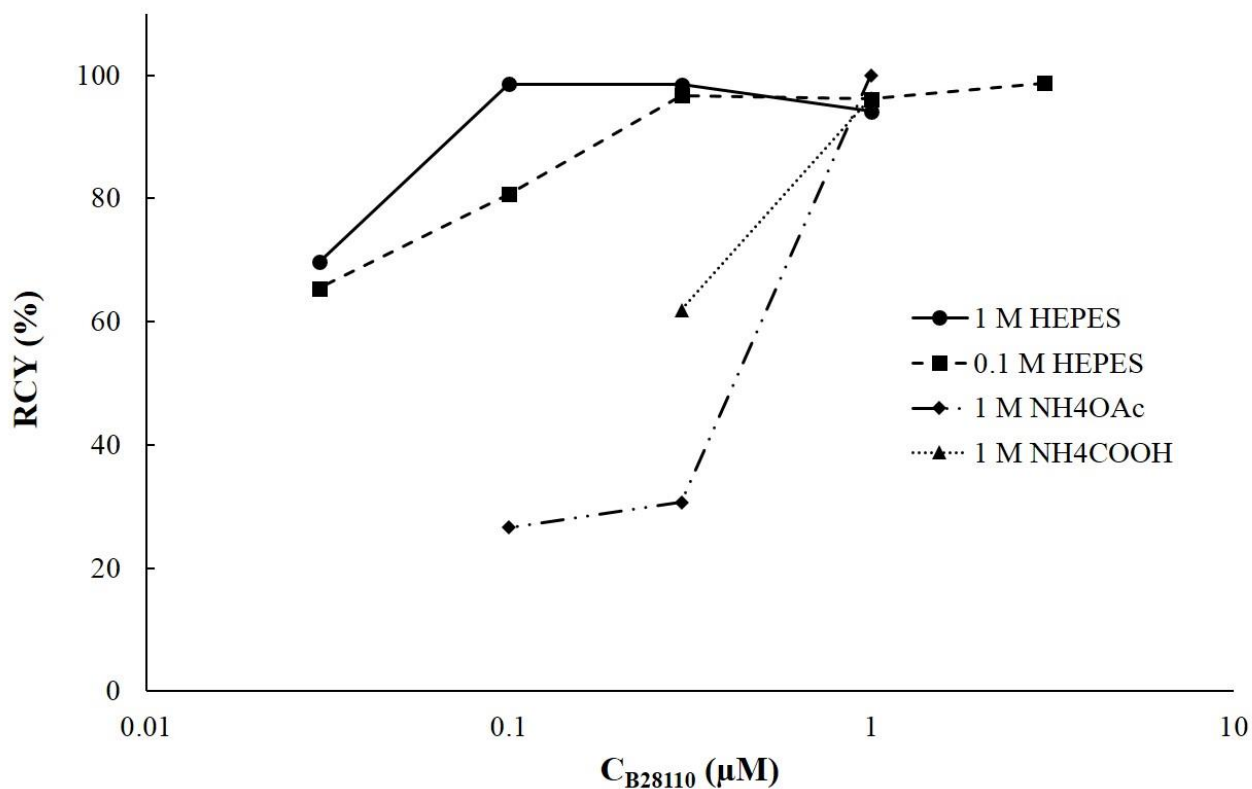


**Fig. 2.** Comparison of the labeling yields of B28110 with scandium-44 at pH 4 and 95 °C in different buffers.

Moreover, the effect of pH in the labeling performance was determined using different reaction time at room temperature in 0.1 M HEPES buffer (Fig. 3). Results show RCY% > 95% (at pH 4) using 1  $\mu\text{M}$  of ligand in 5 min of reaction time.

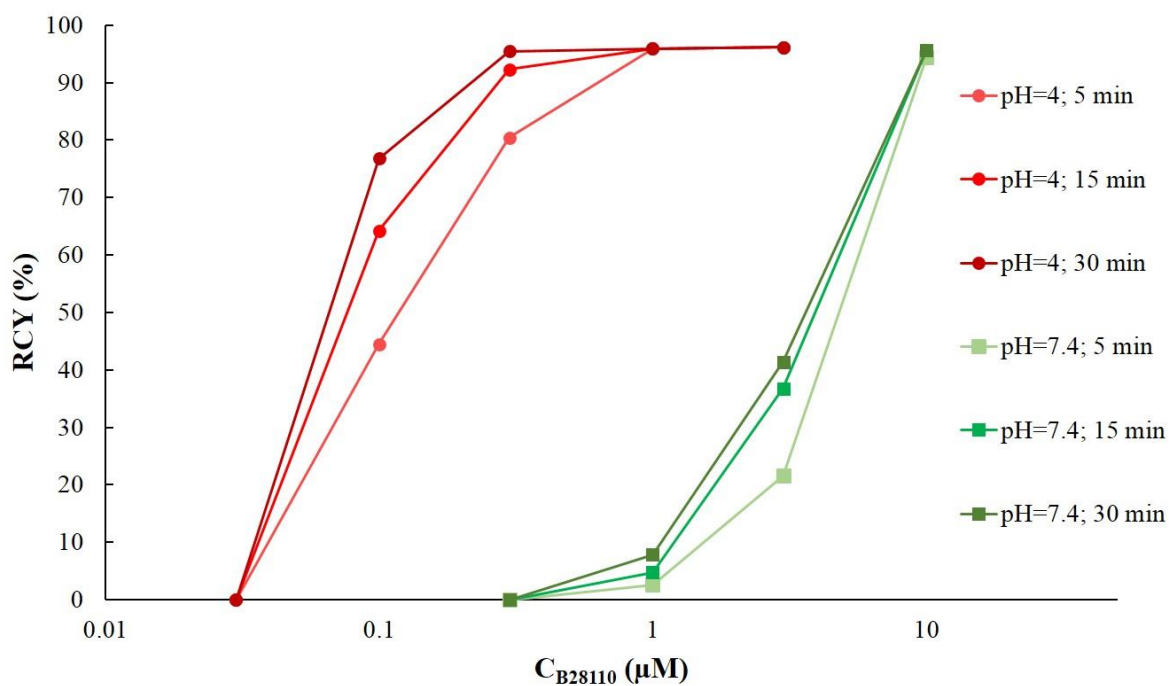


**Fig. 3.** Labeling yields of B28110 with scandium-44 (7-25 MBq) at pH=4, and 7.4 and room temperature in 0.1 M HEPES buffer

### **Radiolabeling for animal experiments**

In order to compare the performance of B28110 and PSMA-617 labeling with scandium-44 *in vivo* experiments, labeling was carried out at 95°C (10 min) to obtain quantitative yields for both ligands. Moreover, with the aim to obtain the highest molar activity as well as quantitative RCY, the concentration of ligand in the labeling solution was set at about 8 μM and 14 μM for B28110 and PSMA-617, respectively. Consequently, the average molar activity of [<sup>44</sup>Sc]Sc-B28110 and of [<sup>44</sup>Sc]Sc-PSMA-617 was about 53 and 26 GBq/μmol respectively.

### **Stability experiments**

The stability of <sup>44</sup>Sc-labeled B28110 was determined by radio HPLC in 0.01 M DTPA solution at pH=7.4 and room temperature, in plasma at 37°C. In all cases, samples were investigated by the HPLC at regular intervals to determine RCP% of the analyzed solution. RCP% of [<sup>44</sup>Sc]Sc-B28110 incubated in DTPA solution decreased to 92 % after 24 hours.

[<sup>44</sup>Sc]Sc-B28110 solution was also mixed with human plasma and kept at 37 °C in well closed vessel. Samples were taken at different time points, mixed with DTPA solution and precipitated with acetonitrile to remove plasma proteins. The supernatant and the pellet were separated by centrifugation. Activity values of the sample, supernatant and pellet were determined by gamma counter. Based on our preliminary experiments, [<sup>44</sup>Sc][Sc(DTPA)<sup>2-</sup>] formed quantitatively by the free scandium-44 in the presence of DTPA excess can be found in the supernatant as well as the intact [<sup>44</sup>Sc]Sc-B28110. However, the pellet contains the intact [<sup>44</sup>Sc]Sc-B28110 only. The amount of the intact [<sup>44</sup>Sc]Sc-B28110 and [<sup>44</sup>Sc][Sc(DTPA)<sup>2-</sup>] formed by the free <sup>44</sup>Sc<sup>3+</sup> that are present in the supernatant can be determined by HPLC analysis. By taking into account the HPLC area of the [<sup>44</sup>Sc]Sc-B28110, the activity values of supernatant ( $A_{\text{supernatant}}$ ) and the pellet ( $A_{\text{pellet}}$ ), the activity of the intact [<sup>44</sup>Sc]Sc-B28110 ( $A_{44\text{Sc-B28110}}$ ) can be calculated by Eq. (1)

$$A_{44\text{Sc-B28110}} = A_{\text{supernatant}} \times \frac{\text{Area}_{44\text{Sc-B28110}}(\%) }{100} + A_{\text{pellet}} \quad (1)$$

where  $\text{Area}_{44\text{Sc-B28110}}(\%)$  is the area percentage of the [<sup>44</sup>Sc]Sc-B28110 in the HPLC of the supernatant. Considering the HPLC area of the [<sup>44</sup>Sc][Sc(DTPA)<sup>2-</sup>] formed by the free scandium-44 and  $A_{\text{supernatant}}$ , the activity of the free scandium-44 can be calculated by Eq. (2).

$$A_{44\text{Sc}} = A_{\text{supernatant}} \times \frac{\text{Area}_{44\text{Sc(DTPA)}}(\%) }{100} \quad (2)$$

where  $\text{Area}_{44\text{Sc(DTPA)}}(\%)$  is the area percentage of the [<sup>44</sup>Sc][Sc(DTPA)<sup>2-</sup>] in the HPLC of the supernatant. By taking into account Eqs. (1) and (2), the radiochemical purity of [<sup>44</sup>Sc]Sc-B28110 (RCP%) can be calculated by Eq. (3)

$$\text{RCP}\% = \frac{A_{44\text{Sc-B28110}}}{A_{44\text{Sc-B28110}} + A_{44\text{Sc}}} \times 100 \quad (3)$$

RCP% of [<sup>44</sup>Sc]Sc-B28110 was found to be 99.62 % and 94.32 % after 2 and 24 hours, respectively.

### **Cellular uptake studies**

The selectivity of <sup>44</sup>Sc- and <sup>68</sup>Ga-labeled B28110 was investigated using PSMA positive LNCaP and negative A2780 cell lines. The accumulation of the <sup>44</sup>Sc- and <sup>68</sup>Ga-labeled molecules in LNCaP cells were significantly higher ( $p < 0.01$ ) than in receptor negative A2780 cells at each investigated time point confirming the specificity of the B28110 radiotracers (Fig. 4).

Furthermore, relatively higher radiotracer accumulation was found in LNCaP cells by using the  $^{44}\text{Sc}$ -labeled probes than that of  $^{68}\text{Ga}$ -labeled analogue. By analyzing the accumulation of the  $^{68}\text{Ga}$ -labeled molecules in LNCaP cells significantly higher ( $p < 0.01$ ) uptake of  $^{68}\text{Ga}$ -B28110 than that of the  $^{68}\text{Ga}$ -PSMA-617 has been evidenced at each time point (Fig. 4). Similar results were found when the  $^{44}\text{Sc}$ -labeled probes were investigated using LNCaP cell line. In LNCaP cells  $^{44}\text{Sc}$ -B28110 showed somewhat higher uptake than that of the  $^{44}\text{Sc}$ -PSMA-617 accumulation at each time point (Fig. 4).

*In vitro* binding experiments indicated a positive correlation between the concentration of  $^{44}\text{Sc}$ -labeled B28110 and PSMA-617 and their binding using PSMA positive LNCaP cells (Fig. 5A and B), and no significant differences were found between the two radiotracers. Moreover, linear relationship was found between the used incubation time and uptake of radiotracers, and linear relationship was observed between the concentration and the accumulation of the radioligands in the cells.

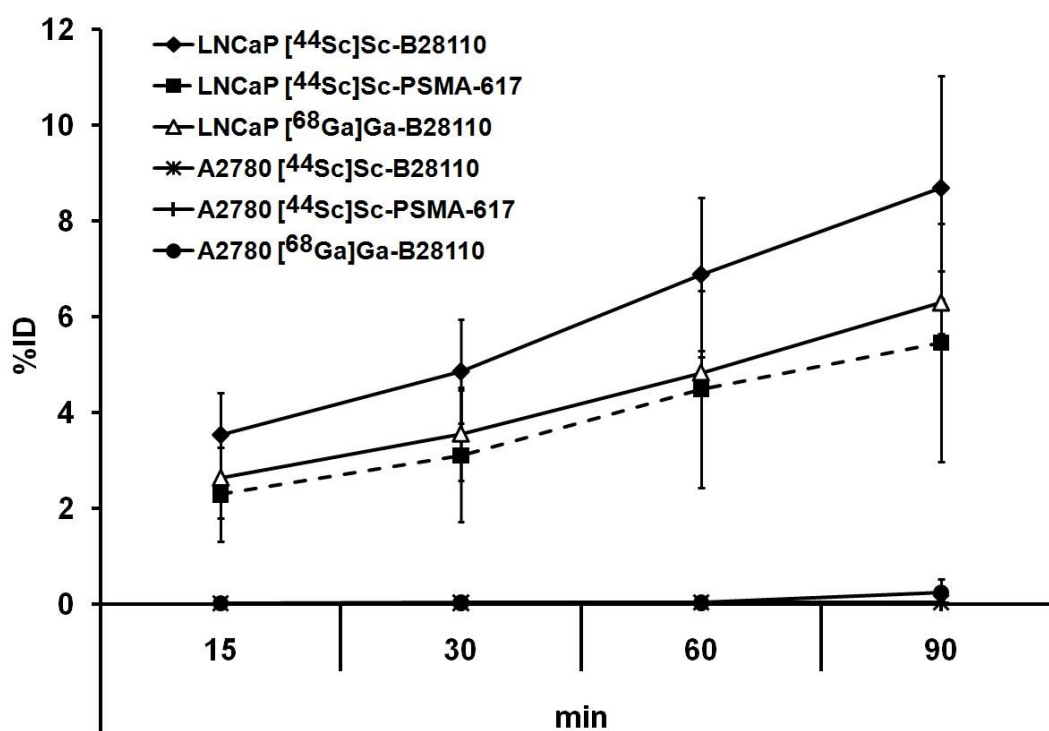


**Fig. 4.** Comparison of time dependent radio tracer uptake results of  $^{68}\text{Ga}$ - and  $^{44}\text{Sc}$ -labeled B28110 and  $^{44}\text{Sc}$ -labeled PSMA-617 probes using receptor positive (LNCaP) and negative (A2780) cell lines. %ID: Tracer accumulation in  $10^6$  cells was expressed as the percentage of the incubating dose. The data shown are means  $\pm$  SD of the results of three independent experiments, each performed in triplicate.

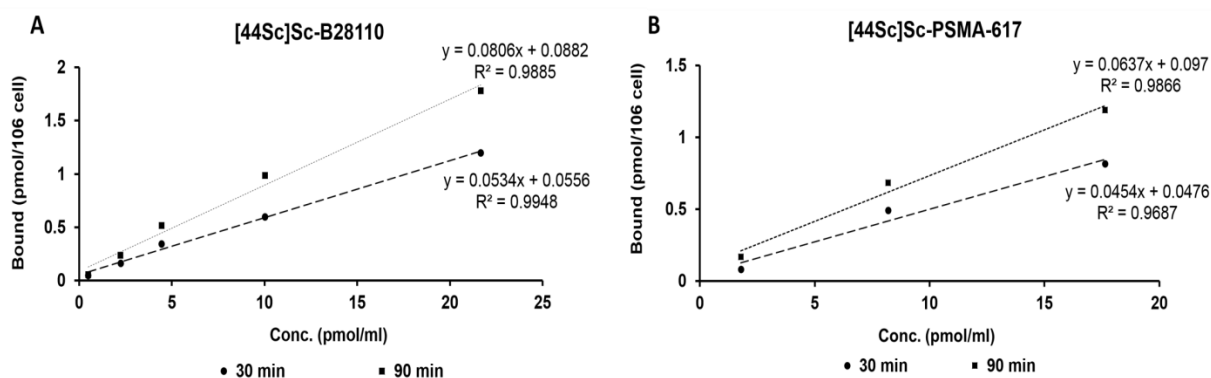


**Fig. 5.** *In vitro* binding studies using LNCaP cells A and B panels. Cells were incubated with different concentrations of [<sup>44</sup>Sc]Sc-B28110 and [<sup>44</sup>Sc]Sc-PSMA-617.

### ***In vivo and ex vivo biodistribution of [<sup>44</sup>Sc]Sc-B28110 in healthy control mice***

To determine the biodistribution of [<sup>44</sup>Sc]Sc-B28110 whole body dynamic PET/MRI scans (0-150 min) and *ex vivo* studies (at 180 min post injection) were performed after intravenous injection of approximately 18 MBq of <sup>44</sup>Sc-labeled B28110 in healthy mice. Representative dynamic PET images and the mean time-activity curve (TAC) after intravenous injection of the radiolabeled probe are shown in Fig. 6. By the quantitative analysis of dynamic PET images, the SUV mean data and the TAC (Fig. 6A) showed the rapid clearance of [<sup>44</sup>Sc]Sc-B28110 from the investigated tissues. The uptake of [<sup>44</sup>Sc]Sc-B28110 by the investigated organs significantly decreases after 5 minutes, and very low [<sup>44</sup>Sc]Sc-B28110 accumulation was observed at 150 min post injection in the abdominal organs (SUVmean intestines: 0.13±0.08, SUVmean liver: 0.07±0.05, SUVmean gall bladder: 0.12±0.07, SUVmean stomach: 0.12±0.06, SUVmean spleen: 0.04±0.01, SUVmean fat: 0.03±0.01, SUVmean kidney: 1.27±0.91), in the thoracic region (SUVmean lung: 0.02±0.01, SUVmean heart: 0.02±0.01), and in the brain (SUVmean: 0.02±0.001) (Fig. 6C). Only the radioactivity of the urine increased from 0 to 150 min post injection (SUVmean: 90.88±12.17 at 150 min). The [<sup>44</sup>Sc]Sc-B28110 is eliminated quickly via renal pathway with maximum uptake in kidney which gradually accumulates in bladder (inset figure 6A) with very low to minimal uptake in abdominal areas.

Representative coronal PET/MRI image of a healthy control SCID mice 150 min after intravenous injection of [<sup>44</sup>Sc]Sc-B28110 is shown in Fig. 6B. By the qualitative analysis of PET/MRI images the urinary system (kidneys and -bladder) were clearly visualized.

*In vivo* PET/MRI images and the SUV data analysis (Fig. 6C) correlated well with the *ex vivo* biodistribution results shown in Fig. 7. *Ex vivo* biodistribution studies were carried out 180 min after intravenous injection of [<sup>44</sup>Sc]Sc-B28110. After autopsy the accumulated activities of the organs were assessed by a calibrated gamma counter. By the %ID/g analysis of the *ex vivo* data low uptake values were found in the brain (0.03±0.02), muscle (0.02±0.01), blood (0.06±0.03), heart (0.05±0.02), lung (0.05±0.02), liver (0.24±0.29), intestines (0.18±0.16), fat (0.12±0.10), and stomach (0.09±0.06). Relatively higher accumulation was found in the spleen (0.89±0.54), gall bladder (1.12±0.77), and notable accumulation was observed in the kidneys (8.58±6.69) and in the urine (79.56±10.23).

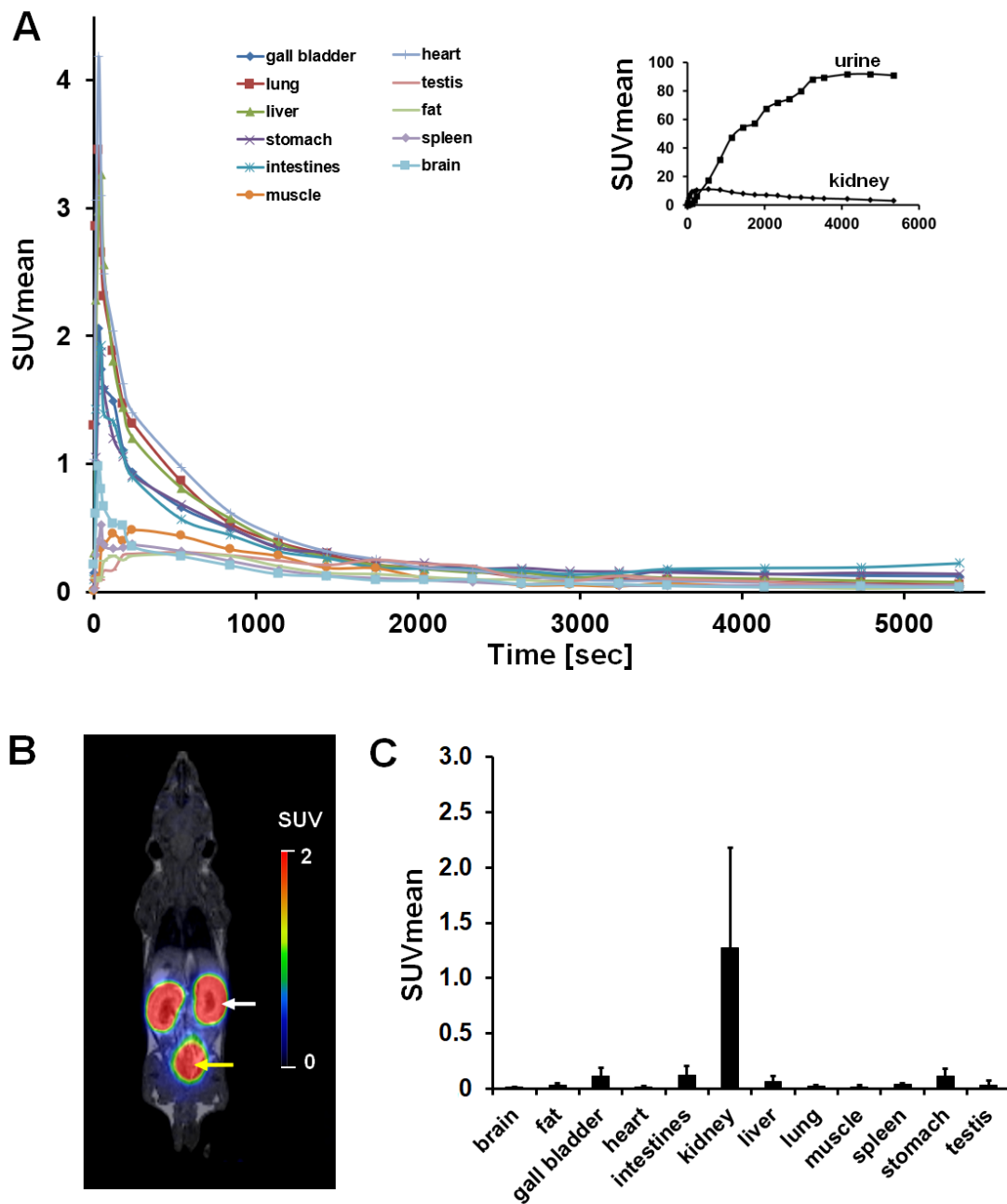


**Fig. 6.** *In vivo* biodistribution of the intravenously injected [ $^{44}\text{Sc}$ ]Sc-B28110 in healthy control SCID mice. Representative SUVmean time-activity curve (A) and representative decay-corrected static coronal PET/MRI image 150 min post injection (B) of [ $^{44}\text{Sc}$ ]Sc-B28110. Quantitative SUV analysis of the biodistribution of [ $^{44}\text{Sc}$ ]Sc-B28110 in selected organs/tissues of healthy SCID mice (n=5) 150 min after intravenous radiotracer injection (C). White arrows: kidneys; yellow arrows: urinary bladder. SUV: standardized uptake value.

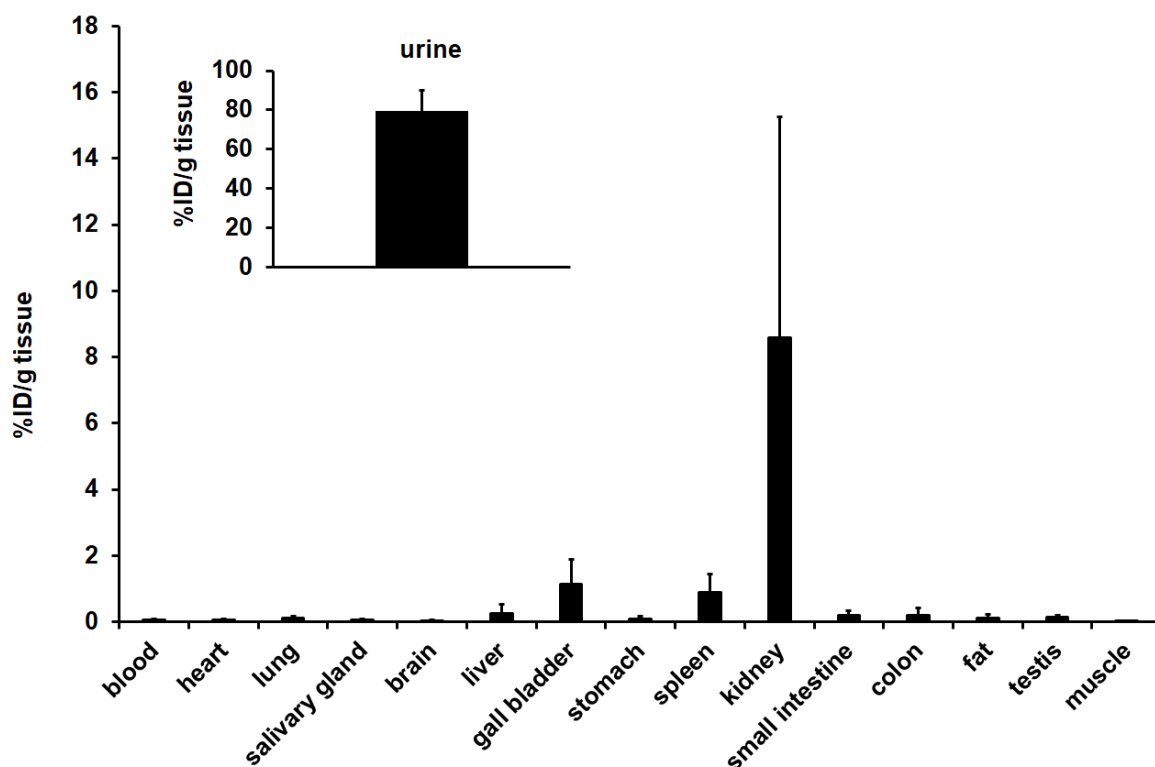


**Fig. 7.** *Ex vivo* biodistribution of [<sup>44</sup>Sc]Sc-B28110 (%ID/g) in healthy control SCID mice (n=5) 180 min after radiotracer injection. %ID/g values are presented as mean ± SD.

#### ***In vivo* PET/MRI imaging and *ex vivo* biodistribution studies of LNCaP tumor-bearing mice**

The biodistribution and tumor targeting properties of [<sup>44</sup>Sc]Sc-B28110, [<sup>68</sup>Ga]Ga-B28110, and [<sup>44</sup>Sc]Sc-PSMA-617 was investigated by dynamic (0-90 min) and static (150 min post injection) *in vivo* PET/MRI imaging using LNCaP tumor-bearing mice. Representative mean time-activity curves (TAC) of the accumulation in subcutaneously growing LNCaP tumors are shown in Fig. 8A. By the quantitative analysis of dynamic PET images, it was found that the uptake of all three radiopharmaceuticals in LNCaP tumor increased for approximately 50 min, followed by an equilibrium state. In self-blocking experiments, the accumulation of [<sup>44</sup>Sc]Sc-B28110 decreased from 5 min post injection. By analyzing the time activity curves, it was clearly visualized, that the accumulation of [<sup>44</sup>Sc]Sc-B28110 in LNCaP tumors was significantly higher at each investigated time point, than that of the other two radiopharmaceuticals (Fig. 8A). The qualitative image analysis confirmed this phenomenon (Fig. 8B-D). Despite these differences in the accumulation, subcutaneously growing LNCaP tumors were well identifiable with all three radiopharmaceuticals.

In self-blocking experiments *in vivo* PET/MRI imaging was performed 150 min post injection with unlabeled B28110 (approx. 200-fold of the radiolabeled probe). The qualitative image analysis showed that the intravenous administration of unlabeled B28110 reduced the accumulation of [<sup>44</sup>Sc]Sc-B28110 in PSMA positive LNCaP tumors (Fig. 8E). After the assessment of the decay-corrected PET images the quantitative SUVmean data (Fig. 8F insert) showed that the SUVmean values significantly ( $p \leq 0.01$ ) decreased (SUVmean:  $0.22 \pm 0.20$ ) in LNCaP tumors after the injection of unlabeled B28110.

Quantitative SUV mean analysis of decay-corrected PET/MRI images of LNCaP tumor-bearing mice 150 min after intravenous injection of all tracers is reported in Fig. 8F, representative decay-corrected static coronal PET/MRI images are also reported in Fig. 1S in ESI.



The *in vivo* observations correlated well with the *ex vivo* biodistribution data (see Table 1 for *ex-vivo* biodistribution data). Table 1 shows that [<sup>44</sup>Sc]Sc-B28110 and [<sup>68</sup>Ga]Ga-B28110 are characterized by the highest uptake in LNCaP tumors 3 hour after tracer injection, and the difference between these radiotracers was not significant. Interesting, the accumulation of <sup>44</sup>Sc-PSMA-617 was two-fold lower, than that of the radiolabeled B28110 probes. In self-blocking experiments [<sup>44</sup>Sc]Sc-B28110 was injected intravenously in the presence of B28110. The %ID values significantly ( $p \leq 0.01$ ) decreased in LNCaP tumors (Table 1).

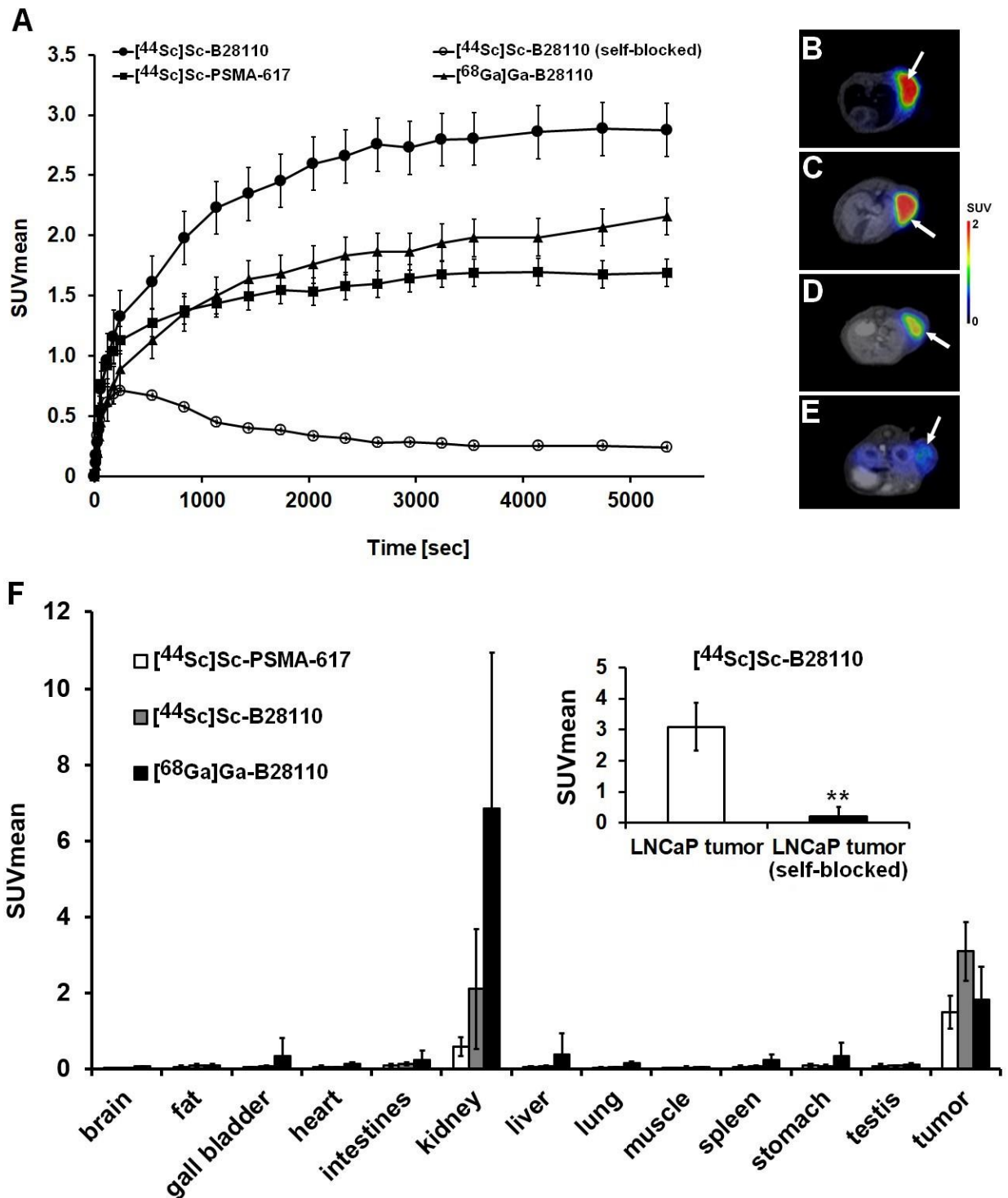


**Fig. 8.** *In vivo* PET/MRI imaging and quantitative image analysis of LNCaP tumors using <sup>44</sup>Sc- and <sup>68</sup>Ga-labeled radiotracers. Representative SUVmean time-activity curve(A) and representative decay-corrected static axial PET/MRI images 150 min post injection of [<sup>44</sup>Sc]Sc-

B28110 (B), [<sup>68</sup>Ga]Ga-B28110(C), [<sup>44</sup>Sc]Sc-PSMA-617 (D), and [<sup>44</sup>Sc]Sc-B28110 blocked (E). Quantitative SUV mean analysis of decay-corrected PET/MRI images of LNCaP tumor-bearing mice 150 min after intravenous injection of [<sup>44</sup>Sc]Sc-PSMA-617(n=5), [<sup>44</sup>Sc]Sc-B28110 (n=5) and [<sup>68</sup>Ga]Ga-B28110(n=5) (F). Insert: quantitative analysis of PET/MRI images of LNCaP tumors 150 min after intravenous injection of [<sup>44</sup>Sc]Sc-B28110 with and without self-blocking. White arrows: LNCaP tumors. Significance level:  $p \leq 0.01$  (\*\*). SUV: standardized uptake value.

**Table 1**

*Ex vivo* assessment of [<sup>44</sup>Sc]Sc-B28110, [<sup>68</sup>Ga]Ga-B28110 and [<sup>44</sup>Sc]Sc-PSMA-617 accumulation (%ID/g) in LNCaP tumors and in different organs, 3 hours after tracer injection. Significance level between the %ID/g data of [<sup>44</sup>Sc]Sc-B28110 and [<sup>44</sup>Sc]Sc-PSMA-617 in LNCaP tumor, and between blocked and non-blocked tumors:  $p \leq 0.01$  (\*\*). B28110 was used for self-blocking.

Organs	[ <sup>44</sup> Sc]Sc-B28110		[ <sup>44</sup> Sc]Sc-B28110 blocked		[ <sup>68</sup> Ga]Ga-B28110		[ <sup>44</sup> Sc]Sc-PSMA-617	
	Mean	SD	Mean	SD	Mean	SD	Mean	SD
blood	0.15	0.15	0.09	0.02	0.57	0.26	0.24	0.27
urine	173.67	133.91	278.96	59.63	74.90	19.82	70.54	33.26
heart	0.15	0.09	0.07	0.03	0.69	0.47	0.10	0.09
lung	0.30	0.10	0.12	0.02	1.05	0.46	0.17	0.12
salivary gland	0.16	0.07	0.04	0.01	1.02	0.53	0.09	0.05
brain	0.04	0.01	0.03	0.00	0.06	0.02	0.04	0.01
liver	0.14	0.04	0.90	0.38	3.85	7.53	0.15	0.10
gall bladder	0.58	0.28	1.05	0.61	1.82	3.13	0.31	0.14
stomach	0.17	0.03	0.09	0.00	1.07	1.66	0.25	0.31
spleen	3.26	3.33	0.61	0.45	17.51	7.50	0.60	0.15
kidney	26.45	16.74	1.64	0.84	163.80	31.45	5.35	2.25
small intestine	0.30	0.31	0.12	0.06	0.35	0.14	0.15	0.12
colon	0.22	0.08	0.97	1.53	0.35	0.19	0.09	0.04
fat	0.23	0.24	0.08	0.08	1.39	1.98	0.07	0.05
testis	0.46	0.27	0.05	0.01	0.67	0.21	0.09	0.06
muscle	0.07	0.02	0.02	0.01	0.20	0.13	0.03	0.02
LNCaP tumor	14.98*	5.69*	1.57	2.27	13.28	5.96	7.49	2.28

## Discussion

There is a gained interest for the use of scandium-44 as a novel radio-metal in positron emission tomography - and the application of  $^{44}\text{Sc}$ -labeled molecules [13]. By comparing scandium-44 and gallium-68, the advantages of scandium-44 can be counted to its radiochemical properties (e.g. half-life, positron range, energy) resulting in a more evaluable and more contrasting PET image than with gallium-68. Moreover scandium-44 can be used in imaging clinics far from the place of production [19-21].

In this work the radiolabeling condition of B28110 with scandium-44 were investigated in detail. The effects of the applied buffer (formate, acetate, HEPES) was studied at pH=4, where 1M HEPES was found to be the best (Fig. 2). Labeling at room temperature requires the peptide concentration of 0.3  $\mu\text{M}$  and 30 min reaction time to reach 95% labeling yield. However, high labeling yield can be reached (RCY > 95%) with HEPES buffer at pH 4 in 5 min at room temperature in the presence of slightly higher concentration of ligand (1  $\mu\text{M}$ ). At pH 7.4 higher peptide concentration is necessary (10  $\mu\text{M}$ ) to achieve quantitative labeling yields (Fig. 3). [ $^{44}\text{Sc}$ ]Sc-B28110 was found to be stable several hours, in particular in human plasma, and the stability of the complex did not decrease significantly during 24 hours.

The PSMA selectivity and specificity of  $^{44}\text{Sc}$ - and  $^{68}\text{Ga}$ -labeled B28110 were investigated and compared with that of [ $^{44}\text{Sc}$ ]Sc-PSMA-617.

The PSMA specificity of  $^{68}\text{Ga}$ - and  $^{44}\text{Sc}$ -labeled B28110 and PSMA-617 probes was assessed using receptor positive (LNCaP) cell line in binding studies. Strong positive correlation was found between the concentration of  $^{44}\text{Sc}$ -labeled B28110 and its binding properties using receptor positive LNCaP tumor cells (Fig. 5). The PSMA selectivity of  $^{44}\text{Sc}$ - and  $^{68}\text{Ga}$ -labeled B28110 and PSMA-617 molecules was investigated using receptor positive (LNCaP) and negative (A2780) cell lines. In cellular uptake studies it was found that the accumulation of the  $^{44}\text{Sc}$ - and  $^{68}\text{Ga}$ -labeled molecules in LNCaP cells were significantly higher ( $p < 0.01$ ) than in receptor negative A2780 cells, due to the high PSMA expression of LNCaP cancer cells [22]. Moreover, the accumulation of the  $^{68}\text{Ga}$ -labeled molecules in LNCaP cells is significantly higher ( $p < 0.01$ ) with B28110 than with PSMA-617 chelator (Fig. 4). Higher cellular uptake was also found for [ $^{44}\text{Sc}$ ]Sc-B28110 comparing with [ $^{44}\text{Sc}$ ]Sc-PSMA-617. In both cases ( $^{68}\text{Ga}$  and  $^{44}\text{Sc}$ -based experiments) the molar activity of labeled B28110 was 2-3 time higher than labeled PSMA-617.

*In vivo* animals studies were set up to compare the performance of  $^{44}\text{Sc}$  and  $^{68}\text{Ga}$ -labeled B28110 with  $^{44}\text{Sc}$ -PSMA-617 and evaluate the pharmacokinetic behavior, the accumulation and the binding affinity of the mentioned radiolabeled compounds.

First, to determine the biodistribution of [ $^{44}\text{Sc}$ ]Sc-B28110 PET/MRI scans and *ex vivo* studies were performed after intravenous injection of the compound in healthy mice. *In vivo* PET/MRI imaging and *ex vivo* biodistribution studies showed high accumulation in the kidneys and high radioactivity in the urine. This phenomenon can be explained by the urinary excretion of [ $^{44}\text{Sc}$ ]Sc-B28110 which was expected by the high hydrophilicity as well as by kidney retention due to its specific uptake (also confirmed by self-blocking experiment in LNCaP tumor-bearing mice study). Low or moderate radiotracer uptake was found in the chest and abdominal organs (Fig. 6). Biodistribution results correlated well with published literature where radiolabeled PSMA molecules ( $^{44}\text{Sc}$ - and  $^{68}\text{Ga}$ -labeled PSMA) showed also low accumulation in abdominal and thoracic organs and high in the urinary system [23, 24].

Successively, the PSMA specificity of  $^{44}\text{Sc}$ - and  $^{68}\text{Ga}$ -labeled B28110, and  $^{44}\text{Sc}$ -PSMA-617 was investigated by dynamic and static *in vivo* PET/MRI imaging using LNCaP tumor-bearing mice.

Representative mean time-activity curves (TAC) and static PET images showed that subcutaneously growing LNCaP tumors were well identifiable with all three radiopharmaceuticals (Fig. 8). Among the examined radiometals and chelators  $^{44}\text{Sc}$ -labeled B28110 conjugate showed the highest accumulation in LNCaP tumors. Similar results were found for  $^{68}\text{Ga}$ - and  $^{44}\text{Sc}$ -labeled DOTA-NAP amide or DOTA- and NODAGA-RGD molecules when the tumor uptake was investigated using *in vivo* tumor models, and higher accumulation was found using the  $^{44}\text{Sc}$ -labeled tracers respect to  $^{68}\text{Ga}$ -labeled compound [13, 25]. *In vivo* observations correlated well with the *ex vivo* biodistribution data (Table 1), where it was also found that the [ $^{44}\text{Sc}$ ]Sc-B28110 showed higher accumulation than that of the  $^{44}\text{Sc}$ -labeled DOTA chelator conjugated probes in LNCaP tumors 3 hour after tracer injection. In this study the molar activity of [ $^{44}\text{Sc}$ ]Sc-B28110 was two times higher than that of PSMA-617. In self-blocking experiments, when [ $^{44}\text{Sc}$ ]Sc-B28110 was injected intravenously in the presence of B28110 *in vivo* and *ex vivo* data show that the SUV mean and %ID values significantly ( $p \leq 0.01$ ) decreased in LNCaP tumors confirming the PSMA specificity of [ $^{44}\text{Sc}$ ]Sc-B28110 (Fig. 8F and Table 1).

On the basis of these consideration, an AAZTA conjugate of a PSMA inhibitor labelled with scandium-44 with enhanced accumulation in the targeted tissues has been designed in this study. The resulting [ $^{44}\text{Sc}$ ]Sc-B28110 exhibits high cellular uptake for PSMA and high LNCaP tumor targeting. The results obtained by using the novel tracer were significantly improved in comparison with [ $^{44}\text{Sc}$ ]Sc-PSMA-617 by taking advantage of the fast complexation kinetic of scandium-44 by AAZTA chelator. Actually, AAZTA can chelate scandium-44 at room temperature, moreover at high temperature a reduced amount of ligand respect to DOTA can also be exploited to obtain labelling solutions characterized by higher molar activity, that may reduce the competition of unlabeled precursor, as well as quantitative RCY. Hence, in the preclinical study we demonstrate the superiority of [ $^{44}\text{Sc}$ ]Sc-B28110 at the labelling condition typically used for PSMA-617 obtaining an evident higher tumor uptake resulting in superior tumor imaging.

## Conclusion

In conclusion, we synthesized a new derivative for PSMA targeting based on 1,4-diazepine scaffold (AAZTA). The resulting B28110 has been shown to be an excellent ligand for the labelling (RCY > 95%) with  $^{44}\text{Sc}$  at room temperature with short reaction time (5 min). Moreover, its fast formation kinetic allowed to obtain quantitative radiochemical yields by using a decreased amount of unlabeled precursor respect to PSMA-617 resulting in a labeling solution characterized by a molar activity two time higher than that of DOTA analogue. Thus, the intrinsic physico-chemical properties of [ $^{44}\text{Sc}$ ]Sc-B28110 as well as the high molar activity resulted in higher tumor (LNCaP) uptake *in vivo* demonstrating high contrast imaging. In addition, overall good performance of [ $^{44}\text{Sc}$ ]Sc-B28110 to detect disease was also demonstrated not only respect to the gallium-68 analogue ([ $^{68}\text{Ga}$ ]Ga-B28110) but also respect the use of one of the most relevant compound studied in clinics for PSMA targeting, i.e. PSMA-617 making a case for its further evaluation as a theranostic agent in clinic.

## Declaration

**Funding** The research was totally supported by Bracco Imaging SpA

**Competing interest** The authors declare that they have no competing interests

**Ethics approval and informed consent** All procedures performed in studies involving animals were in accordance with the ethical standards of the the Hungarian Laws and regulations of the European Union (Permission numbers: animal house: XXVIII-KÁT/2015, ethical licence for the study: 19/2017/DE MÁB). Approval for this study was granted by the Scientific Ethics Council of Animal Experiments.

**Consent to participate** Not applicable

**Availability of data and material** All data generated or analysed during this study are included in this published article.

## Acknowledgements

We thank Lorenzo Tei for supporting synthesis activity.

## References

1. Siegel R, Ma J, Zou Z, Jemal A. Cancer statistics, 2014. *CA Cancer J Clin.* 2014; 64:9-29. doi:10.3322/caac.21208.
2. Sam S, Chang MD. Overview of Prostate-Specific Membrane Antigen. *Rev Urol.* 2004; 6 Suppl 10: S13-8.
3. Silver DA, Pellicer I, Fair WR, Heston WD, Cordon-Cardo C. Prostate-specific membrane antigen expression in normal and malignant human tissues. *Clin Cancer Res.* 1997;3:81-5.
4. Kiess A, Minn I, Chen Y, Hobbs R, Sgouros G, Mease RC, Pullambhatla U, Shen CJ, Foss CA, Pomper, M.G. Auger Radiopharmaceutical Therapy Targeting Prostate-Specific Membrane Antigen. *J. Nucl. Med.* 2015; 56: 1401–1407.
5. Maurer T, Eiber M, Schwaiger M, Gschwend JE. Current use of PSMA-PET in prostate cancer management. *Nat Rev Urol.* 2016;13:226-35. doi:10.1038/nrurol.2016.26.
6. Maresca KP, Hillier SM, Femia FJ, Keith D, Barone C, Joyal JL, et al. A series of halogenated heterodimeric inhibitors of prostate specific membrane antigen (PSMA) as radiolabeled probes for targeting prostate cancer. *J Med Chem.* 2009;52:347-57. doi:10.1021/jm800994j.
7. Benešová M, Bauder-Wüst U, Schäfer M, Klika KD, Mier W, Haberkorn U, et al. Linker Modification Strategies To Control the Prostate-Specific Membrane Antigen (PSMA)-Targeting and Pharmacokinetic Properties of DOTA-Conjugated PSMA Inhibitors. *J Med Chem.* 2016;59:1761-75. doi:10.1021/acs.jmedchem.5b01210.
8. Radchenko V, Engle JW, Medvedev DG, Maassen JM, Naranjo CM, Unc GA, et al. Proton-induced production and radiochemical isolation of. *Nucl Med Biol.* 2017;50:25-32. doi:10.1016/j.nucmedbio.2017.03.006.
9. Chaple IF, Lapi SE. Production and Use of the First-Row Transition Metal PET Radionuclides. *J Nucl Med.* 2018;59:1655-9. doi:10.2967/jnumed.118.213264.
10. Price EW, Orvig C. Matching chelators to radiometals for radiopharmaceuticals. *ChemSoc Rev.* 2014;43:260-90. doi:10.1039/c3cs60304k.

11. Velikyan I, Maecke H, Langstrom B. Convenient preparation of  $^{68}\text{Ga}$ -based PET-radiopharmaceuticals at room temperature. *Bioconjug Chem.* 2008;19:569-73. doi:10.1021/bc700341x.
12. Pfister J, Summer D, Rangger C, Petrik M, von Guggenberg E, Minazzi P, et al. Influence of a novel, versatile bifunctionalchelator on theranostic properties of a minigastrin analogue. *EJNMMI Res.* 2015;5:74. doi:10.1186/s13550-015-0154-7.
13. Domnanich KA, Müller C, Farkas R, Schmid RM, Ponsard B, Schibli R, et al. Sc for labeling of DOTA- and NODAGA-functionalized peptides: preclinical in vitro and in vivo investigations. *EJNMMI Radiopharm Chem.* 2017;1:8. doi:10.1186/s41181-016-0013-5.
14. Gugliotta G, Botta M, Giovenzana GB, Tei L. Fast and easy access to efficient bifunctionalchelators for MRI applications. *BioorgMedChemLett.* 2009;19:3442-4. doi:10.1016/j.bmcl.2009.05.024.
15. Zsolt B, Fulvio U, Alessandro M, Giovanni B. G, Camilla C, Anett T, et al. Equilibrium, Kinetic and Structural Studies of AAZTA Complexes with  $\text{Ga}^{3+}$ ,  $\text{In}^{3+}$  and  $\text{Cu}^{2+}$ . *Eur. J. Inorg. Chem.*; 2013. p. 147-62.
16. Manzoni L, Belvisi L, Arosio D, Bartolomeo MP, Bianchi A, Brioschi C, et al. Synthesis of Gd and ( $^{68}\text{Ga}$ ) complexes in conjugation with a conformationally optimized RGD sequence as potential MRI and PET tumor-imaging probes. *ChemMedChem.* 2012;7:1084-93. doi:10.1002/cmdc.201200043.
17. Nagy G, Szikra D, Trencsényi G, Fekete A, Garai I, Giani AM, et al. AAZTA: An Ideal Chelating Agent for the Development of. *AngewChemInt Ed Engl.* 2017;56:2118-22. doi:10.1002/anie.201611207.
18. Faustino-Rocha A, Oliveira PA, Pinho-Oliveira J, Teixeira-Guedes C, Soares-Maia R, da Costa RG, Colaco B, Pires MJ, Colaco J, Ferreira R, Ginja M, Estimation of Rat Mammary Tumor Volume using Caliper and Ultrasonography Measurements, *Lab Animal.* 2013; 42 (6): 217-224. doi: 10.1038/labon.254
19. Bunka M, Müller C, Vermeulen C, Haller S, Türler A, Schibli R, et al. Imaging quality of ( $^{44}\text{Sc}$ ) in comparison with five other PET radionuclides using Derenzo phantoms and preclinical PET. *ApplRadiatIsot.* 2016;110:129-33. doi:10.1016/j.apradiso.2016.01.006.
20. Chakravarty R, Goel S, Valdovinos HF, Hernandez R, Hong H, Nickles RJ, et al. Matching the decay half-life with the biological half-life: ImmunoPET imaging with ( $^{44}\text{Sc}$ )-labeledcetuximab Fab fragment. *Bioconjug Chem.* 2014;25:2197-204. doi:10.1021/bc500415x.
21. Conti M, Eriksson L. Physics of pure and non-pure positron emitters for PET: a review and a discussion. *EJNMMI Phys.* 2016;3:8. doi:10.1186/s40658-016-0144-5.
22. Gorges TM, Riethdorf S, von Ahsen O, Nastał Y P, Röck K, Boede M, et al. Heterogeneous PSMA expression on circulating tumor cells: a potential basis for stratification and monitoring of PSMA-directed therapies in prostate cancer. *Oncotarget.* 2016;7:34930-41. doi:10.18632/oncotarget.9004.
23. Müller C, Domnanich KA, Umbricht CA, van der Meulen NP. Scandium and terbium radionuclides for radiotheranostics: current state of development towards clinical application. *Br J Radiol.* 2018;91:20180074. doi:10.1259/bjr.20180074.
24. Ray Banerjee S, Chen Z, Pullambhatla M, Lisok A, Chen J, Mease RC, et al. Preclinical Comparative Study of ( $^{68}\text{Ga}$ )-Labeled DOTA, NOTA, and HBED-CC Chelated Radiotracers for Targeting PSMA. *Bioconjug Chem.* 2016;27:1447-55. doi:10.1021/acs.bioconjchem.5b00679.
25. Nagy G, Dénes N, Kis A, Szabó JP, Berényi E, Garai I, et al. Preclinical evaluation of melanocortin-1 receptor (MC1-R) specific. *Eur J Pharm Sci.* 2017;106:336-44. doi:10.1016/j.ejps.2017.06.026.

# Synthesis, radiolabelling and pre-clinical evaluation of <sup>44</sup>Sc-AAZTA conjugate PSMA inhibitor, a new tracer for high-efficiency imaging of prostate cancer (Supporting Information)

## Materials and methods

### Materials and Reagents

9-Fluorenylmethoxycarbonyl (Fmoc) protected amino acids and 2-Chlorotrytil Chloride Resin were purchased from IRIS Biotech (Marktredwitz, Germany) and Novabiochem (Darmstadt, Germany). 2-(1H-benzotriazol-1-yl)-1,1,3,3-tetramethyluronium hexafluorophosphate (HBTU), N,N-Diisopropylethylamine were purchased from Sigma Aldrich (Darmstadt, Germany). PSMA-617 was purchased from ABX Advanced Biochemical Compounds (Radeberg, Germany). All solvents were purchased from VWR International (Radnor, USA) and were used without further purifications. Mass spectra with electrospray ionization (ESI) were recorded by a SQD 3100 Mass Detector (Waters). The HPLC-MS analytical and preparative analysis were carried out by a Waters AutoPurification system (3100 Mass Detector, 600 Quaternary Pump Gradient Module, 2767 Sample Manager and 2487 UV/Visible Detector). Analytical HPLC analyses were performed by using a Waters 2695 Alliance Separation Module equipped with a Waters 2998 Photodiode Array Detector. Desalting processes were performed with an AKTA purifier equipped with UV-900 lamp, P-900 pumps, FRAC-920 collector, 907 Inj valve, PV-908 Outlet valve.

### Purification and characterization of B28110

The crude product was purified by preparative HPLC with the use of Atlantis prepD<sup>®</sup>C18OBD 5um (19X100 mm) column. Eluent: (A) 0.1% TFA in H<sub>2</sub>O, (B) 0.1% TFA in CH<sub>3</sub>CN. Elution profile: 1) isocratic at 25% of B for 8.58 min, 2) linear gradient from 25% to 80% of B in 2.84 min, 3) linear gradient from 80% to 100% in 0.58 min, 4) isocratic at 100% of B for 1.8 min; Flow rate was constant 20 mL/min. B28110 was isolated as a homogenous peak with retention time of ca 8 min. The purity of the product was monitored by analytical HPLC with the use of Atlantis DC18 5um (4.6X150mm) column, the same elution profile and solvent mixtures as mentioned above Flow rate was constant 1 mL/min. The TFA was removed by the desalting AKTA purifier with a Mono S HR 5/5 packed with XAD1600D resin; Eluent: (A) H<sub>2</sub>O, (B) CH<sub>3</sub>CN. Elution profile: 1) isocratic at 16% of B for 5 min, 2) linear gradient from 16% to 100% of B in 5 min, 3) isocratic at 100% of B for 5 min. Flow rate was constant 0.5 mL/min. The fractions containing the pure product were evaporated *in vacuo* and lyophilized from water to give a white solid. HPLC chromatograms were recorded by the use of UV detection at 230 nm. HPLC Purity: 97%. ESI-MS (*m/z*): calc: For C<sub>51</sub>H<sub>72</sub>N<sub>8</sub>O<sub>18</sub> (*M/Z*)<sup>+</sup>1085.18 found: 1085.46; for C<sub>51</sub>H<sub>72</sub>N<sub>8</sub>O<sub>18</sub> (*M+2H*)<sup>2+</sup>543.59 found: 543.26. <sup>1</sup>H-NMR (CDCl<sub>3</sub>, 600 MHz): δ 0.82 (tr, 3H), 1.06 (t, J<sub>1</sub>=12.6 Hz, J<sub>2</sub>=12.8 Hz, 1H), 1.29 (tr, 13H), 1.49 (tr, 2H), 1.68 (tr, 5H), 1.93 (tr, 1H), 2.04 (t, J=7.5 Hz, 1H), 2.25 (tr, 3H), 2.85 (t, J=5.81 Hz, 2H), 2.96 (tr, 2H), 3.05 (tr, 1H), 3.11 (dd, 1H), 3.21 (s, 2H), 3.44 (s, 3H), 3.61 (s, 3H), 3.77 (s, 3H), 4.03 (tr, 1H), 4.12 (q, J<sub>1</sub>=5.34, J<sub>2</sub>=8.06, 1H), 4.11 (q, J<sub>1</sub>=5.34, J<sub>2</sub>=8.06, 1H), 4.54 (q, J<sub>1</sub>=5.45, J<sub>2</sub>=8.57, 1H), 6.29 (tr, 1H), 7.46 (quint, J<sub>1</sub>=8.84, J<sub>2</sub>=15.91, 2H), 7.69 (s, 1H), 7.79 (t, J=7.82, 2H), 7.85 (d, J=7.82, 1H).

B28110 (3):63.6 mg. Overall yield: 9%.

### Radiolabelling experiments

<sup>44</sup>Sc was obtained by the irradiation of 120-170 mg natural calcium target (Sigma Aldrich, 99.99 %) with 30 μA beam current for 30-60 minutes in the 16 MeV Ge PET trace 800 cyclotron

(University of Debrecen). The irradiated target material was dissolved in 3 M ultrapure HCl and loaded on 70 mg DGA resin conditioned with 2 ml portions of 3 M HCl, 1 M HNO<sub>3</sub>, 0.1 M HCl and 3 M HCl. The resin was washed with 3 mL 3 M HCl and 3 mL 1 M HNO<sub>3</sub> in order to remove traces of calcium, iron and nickel, and eluted with 3 mL 0.1 M HCl in 150 µl fractions. The first 250-300 µl of the eluate was discarded, and the next fractions were used for labeling experiments by mixing with appropriate buffer (i.e. 0.1 M and 1M HEPES, 1 M NH<sub>4</sub>OAc and 1 M NH<sub>4</sub>COOH at pH 4) containing B28110 (0.03, 0.1, 0.3, 1, 3 µM). Labelling was performed at 95°C and 5 minutes as reaction time, or concentrated on a small DOWEX cartridge (10-30 mg), washed with 1 mL water and eluted with 8 x 30 µl 1 M NH<sub>4</sub>OAc buffer (pH=4). The activity concentration of the buffered <sup>44</sup>Sc solution was in the range of 1-3 GBq/mL.

Room temperature labelling was performed at pH 4 and 7.4 in 0.1 M HEPES buffer using the same procedure described above. Labelling was carried out by using different reaction time (5, 15 and 30 min) and ligand concentration (0.03, 0.1, 0.3, 1, 3 and 10 µM).

For *in vitro*- and *in vivo* measurements B28110 (0.2 nmol) solution was added to 100 µl solution of <sup>44</sup>Sc (0.1 M HCl, 1 M HEPES, pH=4.3). All radiolabelling experiments were performed with a heating block for 10 minutes, at 95 °C in closed 1.5 mL Eppendorf tubes. After the labelling the sample was passed through a SPE cartridge (Empore™ C18-SD), which had previously been conditioned by purging with ethanol (1 mL, Ph.Eur) and water (5ml). Finally the cartridge was purged with water (1 mL). The labelled product was eluted dropwise from cartridge to PBS buffer – ethanol 1:1 solution in 1.5 mL Eppendorf tube. Two drops (50 µl) were mixed with PBS buffer to a final volume of 300 or 600 µl, depending on the number of animals to be examined from the batch.

Since the ethanol content of the final product is not tolerated in the *in vitro* experiments the Empore cartridge was eluted with 100 µl ethanol and evaporated to dryness in nitrogen stream at 60°C in a heating block. The product was dissolved in 300 µl PBS buffer.

The labelling yield of B28110 with <sup>44</sup>Sc was followed by radio HPLC using a Phenomenex Kinetex XB-C18 column (4.6 x 50 mm, 2.6 µm). Eluent: (A) 0.01 M oxalic acid (pH=3.0), (B) 90 % ACN : 10 % H<sub>2</sub>O. Elution profile: 1) 100% of A for 1 minute, 2) linear gradient from 0 to 100 % of B in 1.5 min, 3) 100 % of B for 0.5 min. Flow rate was constant 1 mL/min. The <sup>44</sup>Sc<sup>3+</sup> eluted with the solvent front (0.55 min), whereas the retention time of <sup>44</sup>Sc-B28110 were found to be 2.3 minutes.

<sup>68</sup>Ga was eluted from an ITG <sup>68</sup>Ge/<sup>68</sup>Ga generator with 0.05 M hydrochloric acid. The eluate was collected in 1 ml fractions. Two fractions with the highest activity (100-120 MBq each) were used for labeling, without further purification. All experiments were performed at 95 °C in closed 1.5 ml Eppendorf tubes in a heating block, with a few drops of water in each cavity to facilitate uniform heating.

For *in vitro*- and *in vivo* experiments 200 µl of <sup>68</sup>Ge/<sup>68</sup>Ga generator eluate (0.05M HCl) was mixed with 184.6 µl 1 M HEPES buffer (pH=4.3) and 13.4 µl of 30 µM B28110 solution. The mixture was heated for 10 minutes at 95 °C. The product was loaded onto an Empore C18 SD cartridge, washed with water and eluted with 2 x 50 µl ethanol. The eluate was evaporated to dryness in nitrogen stream at 60°C in a heating block. The product was dissolved in 300 µl PBS buffer.

### **Cell lines**

LNCaP ((ATCC® CRL-1740™) human prostate carcinoma cancer) and human A2780 (receptor negative human ovary carcinoma) cell lines were purchased from the American Type Culture Collection (ATCC). LNCaP and A2780 cells were cultured in DMEM Medium (GIBCO Life Technologies) supplemented 10% Fetal Bovine Serum (FBS, GIBCO Life technologies) and 1% Antibiotic and Antimicotic solution (Sigma-Aldrich). All cell lines were cultured at 5 % CO<sub>2</sub>



and 37°C. For *in vitro* studies cells were used at 85 % confluence and the viability of the cells was always higher than 95 %, as assessed by the trypan blue exclusion test.

### ***Animals***

Four weeks old male immune deficient CB17 SCID (C17SSMA04W) (n=28 for imaging and *ex vivo* studies) mice were purchased from the Charles River Laboratories with Health Report (DN No: FEW24288, Unit No: 18). Immunodeficient CB17 SCID mice were housed under sterile conditions in IVC cage system (Techniplast S.p.A., Italy) at a temperature of 26±2 °C with 55±10 % humidity and artificial lighting with a circadian cycle of 12 h. Sterile semi-synthetic diet (Akronom Ltd., Budapest, Hungary) and sterile drinking water were available ad libitum to all the animals. All procedures performed in studies involving animals were in accordance with the ethical standards of the the Hungarian Laws and regulations of the European Union (Permission numbers: animal house: XXVIII-KÁT/2015, ethical licence for the study: 19/2017/DE MÁB). Approval for this study was granted by the Scientific Ethics Council of Animal Experiments.

### ***PET/MRI imaging analysis***

PET volumes were reconstructed using the three-dimensional Ordered Subsets Expectation Maximization (3DOSEM) algorithm (Tera-Tomo, Mediso Ltd., Hungary). PET and MRI images were automatically co-registered by the acquisition software (Nucline) of nanoScan PET/MRI instrument. Reconstructed images were analyzed using the InterView™ FUSION (Mediso Ltd, Hungary) image analysis software. Ellipsoidal 3-dimensional Volumes of Interest (VOI) were manually drawn around the edge of the tissue or organ activity by visual inspection. Radiotracer uptake was expressed in terms of standardized uptake values (SUVs). SUV was calculated as follows:  $SUV = [VOI \text{ activity (Bq/ml)}] / [\text{injected activity (Bq)} / \text{animal weight (g)}]$ , assuming a density of 1 g/ml.

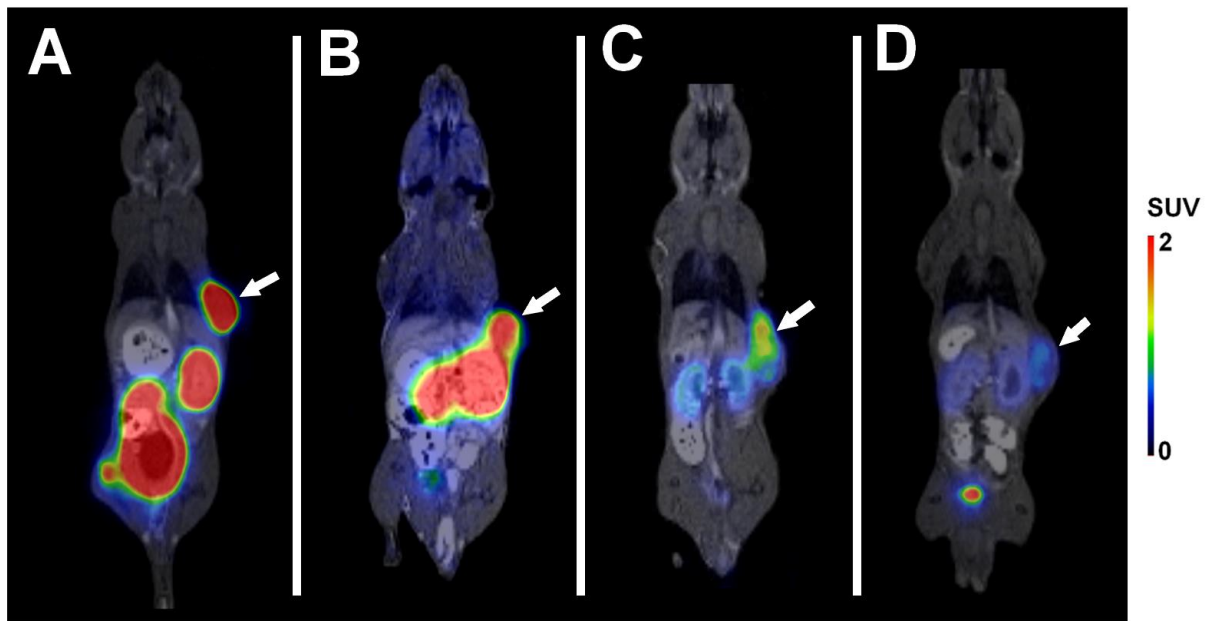


**Fig 1S.** *In vivo* PET/MRI imaging of LNCaP tumors using  $^{44}\text{Sc}$ - and  $^{68}\text{Ga}$ -labeled radiotracers. Representative decay-corrected static coronal PET/MRI images 150 min post injection of  $^{44}\text{Sc}$ -B28110 (A),  $^{68}\text{Ga}$ -B28110 (B),  $^{44}\text{Sc}$ -PSMA-617 (C), and  $^{44}\text{Sc}$ -B28110 blocked (D). White arrows: LNCaP tumors.

## MANUSCRIPTS 2

### An innovative approach for the synthesis of dual modality peptide imaging probes based on the native chemical ligation (Published on ChemCommun)

Ivan Hawala, <sup>a</sup>Lucia De Rosa, <sup>b</sup>Silvio Aime<sup>a</sup> and Luca D. D'Andrea\*<sup>c</sup>

<sup>a</sup> Dipartimento di Biotecnologie Molecolari e Scienze per la salute, Centro di Imaging Molecolare, Università degli Studi di Torino, Via Nizza 52, 10126, Torino (TO), Italy;

<sup>b</sup> Istituto di Biostrutture e Bioimmagini, CNR, Via Mezzocannone 16, 80134 Napoli (NA), Italy;

<sup>c</sup> Istituto di Biostrutture e Bioimmagini, CNR, Via Nizza 52, 10126 Torino (NA), Italy;

\*E-Mail: luca.dandrea@cnr.it

Received 25th December 2019,

Accepted 18th February 2020

DOI: 10.1039/c9cc09980h

#### **Abstract**

Peptide-targeting probes tagged with optical imaging and PET reporters may find application in innovative diagnostic procedures as well as in imaging-guided surgery. The reported synthesis procedure is of general applicability to obtain dual imaging probes using fully unprotected moieties with a selective and rapid chemistry based on the native chemical ligation.

Dual modality imaging probes are under intense scrutiny as they may be useful tools for innovative diagnostic procedures and/or for monitoring therapeutic treatments<sup>1</sup>. Dual-modality optical/PET probes allows for a better correlation between fluorescence and PET imaging experiments, especially when the structural difference between monomodality optical probes and the corresponding PET probes is associated to a not ignorable biological effect<sup>2</sup>.

Peptide-based probes<sup>3</sup> are advantageous as they own a fast body clearance, an easy-to-perform quality control, when compared to the larger size proteins and antibodies. However, the preparation of a doubly labelled peptide probe usually requires a complex multi-step chemistry and the use of orthogonal protecting groups<sup>4-6</sup>. Currently, the preparation of a dual labelled peptides is often performed using solid phase techniques (Solid Phase Peptide Synthesis, SPPS) or combining solid and solution phase. When the preparations are carried out in solution, one has to rely on the availability of properly designed chemoselective reactions. The solid phase approach requires the insertion of a molecule with at least two orthogonal protecting groups, compatible with the chemistry of the SPPS, the use of a large excess of chelating and optical agents which should be stable to the SPPS and cleavage conditions. In alternative, the peptide can be cleaved from the resin fully protected and, after purification, one or both agents can be coupled in solution upon selective deprotection, followed by the final peptide deprotection and purification. In some cases, it could be convenient to prepare preliminary the dual scaffold and then perform the bioconjugation in solid or solution phase. In all cases, multiple synthetic and purification steps are required. To avoid laborious chemical procedures, consumption of large excess of reagents, a limitation in the choice of the imaging probes, chemoselective groups could be inserted for selective labelling in solution working on a fully-deprotected peptides. Several chemoselective chemistries are available for specific bioconjugation steps such those offered by the click chemistry and the chemical ligation approaches. For example, Sun and coworkers exploited a photo-click approach to efficiently generate dual PET/OI peptide imaging probes<sup>2</sup>. However, despite the dual-labelling can be obtained in only one bioconjugation step, the method has limitations as far as concern the chemical nature and properties of the fluorophore moiety. Another interesting approach relies on the conjugation of peptides with strained-internal alkyne for which the labelling with a base-catalyzed double addition of different imaging moieties modified with thiol functional group was reported.<sup>7</sup> In this case, the first thiol addition has to be carefully controlled to avoid undesired double labelling with the same moiety.

The use of chemical ligation approach in the field of peptide chemistry has already found interesting applications, either in chemical syntheses and in bioconjugation procedures.<sup>8-10</sup> In particular it has been stressed how chemical ligation approaches may provide advantageous strategies for protein and peptide site-specific modification.<sup>11-13</sup> Native chemical ligation (NCL) was originally developed to generate long peptide chains (or proteins) while maintaining the native peptide backbone, which for many peptides/proteins is fundamental for preserving the bioactivity.<sup>14</sup> This chemical approach allows for the coupling of two fully-deprotected peptide fragments in an aqueous solution to form an amide bond at the ligation site.<sup>15</sup>

In a typical NCL procedure a C-terminal thioester peptide selectively reacts with a N-terminal cysteinyl peptide to afford a native polypeptide product (Fig. 1). No additional protecting groups are required for any of the amino acids found in the polypeptide, and, furthermore, the presence of internal cysteine residues does not hinder this

reaction. For these reason, thereby, NCL can be considered an invaluable regioselective reaction<sup>16, 17</sup>.

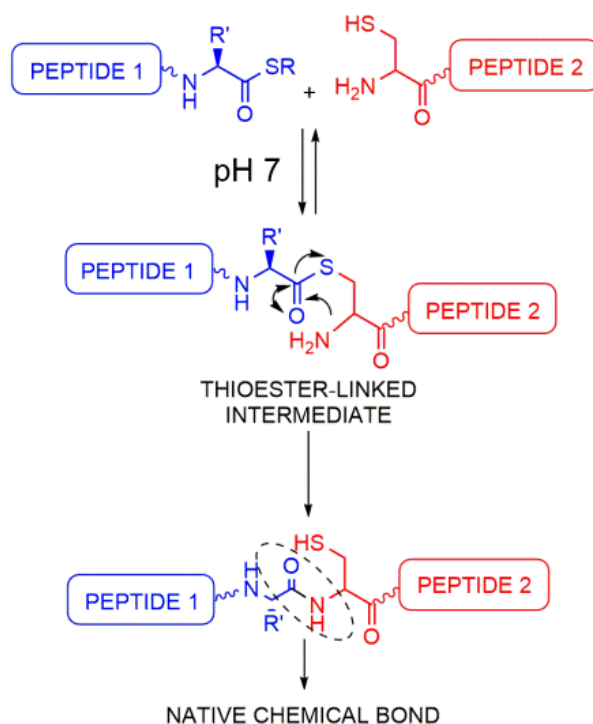


**Figure 1:** Mechanism of the native chemical ligation reaction

Herein, the utility of the NCL approach in the synthesis of dual optical/PET peptide probes is reported. This type of imaging probes may find application also in the field of image-guided surgery, where the PET tracer may act as reporter of the targeting procedure in *in vivo* pre-surgery images and the fluorescent probe may guide the surgeon in the resection of the pathological lesion. Two well established tumour targeting peptides (AE105<sup>18</sup> and *cyclo*RGDfK<sup>19, 20</sup>) were considered. First, they were derivatized with a cysteine residue to yield the a and b compounds reported in Fig. 2. These molecules were then conjugated to AAZTA chelator, preactivated as MESNA thioester (c, in Fig. 2) *via* NCL. After the first NCL reaction was completed, the free thiol group of the Cys residue was exploited for pursuing the second site-specific labelling, *via* the thiol-maleimide chemistry<sup>21</sup> to conjugate the maleimide fluorophore derivative (d, in Fig. 2).

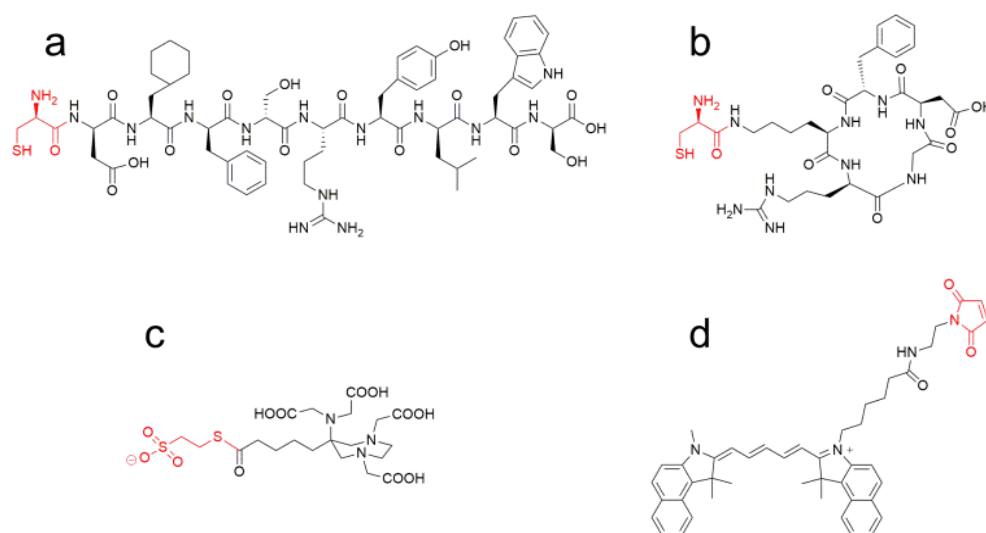


**Figure 2:** Chemical structures of the building blocks used in the procedure reported in Fig. 3: a) Cys-AE105; b) *cyclo*RGDfK(C); c) AAZTA-C4-CO-MES; 4) Cy 5.5 maleimide

The proposed approach can also be extended to protein-based probes, upon the insertion of a Cys residue at the protein N-terminal, thus paving the route to dual selectively labelled proteins.

Currently main used chelators like 1,4,7,10-tetraazacyclododecane-1,4,7,10-tetraacetic acid (DOTA) have certain limitations<sup>22</sup>, associated to the need of accessing to high temperatures for a successful radiolabelling. In this work we used the polyaminopolycarboxylateheptadentate ligand based on a 1,4-diazepine scaffold (AAZTA) that has been thoroughly studied as chelator for  $Gd^{3+}$  ions for MRI applications<sup>23</sup>. This ligand has already been proven to form thermodynamically stable and kinetically inert Gallium complexes<sup>24</sup> and an AAZTA-RGD peptide conjugate was recently shown to complex  $^{68}Ga$  at room temperature in acetate buffer at pH 3.8.

As far as concern the fluorescent reporter, cy 5.5 was selected on the ground of the large number of studies that have been carried out in the field of optical imaging using this molecules<sup>25, 26</sup>.

The synthetic procedure is schematically depicted in Fig.3. It starts from the thioester and 1,2 amino thiol components and consists of two reactions which, in principle, could be performed in sequence without the need of purification of the intermediate product. All reactions are performed in aqueous solution, using unprotected components.

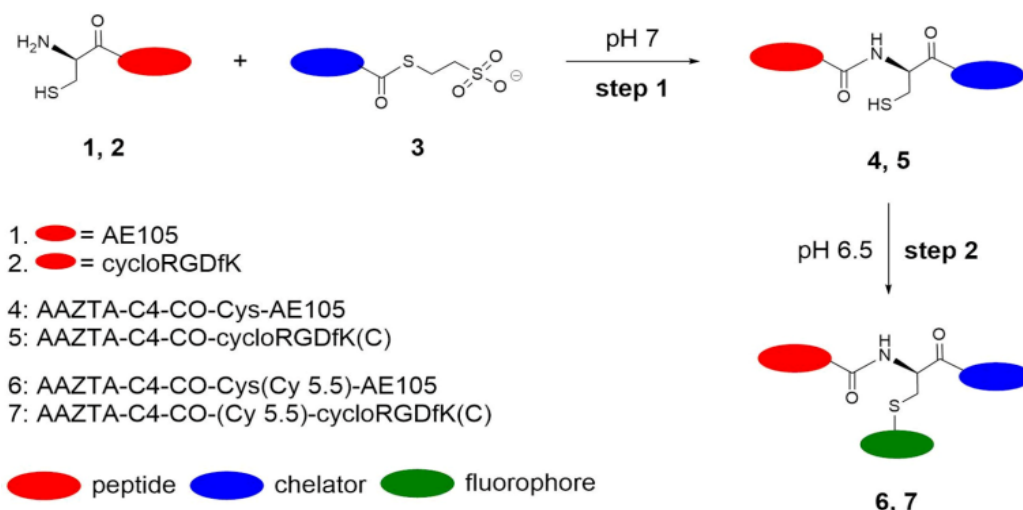


**Figure 3:** Synthesis scheme of the dual labelled peptide probes (6 and 7, Fig. S1 and S2): step 1) phosphate buffer pH 7.4, 5M imidazole, 3M guanidinium chloride, 50mM TCEP, 1h, RT; step 2) cy 5.5 maleimide, acetate pH 6.5, 3h, RT.

The peptides H-Cys(trt)-Asp(t-Bu)-Cha-Phe-D-Ser(t-Bu)-D-Arg(Pbf)-Tyr(t-Bu)-Leu-Trp(Boc)-Ser(t-Bu)-OH(1)(cysteinyll derivative of AE105 peptide, uPAR antagonist<sup>18</sup>) and *cyclo*RGDFK(C) (2) (cysteinyll derivative of *cyclo*RGDFK peptide, integrins antagonist<sup>27</sup>) were synthesized using the solid phase procedure. Then, they were fully deprotected and characterized (Fig.S3). (tBu)<sub>4</sub>-AAZTA-C4-COOH was preactivated as thioester with MESNA and then totally deprotected with a mixture of TFA/TIS/H<sub>2</sub>O (compound 3, Fig.S4 and S5), to allow the subsequent condensation with 1 and 2, using the NCL approach (Fig.3, step 1). The reaction between 1 or 2 and 3, was performed in 0.2M phosphate buffer medium (pH 7.4) supplemented with 5M imidazole, 3M guanidinium chloride and 50mM TCEP. Guanidinium chloride improves the solubility of the starting materials; the increased concentration of the reagents allows to decrease either the reaction time and the reaction volume. Imidazole was used instead of a thiol (e.g. 4-Mercaptophenylacetic acid) as NCL reaction catalyst<sup>28</sup>, and TCEP was added to the mixture as reducing agent with the purpose of getting the full availability of the thiol group of the cysteine residue, avoiding the formation of disulfide bonds that would hinder the NCL reaction. After the transthioesterification step, an intramolecular rearrangement gives a stable amide bond between the N-terminal amino group of the cysteine and the carboxylic group of the externally protruded arm of AAZTA-C4-COOH. Overall the NCL procedure was completed in about 30-60 min yielding, after RP-HPLC purification, a highly pure product (Fig. S6).

The transposition of the chemical bond from the side chain thiol group to the α-amine group made the thiol group of the cysteine available for the subsequent chemoselective reaction with the maleimide pre-activated fluorophore (i.e. cy 5.5) (Fig.3, step 2). For this step maleimide-thiol chemistry was used as maleimide-derivatized fluorophores are commercially available. Of course, other thiol selective chemistry can be also exploited. Final reaction between the free cysteine thiol and the maleimide moiety of the pre-activated fluorophore, carried out in aqueous solution at almost neutral pH, was completed within few hours at room temperature (Fig. S7).

AAZTA-C4-CO-Cys(Cy5.5)-AE105 (6) was synthesized with an overall yield of 24% and a chemical purity of 95%. AAZTA-C4-CO-(Cy 5.5)-*cyclo*RGDFK(C) (7) was synthesized with an overall yield of 6.4% and a chemical purity of 95%. The low values of the overall

yields are mainly related to a low recovery after the purification steps, as bioconjugation reactions proceeded almost to completion as assessed by RP-HPLC analyses.

We also performed the synthesis of 6 and 7 in two consecutive steps avoiding the purification of the species 4 and 5. It was carried out by adding cy 5.5 maleimide to the reaction mixture of the chemical ligation step after having checked the full conversion of the reagent by RP-UPLC. However, the free thiol-containing anion, released during the NCL reaction between AAZTA thioester and the peptides, can react with the fluorophore-maleimide thus subtracting part of the reagent needed for the second labelling reaction. Unfortunately, the side product formed from MES/cy 5.5 maleimide had similar HPLC retention time of the desired product 6. This led to obvious purification inconveniences. In summary, the latter synthetic approach, in the case of the synthesis of 6, gave a similar overall yield of 22% (it was 24% for the former approach). Conversely, the overall yield increased in the case of the synthesis of 7 passing from 6.4% to 23% highlighting the influence of the purification step on the overall yield. In both cases, the final product was obtained with a chemical purity of 95%.

The AAZTA ligand on 6 and 7 yielded the respective Ga(III) complexes by mixing equimolar amounts of the peptide-containing probe and GaCl<sub>3</sub> in a 50:50 solution of 0.1M acetate buffer pH (3.8)/acetonitrile medium, at room temperature for 10 minutes under magnetic stirring. The reactions were monitored by UPLC-MS (8 and 9, Fig. S8). The final products were characterized by UV-Vis spectroscopy. UV-Vis spectra of 8 and 9 showed, according to parent cy 5.5 maleimide spectrum,  $\lambda_{\max}$  at 692 nm, suggesting the preservation of the intact chromophore moiety in the final molecule (Fig. 4). The concentration of the 8 and 9 complexes were quantified by UV-Vis spectroscopy and used as such for the *in vitro* targeting experiments, as the assumption that the tiny amounts of acetonitrile (<0.1% v/v) does not compromise the viability of the cells during the experiment time.

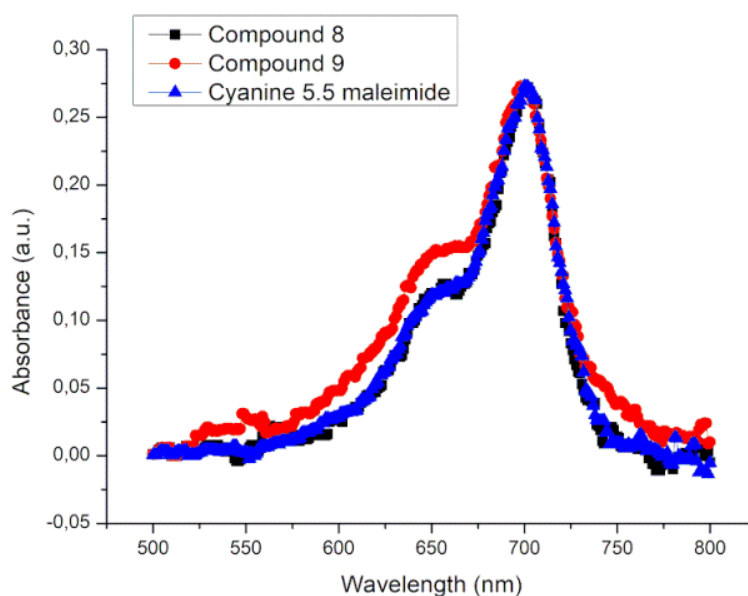


**Figure 4:** UV-Vis spectra of cy 5.5 maleimide, compound 8 and compound 9



Human glioblastoma U-87 MG cells overexpressing either uPAR and  $\alpha\text{v}\beta\text{3}$  integrin receptors were used to assess the binding proprieties of the synthesized dual probes (compound 8 and 9) by flow cytometry. Tumour cells ( $10^5$ /well) were incubated in a medium containing different concentrations of 8 or 9 (from 0 to 0.4  $\mu\text{g}$ ) for 30 minutes at 273 K. Representative results from flow cytometry experiments with Ga-AAZTA-C4-CO-Cys(Cy5.5)-AE105 (8) and Ga-AAZTA-C4-CO-(Cy5.5)-*cyclo*RGDfK(C)(9) are reported in Figures S9 and S10. Both dual probes were able to bind to U-87 MG cells. Furthermore, both probes showed a dose-dependent behaviour (Fig.5a-b). Overall, these *in vitro* experiments demonstrate that the dual-labelled peptides are able to interact with uPAR or integrin receptor<sup>29</sup>.

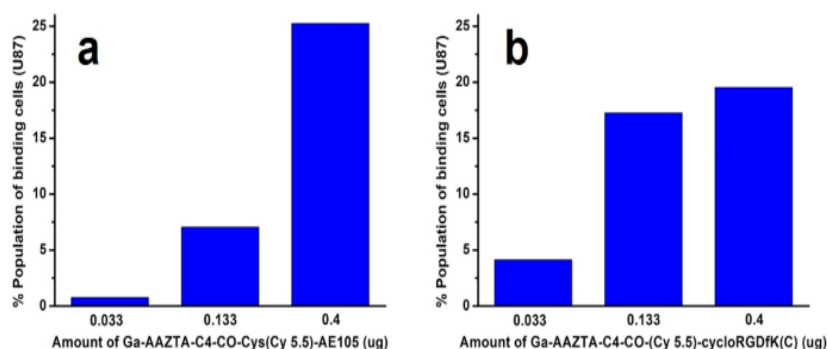


**Figure 5:** a) Histogram plot of U-87 MG cells ( $10^5$ ) analysed at FACS after incubation for 1h at 273 K with 0.033, 0.133 and 0.400  $\mu\text{g}$  of Ga-AAZTA-C4-CO-Cys(Cy5.5)-AE105 (8); b) Histogram plot of U-87 MG cells ( $10^5$ ) analysed after incubation for 1h at 273 K with 0.033, 0.133 and 0.400  $\mu\text{g}$  of Ga-AAZTA-C4-CO-(Cy5.5)-*cyclo*RGDfK(C) (9).

The reported synthetic procedure allows for the preparation of a dual labelled peptide based probe. Using two chemoselective reactions, the fluorescent and the chelating moieties are inserted at site-specific position without the use of protecting groups. The targeting peptide is modified with the introduction of a cysteine residue, which can be easily inserted during peptide synthesis, minimizing the impact on the overall molecular structure even in the case of short peptide sequences. All the bioconjugation reactions are performed in aqueous solution, under mild condition and using unprotected reagents, suggesting that an analogous procedure could be easily translated to the preparation of protein-based probes, not presenting exposed Cys residue, through the introduction of a N-terminal cysteine.

In conclusion, the herein reported results show that a synthetic strategy can be set-up to obtain peptide-containing molecules (e.g. AE105 or *cyclo*RGDfK) functionalized with a fluorophore (e.g. cy 5.5) and a chelator (e.g. AAZTA). The reported synthesis procedure can be generally applied to obtain dual imaging probes. Compounds 6 and 7 if labelled with Ga-68 could be considered as candidates for dual detection with PET and Optical Imaging. Such probes might be particularly useful in imaging-guided surgery *via* the detection of the fluorescence reporters once the occurrence of a successful targeting has been verified pre-surgery by the acquisition of PET image.

### Conflicts of interest

There are no conflicts to declare.

## Acknowledgement

I.H. is grateful to Bracco Imaging Spa for financial support of the PhD program. The authors are very grateful to Marta Tapparo (University of Turin, Italy) for her precious support during the *in vitro* experiments evaluations. L.D.R. was supported by "Fondazione Umberto Veronesi".

## References:

1. A. Louie, *Chem Rev*, 2010, **110**, 3146-3195.
2. L. Sun, J. Ding, W. Xing, Y. Gai, J. Sheng and D. Zeng, *Bioconjug Chem*, 2016, **27**, 1200-1204.
3. S. Mizukami, R. Takikawa, F. Sugihara, M. Shirakawa and K. Kikuchi, *Angew Chem Int Ed Engl*, 2009, **48**, 3641-3643.
4. C. Li, W. Wang, Q. Wu, S. Ke, J. Houston, E. Sevick-Muraca, L. Dong, D. Chow, C. Charnsangavej and J. G. Gelovani, *Nucl Med Biol*, 2006, **33**, 349-358.
5. H. Xu, K. Baidoo, A. J. Gunn, C. A. Boswell, D. E. Milenic, P. L. Choyke and M. W. Brechbiel, *J Med Chem*, 2007, **50**, 4759-4765.
6. K. R. Bhushan, P. Misra, F. Liu, S. Mathur, R. E. Lenkinski and J. V. Frangioni, *J Am Chem Soc*, 2008, **130**, 17648-17649.
7. Y. Sun, X. Ma, K. Cheng, B. Wu, J. Duan, H. Chen, L. Bu, R. Zhang, X. Hu, Z. Deng, L. Xing, X. Hong and Z. Cheng, *Angew Chem Int Ed Engl*, 2015, **54**, 5981-5984.
8. L. D. D'Andrea and A. Romanelli, *Chemical Ligation: Tools for Biomolecule Synthesis and Modification*, Wiley, 2017.
9. W. R. Algar, P. Dawson and I. L. Medintz, *Chemoselective and Bioorthogonal Ligation Reactions. Concepts and Applications.*, Wiley, 2017.
10. L. De Rosa, A. Russomanno, A. Romanelli and L. D. D'Andrea, *Molecules*, 2013, **18**, 440-465.
11. L. De Rosa, A. L. Cortajarena, A. Romanelli, L. Regan and L. D. D'Andrea, *Org Biomol Chem*, 2012, **10**, 273-280.
12. C. P. Hackenberger and D. Schwarzer, *Angew Chem Int Ed Engl*, 2008, **47**, 10030-10074.
13. L. De Rosa, R. Di Stasi, L. Longhitano and L. D. D'Andrea, *Bioorg Chem*, 2019, **91**, 103160.
14. P. E. Dawson, T. W. Muir, I. Clark-Lewis and S. B. Kent, *Science*, 1994, **266**, 776-779.
15. S. Chandrudu, P. Simerska and I. Toth, *Molecules*, 2013, **18**, 4373-4388.
16. S. Kent, Y. Sohma, S. Liu, D. Bang, B. Pentelute and K. Mandal, *J Pept Sci*, 2012, **18**, 428-436.
17. T. M. Hackeng, C. M. Mounier, C. Bon, P. E. Dawson, J. H. Griffin and S. B. Kent, *Proc Natl Acad Sci U S A*, 1997, **94**, 7845-7850.
18. Z. B. Li, G. Niu, H. Wang, L. He, L. Yang, M. Ploug and X. Chen, *Clin Cancer Res*, 2008, **14**, 4758-4766.
19. R. Haubner, R. Gratias, B. Diefenbach, S. L. Goodman, A. Jonczyk and H. Kessler, *J. Am. Chem. Soc.*, 1996, **118**, 7461-7472.
20. H. P. Hammes, M. Brownlee, A. Jonczyk, A. Sutter and K. T. Preissner, *Nat Med*, 1996, **2**, 529-533.
21. B. H. Northrop, S. H. Frayne and U. Choudhary, *Polym. Chem.*, 2015, **6**, 3415-3430.
22. E. W. Price and C. Orvig, *Chem Soc Rev*, 2014, **43**, 260-290.
23. L. Manzoni, L. Belvisi, D. Arosio, M. P. Bartolomeo, A. Bianchi, C. Brioschi, F. Buonsanti, C. Cabella, C. Casagrande, M. Civera, M. De Matteo, L. Fugazza, L. Lattuada, F. Maisano,

- L. Miragoli, C. Neira, M. Pilkington-Miksa and C. Scolastico, *ChemMedChem*, 2012, **7**, 1084-1093.
24. Z. Baranyai, F. Uggeri, A. Maiocchi, G.B. Giovenzana, C. Cavallotti, A. Takàcs, I. Toth, I. Benyei, E. Brucher and S. Aime, *Eur J Inorg Chem*, **2013**, 147-162.
25. Y. Shimizu, T. Temma, I. Hara, R. Yamahara, E. Ozeki, M. Ono and H. Saji, *J Fluoresc*, 2012, **22**, 719-727.
26. V. Ntziachristos, J. Ripoll, L. V. Wang and R. Weissleder, *Nat Biotechnol*, 2005, **23**, 313-320.
27. M. A. Russo, M. Paolillo, Y. Sanchez-Hernandez, D. Curti, E. Ciusani, M. Serra, L. Colombo and S. Schinelli, *Int J Oncol*, 2013, **42**, 83-92.
28. K. Sakamoto, S. Tsuda, M. Mochizuki, Y. Nohara, H. Nishio and T. Yoshiya, *Chem. Eur. J.*, 2016, **22**, 17940-17944.
29. K. Chen, L. P. Yap, R. Park, X. Hui, K. Wu, D. Fan, X. Chen and P. S. Conti, *Amino Acids*, 2012, **42**, 1329-1337.

## Supporting Information

### ***An innovative approach for the synthesis of dual modality peptide imaging probes based on the Native Chemical Ligation***

Ivan Hawala, Lucia De Rosa, Silvio Aime, Luca Domenico D'Andrea

#### **Contents**

I. Abbreviations

II. Materials and methods

III. Experimental synthesis procedures and analytical characterizations

IV. Experimental labelling procedures and analytical characterizations

V. Experimental procedure of *in vitro* receptor binding analyses

VI. Supplementary figures:

- Figure S1: Chemical structure of **6**
- Figure S2: Chemical structure of **7**
- Figure S3: UPLC-MS analysis of **1** and **2**
- Figure S4: UPLC-MS analysis of **3**
- Figure S5: <sup>1</sup>H-NMR of **3**
- Figure S6: UPLC-MS analysis of **4** and **5**
- Figure S7: UPLC-MS analysis of **6** and **7**
- Figure S8: UPLC-MS and ESI-ToF analyses of **8** and **9**
- Figure S9: Flow cytometry plots of **8**
- Figure S10: Flow cytometry plots of **9**

## I. Abbreviations

Fmoc (9-Fluorenylmethoxycarbonyl), AA (Amino acid), PyBOP (Benzotriazol-1-yl-oxytrypyrrolidinophosphonium hexafluorophosphate), DMAP (4-dimethylaminopyridine), HATU (1-[Bis(dimethylamino)methylene]-1H-1,2,3-triazolo[4,5-b]pyridinium 3-oxide hexafluorophosphate), DIC (N,N'-Diisopropylcarbodiimide), RP-HPLC (Reverse Phase High Performance Liquid Chromatography), UPLC (Ultra Performance Liquid Chromatography), MS (Mass Spectrometry), NMR (Nuclear Magnetic Resonance), DCM (methylene chloride), DMF (dimethylformamide), NMP (N-methyl-2-pyrrolidone), (tBu)<sub>4</sub>-AAZTA-C4-COOH (6-[Bis[2-(1,1-dimethylethoxy)-2-oxoethyl]amino]-6-(5-carboxypentyl)tetrahydro-1H-1,4-diazepine-1,4(5H)-Diacetic acid  $\alpha,\alpha'$ -bis(1,1-dimethylethyl)ester), TIS (triisopropylsilane), DIPEA (N,N-diisopropylethylamine), TFA (trifluoroacetic acid), CH<sub>3</sub>CN (acetonitrile), ESI-MS (Electron Spray ionization Mass Spectrometry), TCEP (Tris(2-carboxyethyl)phosphine hydrochloride), MEM (Minimmun Essential Medium), MESNA (2-Mercaptoethanesulfonic acid sodium salt), NCL (Native Chemical Ligation), EDC (1-ethyl-3-(3-dimethylaminopropyl)carbodiimide hydrochloride). PET (positron emission tomography), OI (optical imaging). tBu (tert-butyl), Boc (tert-butyloxycarbonyl) Pbf (2,2,4,6,7-pentamethylidhydrobenzofuran-5-sulfonyl).

## II. Materials and methods

### *Chemical Synthesis*

All Fmoc protected amino acids, preloaded Wang Resin with Fmoc-Ser(*t*Bu)-OH and PyBOP were purchased by Novabiochem (Darmstad, Germany), Sigma Aldrich (Darmstad, Germany) and Iris Biotech (Marktredwitz, Germany). Fmoc-Asp-OAll was purchased by Fluka. Wang ChemMatrix<sup>®</sup> resin was purchased by Biotage (Uppsala, Sweden). Sodium acetate, acetic acid and anhydrous GaCl<sub>3</sub> were purchased by Sigma Aldrich (Darmstad, Germany). Cyanine 5.5 maleimide was purchased by Lumiprobe GmbH (Hannover, Germany). All other reagents were purchased by Sigma Aldrich (Darmstad, Germany). All solvents were purchased by VWR International (Radnor, USA) and were used without further purifications. 6-[Bis[2-(1,1-dimethylethoxy)-2-oxoethyl]amino]-6-(5-carboxypentyl)tetrahydro-1H-1,4-diazepine-1,4(5H)-Diacetic acid  $\alpha,\alpha'$ -bis(1,1-dimethylethyl)ester ((*t*Bu)<sub>4</sub>-AAZTA-C4-COOH) was synthesized in accordance with Manzoni et al protocol.<sup>1</sup>

NMR spectra were recorded at 298 K on a Bruker AVANCE 600 spectrometer. CD<sub>3</sub>OD and NMR tube were purchased from Sigma Aldrich.

Mass spectra with electrospray ionization (ESI) were recorded on a SQD 3100 Mass Detector (Waters) and on an LC-MS system Agilent 1200 Infinity Series (Agilent Technologies). The HPLC-MS analytical and preparative purifications were carried out on a Waters AutoPurification system (3100 Mass Detector 600 Quaternary Pump Gradient Module, 2767 Sample Manager and 2487 UV/Visible Detector) and on a HP 1200 Series (Agilent Technologies). UPLC-MS analyses were performed using a Waters Acquity UPLC H-Class coupled with an ESI source, a quadrupole (QDa) mass analyzer and dual-wavelength UV/Vis TUV Detector. High resolution mass analysis was performed on an Agilent 1200 Infinity Series (Agilent Technologies) equipped with ESI source and a ToF analyzer.

AE105-Cys linear peptide was synthesized automatically with a CEM Microwave Peptide Liberty Synthesizer.

UV-Vis spectra were acquired by a 6715 UV-Vis spectrophotometer (JENWAY) in the spectral range 500-800 nm using rectangular quartz cells having an optical path length of 1 cm (Hellma Analytics).

### *Cell culture and flow cytometry*

U-87 MG human glioblastoma cell line was purchased from American Type Culture Collection (ATCC, Manassas, VA, USA) and were grown in MEM modified medium (Euroclone, Milan, Italy) supplemented with 1% glutamine, 1% sodium pyruvate, 1% Non-Essential Aminoacids, 100 U/mL penicillin, 100 U/mL streptomycin and 10% (v/v) fetal bovine serum (FBS) at 310 K in humidified atmosphere containing 5% of CO<sub>2</sub>.

In vitro binding evaluations were performed by Guava<sup>®</sup> easyCyte 8 Benchtop Flow Cytometer (Merck Millipore, Burlington, Massachusetts, USA) using RED2 filter (661/19 nm). Fluorescent profiles and binding percentages of the cell populations were obtained and analyzed using InCyte Software (Merck Millipore, Burlington, Massachusetts, USA).

### III. Experimental synthesis procedures and analytical characterizations

#### Cys-AE105 (1)

The immobilized linear peptide H-Cys(trt)-Asp(tBu)-Cha-Phe-D-Ser(tBu)-D-Arg(Pbf)-Tyr(tBu)-Leu-Trp(Boc)-Ser(tBu)-Wang resin was synthesized automatically with the support of microwaves (MW) on a Wang Resin preloaded with H-Ser(tBu)-OH (156 mg, 0.64 mmol/g) by standard Fmoc protocol. Cleavage of Fmoc group was achieved with 20% piperidine in DMF. Each coupling reaction was performed adding to the reaction vessel 5 equivalents of the Fmoc protected amino acid, 10 equivalents of DIPEA and 5 equivalents of the activator agent (PyBOP). The peptide was cleaved from the solid support by addition of TFA/Phenol/H<sub>2</sub>O/TIS (88:5:2:5) overnight at room temperature. Final purification was achieved by preparative RP-HPLC by employing an Atlantis prepD<sup>®</sup> C18OBD 5 $\mu$ m (19X100 mm) column. Eluent: (A) 0.1% TFA in H<sub>2</sub>O, (B) 0.1% TFA in CH<sub>3</sub>CN. Gradient profile; isocratic at 20% of B for 8.52 min, linear gradient from 20% to 40% of B in 8.48 min, linear gradient from 40% to 100% in 2.9 min, isocratic at 100% for 1.1 minutes. Flow rate; 15 mL/min. Cys-AE105 was isolated as a homogenous peak with a retention time of ab. 18 minutes. The solvent was removed *in vacuo* and the product lyophilized from water to give **1** as a white solid (39 mg, 29%). The purity of the product was checked by analytical UPLC-MS by employing an ACQUITY UPLC<sup>®</sup> Peptide BEH C18 column (300 $\text{\AA}$ , 1.7 $\mu$ m, 2.1X100mm). Eluent: (A) 0.05% TFA in H<sub>2</sub>O, (B) 0.05% TFA in CH<sub>3</sub>CN. Gradient profile; linear gradient from 5% to 50% of B in 7 min, linear gradient from 50% to 100% in 3 min, isocratic at 100% for 3 minutes. Flow rate of 0.4 mL/min and UV detection at 210 nm. Purity 98%. ESI-MS (*m/z*): calcd: For C<sub>67</sub>H<sub>91</sub>N<sub>13</sub>O<sub>21</sub>S<sub>2</sub> (M+2H)<sup>2+</sup> 665.37 found: 665.73.

#### cycloRGDFK(C) (2)

*Synthesis of the linear peptide.* The linear peptide H-D-Phe-Lys(Mtt)-Arg(Pbf)-Gly-Asp-O-All was synthesized manually on a Wang ChemMatrix<sup>®</sup> resin (loading: 0.39 mmol/g) using Fmoc chemistry. The C-terminal Asp residue was loaded on the resin through the side chain carboxyl group. 154.2 mg (0.39 mmol, 1 equiv) of Fmoc-Asp-OAll were dissolved in 5 mL of dry DCM, and 30.6  $\mu$ L (0.195 mmol, 0.5 equiv) of DIC were added to the solution. The mixture was incubated on ice for 30 min, under stirring. Then, DCM was removed under N<sub>2</sub> flux, the mixture was resuspended in DMF, and added to 0.39 mmol (1 g, 1 equiv) of Wang ChemMatrix<sup>®</sup> resin swollen in DMF, with 4.7 mg (0.039 mmol, 0.1 equiv) of DMAP. The reaction mixture was stirred for 2 h at room temperature. The substitution degree of the resin was evaluated by Fmoc-test<sup>2</sup>, resulting in 0.21 mmol/g. Peptide synthesis was completed on a 0.2 mmol scale, using a standard Fmoc protocol and the amino acids Fmoc-Gly-OH, Fmoc-Arg(Pbf)-OH, Fmoc-Lys(Mtt)-OH, Fmoc-D-Phe-OH. Coupling reactions were carried out for 30 min under stirring using 5 equiv of the Fmoc protected amino acid, 4.9 equiv of HATU as the activating agent, 10 equiv of DIPEA as base in DMF. A capping reaction was performed after each amino acid coupling by treatment of the resin with a solution of 2.0 M acetic anhydride, 0.55 M DIPEA in NMP, for 5 min under stirring. Fmoc deprotection reactions were performed by incubation of the resin with a solution of 20% piperidine in DMF, twice for 5 min. After the coupling of the Fmoc-D-Phe-OH, the resin was dried under *vacuo* and the substitution degree of the resin was evaluated by Fmoc-test, resulting in 0.072 mmol/g (1.2 g, 86.4  $\mu$ mol).

*Allyl group removal.* The resin (1.2 g, 86.4  $\mu$ mol) was swollen in dry DCM, under N<sub>2</sub> flux. Allyl-protecting group was removed from the  $\alpha$ -carboxyl group of the Asp residue at the C-terminus of the linear peptide by treatment with tetrakis (triphenylphosphine) palladium(0) (25 mg, 0.25 equiv) and phenylsilane (255  $\mu$ L, 24 equiv) in dry DCM, which were added to the resin

under N<sub>2</sub> flux and gently shaken for 30 min. The procedure was repeated twice. The resin was subsequently washed with DCM and DMF and the N-terminal Fmoc group was removed by treatment with 20% piperidine in DMF (2 × 5 min).

*On resin peptide head-to-tail cyclization.* The cyclization reaction between the N-terminal α-amino group of the D-Phe and the C-terminal α-carboxy group of the Asp residue was carried out by adding to the resin 44.7 mg of PyBOP (86 μmol, 1 equiv) and 30.2 μL of DIPEA (172 μmol, 2 equiv) in DMF. The reaction was incubated over night at room temperature, under stirring. The resin was then washed with DMF, DCM and diethyl ether and dried under *vacuo*.

*Mtt removal and coupling of a Cys residue on ε-amine group of the Lys2.* After peptide head-to-tail cyclization, methyltrityl (Mtt) side chain protecting group of the Lys2 was selectively removed on solid phase by treatment with a solution of 0.5% TFA, 5% TIS in DCM, performing washes of 1 min with the solution until a uncolored eluate solution was obtained. The resin was washed with DCM and DMF and then 200 mg of Boc-Cys(trt)-OH (432 μmol, 5 equiv), 160 mg of HATU (422 μmol, 4.9 equiv) and 97 μL of 4-methylmorpholine (860 μmol, 10 equiv) were added to the resin and the mixture was incubated for 1 h at room temperature, under stirring. The resin was then washed with DMF, DCM and diethyl ether and dried under *vacuo*.

The branched cyclic peptide *cyclo*RGDfK(C) was cleaved off the resin and deprotected using a mixture of TFA/H<sub>2</sub>O/TIS (95:2.5:2.5; v/v/v) for 2 h at room temperature. The resin was finally filtered, and the peptide *cyclo*RGDfK(C) was precipitated using cold diethyl ether. The crude product (53 mg) was purified by preparative RP-HPLC on a HP 1200 Series (Agilent Technologies) using the column Axia 50×21.2 mm, Synergi, 4 mm, Fusion RP 80 Å (Phenomenex), applying a gradient of CH<sub>3</sub>CN (0.1% TFA) in H<sub>2</sub>O (0.1% TFA) from 5% to 25% in 20 min, at a flow rate of 20 mL/min. Pure fractions were pooled and lyophilized. 13.5 mg of pure (>95%) *cyclo*RGDfK(C) were obtained (yield 10%). The purity of the product was checked by analytical UPLC-MS by employing an ACQUITY UPLC® Peptide BEH C18 column (300Å, 1.7μm, 2.1X100mm). Eluent: (A) 0.05% TFA in H<sub>2</sub>O, (B) 0.05% TFA in CH<sub>3</sub>CN. Gradient profile: linear gradient from 5% to 50% of B in 7 min, linear gradient from 50% to 100% in 3 min, isocratic at 100% for 3 minutes. Flow rate of 0.4 mL/min and UV detection at 210 nm. ESI-MS (*m/z*): calcd: For C<sub>30</sub>H<sub>46</sub>N<sub>10</sub>O<sub>8</sub>S (M+H)<sup>+</sup> 707.33 found: 707.43, (M+2H)<sup>2+</sup> 354.41 found: 354.38

### **2-((5-(6-(bis(carboxymethyl)amino)-1,4-bis(carboxymethyl)-1,4-diazepan-6-yl)pentanoyl)thio)ethane-1-sulfonate, AAZTA-C4-CO-MES (3)**

In a round bottom flask, 108.1 mg of (tBu)<sub>4</sub>-AAZTA-C4-COOH (1 eq, 0.161 mmol) were dissolved in 5 mL of DCM. The solution was cooled at 273 K and DMAP (0.09 eq, 1.8 mg) and EDC (1 eq, 30.8 mg) were added. After 10 minutes the ice bath was removed and MESNA (0.9 eq, 23.8 mg) were added to the solution and the reaction was stirred overnight at room temperature. The solvent was evaporated and the obtained product re-dissolved in 5 mL of TFA/TIS/H<sub>2</sub>O(95:2.5:2.5) and the reaction was stirred overnight at room temperature. The solvent was evaporated and the final purification was achieved by preparative RP-HPLC on Waters AutoPurification system by employing an Atlantis prepD® C18OBD 5μm (19X100 mm) column. Eluent: (A) 0.1% TFA in H<sub>2</sub>O, (B) 0.1% TFA in CH<sub>3</sub>CN. Gradient profile: isocratic at 10% of B for 2.8 min, linear gradient from 10% to 35% of B in 5.7 min, linear gradient from 35% to 100% in 2.8 min, isocratic at 100% for 1 min. Flow rate; 15 mL/min. AAZTA-C4-CO-MES was isolated as a homogenous peak with a retention time of ab. 5 minutes. The solvent was removed *in vacuo* and the product lyophilized from water to give **2** as a white solid (35 mg, 38%). The purity of the product was checked by analytical UPLC-MS by employing an ACQUITY UPLC® Peptide BEH C18 column (300Å, 1.7μm, 2.1X100mm). Eluent: (A) 0.05% TFA in H<sub>2</sub>O, (B)



0.05% TFA in CH<sub>3</sub>CN. Gradient profile; linear gradient from 5% to 50% of B in 7 min, linear gradient from 50% to 100% in 3 min, isocratic at 100% for 3 minutes. Flow rate of 0.4 mL/min and UV detection at 210 nm. Purity 95%. ESI-MS (*m/z*): calcd: For C<sub>20</sub>H<sub>33</sub>N<sub>3</sub>O<sub>12</sub>S<sub>2</sub> (M+H)<sup>+</sup> 572.16 found: 572.31. <sup>1</sup>H-NMR (CD<sub>3</sub>OD, 600 MHz): δ 1.63 (tr, 6H), 2.37 (t, J=7.45 Hz, 2H), 2.62 (t, J=7.45, 4H), 3.02 (tr, 4H), 3.26 (tr, 2H), 3.58 (tr, 2H), 3.74 (s, 8H).

#### **AAZTA-C4-CO-Cys-AE105 (4)**

2 mg of **1** (1.50 μmol, 1 eq) were dissolved in 100 μL of ligation buffer (0.2M phosphate buffer pH 7.4, 5M Imidazole, 3M Guanidinium chloride, 50mM TCEP. Final pH: 7.4) and the pH is adjusted to 7.4. A solution of **3** (3.00 μmol, 2 eq) in 100 μL of ligation buffer was added to the previous solution and the pH was adjusted to 7.4. The reaction was stirred for 1 h at room temperature. The reaction was monitored by HPLC-MS. Final purification was achieved by preparative RP-HPLC on Waters AutoPurification system by employing an XBridge™ BEH300 Prep C18 10 μm (10X100 mm) column. Eluent: (A) 0.1% TFA in H<sub>2</sub>O, (B) 0.1% TFA in CH<sub>3</sub>CN. Gradient profile; isocratic at 20% of B for 10 min, linear gradient from 20% to 35% of B in 10 min, linear gradient from 35% to 100% in 3.33 min, isocratic at 100% for 4 min. Flow rate; 5 mL/min. **4** was isolated as a homogenous peak with a retention time of ab. 22.5 minutes. The solvent was removed *in vacuo* and the product lyophilized from water to give **4** as white solid (1.64 mg, 62%). The purity of the product was checked by analytical UPLC-MS by employing an ACQUITY UPLC® Peptide BEH C18 column (300Å, 1.7μm, 2.1X100mm). Eluent: (A) 0.05% TFA in H<sub>2</sub>O, (B) 0.05% TFA in CH<sub>3</sub>CN. Gradient profile; linear gradient from 5% to 50% of B in 7 min, linear gradient from 50% to 100% in 3 min, isocratic at 100% for 3 minutes. Flow rate of 0.4 mL/min and UV detection at 210 nm. Purity 98%. ESI-MS (*m/z*): calcd: For C<sub>81</sub>H<sub>115</sub>N<sub>17</sub>O<sub>25</sub>S (M+2H)<sup>2+</sup> 880.36 found: 880.16.

#### **AAZTA-C4-CO-cycloRGDfK(C) (5)**

1.09 mg (1.91 μmol, 1 equiv) of **3** were dissolved in 283 μL of ligation buffer (0.2 M phosphate buffer pH 7.4, 5 M imidazole, 3 M guanidinium chloride, 2 mM EDTA, in ultra-gradient water. Final pH: 7.4) and the solution was immediately added to 0.98 mg (1.39 μmol, 0.75 equiv) of **2**. The mixture was incubated for 30 min at room temperature and then analyzed by LC-MS on HP 1200 Series (Agilent Technologies) using a column Aeris 100 × 2.1 mm, PEPTIDE XB-C18, 3.6 μm and applying a gradient of CH<sub>3</sub>CN (0.05% TFA) in H<sub>2</sub>O (0.05% TFA) from 5% to 70% in 15 min. The analysis showed the complete conversion of the cyclic peptide in the ligation product AAZTA-C4-CO-cycloRGDfK(C). The reaction mixture was diluted with 0.25 mL of CH<sub>3</sub>CN (0.1% TFA) and 4.47 mL of H<sub>2</sub>O (0.1% TFA) (final volume of 5 mL) and purified by RP-HPLC on HP 1200 Series (Agilent Technologies) on a column Axia 50 × 21.2 mm, Synergi, 4 μm, Fusion RP 80 Å, applying a gradient of CH<sub>3</sub>CN (0.1% TFA) in H<sub>2</sub>O (0.1% TFA) from 5% to 60% in 10 min, at a flow rate of 20 mL/min. The product was lyophilized to give **5** (0.5 mg, 32%). The purity of the product was checked by analytical UPLC-MS by employing an ACQUITY UPLC® Peptide BEH C18 column (300Å, 1.7μm, 2.1×100mm). Eluent: (A) 0.05% TFA in H<sub>2</sub>O, (B) 0.05% TFA in CH<sub>3</sub>CN. Gradient profile; linear gradient from 5% to 50% of B in 7 min, linear gradient from 50% to 100% in 3 min, isocratic at 100% for 3 minutes. Flow rate of 0.4 mL/min and UV detection at 210 nm. Purity 95%. ESI-MS (*m/z*): calcd: For C<sub>48</sub>H<sub>73</sub>N<sub>13</sub>O<sub>17</sub>S (M+H)<sup>+</sup> 1136.25 found: 1136.64.

### **AAZTA-C4-CO-Cys(Cy 5.5)-AE105 (6): procedure 1**

3.09 mg of **4** (1.76  $\mu\text{mol}$ ) were dissolved in 600  $\mu\text{L}$  of 50 mM acetate at pH 6.5. 1.14 mg of Cyanine 5.5 Maleimide (0.875 eq, 1.53  $\mu\text{mol}$ ) were added to the previous solution and the reaction was stirred at room temperature for 3h. The reaction was monitored by UPLC-MS. Final purification was achieved by preparative RP-HPLC on Waters AutoPurification system by employing an XBridge™ BEH300 Prep C18 10  $\mu\text{m}$  (10 $\times$ 100 mm) column. Eluent: (A) 0.1% TFA in H<sub>2</sub>O, (B) 0.1% TFA in CH<sub>3</sub>CN. Gradient profile; isocratic at 25% of B for 5.25 min, linear gradient from 25% to 50% of B in 15.77 min, isocratic at 50% of B in 5.25 min, linear gradient from 50% to 100% in 5 min, isocratic at 100% for 5 min. Flow rate; 4.5 mL/min. AAZTA-C4-CO-Cys(Cy 5.5)-AE105 (**6**) was isolated as a homogenous peak with a retention time of ab. 24 min (1.68 mg, 39%). The purity of the product was checked by analytical UPLC-MS by employing an ACQUITY UPLC® Peptide BEH C18 column (300 $\text{\AA}$ , 1.7  $\mu\text{m}$ , 2.1 $\times$ 100mm). Eluent: (A) 0.05% TFA in H<sub>2</sub>O, (B) 0.05% TFA in CH<sub>3</sub>CN. Gradient profile; linear gradient from 5% to 50% of B in 7 min, linear gradient from 50% to 100% in 3 min, isocratic at 100% for 3 minutes. Flow rate of 0.4 mL/min and UV detection at 210 nm and 672 nm. Purity<sub>210 nm</sub>: 95%. ESI-MS (*m/z*): calcd: For C<sub>127</sub>H<sub>164</sub>N<sub>21</sub>O<sub>28</sub>S<sup>+</sup> (M+2H)<sup>3+</sup> 822.11found: 822.35.

### **Synthesis of AAZTA-C4-CO-Cys(Cy 5.5)-AE105 (6): procedure 2**

2.5 mg of **1** (1.88  $\mu\text{mol}$ , 1 eq.) were dissolved in 300 $\mu\text{L}$  of the reaction buffer (0.2M phosphate buffer pH 7.4, 5M imidazole, 3M guanidinium chloride. Final pH: 7.0) and 2.14 mg of **3** (3.75  $\mu\text{mol}$ , 2 eq.) were added to the solution. The obtained solution was stirred at room temperature for 30 min. After the reaction time an UPLC-MS chromatogram shows the total conversion to the desired product.

Subsequently, without performing any further purification, 1.39 mg of Cy 5.5 maleimide (1.87  $\mu\text{mol}$ , 1 eq.) were added to the solution. After 3 h the solution was directly purified on preparative RP-HPLC (same condition of synthesis of **6**). The final product was lyophilized from water to give **6** as dark blue solid (1.0 mg, 22%). The purity of the product was checked by analytical UPLC-MS by employing an ACQUITY UPLC® Peptide BEH C18 column (300 $\text{\AA}$ , 1.7  $\mu\text{m}$ , 2.1 $\times$ 100mm). Eluent: (A) 0.05% TFA in H<sub>2</sub>O, (B) 0.05% TFA in CH<sub>3</sub>CN. Gradient profile; linear gradient from 5% to 50% of B in 7 min, linear gradient from 50% to 100% in 3 min, isocratic at 100% for 3 minutes. Flow rate of 0.4 mL/min and UV detection at 210 nm and 672 nm. Purity<sub>210 nm</sub>: 95%. ESI-MS (*m/z*): calcd: For C<sub>127</sub>H<sub>164</sub>N<sub>21</sub>O<sub>28</sub>S<sup>+</sup> (M+2H)<sup>3+</sup> 822.11found: 822.15.

### **AAZTA-C4-CO-(Cy 5.5)-cycloRGDfK(C) (7): procedure 1**

0.5 mg (441 nmol, 1 equiv) of **5** were dissolved in 440  $\mu\text{L}$  of 20 mM phosphate buffer, pH 7.2. 0.39 mg of Cy 5.5 Maleimide (529 nmol, 1.2 equiv) were dissolved in 25  $\mu\text{L}$  of CH<sub>3</sub>CN and added to the solution of **5**. Reaction was carried out for 1 h at room temperature, in the dark, and analyzed by LC-MS on HP 1200 Infinity Series (Agilent Technologies) on a column Aeris 100  $\times$  2.1 mm, PEPTIDE XB-C18, 3.6 mm and applying a gradient of CH<sub>3</sub>CN (0.05% TFA) in H<sub>2</sub>O (0.05% TFA) from 5% to 95% in 25 min. The analysis showed the complete conversion of the **5** in the doubly labelled peptide AAZTA-C4-CO-(Cy 5.5)-cycloRGDfK(C) (**7**). The reaction mixture was diluted with 0.25 mL of CH<sub>3</sub>CN (0.1% TFA) and 4.28 mL of H<sub>2</sub>O (0.1% TFA) (final volume of 5 mL) and purified by RP-HPLC on HP 1200 Series (Agilent Technologies) on a column Jupiter C18 250  $\times$  10 mm, 5  $\mu\text{m}$ , 300  $\text{\AA}$  (Phenomenex) applying a gradient of CH<sub>3</sub>CH (0.1% TFA) in H<sub>2</sub>O (0.1% TFA) from 5% to 70% in 40 min), at a flow rate of 5 mL/min. The pure **7** was quantified

by UV absorption spectroscopy, using the Cy5.5 molar extinction coefficient at 684 nm of  $1.98 \times 10^5 \text{ M}^{-1} \text{ cm}^{-1}$  (0.160 mg, 86.7 nmol, 20% yield). The purity of the product was checked by analytical UPLC-MS by employing an ACQUITY UPLC® Peptide BEH C18 column (300Å, 1.7µm, 2.1X100mm). Eluent: (A) 0.05% TFA in H<sub>2</sub>O, (B) 0.05% TFA in CH<sub>3</sub>CN. Gradient profile; linear gradient from 5% to 50% of B in 7 min, linear gradient from 50% to 100% in 3 min, isocratic at 100% for 3 minutes. Flow rate of 0.4 mL/min and UV detection at 210nm and 672 nm. Purity<sub>210nm</sub>: 95%.ESI-MS (*m/z*): calcd: For C<sub>94</sub>H<sub>122</sub>N<sub>17</sub>O<sub>20</sub>S<sup>+</sup> (M+H)<sup>2+</sup>921.58 found: 921.37.

#### **AAZTA-C4-CO-(Cy 5.5)-cycloRGDfK(C) (7): procedure 2**

1.1mg (1.92 µmol, 1 equiv) of **3** were dissolved in 283 µL of ligation buffer (see previous procedure) and the solution was immediately added to 1.0 mg (1.41 µmol, 0.75 equiv) of **2**. The mixture was incubated for 30 min at room temperature and analyzed by LC-MS on HP 1200 Infinity Series (Agilent Technologies) showing the complete conversion of the cyclic peptide in the ligation product **5**. Without performing any purification, 2.17 mg (2.92 µmol, 1.5 equiv) of Cy 5.5 maleimide were dissolved in 50 µL of CH<sub>3</sub>CN and added to the reaction mixture. After 30 min of reaction in the dark, at room temperature, the reaction was checked by LC-MS on HP 1200 Infinity Series (Agilent Technologies) showing the complete conversion of the **5** in the doubly labelled peptide AAZTA-C4-CO-(Cy 5.5)-cycloRGDfK(C) (**7**). The mixture was diluted with 0.5 mL of CH<sub>3</sub>CN (0.1% TFA) and 3.87 mL of H<sub>2</sub>O (0.1% TFA) (final volume of 5 mL) and purified by RP-HPLC on HP 1200 Series (Agilent Technologies) on a column Axia 50 × 21.2 mm, Synergi, 4 mm, Fusion RP 80 Å, applying a gradient of CH<sub>3</sub>CN (0.1% TFA) in H<sub>2</sub>O (0.1% TFA) from 5% to 70% in 25 min, at a flow rate of 20 mL/min. After lyophilization 0.6 mg of pure **7** were recovered (yield:23%). Purity<sub>210nm</sub>: 95%. ESI-MS (*m/z*): calcd: For C<sub>94</sub>H<sub>122</sub>N<sub>17</sub>O<sub>20</sub>S<sup>+</sup> (M+H)<sup>2+</sup>921.58 found: 921.47.

#### IV. Experimental labelling procedures and analytical characterizations

##### **Ga-AAZTA-C4-CO-Cys(Cy 5.5)-AE105 (8)**

0.38 mg of **6** (0.154  $\mu\text{mol}$ ) were dissolved in 300  $\mu\text{L}$  of a solution 50:50 of 0.1M acetate buffer at pH 3.8/ $\text{CH}_3\text{CN}$ . 10  $\mu\text{L}$  of a 1000ppm standard water solution of  $\text{GaCl}_3$  were added and the solution was stirred at room temperature for 1h. Product **8** was quantified by UV absorption spectroscopy in ethanol, using the Cy5.5 molar extinction coefficient at 684 nm of  $1.98 \cdot 10^5 \text{ M}^{-1} \text{ cm}^{-1}$ . The purity of the product was checked by analytical UPLC employing an ACQUITY UPLC<sup>®</sup> Peptide BEH C18 column (300 $\text{\AA}$ , 1.7 $\mu\text{m}$ , 2.1X100mm). Eluent: (A) 0.05% TFA in  $\text{H}_2\text{O}$ , (B) 0.05% TFA in  $\text{CH}_3\text{CN}$ . Gradient profile; linear gradient from 5% to 50% of B in 7 min, linear gradient from 50% to 100% in 3 min, isocratic at 100% for 3 minutes. Flow rate of 0.4 mL/min and UV detection at 210nm and 672 nm. Purity<sub>210 nm</sub>: 96%. ESI-MS ( $m/z$ ): calcd: For  $\text{C}_{127}\text{H}_{161}\text{GaN}_{21}\text{O}_{28}\text{S}^+$  ( $\text{M}+2\text{H}$ )<sup>3+</sup> 844.42 found: 844.25. High resolution mass spectrometry monoisotopic peak ( $\text{M}+2\text{H}$ )<sup>3+</sup>: calcd: 843.6932 found: 843.6893.

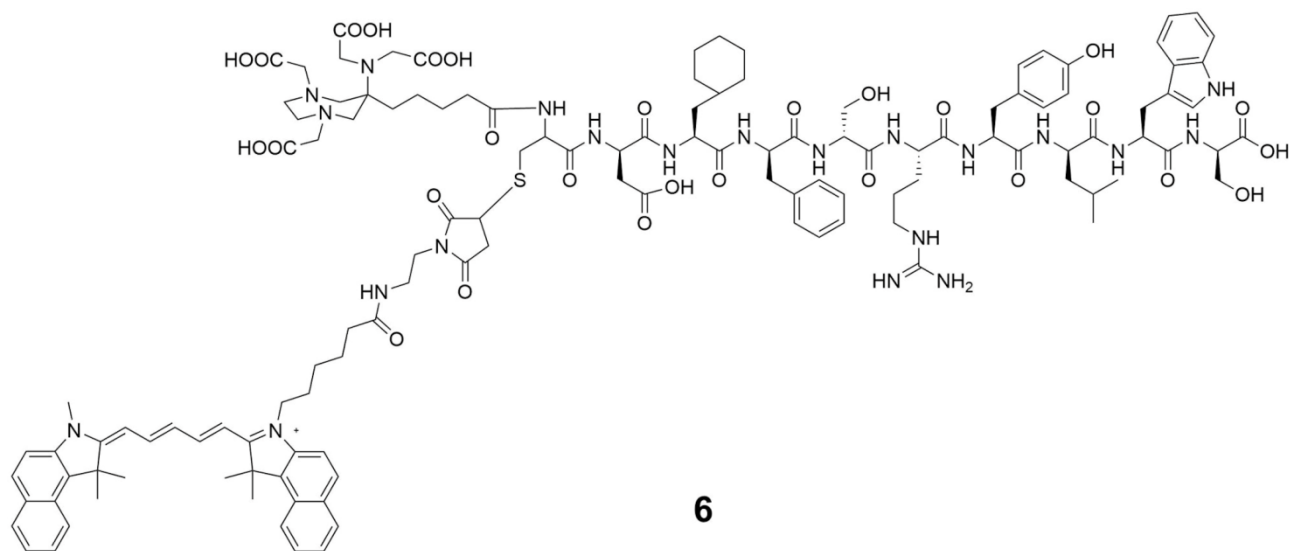
##### **Ga-AAZTA-C4-CO-(Cy 5.5)-cycloRGDFK(C) (9)**

0.54 mg of **7** (0.293  $\mu\text{mol}$ ) were dissolved in 450  $\mu\text{L}$  of a solution 50:50 of 0.1M acetate buffer/ $\text{CH}_3\text{CN}$  at pH 3.8. 20  $\mu\text{L}$  of a 1000ppm standard water solution of  $\text{GaCl}_3$  were added and the solution was stirred at room temperature for 1h. The pure **9** was quantified by UV absorption spectroscopy in ethanol, using the Cy5.5 molar extinction coefficient at 684 nm of  $1.98 \cdot 10^5 \text{ M}^{-1} \text{ cm}^{-1}$ . The purity of the product was checked by analytical UPLC by employing an ACQUITY UPLC<sup>®</sup> Peptide BEH C18 column (300 $\text{\AA}$ , 1.7 $\mu\text{m}$ , 2.1X100mm). Eluent: (A) 0.05% TFA in  $\text{H}_2\text{O}$ , (B) 0.05% TFA in  $\text{CH}_3\text{CN}$ . Gradient profile; linear gradient from 5% to 50% of B in 7 min, linear gradient from 50% to 100% in 3 min, isocratic at 100% for 3 minutes. Flow rate of 0.4 mL/min and UV detection at 210 nm and 672 nm. Purity<sub>210 nm</sub>:95%. ESI-MS ( $m/z$ ): calcd: For  $\text{C}_{94}\text{H}_{119}\text{GaN}_{17}\text{O}_{20}\text{S}^+(\text{M}+\text{H})^{2+}$ 954.94 found: 954.97. High resolution mass spectrometry monoisotopic peak ( $\text{M}+\text{H}$ )<sup>2+</sup>: calcd: 953.8897 found: 953.8832.

## V. Experimental procedure of *in vitro* receptor binding analyses

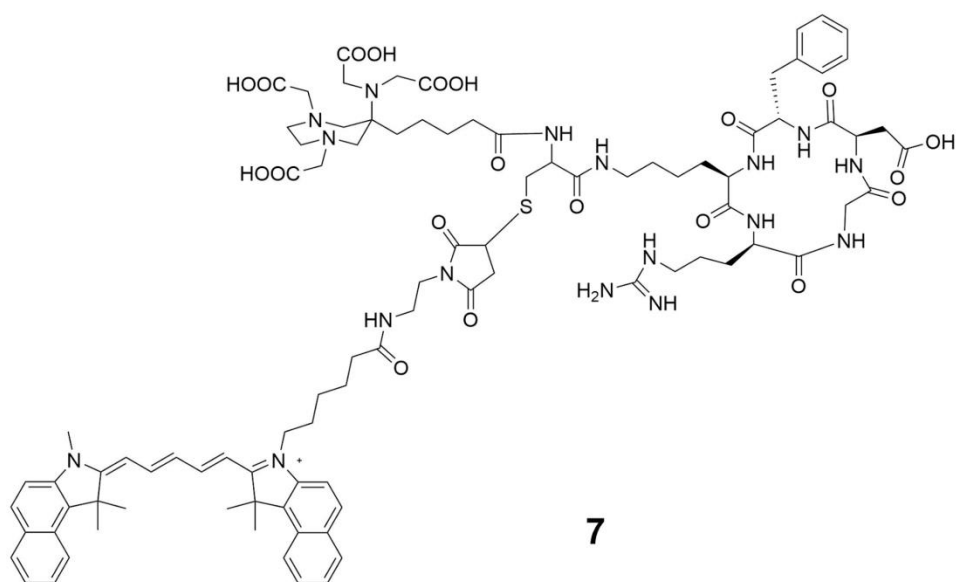
Human U-87 MG glioblastoma cells were used to determine cell binding of Ga-AAZTA-C4-CO-Cys(Cy 5.5)-AE105 (compound **8**) and Ga-AAZTA-C4-CO-(Cy 5.5)-*cyclo*RGDfK(C) (compound **9**). To minimize the non-specific uptake, incubations were performed on ice and followed immediately by flow cytometry. All cells groups ( $10^5$ ) were incubated with Ga-AAZTA-C4-CO-Cys-(Cy 5.5)-AE105 or Ga-AAZTA-C4-CO-(Cy 5.5)-*cyclo*RGDfK(C) (0, 0.033, 0.133 and 0.400  $\mu$ g) for 30 min at 273 K. After centrifugation of the tubes and the elimination of the supernatant, cells were washed twice with PBS 1X. 100uL of PBS 1X supplemented with 0.1% BSA were added to each tube.

1. L. Manzoni, L. Belvisi, D. Arosio, M. P. Bartolomeo, A. Bianchi, C. Brioschi, F. Buonsanti, C. Cabella, C. Casagrande, M. Civera, M. De Matteo, L. Fugazza, L. Lattuada, F. Maisano, L. Miragoli, C. Neira, M. Pilkington-Miksa and C. Scolastico, *ChemMedChem*, 2012, **7**, 1084-1093.
2. G. W. L. Mikhail F. Gordeev , Hon C. Hui , Eric M. Gordon , Dinesh V. Patel, *Tetrahedron*, 1998, **54**, 15879-15890.



**6**

**Figure S1:** Chemical structure of **6**



**7**

**Figure S2:** Chemical structure of **7**

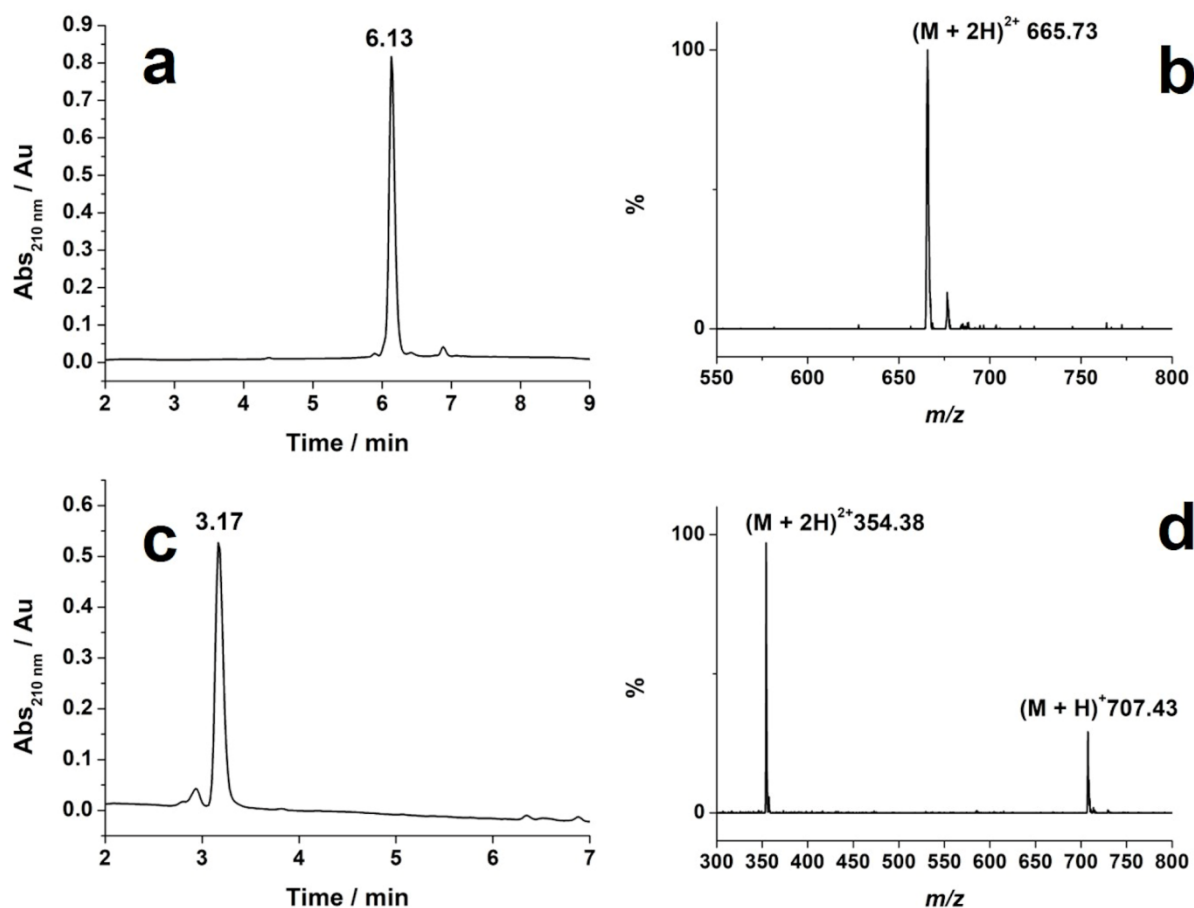


**Figure S3:** UPLC-MS analysis of pure compounds **1** and **2**: a) chromatographic profile of **1** revealed at 210 nm and ESI-MS spectrum (b) of the peak at 6.13 min retention time; c) chromatographic profile of **2** revealed at 210 nm and ESI-MS spectrum (d) of the peak at 3.17 min retention time

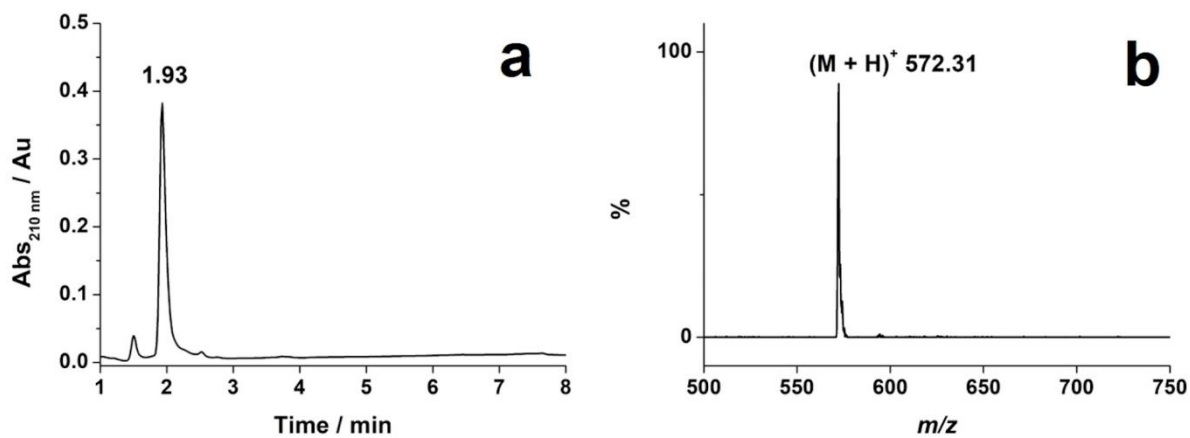


**Figure S4:** UPLC-MS analysis of pure compound **3**: a) chromatographic profile of **3** revealed at 210 nm and ESI-MS spectrum (b) of the peak at 1.93 min retention time



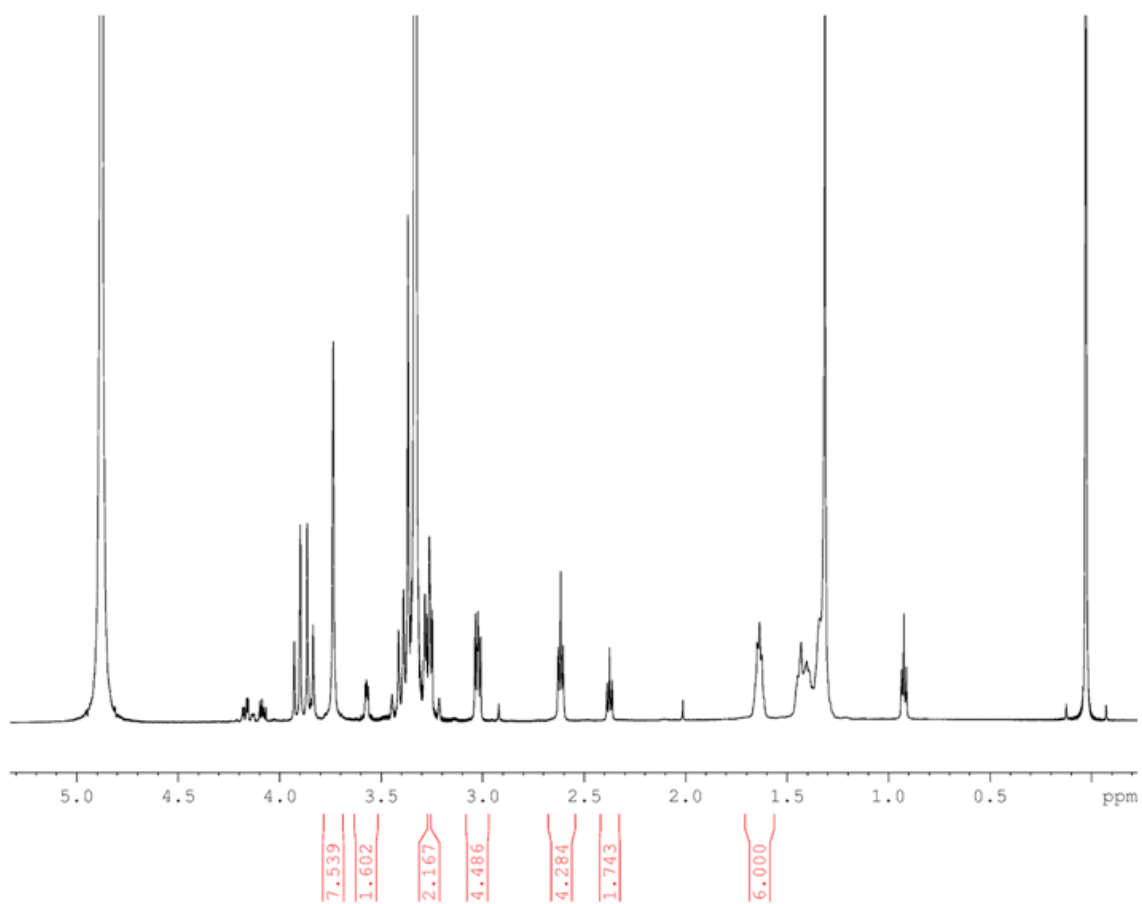


**Figure S5:** <sup>1</sup>H-NMR spectrum of **3** in CD<sub>3</sub>OD at 14.6 mM

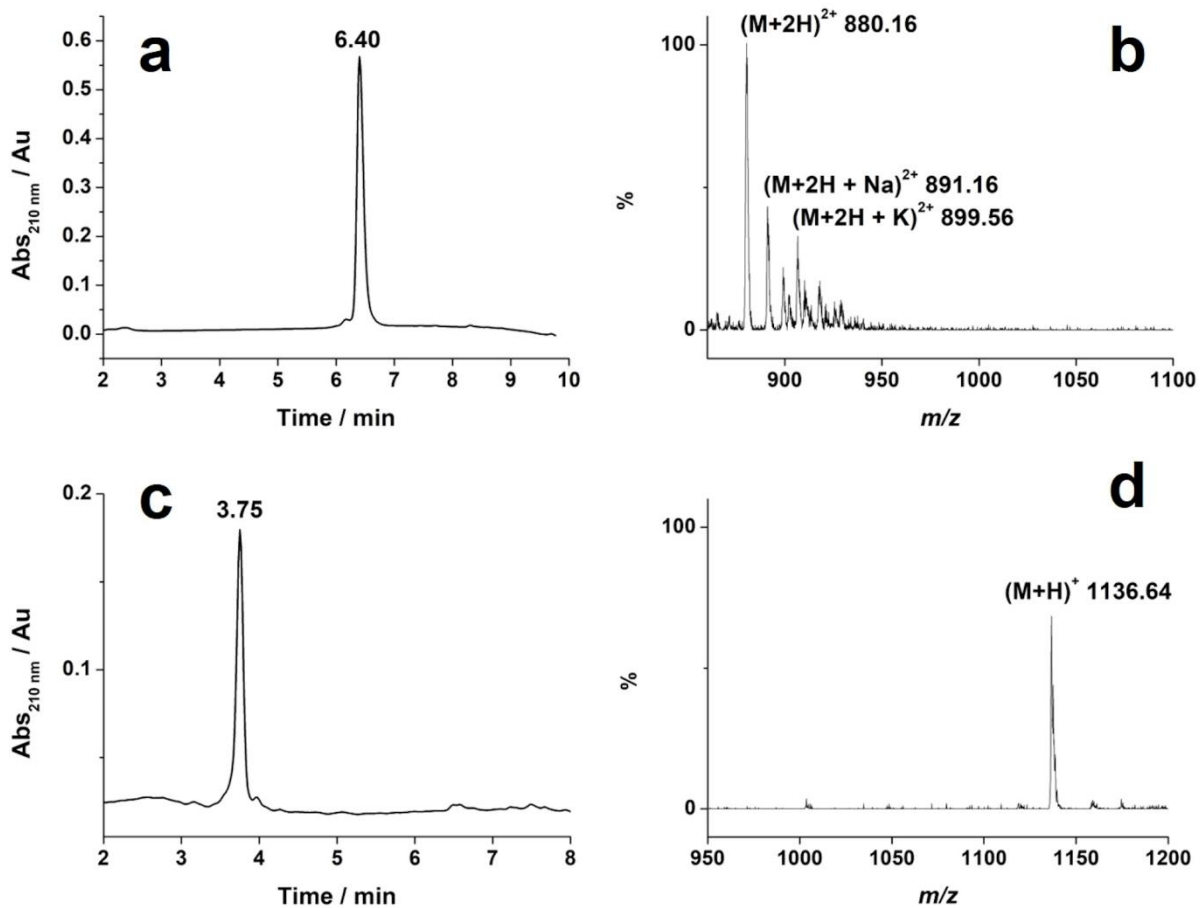


**Figure S6:** UPLC-MS analysis of pure compounds 4 and 5: a) chromatographic profile of 4 revealed at 210 nm and ESI-MS spectrum (b) of the peak at 6.40 min retention time; c) chromatographic profile of 5 revealed at 210 nm and ESI-MS spectrum (d) of the peak at 3.75 min retention time

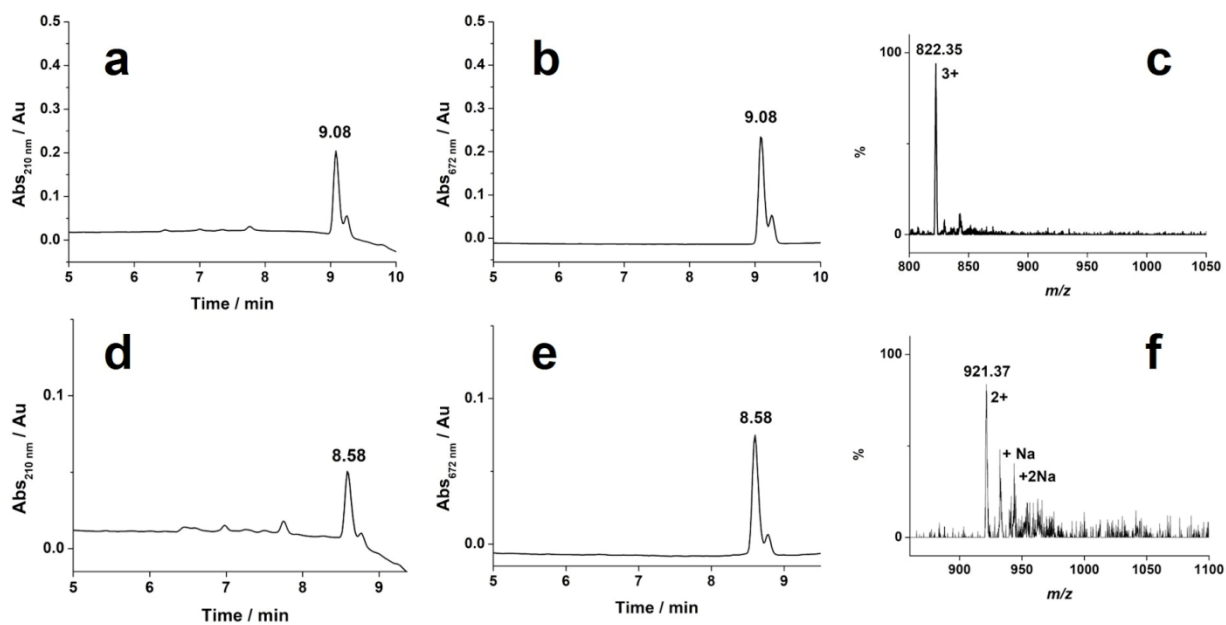


**Figure S7:** UPLC-MS analysis of pure compounds **6** and **7**: a) chromatographic profile of **6** revealed at 210 nm and 672 nm (b), and ESI-MS spectrum (c) of the peak at 9.08 min retention time; d) chromatographic profile of **7** revealed at 210 nm and 672 nm (e) and ESI-MS spectrum (f) of the peak at 8.58 min retention time

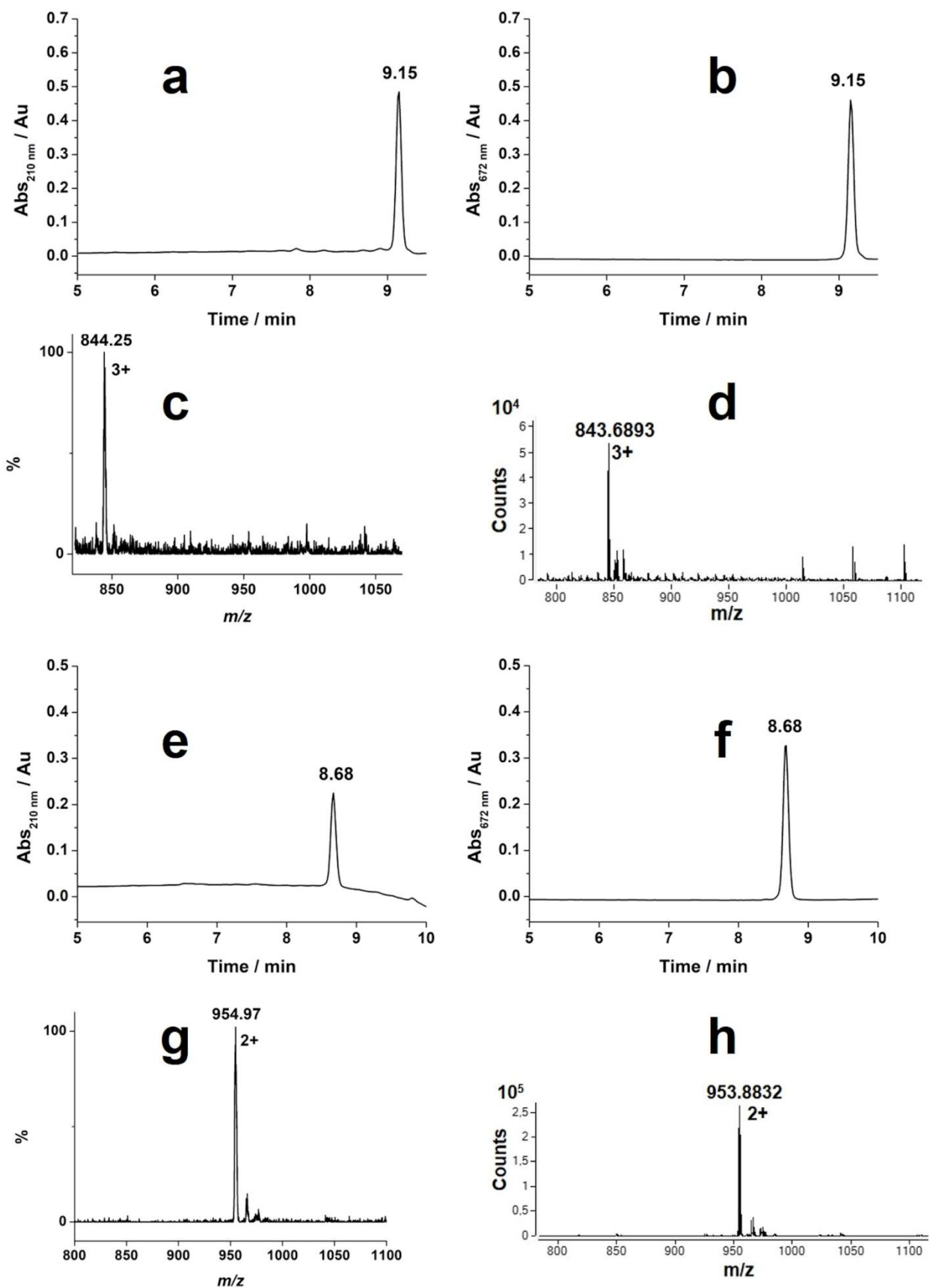


**Figure S8:** UPLC-MS and High Resolution Mass analyses of pure compounds **8** and **9**. Compound **8**: chromatographic profile revealed at 210 nm (a) and 672 nm (b), ESI-MS (c) and ESI-ToF (the monoisotopic peak is indicated) (d) spectra of the peak at 9.15 min retention time; Compound **9**: chromatographic profile revealed at 210 nm (e) and 672 nm (f), ESI-MS (g)

and ESI-ToF (the monoisotopic peak is indicated) (h) spectra of the peak at 8.68 min retention time.

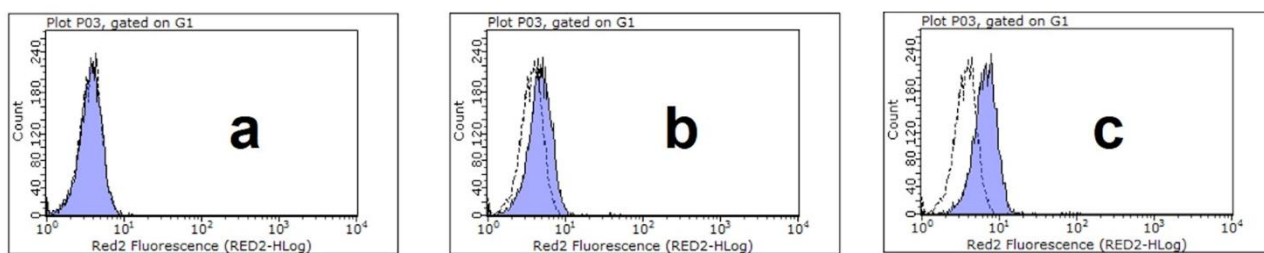


**Figure S9:** Flow Cytometry plot of U-87 MG cells ( $10^5$ ) analysed after incubation of 30 min at 273 K with (a) 0.033, (b) 0.133 and (c) 0.400  $\mu\text{g}$  of Ga-AAZTA-C4-CO-Cys(Cy5.5)-AE105 (**8**).

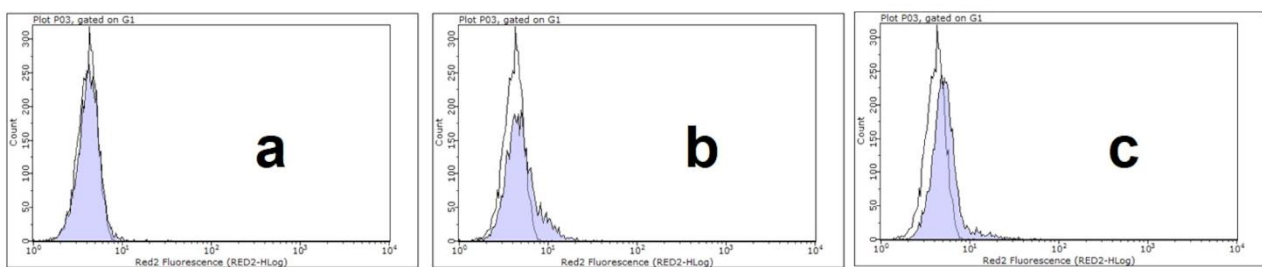


**Figure S10:** Flow Cytometry plot of U-87 MG cells ( $10^5$ ) analysed after incubation of 30 min at 273 K with (a) 0.033, (b) 0.133 and (c) 0.400  $\mu\text{g}$  of Ga-AAZTA-C4-CO-(Cy5.5)-*cyclo*RGDfK(C) (**9**).